The Dissertation Committee for Carla Kantara Certifies that this is the approved version of the following dissertation:

GROWTH FACTORS UP-REGULATE EPITHELIAL STEM CELLS: TREATMENT STRATEGIES FOR COLORECTAL CANCERS

APPROVED BY THE SUPERVISORY COMMITTEE

Pomila Singh, PhD

Robert Ullrich, PhD

Rakez Kayed, PhD

Darrell Carney, PhD

Shahid Umar, PhD

Dean, Graduate School

GROWTH FACTORS UP-REGULATE EPITHELIAL STEM CELLS: TREATMENT STRATEGIES FOR COLORECTAL CANCERS

by

Carla Kantara, B.S.

DISSERTATION

Presented to the Faculty

of the

GRADUATE SCHOOL OF

THE UNIVERSITY OF TEXAS MEDICAL BRANCH

in Partial Fulfillment

of the Requirements

for the Degree of

Doctor of Philosophy

THE UNIVERSITY OF TEXAS MEDICAL BRANCH

March, 2012

To my family and friends for their unconditional love and support throughout the years.

Thank you for believing in me.

ACKNOWLEDGEMENTS

I would like to take this opportunity to express my heartfelt appreciation to my mentor, Dr. Pomila Singh, for her invaluable guidance and support throughout my graduate career. I am honored to have had the privilege of working with and learning from someone who is so highly esteemed by the scientific community. It has been a true honor to have had you as my mentor, thank you for inspiring me, and for your constant support and encouragement both in and out of the lab and for challenging me to my true potential. I am forever grateful to you.

I would also like to thank my co-mentor Dr. Robert Ullrich for his expertise and support throughout the years and my committee members Dr. Rakez Kayed, Dr. Darrell Carney, and Dr. Shahid Umar. Thank you for your guidance and commitment to my dissertation. I truly appreciate your support, guidance and commitment throughout my dissertation project.

I also owe a debt of gratitude to my lab members Dr. Shubhashish Sarkar and Carrie Maxwell for their friendship, encouragement and assistance on many aspects of my project.

I am deeply grateful to the administration and staff of the Graduate School of Biomedical Sciences and the Cell Biology Program for their invaluable support and guidance throughout my graduate career. I would especially like to thank Mrs. Lisa Davis for graciously assisting me with all of my administrative needs and for her friendship; Dr. Dorian Coppenhaver for his helpful advice and guidance throughout my graduate experience; Dr. Golda Leonard and Dr. Darren Boehning for their guidance and for always believing in me.

The completion of my project would not have been possible if not for the valuable resources and expertise of Kenneth Escobar, at the UTMB histology core. Thank you for dedicating your time to training me and helping me develop new methods for embedding spheroids. In addition, I would like to thank Mark Griffin from the Flow Cytometry core at UTMB for his help and assistance throughout the years.

To my dear friends, Claiborne, A.C, Kira, Tina, Christine, Edna and Marlene, thank you for your friendship, support and for keeping me sane until the end.

Finally, I would like to thank my family and friends, for their love, support, and encouragement throughout my graduate career and for always believing in me.

GROWTH FACTORS UP-REGULATE EPITHELIAL STEM CELLS: TREATMENT STRATEGIES FOR COLORECTAL CANCERS

Publication No._____

Carla Kantara, B.S.

The University of Texas Medical Branch, Galveston, 2012

Supervisor: Pomila Singh

Colorectal-cancer is a leading cause of cancer deaths in United States. Accumulating evidence suggests that elevated progastrins (PG) increase the risk of colon carcinogenesis, however mechnaims involved remain ill-defined. Recently, cell-surface AnnexinA2 (CS-ANXA2) was discovered as a non-conventional receptor for progastrin. Therefore, the first goal was to examine whether ANXA2 expression is required to mediate proliferative/anti-apoptotic effects of progastrin on target cells. The studies in chapter 2, conclude that ANXA2 mediates growth effects of PG on target cells (including colonic-epithelial-cells), *in vitro* and *in vivo*, associated with up-regulation of stem/progenitor cell markers. Surprisingly, overexpression of autocrine PG in HEK-293 cells, imparted tumorigenic/metastatic potential to the cells (chapter 3). Based on these

data, the second goal was to investigate the phenotypic differences between non-transformed and transformed stem cell using non-tumorigenic (HEK-C) and tumorigenic (HEK-mGAS) isogenic cells. The studies in chapter 3, conclude that transformed stem cells, unlike normal stem cells, co-express CS-ANXA2 with stem-cell-markers DCAMKL-1/CD44. Interestingly, CS-ANXA2 dictates morphology/growth characteristics of spheroidal growths, *in vitro.*

The third goal was to identify cancer stem cell (CSC) marker(s), for developing targeted therapies against colon cancers. Since both DCAMKL-1/LGR5 have been reported as colonic CSC markers, the possible phenotypic/proliferative differences between DCAMKL-1+ve and LGR5+ve human colon CSCs was examined. Results in chapter 4 suggest that DCAMKL-1+ve cells are significantly more proliferative than either DCAMKL-1-ve or LGR5+ve stem cells. Thus targeting DCAMKL-1+ve cells may be more effective in treating/eradicating colon-cancers; this possibility was examined as part of my fourth goal.

Although several therapies are currently available for treating cancers, recurrence remains a challenge. It is believed that CSCs are resistant to radiation and chemotherapeutic treatments, and are the likely cause of cancer relapse. It is therefore important to develop novel therapies which are relatively non-toxic and specifically target CSCs. Therefore the fourth goal was to examine the inhibitory efficacy of non-toxic dietary agent (Curcumin) ± RNAi against DCAMKL-1. The results in chapter 5 suggest that combination of curcumin+siRNA-DCAMKL-1 effectively attenuates growth of colon-cancer-cells *in vitro* and *in vivo*, by synergistically augmenting autophagic/apoptotic cell-death mechanisms. It is hypothesized that the combinatorial treatment will significantly reduce the risk of relapse.

TABLE OF CONTENTS

LIST OF ILLUSTRATIONS

LIST OF TABLES

LIST OF ABBREVIATIONS

Abs	Antibodies
ALDH1	Aldehyde Dehydrogenase
AnxA2	Annexin A2
ANXA2+/+ mice	Wildtype C57Bl/J6 mice
ANXA2-/- mice	C57Bl/J6 mice knocked down for the expression of annexin A2
CCK_1R	Cholecystokinin type 1 receptors
CCK_2R	Cholecystokinin type 2 receptors
CD44	Cluster of differentiation44
co-IP	Co-immunoprecipitation
CRC	Colorectal cancer cells
CS-ANXA2	Cell-surface associated annexinA2
CSCs	Cancer stem cells
Cu	Curcumin
DCAMKL-1	Doublecortin Ca^{+2}/Calmodulin kinase-like 1
DLD-1	Colorectal adenocarcinoma cell line (D.L.Dexter)
DMSO	Dimethyl sulfoxide
EMT	Epithelial-mesenchymal-transition
ERK	Extracellular regulated kinases
FACScan	Fluorescence-activated cell scanning
FACSorting	Fluorescence-activated cell sortin
FCS	Fetal calf serum

HCT-116	Human colorectal cancer cell line
HEK-C	Wildtype HEK-293 cells expressing control empty vector
HEK-mGAS mice	HEK-293 clones over-expressing mutant gastrin gene
hPG	Human progastrin
HT-29	Human colon adenocarcinoma grade II cell line
IF	Immunofluorescence
IHC	Immunohistochemistry
LGR5	Leucine-rich repeat-containing G-protein coupled receptor 5
Luc	Firefly-luciferase
MMPs	Matrix metalloproteinases
NF-κB	Nuclear factor-κB
Oct-4	Octamer-binding transcription factor 4
p65	p65NF-κB
PCNA	Proliferating cell nuclear antigen
PG	Progastrin
rhPG	Recombinant human progastrin
shRNA	Small hairpin RNA
siRNA	Small inhibitory double stranded RNA oligonucleotides
Sox-2	SRY (sex determining region Y)-box 2
vs	Versus
WB	Western blot
2-D	2-dimentional
3-D	3-dimentional
3-MA	3-methyladenine

>*	Significantly higher values between the indicated groups
-ve	Negative
+ve	Positive

CHAPTER 1

INTRODUCTION

Colorectal cancer is characterized by the uncontrolled growth of abnormal epithelial cells which undergo perpetual divisions and result in malignant tumors. The transformation from a normal to a malignant phenotype is triggered by many genetic and epigenetic mechanisms. Our laboratory and several other investigators have demonstrated that the aberrant up-regulation of growth factors within the epithelial cell microenvironment can significantly increase the risk of transformation.

We now know that elevated levels of growth factors, such as gastrins and precursor form of gastrins, progastrins (PG), significantly increase the proliferative and tumorigenic potential of intestinal epithelial and gastrointestinal cancer cells, by potently up-regulating the activation of MAPKs, NFκB and β-catenin signaling molecules (5). Recently, our laboratory reported that annexinA2, present on the cell-surface of target cells (CS-ANXA2), represents a novel, non-conventional receptor for progastrin peptides (182). However, the question remained as to whether ANXA2 expression was required to measure downstream signaling events in response to PG. Therefore, the first aim of my dissertation was to examine the role of ANXA2 in mediating biological effects of PG *in vitro* and *in vivo*. *The experiments conducted to address this aim are presented in Chapter 2 of my dissertation*. The results of our studies revealed that Annexin A2 (ANXA2) is critically required for mediating hyperproliferative effects of PG on colonic crypts in mice, via activation of the potent transcription factors, p65NFκB and β-catenin. Surprisingly, we also observed that ANXA2 mediated up-regulatory effects of PG on stem cell populations, positive for DCAMKL-1 and CD44, in both colonic crypts, *in vivo*,

and *in vitro* in an embryonic epithelial cell line, HEK-293. Importantly, over-expression of autocrine PG in HEK-293 cells (HEK-mGAS cells), lead to a significant increase in the proliferative potential of the cells compared to that of the control HEK-293 cells (HEK-C). These findings may explain previously reported hyperproliferative and co-carcinogenic effects of elevated progastrin on colonic crypts of mutant mice by several laboratories, including our laboratory.

Since over-expression of PG in HEK-mGAS cells resulted in up-regulating proliferative potential of the cells, I next examined if the tumorigenic and metastatic potential of the cells was also increased, using athymic nude mouse as a model. *The results of these studies are presented in chapter 3*, and demonstrate for the first time that over-expression of PG in the background of immortalized embryonic epithelial cells was sufficient for transforming the cells and imparting tumorigenic and metastatic potential to the cells. The significance of these novel findings are discussed in chapter 3.

Stem cells play a critical role in maintaining normal homoeostasis of cells within the colonic crypts. It is postulated that upon disruption of the microenvironment and/or genetic/epigenetic changes in colonic crypts, adult stem cells lose normal homeostatic responses and develop a transformed phenotype, labeled as cancer stem cells. To date, several stem cell markers have been described, including DCAMKL-1 and LGR5. Stem cells positive for DCAMKL-1 or LGR5 have been identified in both normal colonic crypts and colorectal cancers; however phenotypic characteristics of normal versus cancer stem cells remains ill-defined. Therefore, my second aim was to investigate phenotypic differences between non-transformed (normal) stem-cells and transformed/tumorigenic stem-cells, using isogenic cells lines, *as described in Chapter 3*. My results suggest the novel possibility that transformation of stem cells results in co-expression of stem cell markers, DCAMKL-1 and CD44, with CS-ANXA2, which

significantly impacts the morphology of spheroidal growths arising from these cells.

As discussed above, several stem cell markers have been identified, including DCAMKL-1 and LGR5. However, the role of DCAMKL-1+ve versus LGR5+ve stem cells has remained controversial. Thus, the third aim of my studies was to examine the phenotypic/proliferative differences, if any, between these two cell populations, using human colon cancer cells as a model; the *results are presented in Chapter 4*. My results suggest that DCAMKL-1+ve and LGR5+ve colon cancer stem cells may represent two distinct cell populations. An unexpected finding was that DCAMKL-1+ve cells were significantly more proliferative compared to the LGR5+ve stem cells in spheroidal assays; surprisingly LGR5-ve cells were more proliferative than the LGR5+ve cells. My results suggest the novel possibility that DCAMKL-1+ve colon cancer stem cells may have more potent 'stemness' qualities, and that enhanced proliferation of LGR5-ve cells as spheroids may be due to the presence of DCAMKL+ve stem cells within this population.

Conventional therapies do not differentiate between normal and cancer cells, and thus elicit many side effects on normal cells as well. Another limiting feature of currently available treatment strategies is that it targets mainly the bulk of the rapidly proliferating tumor cells, without eliminating the subpopulation of cancer stem cells, thus resulting in tumor relapse. To address this major issue, researchers have focused on developing novel therapies which not only promotes the use of non-toxic drugs but are also aimed at directly targeting cancer stem cells, in hopes of preventing recurrence of the disease (1) (**Fig 1.1**).

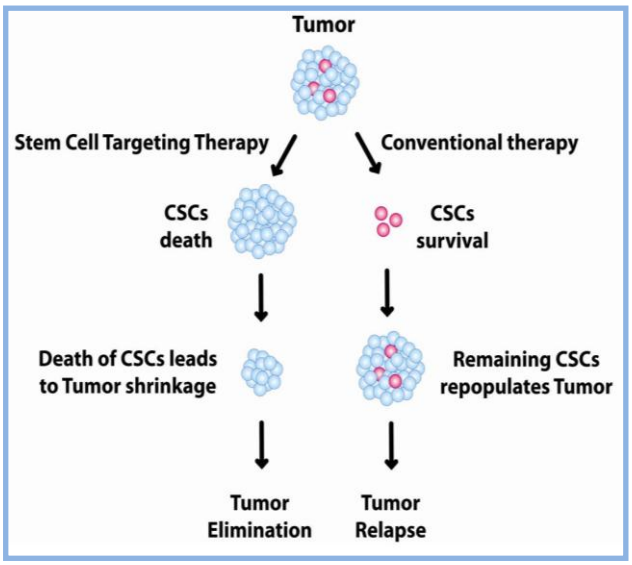

Figure 1.1: Cancer Stem Cell Hypothesis

Curcumin is a non-toxic, natural dietary agent, currently being used in clinical trials to treat cancers. In addition, our results demonstrated that DCAMKL-1+ve cells characterize a population of transformed stem cells which are highly proliferative and possess 'stemness' qualities. Therefore, the *fourth aim* of my studies was to examine whether the combination of curcumin + RNAi methods against DCAMKL-1 can effectively attenuate the growth of colon cancer cells *in vitro* and *in vivo*, compared to the individual agent itself. My results, *described in chapter 5*, show that treating colon cancer cells/xenografts with either DCAMKL-1 siRNA or an optimal dose of curcumin was insufficient in significantly reducing the *in vitro*/*in vivo* growth of colon cancer cells; however the combined regimen was extremely effective. This may be due to the fact that while curcumin treatment induced autophagic death, treatment with DCAMKL-1 siRNA resulted in apoptotic death; combination of the two agents synergistically increased both autophagic and apoptotic death of colon cancer cells/xenografts, suggesting that the combined treatment with these agents may be significantly more effective in eradicating

not only the bulk of the tumor but also the cancer stem cell subpopulations.

The significance of the molecules and mechanisms examined in my dissertation project are described in the background section below.

1.1 The Anatomy of the Colon

The main function of the colon, also known as the large intestine, is to extract water, electrolytes and energy from solid wastes before elimination from the body (2). The human colon consists of four sections: the ascending, transverse, descending and sigmoid colon. The colon is furthermore divided into two regions: Proximal (including cecum, appendix, ascending colon, hepatic flexure, transverse colon and splenic flexure) and Distal (including descending colon and sigmoid colon) (3) (**Fig 1.2**). Several investigators have reported differences in the growth of cancer in proximal versus distal colons (4). Our laboratory has also reported differences in the effects of PG on proximal versus distal colonic crypts, wherein proximal colonic crypts were shown to be highly responsive to PG, resulting in a significant increase in activated *p*p65NFκB levels, in contrast to distal colonic crypts which were not as responsive (5).

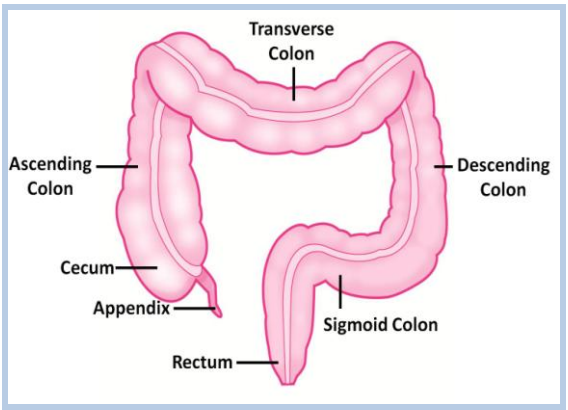

Figure 1.2: The Anatomy of the Human Colon

The colonic epithelium is a very dynamic structure composed of columnar cells which make up the crypts of Lieberkühn (6). The colonic epithelium undergoes continuous regeneration supported by three cell types: columnar absorptive cells (also known as colonocytes), mucous secreting cells (goblet cells) that are located within tubular crypts, extending downward towards the muscularis mucosa, and enteroendocrine cells (7). Colonocytes and Goblet cells are thought to arise from a single progenitor/stem cell situated towards the base of the crypt which give rise to proliferating 'stem' cells in the lower 1/3rd region of the crypt (8-11) (**Fig 1.3**). For my dissertation project, I focused on isolating and characterizing stem cells to further understand their role in the growth of colonic crypt cells and colon cancer cells (chapters 3-5).

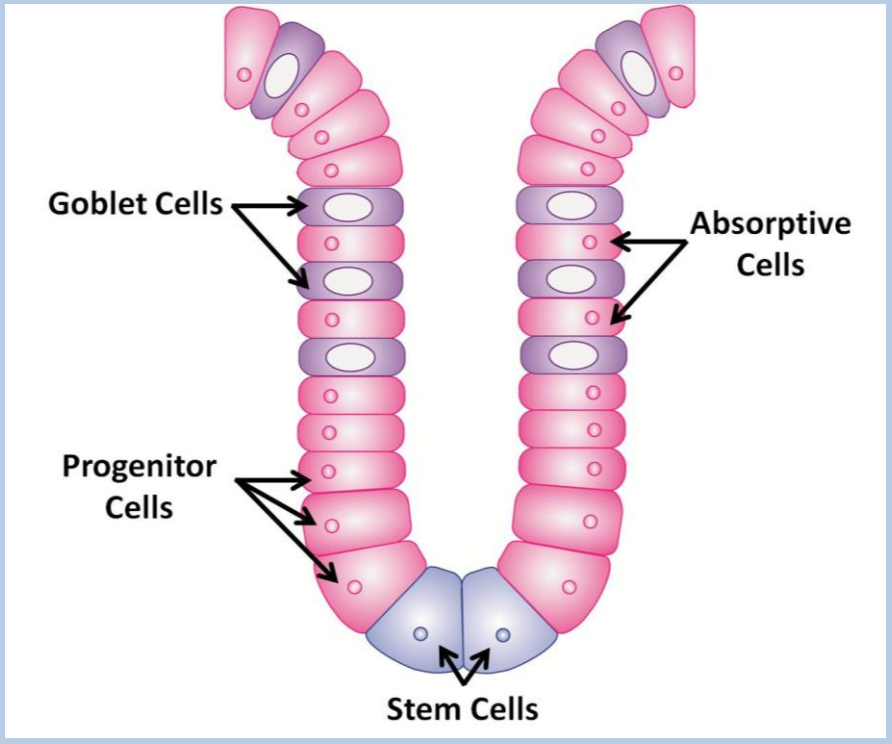

Figure 1.3: The Colonic Epithelium

1.2 Normal Intestinal and Colonic Stem Cells

Stem cells are multi-potent cells which can differentiate into various cell types (12). They are characterized by their unique ability to perpetually self-renew through unlimited cell divisions and their ability to differentiated into any cell type within the tissue of their origin (13,14). When a stem cell divides, each new daughter cell has the potential to either revert back to a quiescent stem cell or commit to further proliferation, followed by terminal differentiation into a specialized cell type (15-17) (**Fig 1.4**).

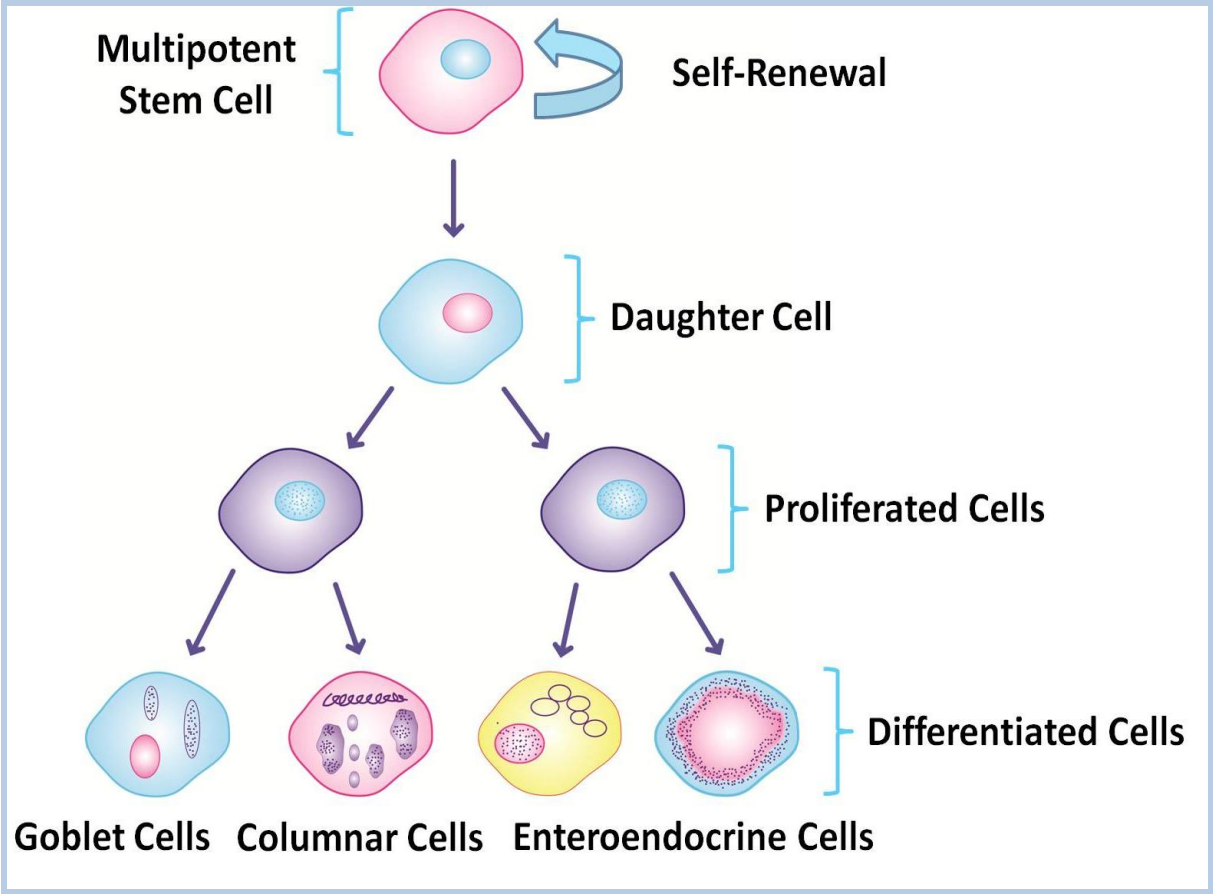

Figure 1.4: Asymmetrical Division of Quiescent Stem Cells

In the small intestine, it is speculated that 4-6 independent stem cells or a single intestinal stem cell are present within the crypts (18,19). Two stem cell models have been proposed within the small intestinal crypts. In the first model proposed, quiescent stem cells are believed to be located at the +4 position of the small intestinal crypts (14,20,21). Quiescent stem cells divide asymmetrically, wherein one daughter cell reverts back to the quiescent state and the second daughter cell continues to divide and eventually differentiate, suggesting that the quiescent stage of the non-dividing stem cell is perhaps regulated by inhibitory factors in the niche microenvironment of stem cells (22). The second model proposed is known as the 'stem cell zone' hypothesis, based on proliferating daughter stem cells, also known as the crypt base columnar cells (CBCs), which are believed to be situated at the bottom of the intestinal crypt, in between Paneth cells (14,23). This population is speculated to represent the true stem cells within crypts and actively responds to growth and differentiation signals from adjacent mesenchymal cells (22). Both models proposed are still under investigation, as the lack of robust stem cell markers have rendered these studies very challenging.

The study of stem/progenitor cell populations has been examined mostly in the small intestine of mice. However, more recent studies are focusing on understanding the mechanisms in the growth of colonic crypts as it is the major site, in an intestine, which gives rise to tumorous growth (colorectal cancers).

Unlike in the small intestine, the colonic stem cells remain largely undefined to date (22,24). It is believed that 5-10 stem cells are present at the bottom of each colonic crypt (13). In addition to these stem cells, there are approximately 16-36 cells which can functionally act as stem cells within the same crypt (25). Due to differences in the embryonic origin of proximal versus distal colon, the location of stem cells and pattern of cell migration differs within the two regions of the colon (7). Stem cells in the distal

colon are situated at the lower region of the crypt and their progeny migrate upwards, along the crypt axis (18). Stem cells in proximal colonic crypts, at one time, were speculated to reside in the middle of the crypts, wherein daughter cells moved downward and upward along the crypt axis (26); this theory however has not been confirmed. More recently, it has been speculated that within the colonic crypts the proliferating cells are thought to be present in the transit-amplifying region (lower 1/3rd of the crypts), and terminally differentiated cells are located in the upper region of the crypt (27). As the proliferating cells migrate, they stop dividing and differentiate into mature colonocytes or goblet cells. Within one week, cells travel from the bottom to the luminal surface of the crypts and undergo apoptosis and are sloughed off into the lumen of the gut (28).

The epithelial homeostasis of the large intestine is based on a calculated coordination between self-renewal, proliferation and differentiation which must be maintained throughout life (24); perturbance of the normal homeostasis can result in either hyperproliferation/carcinogenesis or other IBD-like diseases. Therefore it is critical to understand the dynamics involved in stem/progenitor cell regulation and the key factors involved in maintaining or perturbing the supporting environment of a stem cell.

1.3 Stem Cell Niche

The intestinal epithelium undergoes constitutive regeneration as described above (24). The stem cells must stay within its protective niche in order to maintain normal homeostasis and are instructed by their surrounded mesenchymal cells when to proliferate or differentiate (27,29,30) (**Fig 1.5**).

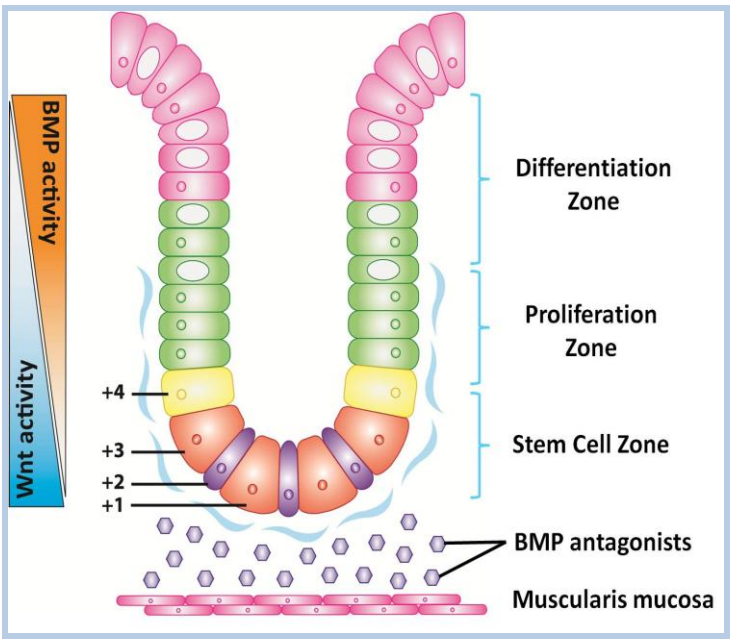

Figure 1.5: The Colonic Crypt

Regulatory/secretory factors within the niche microenvironment tightly regulate the crosstalk between epithelial cells (such as stem cells) and surrounding mesenchymal cells (31). This system is believed to be required for maintaining a normal stem cell milieu and prevent the aberrant proliferation of stem cells which can result in hyperplasia/cancer (31). Therefore, maintaining a tight regulation of stem cell quiescence and activity is characteristic of a functional niche.

1.4 Signaling Pathways and Stem Cell Microenvironment

It is believed that there are four prominent signaling pathways, Bone Morphogenic proteins (BMP), Wnt/β-catenin, Notch, and Hedgehog, which constitute the stem cell signaling network, regulating a tight balance of self-renewal, proliferation and differentiation (32-34).

BMPs are bone morphogenic proteins secreted by stromal cells (34). When BMPs are inhibited by a specific BMP antagonist such as Noggin, β-catenin translocates to the nucleus leading to activation of target gene expression which promotes proliferation and inhibits apoptosis, thus BMPs are believed to be strong inhibitors of the Wnt/β-catenin signaling pathway (11,34). High levels of BMP antagonists, such as Noggin, are found at the base of the crypt promoting cell proliferation. However, levels of BMP antagonists decreases in the microenvironment of the crypt, as one moves up along the axis, while BMP levels increase. This leads to a decrease in proliferation, and an increase in differentiation of the cells, as the cells move up towards the luminal surface of the crypts (11,34).

The Wnt pathway is triggered by the binding of Wnt glycoproteins to the frizzled (Fz) receptor together with the low-density lipoprotein receptor (35). The APC protein controls β-catenin levels by binding to the cytoplasmic β-catenin protein which is then targeted for degradation. However, when the APC gene is mutated or functionally deleted, β-catenin is spared from degradation and accumulates within the cytoplasm (36). The accumulation of β-catenin within the cytoplasm leads to its translocation into the nucleus and binds to Tcf/Lef transcription factors, resulting in up-regulation of the expression of several target genes (35). In transformed cells, elevated levels of nuclear β-catenin can be measured; this can reflect either mutations of APC/β-catenin or sustained up-regulation of the Wnt/β-catenin pathway (35,37). The sustained up-regulation of Wnt/β-catenin levels can potentially result in transformation of cells and tumorigenesis (30,35).

The Wnt signaling pathway is believed to regulate Notch signaling by driving cell proliferation (338-40, 34). Notch pathway is activated by the direct cell-cell contact; wherein one cell expresses the Notch receptors and a neighboring cell expresses the cell

surface ligands such as Delta or Jagged. The binding of ligand-receptor results in cleavage of Notch intracellular domain (NICD) which internalizes to the nucleus and binds to specific transcription factors and drives the activation of Notch target genes. Wnt/β-catenin up-regulates Jagged-1 (Notch ligand), expressed in progenitor cells, and mediates activation of Notch signaling (41). The activity of Notch regulates whether a cell will differentiate into an enterocyte or a secretory cell and plays an important function in stem cell regulation (34). Sustained activation of Notch and WNT pathway within the stem cells can potentially transform normal stem cells into transformed stem cells (34). Inhibition of Notch has been reported to result in differentiation of cancer stem cells into secretory cells (24) and a significant reduction in the growth of colorectal cancer (34).

The Hedgehog pathway is also known to regulate the stem cell niche via the interaction of Smoothened and Patched proteins (42). Patched protein is a repressor of Smoothened transmembrane protein. However, when Hedgehog binds to Patched, Patched is unable to repress smoothened, allowing for the activation and translocation of GLI transcription factor into the nucleus to drive Sonic Hedgehog (SHH) target genes as reviewed in (42). Within the colonic crypts the activation of Shh is believed to be located at the +4 position (42).

To summarize, BMP, Wnt, Notch and Shh play an critical role in regulating the normal homeostasis of colonic crypts. Wnt molecules are present at the base of the crypt and promote proliferation whereas BMPs are located in towards the luminal end of the crypts and promote differentiation. Notch activation usually occurs in the transit amplifying region of the crypts and is responsible for controlling the fate of newly formed daughter cells reviewed in (30). The stem cell niche dynamics is therefore tightly controlled and regulated by several pathways which ensure a normal homeostasis of the

intestinal crypts (**Fig 1.6**). Although several signaling pathways have been demonstrated to be crucial in maintaining a normal niche, the detailed mechanisms of how key regulators coordinate and crosstalk to create this functional colonic stem cell niche remain largely unknown (29,34). However, it has been well established that the disruption of the microenvironment results in the initiation of colorectal cancers, hence understanding the mechanisms involved may aid in the prevention of this disease. My experiments in chapters 2 and 3, showed that PG up-regulates stem cell expression via the activation of NFκB and β-catenin in immortalized embryonic HEK-293 cells. We also demonstrated that NFκB and β-catenin is activated in colon cancer stem cells and is decreased in response to curcumin and/or down-regulation of DCAMKL-1 expression, suggesting that these pathways are very critical in regulating proliferation of cancer cells (chapters 4&5).

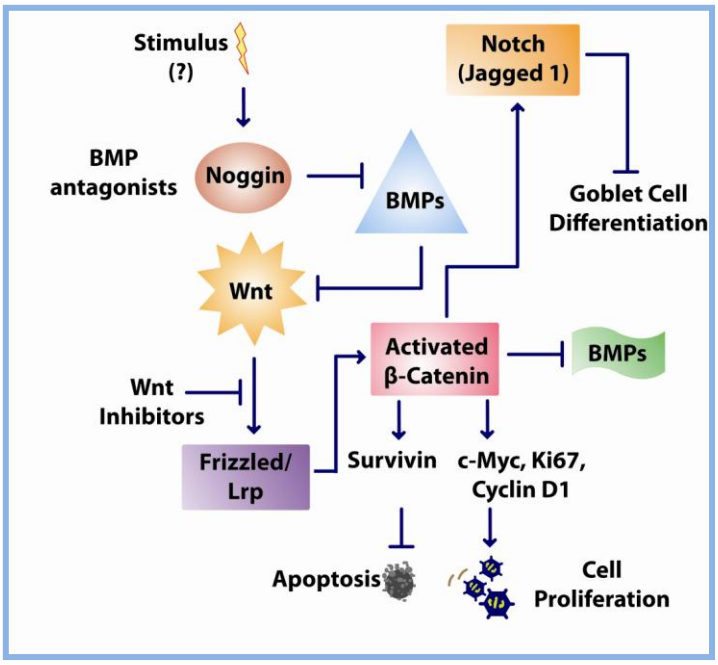

Figure 1.6: Interactive Signaling Pathways mediating stem cell proliferation and differentiation

1.5 Sequence of Events leading to the Progression of Colorectal Cancer

In the early 1990's Fearon and Vogelstein proposed a genetic model describing the multi-step tumor progression of colorectal cancer in humans from adenoma to carcinoma (36). The progression is based on the accumulation of genetic and epigenetic mutations, triggered by the activation of specific oncogenes such as KRAS and the inactivation of APC tumor suppressor gene which operates as the initial trigger of colon carcinogenesis (43). In contrast, mutations in p53 tumor suppressor gene appear to be involved in the advanced stages of adenomas and carcinomas progression (44-46). Additional mutations, such as gastrin gene (resulting in elevating levels of progastrin) are also involved in the progression of colorectal cancer (**Fig 1.7**).

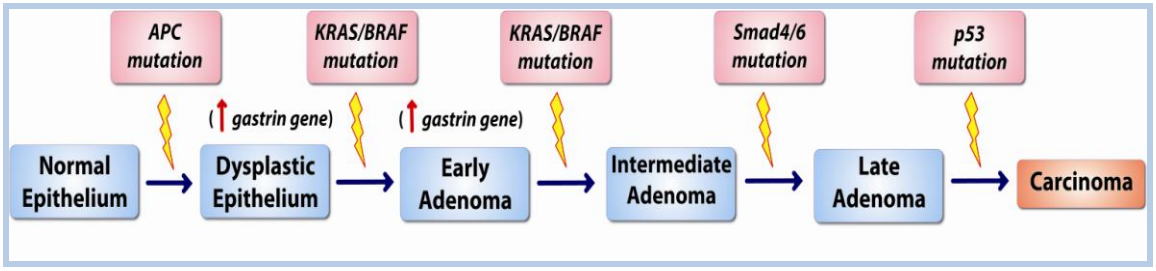

Figure 1.7: Progression of Colorectal Cancer

1.6 Colon Cancer Stem Cells (CSCs)

The role of stem cells in the origin of colon cancer remains controversial. Colon cancer has been postulated to arise from either: mutated/abnormal stem cells in colonic crypts (47) or aberrant progenitor cells (48), or fully differentiated cells (49) or hematopoietic stem cells (22). Based on the CSCs theory, it is now believed that cancer stem cells arise from stem cells located at the base of the colonic crypts that have

acquired specific mutational hits and/or due to a possible imbalance in the stem cell niche (6). Stem cells are believed to require fewer mutations than differentiated cells to promote transformed phenotypes as they already possess self-renewal properties (6). The lack of knowledge relating to the colonic stem cell niche and the stem cells within the milieu is derived from the technical challenges that scientists are continuously experiencing: lack of unique markers and stem cell bioassays (23). Conventional wisdom would suggest that isolating stem cells from colonic crypts or from tumor bulks would be the most efficient method to examine the biology of stem cells. However, in order to do so, specific stem cell markers have to be expressed by the stem cells and, most importantly, identified. Although some stem cell markers have been identified, it remains debatable as to whether these markers truly represent stem cells. Another problem stems from the lack of markers capable of distinguishing between normal stem cells and cancer stem cells. Both possess similar markers and *in situ* may appear to look similar. Therefore isolating normal stem cells versus cancer stem cells has been shown be a very tedious task. In addition, the possibility remains that the markers may be identifying cells other than stem cells. Therefore, the question remains, can stem cells be isolated from colonic crypts and colorectal cancers and if so, which markers will be most appropriate to exploit/target for preventing cancers? Quiescent stem cells appear to be expressing a distinct set of markers (such as DCAMKL-1) compared to the actively stem cells (such as LGR5) within the same crypt (20), thus making these markers more useful for identifying the stem cells. Our laboratory has established the method that allows for the isolation of intact colonic crypts from mouse colon, based on the methods developed by Dr. Umar (50). The intact crypts can be further dissociated into single cells and stained for specific stem cell markers. My preliminary data suggested that DCAMKL-1+ve cells in the mouse colonic crypts are of many different phenotypes (unpublished data from our

laboratory). At the present time we do not know if these different phenotypes represent differences in their genotypes.

We were also successful in FACSorting cells positive for DCAMKL-1, CD44 and LGR5 from colonic crypts and established the methods for growing colonic stem cells as colonospheres and organoids (unpublished data from our laboratory). In a recent study, we reported an increase in the expression and cell numbers of DCAMKL-1+ve and CD44+ve cells in colonic crypts of mice stimulated with progastrin (51), as described in chapter 2 of my dissertation. The latter findings strongly suggest that growth factors such as progastrin can significantly increase the expression levels and census of stem cells in colonic crypts, which may explain previous findings from our laboratory demonstrating a co/carcinogenic role of progastrin in colon carcinogenesis (52,53). Thus, for my dissertation, I examined colon cancer stem cells in more depth and also looked at the possible transformation of normal stem cells to cancer stem cells using an isogenic model of HEK-293 cells developed by our laboratory (described in chapter 4).

Researchers in the field have come to a common consensus that targeting stem cells directly rather than the bulk of tumors cells may be a better strategy for treating and preventing cancer relapse (54-57). The ratio of CSCs to tumor cells in colon cancers has been postulated to be as low as 1:60000 in some tumors (58). Therefore, it is important that we examine isolated CSCs using precise stem cell markers. Several stem cell markers are currently being used to isolate and characterize colon CSCs (59) (**Table 1.1**). For the purpose of my studies, I chose to focus on three stem cell markers, DCAMKL-1, CD44 and LGR5, which are currently believed to be precise stem cell markers with available extracellular domains. Availability of extracellular domains is critical for isolating stem cells and further investigating these cells.

Markers	Function
	Normal Colon Stem Cells
DCAMKL-1	Doublecortin Ca^2/Calmodulin Kinase-like 1
LGR5	Leucine-Rich Repeat containing G protein receptor 5, Wnt Target gene
Msi-1	Musashi-1, RNA binding Protein
CD29	β1 integrin, Cell Adhesion Molecule
	Colon Cancer Stem Cells
DCAMKL-1	Doublecortin Ca^{2+} /Calmodulin Kinase-like 1
LGR5	Leucine-Rich Repeat containing G protein receptor 5, Wnt Target gene
CD44	Cell Adhesion molecule, Hyaluronic acid receptor
ALDH1	Aldehyde Dehydrogenase 1 family Enzyme
Oct4	POU5F1, Octamer-binding transcription factor 4
Sox-2	Invasion and metastasis
CD24	Cell Adhesion Molecule
CD166	Cell Adhesion Molecule
CD29	β1 integrin, Cell Adhesion Molecule
ESA	Epithelial Specific Antigen, Cell Adhesion Molecule
c-Myc	Enhanced self-renewal

Table 1.2: List of Normal and Cancer Colon Stem Cells

1.7 DCAMKL-1

1.7.1 Structure of DCAMKL-1 protein

Doublecortin Ca^{+2}/Calmodulin-dependent kinase like-1 (DCAMKL-1) is a 740 amino acid long transmembrane protein. It is composed of a serine/threonine catalytic domain at the C-terminus with a 65% homology to the calcium-calmodulin family of serine/threonine kinases (60). It also possesses two ubiquitin like domain with a 35% homology to Doublecortin at the N-terminus which is required to bind microtubules (60, 61) (**Fig 1.8**). The DCAMKL-1 gene encodes for multiple alternative splice variants including 2 long forms (α and β), 2 shorts forms (α and β), DCL and the smallest form known as CARP which lacks both the DCL and CaMK domains (61,62). DCAMKL-1 was first identified as a critical developmental protein in the nervous system (61).

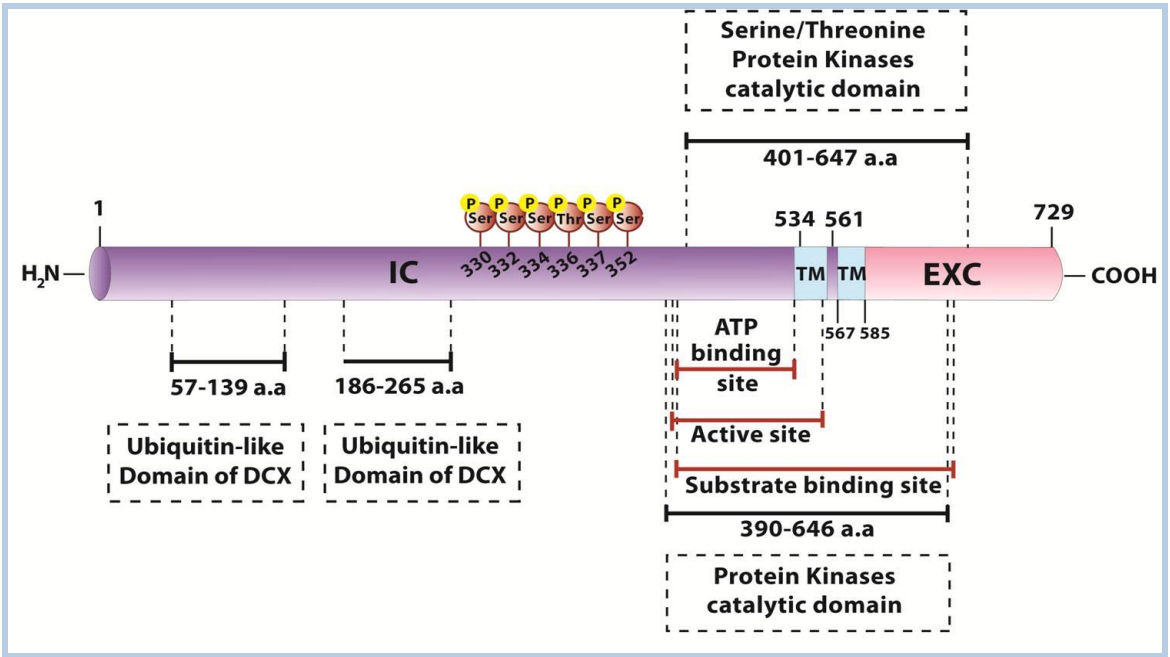

Figure 1.8: DCAMKL-1 Transcript

1.7.2 Role of DCAMKL-1 in the Nervous System

DCAMKL-1 is a microtubule-associated kinase expressed in postmitotic neurons (60) and the developing brains (63). The transmembrane protein plays a crucial role in: mitotic cell division by regulating the spindle formation in neuroblasts (64); regulating neuronal migration, neurogenesis and apoptosis (65); maintaining the axonal system in check (61, 66). More recently studies have shown that silencing DCAMKL-1 expression induced apoptosis in neuroblastoma cells (62), suggesting that DCAMKL-1 plays an important role in neuronal biology. It is believed that the protein plays an important role in calcium signaling pathways due to its kinase homology (60). However, ligands to DCAMKL-1 and key regulatory molecules involved in its intracellular function activation remain to be identified.

1.7.3 DCAMKL-1 a Putative Stem Cell Marker

In 2007, DCAMKL-1 was charaecterized as a novel putative colonic and intestinal stem cell marker (20,67). DCAMKL-1 positive cells were found to be located at the base of the crypts, specifically at the +4 position within the crypts (67,68). DCAMKL-1+ve cells are believed to represent the quiescent stem cells within the intestinal crypts since the cells were negative for proliferative marker, PCNA (20,67). DCAMKL-1+ve cells also co-express Musashi-1 (msi-1), another well characterized stem cell marker (69), hence confirming DCAMKL-1's role as a stem cell marker.

More recently, DCAMKL-1 was also identified as a potential stem cell marker within the gastric epithelium and was apparently expressed by parietal cells within the isthmus region of the stomach also known as the "stem/progenitor cell zone" (66). These cells were also shown to be positive for Msi-1 and quiescent in the gastric epithelium (66, 70). These findings support the notion that DCAMKL-1+ve cells are slow cycling and

represent the quiescent stem cells populations, as demonstrated in the gastric, colonic and intestinal epithelium. The slow cycling 'quiescent' stem cells, such as DCAMKL-1, may possibly play a critical role in homeostasis of normal crypt-like structures.

Kikuchi et al. 2010, recently reported that DCAMKL-1+ve and PCNA+ve cells in a gastric gland can also be located at the base of the gland instead of the isthmus region due to ulcer formation or radiation injury (66,70). Also, DCAMKL-1 has been identified as a potential pancreatic stem/progenitor cell marker and researchers are currently investigating its role in various cancers (67, 71).

Therefore, one of the goals of my dissertation was to examine the role of DCAMKL-1 in colon cancer cells by characterizing the expression, localization, phenotypic and growth patterns of these cells and to examine the effects of down-regulating DCAMKL-1 in colon cancer cells (Chapters 4,5).

1.7.4 DCAMKL-1 and Cancer

DCAMKL-1 is over-expressed in various tumors types including colorectal, pancreatic, breast and prostate cancers (72). Down-regulation of DCAMKL-1 expression in colon cancer cell and pancreatic cancer cell lines resulted in inhibition of cell proliferation, tumor growth arrest, decrease in oncogenic expression of c-myc and KRAS, inhibition of Nocth-1 expression and epithelial-mesenchymal transition (72-74). These findings reiterate the importance of DCAMKL-1 in tumor growth formation and suggest that targeting DCAMKL-1 may be a novel therapeutic method of treating many epithelial cancers including colorectal cancers. Therefore, one of my goals was to examine the effects of down-regulating DCAMKL-1 on the biology of colon cancer cells growing either as spheroids *in vitro* or xenografts *in vivo* as described in chapter 5.

1.8 LGR5

1.8.1 LGR5 and the intestinal crypt

LGR5, also known as GPR49, is a leucine-rich orphan G protein-coupled receptor found to be expressed in a unique fashion in human colon cancer cells and intestinal crypt cells (23,24). The protein consists of a large extracellular leucine rich repeats and a short cytoplasmic tail (6,23,75) (**Fig 1.9**).

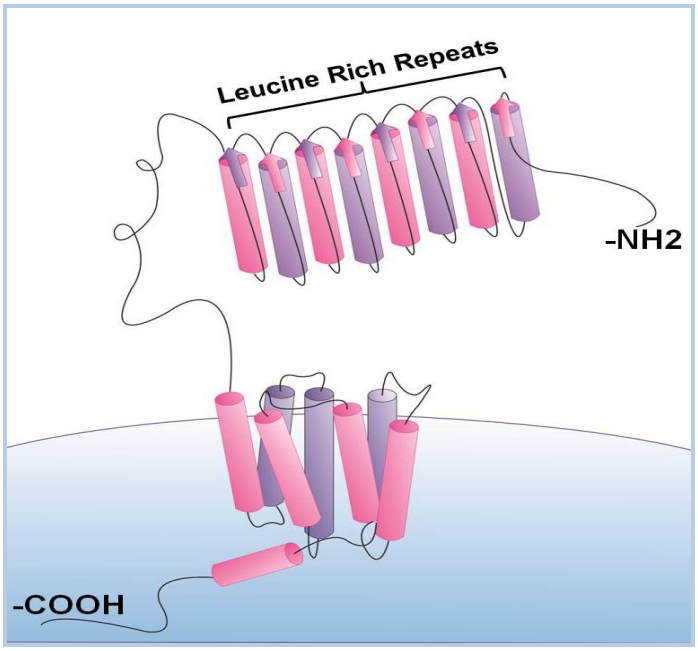

Figure 1.9: LGR5 Transmembrane Protein

Hans Clevers and colleagues generated a novel LGR5-EGFP-IRES-Cre-ERT2/*RosaLacZ* mouse model and conducted lineage tracing studies (23). These studies helped them to identify LGR5+ve cells as the normal stem cells at the base of the crypts in the intestinal cryopts, which is believed to be distinct from the +4 DCAMKL-1+ve cells, as previously described previously (76). Unlike DCAMKL-1+ve cells, LGR5+ve cells are negative for Msi-1 but positive for PCNA. LGR5+ve cells are considered the

active cycling stem cells which are located at the base of the crypts and divide every 24 hours in a normal homeostatic environment (23, 77). It is believed that there are about 4 LGR5+ve cells within each crypt (23,30) (**Fig 1.10**). Cells positive for LGR5 were described to be multipotent and a single LGR5+ve cell seeded in culture, was able to regenerate the entire crypt and villus structure (organoid), giving rise to differentiated cell type lineages found within the intestinal crypts even in the absence of a niche microenvironment (23, 78). These findings suggest that besides DCAMKL-1+ve cells (as described above), LGR5+ve cells may also represent stem cells which are equally important in normal homeostasis and in tumor growth. Therefore, I also wanted to characterize LGR5+ve colon cancer cells, in order to better understand its role in the proliferation of colon cancers, as described in chapter 4.

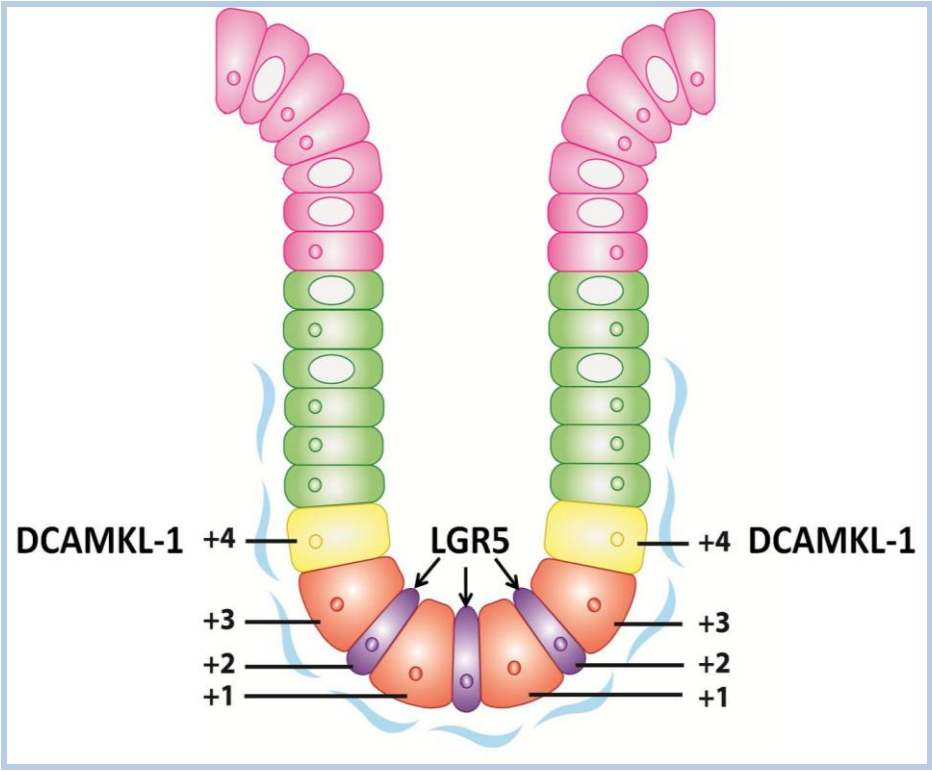

Figure 1.10: Stem Cells within the Small Intestinal Crypt

Using an APC mouse mutant model, researchers were able to observe an increase in β-catenin levels in LGR5+ve cells, followed by formation of micro-adenomas which eventually progressed to larger adenomas (76). Clevers and colleagues believe that the LGR5+ve cells in APC mutant mice gave rise to the aberrant growth observed in the small intestinal mucosa as previously described. However, it is not known if APC mutant LGR5+ve cells can similarly give rise to colonic growth.

1.8.2 LGR5 in the gastric epithelium

LGR5+ve cells are also found in the gastric epithelium. Unlike DCAMKL-1+ve cells which are located in the isthmus region of the gastric glands, LGR5+ve cells were found to be located at the base of the mature pyloric glands (79). About 2-4 LGR5+ve cells were found to be located within the base of glands and were positive for PCNA, indicating their proliferative potential (79). In addition, a single LGR5+ve cell *in vitro* gave rise to organoid-like structures resembling pyloric glands. While LGR5+ve cells can potentially regenerate either a gastric gland or intestinal crypts, it is not known whether LGR5+ve colon cancer cells can maintain the growth of a tumor. This possibility was examined in chapter 4.

1.8.3 Role of LGR5 in the growth of colon cancers

LGR5 is over expressed in various tumor types including colorectal, ovarian and hepatocellular carcinomas reviewed by (30). More specifically, LGR5 is over-expressed in 70% of all human colorectal cancers (80,81), but in only 50% of metastatic colorectal growths (82). The expression levels of LGR5 have been shown to increase progressively

during the hyperplasia-adenoma-adenocarnima sequence of colon carcinogenesis in humans (83,84). Levels of LGR5 were reported to be higher in metastatic versus non metastatic cell lines (84, 85). These results suggest that LGR5 may be a useful diagnostic marker for colorectal cancers.

LGR5 is a well established WNT target gene; the majority of colorectal cancers arise due to mutations in either APC or β-catenin resulting in constitutive activation of the Wnt signaling pathway. Thus overexpression of LGR5 in colorectal cancers probably reflects constitutive activation of β-catenin. However, it is not known if elevated levels of LGR5 are directly involved in driving tumorigenesis within the colons or if constitutively activation of the Wnt signaling pathway is sufficient to initiate tumorigenesis. LGR5+ve cells, however, are localized at the leading edge of colonic tumors in close proximity with the stromal microenvironment (81), suggesting that stromal cues may be required for LGR5+ve cells to function as cancer stem/progenitor cells.

Ligands which bind or activate the extracellular domain of LGR5 protein remain to be identified. It is however believed that LGR5 is essential in the development of intestinal epithelium since mice deleted for the LGR5 gene fail to survive post-natally due to gastrointestinal swelling and malformation of the tongue and lower jaw (23,86).

LGR5 has been suggested as a prognostic marker for CRCs since patients expressing elevated levels of LGR5 in their tumors demonstrated lower survival rate (81,83). However, Walker et al 2011, demonstrated that silencing of LGR5 expression surprisingly promoted tumorigenesis by up-regulating the Wnt signaling pathway (87). The reduced expression of LGR5 in colon cancer cells resulted in the formation of amorphous spheroids in culture, increased cell migration and rearrangements of cell surface proteins including CD44 (87). The investigators believed that CD44 becomes uniformly distributed on the cell membranes in the presence of matrix metalloproteinases

(MMPs) which may play an important role in promoting the invasion and migration of metastatic cancer cells (87). At the same time, other investigators have reported that not all colon cancer tumors positive for β-catenin are also positive for LGR5 and vice-versa (82); it is thus possible that besides β-catenin, other cancer related oncogenic pathways may also upregulate the expression of LGR5 in tumors.

Based on available literature, as described above, LGR5 likely plays a critical role in maintaining normal homeostasis of the colonic crypts and may prevent abnormal migration of the cells based on the results of Walker et.al 2011. Since LGR5 is a target gene of activated Wnt signaling pathway it may also play a secondary role in the generation of colonic tumors.

1.9 CD44

1.9.1 Role of CD44 in colon cancer

CD44 (cluster of differentiation) is a cell surface glycoprotein which binds the extracellular matrix hyaluronic acid with high affinity. In a normal colonic crypt, CD44 is expressed in the lower $1/3^{rd}$ compartment of the colonic crypts known as the stem/progenitor cell zone and is a prominent target of Wnt signaling in the intestinal mucosa (88,89). CD44 is selectively expressed by proliferating epithelial cells lining the intestinal crypts (90) and are believed to represent progenitor cells. However, it is not known whether CD44+ve cells in colonic crypts can give rise to the different lineages of differentiated cells in the intestine.

Originally, CD44 was identified as a cancer stem marker for breast cancers (91). Since then, CD44 has been described as a stem cell marker for prostate, pancreatic, head and neck and colorectal cancers (92-95). Several CD44 alternative splice variants have

been identified in various cancers, including colon cancers, and were found to correlate with cancer progression (96,97).

CD44 regulates tumor growth and cancer cell migration in human colorectal cancers (98,99). In colon cancer cells, the activation of CD44 is mediated by the β-catenin signaling pathway (100). CD44 is considered to be a very selective and robust cancer stem cell marker which mediates cell survival, cell growth, cell motility and cell differentiation (101). Thus, it is believed that CD44 may regulate stemness of cancer stem cells by activating several proliferative pathways required for the growth of cancer cells (102).

Down-regulation of CD44 expression results in the loss of colony formation and migratory potential of colon cancer cells *in vitro* and attenuation of tumor formation *in vivo*, strongly suggesting a functional role for CD44 in the growth and metastasis of CRCs (102). Enriched population of either a single or several CD44+ve cells grew as spheroids *in vitro* and as xenogrfats *in vivo* (102). CD44+ve cells were shown to have significantly higher metastatic and tumorigenic potential compared to CD44-ve cells (102,103). The studies strongly suggest that CD44+ve cancer stem cells can support the growth of a tumorosphere. Therefore, for my dissertation studies, I used CD44 as a colon cancer stem cell marker, in addition to DCAMKL-1 and LGR5 as described in chapters 2-5.

1.9.2 CD44 as a prognostic marker

Levels of CD44 expression in colorectal cancers have been shown to be proportionally increased in relation to the stage of the disease as reviewed by (104). Higher levels of CD44 were reported to be associated with poor prognosis (105). Treatment of mice with carcinogenic agent resulted in increased expression of CD44

(106). Interestingly, increased expression of CD44 in the colonic mucosa precedes mutational changes observed in KRAS and p53 gene (92), which may be secondary to activation of the Wnt/β-catenin pathway. However, it is not known at what stage specific splice variants of CD44 are expressed (107).

1.10 Progastrin up-regulates stem cells in colonic crypts and colon cancers

The stem niche of intestinal crypts has several cytokines and growth factors which control the fate of stem cells. Growth factors such as progastrin can potentially dictate proliferation and differentiation of stem cells. Several investigators, including our laboratory have demonstrated that aberrant up-regulation of growth factors, such as Progastrin can significantly increase the risk of colon carcinogenesis (53,108,109).

In the early 1990's, it was discovered that the majority of the human colon cancer cell lines and colonic adenocarcinomas expressed the gastrin gene (110,111). Normally, only processed and amidated forms of gastrins (G17/G34) are present in circulation; however in certain pathological conditions such as colorectal cancers, the gastrin gene products are not processed completely, resulting in the expression of progastrins (112,113) (**Fig 1.11**). Progastrin (PG) and glycine-extended-gastrins are highly expressed in colon cancers reviewed in (112). Down-regulation of the gastrin gene (progastrin) resulted in the loss of clonogenic and tumorigenic potential of colon cancer cells (114). Progastrin has been shown to exert proliferative (115), anti-apoptotic (116) and co-carcinogenic effects on the colonic epithelium cells (110,111,117).

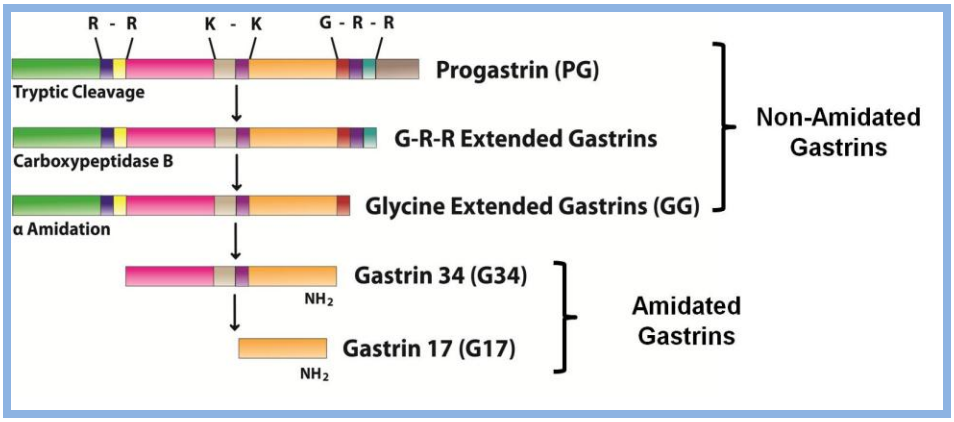

Figure 1.11: Processing of Progastrin peptide

Several laboratories including our laboratory have been examining the intracellular mechanisms by which PG increases the proliferation of normal and cancerous intestinal epithelial cells. Both NFκB and β-catenin pathway were found to be important in mediating anti-apoptotic and proliferative effects of PG *in vitro* and *in vivo* (112,119).

Recently, our laboratory identified annexinA2, as a novel, non-conventional receptor for progastrin peptides. Our studies in chapter 2, demonstrate that AnnexinA2 is required for mediating stimulatory effects of PG on the NFκB and β-catenin signaling pathway. We also demonstrated that PG significantly up-regulates expression of stem cell markers DCAMKL-1, CD44 and LGR5 *in vivo* in intestinal crypts as well *in vitro* in an embryonic epithelial cell line (HEK-293).

1.11 ALDH (Aldehyde dehydrogenase)

Various isoforms and splice variants of the ALDH enzyme were reported to be found in the cytoplasm, mitochondria, nucleus and endoplasmic reticulum (119). One of

the isoforms, ALDH1A1, has been reported to be a specific marker for normal and cancer stem cells.

1.11.1 Role of ALDH1A1 in cancer

Aldehyde dehydrogenase 1A1 is a detoxification enzyme expressed in both normal and cancer stem cells, in the breast (120) and colon (121). The activity of ALDH1A1 is significantly elevated in colonic adenomas compared to normal colonic mucosa (121) and therefore ALDH1A1 may be a unique marker of colon cancer cells. ALDH1A1, has also been reported to be expressed in colonic stem cells in the proliferative zone of crypts (121) and may represent a marker of proliferative cells. ALDH1A1 has been used as a marker to isolate normal and cancer stem cells. Cells positive for ALDH1A1 are also positive for CD44 and CD133, two well established cancer stem cell markers (122). Colon cancer cells positive for ALDH1A1 have been reported to grow as xenografts in athymic nude mice suggesting that ALDH1A1+ve colon cancer cells are tumorigenic. Expression of high levels of ALDH1A1 in tumors is believed to reflect poor prognosis (123).

The functional importance of ALDH1A1 in cancer cells is probably derived from its role as an aldehyde dehydrogenase which protects the stem cells from inhibitory effects of chemotherapeutic agents (124). Therefore, treatment strategies are being developed to target ALDH1A1 in order to sensitize cancer stem cells and decrease their resistance to chemotherapeutic agents (124)

Unlike colonic and gastric epithelial cells, the pancreatic and liver tissues express high levels of ALDH1A1. Thus ALDH1A1 will serve as a strong marker of cancer stem cells in tissues normally expressing low levels of ALDH1A1 (colonic and gastric epithelium) while ALDH1A1 will not be as reliable for cancer arising from pancreas and

livers (123). Since ALDH1A1 can serve as a useful marker for colon cancer stem cells, I examined the effects of inhibitory agents such as curcumin on the growth colon cancer cells in relation relative levels of ALDH1A1 as described in chapter 5.

1.12 Pluripotent markers

Normal stem cells have the ability to perpetually self-renew and differentiate into specific cell types associated with the organ of origin. Stem cells have been described as being either pluripotent, multipotent or unipotent (125). Pluripotent cells are characterized by the ability of the cells to form all three germ layers: endoderm, mesoderm and ectoderm, and be induced to form specific cell types. Multipotent cells, also known as progenitor cells, have the ability to give rise to only the cell lineages of a specific organ. Unipotent cells can differentiate into only one single functional cell type in a tissue (125). However, cancer stem cells, unlike normal pluripotent/multipotent/unipotent stem cells, have lost the ability to form functionally differentiated lineages and continuously proliferate.

Several transcription factors have been discovered which control 'stemness' of both normal and cancer stem cells. For my dissertation project, I have chose to focus on 3 of the following transcription factors, Nanog, Oct-4 and Sox-2, based on literature illustrating their role in cancer cells as described below.

1.12.1 Nanog

Nanog is a homeobox-containing transcription factor which is responsible for maintaining stemness/pluripotency of embryonic and pluripotent stem cells (126). Nanog interacts with Oct-4 and Sox2 to form a complex which induces the pluripotent

phenotypes within the cells (127). Nanog expression is elevated in various tumor types including breast cancers (128), prostate cancers (129), ovarian cancers (130) and colon cancers (131). Overexpression of Nanog has been demonstrated to promote transformation, tumorigenecity and metastasis of cancer cells (132); hence Nanog is a putative marker of tumor cells and predicts poor prognosis for patients whose colorectal cancers are positive for high levels of Nanog (133). Overexpression of Nanog in colon cancer cells have been shown to increase proliferation, invasion and migration of the cells (133-135).

1.12.2 Oct-4

Oct-4 is an octamer-binding transcription factor 4, also known as POU5F1 (POU domain, class 5, transcription factor 1. Elevated expression of Oct-4 was reported in bladder cancers (135), breast cancers (136), gastric cancers (137) and colorectal cancers (58). Oct-4 has been to shown to play an important role in self-renewal of cells and in inducing 'stemness' of pluripotent and embryonic stem cells (138,139). Oct 4 is one of the reprogramming genes currently being used to induce pluripotency of stem cells (140). Oct-4 has been reported to promote proliferation of the cells and prevent the cells from differentiating, thus resulting in dysplasia within the colonic crypts (141). The functional effects of Oct-4 has been shown to be dose dependent, wherein an increase by 2 fold promotes self-renewal while a reduction promote differentiation (142). Loss of Oct-4 expression results in the loss of metastatic potential of lung cancers and sensitizes the cells to radiation therapy (143). The latter results further support an important role of Oct 4 in maintaining tumorigenic/metastatic potential of tumor cells.

1.12.3 Sox-2

Sox-2 is a transcription factor which plays an important role in maintaining self-renewal of pluripotent stem cells. Recent studies have noted elevated levels of Sox-2 in various cancer types including colorectal cancers (144). Relative expression levels of Sox-2 are increased in relation to the stage of the disease (114).

Tumors expressing higher levels of Sox-2 were generally poorly differentiated (145). Cancer cells generally co-express Oct 4 and Sox-2. In normal tissues, proliferation is generally associated with heterodimerization of Oct 4 with Sox-2 which activates downstream targets such as Nanog (146). Constitutive co-expression of Oct4 and Sox-2 in cancer cells is associated with metastatic growth and higher recurrence rate in patients, resulting in poor prognosis (6).

To summarize, Nanog, Oct4 and Sox-2 are well characterized pluripotency markers of stem cells both *in vitro* and *in vivo.* Nanog has been referred to as the master switch within the regulatory network complex. Oct4 and Sox-2 heterodimerizes on the Nanog promoter and transcriptionally activates the expression of Nanog. Thus all 3 proteins likely play a cooperative role towards increase 'stemness' of cancer cells.

For my dissertation project, I examined the effects of inhibitory agents such as curcumin or DCAMKL-1 siRNA on the growth of colon cancer cells in relation to relative levels of Nanog, Oct 4 and Sox-2.

1.13 Treatments for Colorectal Cancers

Cancer is a very complex disease; each cancer is characterized by the activation or deactivation of specific genes, thus leading to the constitutive activation of signaling pathways. The standard treatment currently available includes surgery, radiation and

chemotherapy. The majority of patients who are surgically treated for this disease are also given adjuvant therapy. The most commonly used adjuvant therapy for colorectal cancers is a treatment with FOLFOX, a combination of 5-Fluorouracil (5-FU), a vitamin known as leucovorin and oxaliplatin (147,148). Other chemotherapeutic drugs also used can include Paclitaxel, Adriamycin, Cisplatin, Cytarabine and Adriamycin, which are well established and clinically approved chemotherapeutic drugs as reviewed in (148).

To date, chemotherapy and radiation are the best available therapies to prevent relapse of the disease, however these treatments do not differentiate between normal and cancer cells. To address this concern, targeted therapies have been developed to specifically target cancer cells and spare normal cells. These therapies include monoclonal antibodies against receptor proteins expressed at elevated levels on cell membranes of cancer cells, such as Herceptin or antibodies targeted against other forms of EGF receptors (149,150). Antibodies have also been developed against angiogenic factors such as VEGF but have significant side effects (151). The reason the currently available therapies fail is because cancer stem cells are resistant to these interventions. Therefore, developing therapeutic strategies for specifically targeting cancer stem cells may improve the outcome of treating cancer (152).

Additionally, novel therapies are being developed, which include a combination of natural dietary agents and chemotherapeutic drugs. Many dietary agents have anti-tumor effects and have been shown to sensitize cancer cells to treatment with chemotherapeutic agents at non-toxic concentrations. However, it is not known if these chemotherapeutic dietary agents (non-toxic even at high concentrations) target cancer stem cells. One of my goals for my dissertation project was to examine if a prototype of dietary chemotherapeutic agent, such as curcumin, can target cancer stem cells (chapter 5).

1.14 Curcumin

Curcumin, chemically known as diferuloymethane, is the major pigment in the turmeric powder, which is isolated from the rhizomes of the leafy plant *Curcuma longa* (153). Curcumin possesses anti-inflammatory and anti-oxidant properties (154, 155) and has long been used as traditional medicine in Asian countries (153). Curcumin also possesses anti-tumoral activities and anti-proliferative effects on cancer cells (156) and is currently being used in clinical trials as a chemotherapeutic agent against colorectal cancers (157). The natural dietary agent curcumin possesses many advantages, as it is non-toxic to humans even at high doses even up to 12g/day, and targets multiple signaling pathways concurrently such as the NFκB and β-catenin pathways which have been demonstrated to be key regulators in cancer (158). Curcumin is a polyphenolic compound which suppresses proliferation, induces apoptosis and inhibits angiogenesis (159). Unlike conventional chemotherapeutic drugs, curcumin is believed to target cancer cells while sparing normal cells from any damages. Curcumin has been shown to down-regulate activation of NFκB and COX-2 by perhaps directly interacting with proximal kinases or cyclooxygenase enzyme itself (160). Curcumin also induces p53-independent apoptosis, hence improving its inhibitory effects on cancer cells (161,162). Curcumin in combination with FOLOFOX was reported to significantly inhibit the growth of colon cancer cells as spheroids (163,164). Given all the advantages and efficacy of curcumin as a potential natural chemotherapeutic agent, I focused my studies on examining the effects of curcumin on the growth of colon cancer stem cells in combination with RNAi targeting stem cell marker DCAMKL-1, as a potential novel therapeutic strategy (chapter 5). Our studies revealed the novel possibility that while curcumin induces autophagic death of colon cancer cells, DCAMKL-1 induces apoptotic death.

1.15 Autophagy

Autophagy is an intracellular multi-step process which results in the bulk degradation of proteins and cytoplasmic organelles within cells (165). The process is also referred to as programmed cell death type II and is necessary for maintaining cell survival, cell viability, differentiation and cellular development (166, 167). This catalytic pathway is usually activated when cells are deprived from nutrients; however other conditions such as stress, infection and cancer have been reported to induce autophagic activity. The recycling and removal of damaged organelles and macromolecules from cells via the autophagic pathway improves overall survival of the cells, and hence prevents the cells from undergoing apoptosis/necrotic (165).

1.15.1 Steps of Autophagy

Autophagy is regulated by *atg* genes which are essential to the formation of the double-membrane-bound autophagosomes. The mammalian homologs of these autophagy-related genes have recently been identified, and include LC3 (light chain 3). LC3 has been shown to be a robust marker of autophagy activity. LC3 is a microtubule-associated protein 1 light chain 3 which is normally present in the cytoplasm and plays an important role in the formation of autophagosomes (167). The initial step of autophagy involves the formation and elongation of isolation membranes within the cells (**Fig 1.12).** The isolation membranes extend, curve and form autophagosomes which engulf the cellular organelles predestined for degradation. Concurrently, LC3 is activated and cleaved (LC3-I), allowing for its glycine extended C-terminal end to conjugate to phosphatidylethanolamine resulting in the formation of LC3-II. The now lipidated LC3-II protein binds to the isolation membranes and autophagosomes in order to secure closure and structural stability of these vesicles (168). Subsequently, the autophagosomes

fuse with lysosomes resulting in the formation of autolysosomes which are in turn degraded by lysosomal hydrolases; the remaining macromolecules are recycled into the cytosol (169).

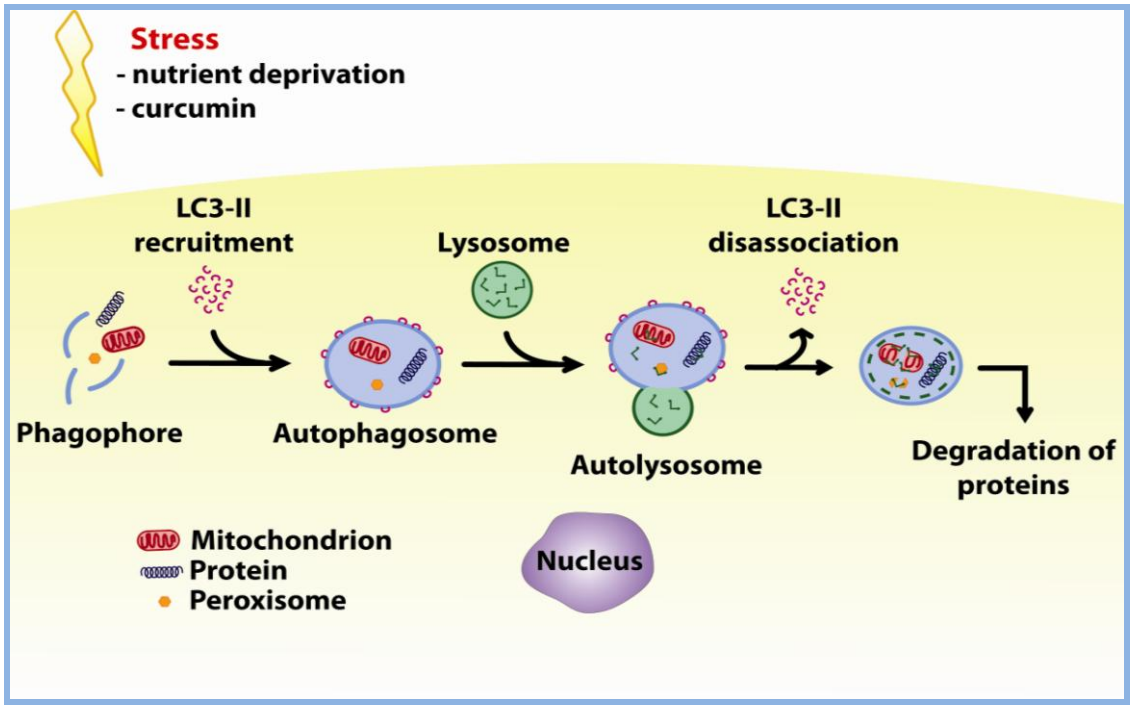

Figure 1.12: Steps of Autophagy

1.15.2 Curcumin induced autophagy and its role in cancer

Autophagy is usually activated as a rescue mechanism in normal cells but in cancer it is suppressed. In fact, autophagy has been shown to be inversely correlated with malignant phenotype of tumor cells (170). However, in response to chemotherapeutic agents, such as curcumin, cancer cells activate autophagic mechanisms (170). In cancer cells, autophagy is regulated by the activation of several signaling pathways including the Akt/mTOR/p70S6K pathway which determines whether a cell survives or undergoes apoptosis (171). The upstream activation of Akt leads to the phosphorylation and

activation of mTOR signaling molecule, which acts as a negative regulator of autophagy. Curcumin has been shown to activate calyculin A-sensitive protein phosphatases which inhibit mTOR phosphorylation, hence inducing autophagy *in vitro* and *in vivo* in cancer cells (171,172). Curcumin has also been shown to arrest cells in the G2/M phase while still promoting apoptosis and is believed to be a very potent anti-cancer drug. Curcumin has been shown to suppress tumor growth by inducing autophagy activity in various cancers (173, 174). However, it remains to be determined whether autophagy is activated as a death mechanism or a protective mechanism in cancer cells. Therefore, for my dissertation, I further examined the specific role of autophagy in response to the inhibitory effects of curcumin on tumor growth.

CHAPTER 2

ANNEXIN A2 MEDIATES UP-REGULATION OF NFKB, B-CATENIN, AND STEM CELL IN RESPONSE TO PROGASTRIN IN MICE AND HEK-293 CELLS

***This chapter is a copy of a manuscript published from our laboratory in 2011. I was granted copyright permission by Elsevier to reuse full article for thesis purpose: License # 2784211378313.**

2.1 Introduction

As briefly discussed under Background and Significance section in chapter 1, accumulating evidence suggests that exogenous/autocrine gastrins up-regulate proliferation/co-carcinogenesis of gastrointestinal and pancreatic cancers (175,176). Progastrin (PG) and glycine-extended gastrins are predominant forms found in colonic/ovarian/pancreatic/lung cancers (175). PG exerts potent proliferative/anti-apoptotic effects on target cells *in vitro* and *in vivo* (112,115,177-179). Transgenic mice overexpressing progastrin are at a high risk for developing preneoplastic/neoplastic colonic lesions in response to azoxymethane (53,68,117,180).

Under physiologic conditions, only processed forms of gastrins (G17/G34) are present in the circulation (175). In certain disease states, however, elevated levels of circulating PG are detected (175). Because co-carcinogenic effects of PG are measured in Fabp-PG mice, expressing "pathophysiologic" concentrations of hPG (53), elevated levels of circulating PG may increase the risk of tumor development, in response to DNA damage. Our laboratory has previously reported a critical role of nuclear factor-κB (NFκB) activation in mediating PG-induced proliferation/anti-apoptosis *in vitro* and *in*

vivo (5,112). Additionally our laboratory reported the novel possibility that β-catenin activation in response to PG is downstream of p65NFκB activation *in vivo* (118). It is, however, not known whether β-catenin also signals to p65NFκB and whether activation of both p65 and β-catenin are required for mediating growth effects of PG. I addressed these questions using a gastrin/PG responsive cell line (HEK-293) (181) because HEK-293 cells are amiable to multiple transfections.

Annexin A2 (AnxA2) represents a nonconventional "receptor" for PG/gastrin peptides (182). Down-regulation of AnxA2 was reported by our laboratory to reduce growth-stimulatory effects of PG on various target cells by ~50%–80% (182). It is, however, not known whether PG binding to AnxA2 is required for activating NFκB and/or β-catenin *in vitro* and *in vivo*. I therefore used $ANXA2^{-/-}$ mice and PG-expressing clones of HEK-293 cells to address this important question.

Recent reports suggest that PG up-regulates the census of cells expressing the putative stem cell marker doublecortin CAM kinase-like 1 (DCAMKL-1) in colonic crypts (68). Stem/progenitor cell marker CD44 is also known to be up-regulated in cancer cells that overexpress autocrine PG (183). In the following studies, I therefore examined whether autocrine PG directly up-regulates DCAMKL-1 expression and whether AnxA2 expression is required for measuring stimulatory effects of PG on DCAMKL-1/CD44 levels. Results of the studies I conducted with the help of other laboratory researchers, strongly suggested that AnxA2 expression is required for up-regulation of NFκB, β-catenin, CD44, and DCAMKL-1 in response to PG both *in vitro* and *in vivo.*

2.2 Materials and Methods

2.2.1 Materials

Antibodies used included anti-total-p65, antiphospho-p65NFκB(Ser^{276}), anti-phospho-p44/42-extracellular-regulated kinase, anti-phospho-p38 mitogen-activated protein kinase, anti-proliferating cell nuclear antigen (PCNA), anti-CyclinD1 (Cell Signaling Technology, Danvers, MA), anti-cylooxygenase (COX)-2 (Chemicon International, Billerica, MA), anti-c-Myc (Santa Cruz Biotechnology, Santa Cruz, CA), anti-β-actin (total) (Sigma, St Louis, MO), anti-AnxA2, anti-CD44 and anti-DCAMKL-1 (BD Biosciences, Carlsbad, CA). Recombinant human PG (rhPG) and anti-PG antibodies were generated in our laboratory (53,115). NFκB DNA binding kit was from Active Motif (Carlsbad, CA). Anti-immunoglobulin G (IgG), coupled to horseradish peroxidase, were from Amersham. Alexa Flour-594 and Alexa Flour-488 coupled secondary IgG were from Invitrogen (Carlsbad, CA). Luciferase reporter plasmids for measuring activation of β-catenin (TOPFlash wild type and FOPFlash mutant) were obtained from Dr. Bert Vogelstein (Johns Hopkins, Baltimore, MD).

2.2.2 Cell culture

HEK-293 cells (obtained from American Type Culture Collection) were cultured in Dulbecco's modified Eagle medium/F12 medium supplemented with 10% fetal calf serum (FCS) containing 1% penicillin/streptomycin in a humid atmosphere at 37°C with 5% CO_2. The cell line was regularly monitored for absence of mycoplasma.

2.2.3 Generation of HEK-293 clones stably overexpressing full-length PG

An eukaryotic expression plasmid was created for expressing full-length coding sequence of hGAS gene mutated at 3 di-basic sites (R57A-R58A/K74A-K75A/R94A-

R95A), as previously described in (53). HEK-293 clones, stably expressing full-length human progastrin (hPG) (HEK-mGAS), were generated as described in (184). Vector transfected clones (HEK-C) served as controls.

2.2.4 Transient transfection

Cells were transiently transfected with indicated plasmids, including promoter-reporter-plasmids (TOPFlash/FOPFlash) for measuring activation of β-catenin, as described in (112).

2.2.5 Transfection with small interfering RNA oliglionucleotides

Smart Pool of target-specific small interfering RNA (siRNA) and Non-Targeting (control) siRNA Pool, were obtained from Dharmacon (Lafayette, CO). Cells, seeded in 6-well dishes, were transfected with 1–1.5 μg of specific/control siRNA using Fugene (Roche, Indianapolis, IN). Transfected cells were propagated in normal medium containing 10% FCS for 48–72 hours and processed for immunoblot analysis.

2.2.6 In vitro growth assays

Cell growth was quantified in either an MTT (3-(4,5-Dimethylthiazol-2-yl)-2,5-diphenyltetrazolium bromide) assay or cell-count assay as described in (115, 185).

2.2.7 Immunoblot analysis

Cell/nuclear extracts were prepared from isolated colonic crypts and from control/treated cells in culture. Samples were processed for electrophoresis and transferred to polyvinylidene difluoride membranes, as described in (112). Blots were cut into horizontal strips containing target or loading-control proteins and processed for

immunoblot analysis. Antigen-antibody complexes were detected with chemiluminescence reagent kit (GE Health Care, Piscataway, NJ). Membrane strips containing either target or loading control proteins were simultaneously exposed to autoradiographic film(s). Relative band density on scanned autoradiograms was analyzed densitometrically using Image J Program (rsb.info.nih.gove/ij/download; National Institutes of Health, Bethesda, MD) and expressed as a ratio of β-actin or total kinase levels in the corresponding samples.

2.2.8 DNA binding assay

Activation of NFκB was determined using TransAM p65NFκB transcription factor assay, as described (5,112).

2.2.9 Promoter-Reporter assays

Cells transfected for 24 hours with either TOPFlash or FOPFlash plasmids were either treated (wtHEK-293 cells) or untreated (HEK-C/HEK-mGAS cells) with rhPG for 24–48 hours, followed by lysis. Luciferase Assay Reagent (Promega) was added to liquots of samples, and luciferase units were measured with a luminometer (Dynex Technologies, Chantilly, VA). Cells transfected with FOPFlash plasmid served as negative controls. In some experiments, cells were pretransfected with the indicated siRNA oligonucleotides.

2.2.10 Membrane binding and internalization of PG/AnxA2

Cells were seeded on glass coverslips, cultured overnight in complete growth medium, washed with phosphate-buffered saline (PBS) and incubated for 0–15 minutes with 10 nmol/L rhPG in Dulbecco's modified Eagle medium containing 0.1% serum at

37°C. Binding was terminated with ice-cold PBS, followed by fixation in acetone:methanol (1:1) for 20 minutes at -20°C. Fixed cells were washed with PBS, blocked with 5% bovine serum albumin, and incubated at 4°C with rabbit antirhPG-antibody (1:200) and mouse anti-AnxA2-antibody (1:500). Excess antibody was removed, and samples were incubated with goat anti-rabbit IgG coupled to Alexa Flour-594 (for detecting PG) and rabbit-anti-mouse IgG coupled to Alexa Flour-488 (for detecting AnxA2). Excess antibody was removed, and cells were incubated with 4□,6-diamidino-2-phenylindole for 5 minutes. Cover slips were mounted on glass slides with anti-fade-fixative (DAKO, Carpinteria, CA), and images acquired with Zeiss LSM 510 confocal microscope (META, NY). Images were analyzed using METAMORPH, v6.0 software (Molecular Devices, Sunnyvale, CA).

2.2.11 Treatment of ANXA2-/-/ANXA2+/+ mice with PG and analysis of colons/ colonic crypts

ANXA2$^{-/-}$ mice, on the C57Bl/6 background were generated as described (186) and shipped to animal facilities at University of Texas Medical Branch, Galveston, TX. C57Bl/J6-WT (ANXA2$^{+/+}$) mice were purchased from Jackson Laboratories (Bar Harbor, ME). Mice (~14 weeks old) were injected in groups of 5–10 with rhPG (1–10 nmol/L), intraperitioneally, 2 times/day for 10 days as described in (118) and then killed. Colons were fixed in 4% paraformaldehyde and processed for immunohistochemical/ immunofluorescence staining, as described in (5,118). Colonic crypts were also isolated and processed for immunoblots as described in (5,118).

2.2.12 Statistical analysis

Data are presented as mean ± standard error of mean of values obtained from 4–8 samples from 2 or 3 experiments. To test significant differences between means, nonparametric Mann–Whitney test was employed using Statview 4.1 (Abacus Concepts, Inc, Piscataway, NJ); *P* values < .05 were considered to be statistically significant.

2.3 RESULTS

2.3.1 Generation of HEK-293 clones overexpressing PG

HEK-293 cells respond to growth effects of gastrins (181). In our studies, conducted as above, we demonstrated for the first time that full-length PG (rhPG) also stimulates growth of HEK-293 cells **(Fig 2.1A)** and activates both p65 and β-catenin in HEK-293 cells *in vitro* **(Fig 2.1*B*–*D*)**. HEK-293 clones were generated for stably expressing either the empty vector (HEK-C) or triple mutanthGastrin gene (HEK-mGAS) as previously described in (53, 184). As a result, HEK-mGAS cells expressed full-length PG, which was resistant to processing into smaller fragments **(Fig 2.2A)**. Basal growth of HEK-mGAS clones was ~2-fold higher than that of HEK-C clones, irrespective of serum concentration, confirming mitogenic effects of autocrine PG **(Fig 2.2B)**. PCNA levels were increased ~2-fold in HEK-mGAS vs HEK-C clones **(Fig 2.2- 1D)**.

2.3.2 AnxA2 Is Expressed on Membranes of HEK-293 Cells

HEK-293 cells, on glass coverslips, were stimulated with 10 nmol/l PG. Strong co-localization of PG with membrane-associated AnxA2 was observed at 0–2 minutes **(Fig 2.2E)**. Within 5–15 minutes, the majority of PG/AnxA2 complexes was observed as punctate bodies in the perinuclear region **(Fig 2.2E)**, suggesting intracellular translocation of AnxA2/PG complexes. More recently we have confirmed these findings

by using an intestinal cell line (IEC-18) as well, and further demonstrated that internalization of PG/ANXA2 complexes in target cells is clathrin mediated, and is required for measuring functional activation of signaling pathways in response to PG (187).

2.3.3 AnxA2 expression is required for measuring activation of NFκB/ β-catenin in response to PG in vitro

Initially, we confirmed a significant increase in relative levels of $p65^{276}$/COX2 **(Fig 2.3A)**, β-catenin/c-Myc/cyclinD1 **(Fig 2.3B)**, as a readout of activated p65/β-catenin, in non-transfected HEK-mGAS vs HEK-C clones. HEK-mGAS/HEK-C cells were transfected with either control or AnxA2-specific siRNA. Transfection with control siRNA had no effect on $p65^{276}$/total-β-catenin levels in HEK-mGAS and HEK-C cells **(Fig 2.3C)**. However, transfection with AnxA2 siRNA resulted in attenuation of activated p65 and significant loss of total β-catenin in HEK-mGAS clones **(Fig 2.3*C*)**. HEK-C cells demonstrated negligible activation of β-catenin/NFκB in both control siRNA and AnxA2 siRNA transfected cells **(Fig 2.3D-E)**. HEK-mGAS cells transfected with control siRNA demonstrated significant activation of β-catenin and NFκB **(Fig 2.3D-E)**, similar to that measured in PG simulated wtHEK-293 cells **(Fig 2.1)**. HEK-mGAS cells transfected with AnxA2 siRNA, on the other hand, demonstrated significant attenuation in activated β-catenin **(Fig 2.3D)** and NFκB **(Fig 2.3E)**, compared with that observed in HEK-mGAS cells transfected with control siRNA. Thus, even though increased stabilization of total β-catenin was measured in AnxA2 siRNA transfected HEK-mGAS cells **(Fig 2.3C)**, levels of activated β-catenin remained negligible in these cells **(Fig 2.3D)**. The data suggest that AnxA2 expression is required for measuring activation of both NFκB/β-catenin at the nuclear level, in response to autocrine PG.

2.3.4 PG up-regulates stem cell markers DCAMKL/CD44 in vitro in an AnxA2-dependent manner

In cells stained with antibodies against DCAMKL-1/CD44, intensity of immunohistochemical staining/cell, and proportion of labeled cells were higher in HEK-mGAS vs HEK-C cells **(Fig 2.4A, Fig 2.5)**. Up-regulation of DCAMKL-1/CD44 expression in HEK-mGAS cells was further confirmed by immunoblot analysis **(Fig 2.4B-C)**. To examine the role of AnxA2, cells were transfected with either control or AnxA2 siRNA **(Fig 2.4B-C)**. Control siRNA had no effect on the increase in DCAMKL-1/CD44 seen in HEK-mGAS vs HEK-C cells. Treatment with AnxA2 siRNA, however, almost completely reversed stimulatory effect of autocrine PG on DCAMKL-1 levels. Surprisingly, CD44 levels remained elevated in AnxA2 siRNA treated HEK-mGAS cells **(Fig 2.4B-C)**, suggesting that up-regulation of CD44 may be more distal than stimulatory effect on DCAMKL-1.

2.3.5 Activation of both β-catenin and p65NFκB are required for measuring proliferative response of HEK-mGAS cells to autocrine PG

Cells growing in the presence of 1% FCS were treated with siRNA directed against either β-catenin or p65NFκB. siGenome non-targeting pool of siRNAs served as controls. β-catenin/p65 expression was reduced by >80% in samples treated with target-specific siRNA **(Fig 2.4D)**. The growth response was examined 48–72 hours after siRNA treatment in a cell-count assay. The number of control siRNA transfected HEK-mGAS cells was ~2- to 3-fold higher than that of control siRNA transfected HEK-C cells **(Fig 2.4E)**. Total number of HEK-C cells, transfected with either β-catenin siRNA or p65 siRNA, was only slightly lower compared with that of control siRNA transfected HEK-C cells **(Fig 2.4E)**. Growth of HEK-mGAS clones was significantly reduced to

control levels upon transfection with p65 siRNA and significantly reduced upon transfection with β-catenin siRNA **(Fig 2.4E)**. However, growth of HEK-mGAS cells transfected with β-catenin siRNA remained elevated compared with HEK-C cells **(Fig 2.4E)**, suggesting a critical role of p65NFκB for mediating growth effects of PG.

2.3.6 Down-regulation of p65NFκB attenuates β-catenin activation in HEK-mGAS clones

HEK-mGAS cells transfected with control siRNA demonstrated significant elevation in $p65^{276}$, total-β-catenin, COX-2, and nuclear-β-catenin, compared with that in control siRNA transfected HEK-C cells **(Fig 2.6A-B)**. HEK-mGAS and HEK-C cells, transfected with p65 siRNA, were down-regulated for p65 expression by ~80% **(Fig 2.6A-B)**. Down-regulation of p65NFκB expression attenuated the increase in $p65^{276}$, total β-catenin, and nuclear-β-catenin in HEK-mGAS cells **(Fig 2.6A-B)**. Relative levels of COX-2, while significantly reduced in p65 siRNA transfected cells, remained elevated in HEK-mGAS vs HEK-C clones **(Fig 2.6A-B)**, suggesting that factors in addition to p65/β-catenin may maintain basal levels of COX-2 in HEK-mGAS cells.

2.3.7 Activation of p65NFκB is independent of β-catenin activation in HEK-mGAS cells

Relative levels of total β-catenin, $p65^{276}$, and cyclin-D1 were significantly elevated in control siRNA transfected HEK-mGAS vs HEK-C cells **(Fig 2.6C-D)**. Transfection of β-catenin siRNA reduced β-catenin expression by >60%–80% in HEK-C/HEK-mGAS cells **(Fig 2.6C-D)**. However, loss of β-catenin expression had no effect on expression of p65NFκB in either HEK-C or HEK-mGAS cells **(Fig 2.6C-D)**. Relative levels of *p*p65 remained significantly elevated in β-catenin siRNA-transfected HEK-

mGAS vs HEK-C cells **(Fig 2.6C-D)**, strongly suggesting that phosphorylation-related activation of p65NFκB is independent of β-catenin, in response to PG. Relative levels of cyclin-D1 in HEK-mGAS cells, transfected with β-catenin vs control siRNA, were significantly reduced. However, levels of cyclin-D1 remained slightly elevated in HEK-mGAS vs HEK-C cells **(Fig 2.6C-D)**. Thus, data in Figure 4 demonstrate for the first time that, whereas β-catenin activation is downstream of NFκB, activation of NFκB, in response to autocrine PG, is independent of β-catenin, as diagrammatically presented in **Fig 2.7**, in relation to what is known in this field.

2.3.8 AnxA2 expression is required for signaling growth effects of PG to colonic crypt cells in vivo

ANXA2$^{-/-}$/ANXA2$^{+/+}$ mice following genotyping were confirmed **(Fig 2.8A)**. Mice were treated with either rhPG or saline as described in Materials and Methods section. In response to 1–10 nmol/L rhPG, significant increase in the length of colonic crypts was observed in ANXA2$^{+/+}$ but not ANXA2$^{-/-}$ mice. Data obtained with 10 nmol/L PG are shown in **Fig 2.8B-C, Fig 2.9**. Representative immunohistochemical data obtained with 10 nmol/L PG are shown in **Fig 2.8B**, and representative colonic crypts isolated from the different groups of mice are presented in **Fig 2.9**. Relative levels of *p*p65^{Ser276}/cellular β-catenin were significantly increased in rhPG vs saline-treated ANXA2$^{+/+}$ mice **(Fig 2.8D)**. Relative levels of p65/β-catenin from PG vs saline-treated ANXA2$^{-/-}$ mice, on the other hand, were similar **(Fig 2.8D)**, strongly implying that AnxA2 expression is required for activating NFκB/β-catenin in colonic crypts of mice, in response to PG.

Relative levels of CD44/DCAMKL-1 were also increased by ~1.5- to 2-fold in colonic crypt cells of PG treated ANXA2$^{+/+}$ mice **(Fig 2.10A-B)** and reflected the

increase in percent cells positive for DCAMKL-1/CD44 in colonic crypts of rhPG vs saline-treated ANXA2$^{-/-}$ mice **(Fig 2.10C-D, Fig 2.11)**. In ANXA2$^{-/-}$ mice, on the other hand, significant differences were not measured in either DCAMKL-1 or CD44 expression, in response to PG stimulation **(Fig 2.10A-B)**. Percentage of cells positive for CD44 in rhPG vs saline-treated ANXA2$^{-/-}$ mice were also not different **(Fig 2.10C-D, Fig 2.11)**. However, proportion of DCAMKL-1 positive cells remained slightly elevated in rhPG vs saline-treated ANXA2$^{-/-}$ mice **(Fig 2.10C-D, Fig 2.11)**. An important finding was that cells staining for CD44/DCAMKL-1 were distinctly different and did not co-stain with each other.

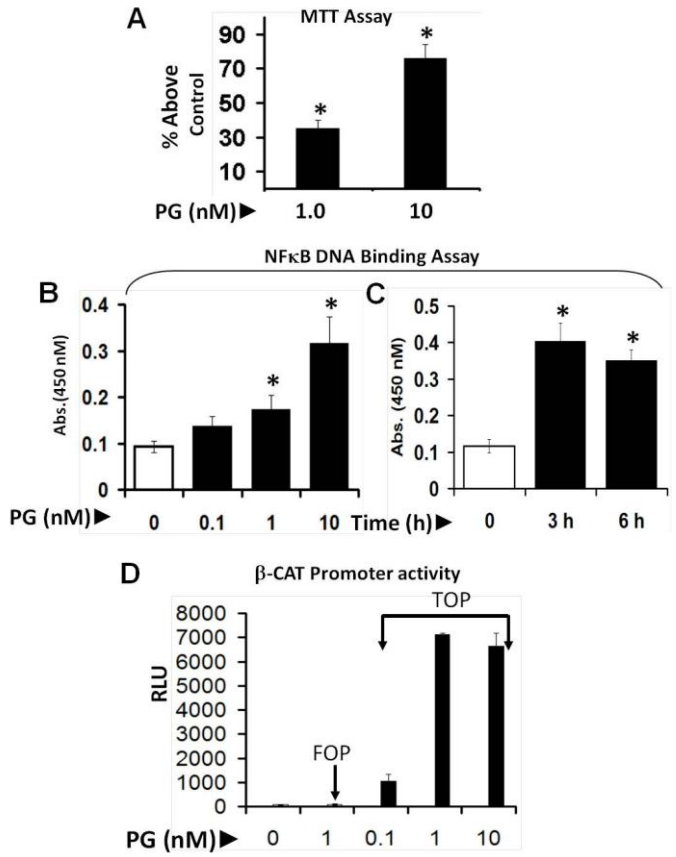

Figure 2.1 (*A-D*). Effect of exogenous progastrin on cell proliferation and activation of NFκB and β-catenin in HEK-293 cells. **A=** The growth response of HEK-293 cells, in culture, was examined in response to the indicated doses of progastrin, using an MTT assay as described in Methods. Each *bar* represents data from 6 replicate measurements from a representative of a total of 3 experiments. **B and C=** In *panel B*, wtHEK-293 cells, in culture, were treated with indicated concentrations of progastrin for 3h (based on results in *C*). For data presented in *panel C*, cells were treated with 10nM progastrin for the indicated time periods. Relative levels of activated NFκB were measured in an *in vitro* DNA binding assay in the nuclear extracts of the treated cells, as described in Methods. Each *bar* represents data from 3 separate dishes and is representative of 3 experiments. **D=** HEK-293 cells were transfected with either wt reporter-promoter plasmid (TOPFlash) or mutant plasmid (FOPFlash) for measuring activation of β-catenin promoter, as described in Methods. After 24h of transfection, cells were treated with the indicated concentrations of progastrin, and processed for measuring relative levels of luciferase after 48h of progastrin treatment. Each *bar* represents mean ± SEM of 3 separate measurements from 1 experiment, and is representative of 3 similar experiments. **P*<.05 vs control levels measured in the absence of progastrin (PG).

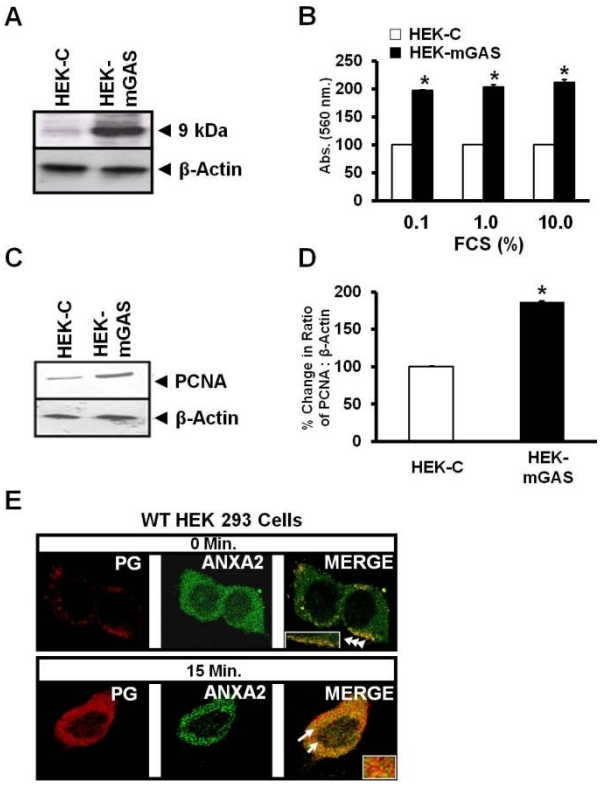

Figure 2.2 (*A*–*E*) Proliferative potential of HEK-mGAS and HEK-C cells. **A=** Expression of full-length 9-kilodalton progastrin peptide by HEK-mGAS clones. **B=** Growth response of an equal number of HEK-C and HEK-mGAS cells to increasing concentrations of FCS, measured in an MTT assay. Absorbance values are plotted against FCS concentrations. Each value represents data from 6 separate wells/experiment, from a representative of 2 similar experiments. **C=** Relative levels of proliferating cell nuclear antigen (PCNA) in the cellular lysates of subconfluent clones, growing in 5% FCS, measured by immunoblot analysis. A representative blot from a total of 6 blots from 3 experiments is presented. **D=** Basal intensity of bands, determined densitometrically, is plotted as percent change in the ratio of PCNA:β-actin (ratio for HEK-C cells was arbitrarily designated 100%); data from 6 blots are presented as mean ± standard error of mean, in *bar graphs*. **P* < .05 vs HEK-C values. **E=** Co-localization and internalization of progastrin/AnxA2 complexes in response to exogenous progastrin (*PG*). wtHEK-293 cells on glass coverslips were incubated with progastrin for indicated time periods and processed for detection of progastrin/AnxA2 by confocal microscopy. *Red fluorescence*, progastrin staining; *green fluorescence*, AnxA2 staining. Colocalization of progastrin/AnxA2 appears bright yellow in merged images at 60x magnification. *Insets* presented for merged images are computer enhanced. Colocalized progastrin/AnxA2 on membranes (*short arrows*) and intracellularly (*long arrows*) are shown.

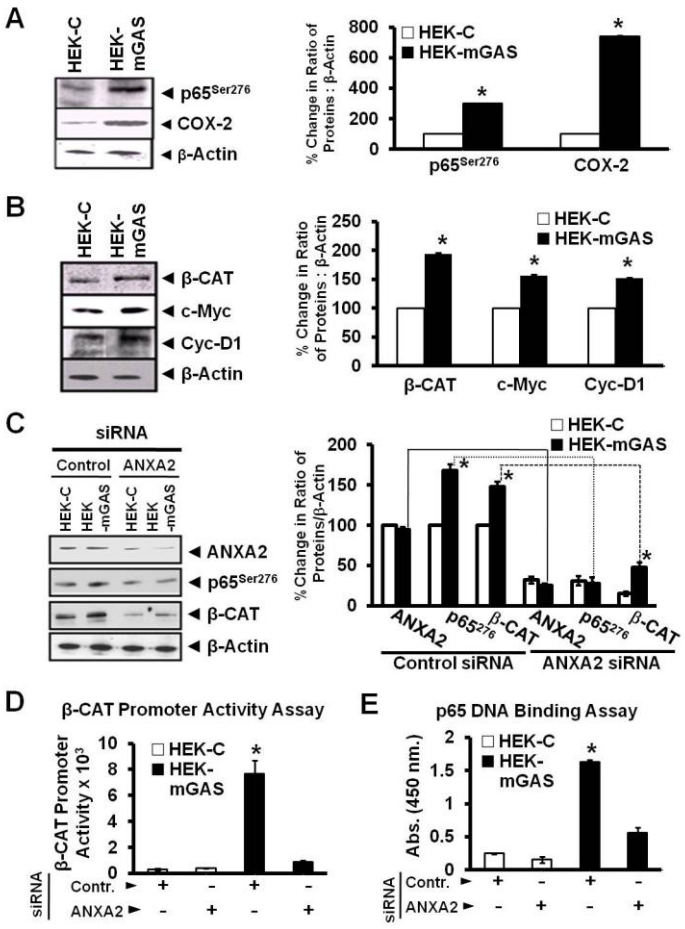

Figure 2.3 (*A-E*) Activation of p65NFκB/β-catenin in response to autocrine-progastrin in HEK-mGAS clones. Relative levels of p65Ser^{276}/COX-2 (A) and β-catenin/c-Myc/CyclinD1/β-actin **(B)** in cellular lysates of HEK-mGAS vs HEK-C cells, measured by immunoblot analysis, are presented. In *A* and *B*, data from a representative blot of 4 blots/2 experiments are presented. In *A* and *B*, percent change in ratio of the indicated proteins to β-actin are presented as mean ± standard error of mean of data from 4 blots, as described in **Figure 2.2** legend. In each case, **P* < .05 vs HEK-C values. **C=** Down-regulation of AnxA2 in HEK-mGAS cells results in loss of relative levels of p65NFκB and β-catenin. HEK-C/HEK-mGAS clones were treated with either control siRNA or AnxA2 siRNA, and cellular lysates were processed for immunoblot analysis. β-actin was analyzed as an internal control. Representative blots from a total of 4 blots/2 experiments are presented in the *left panel*. In the *right panel*, data from 4 blots are presented as percent change in the ratio of indicated proteins:β-actin as mean ± standard error of mean. **P* < .05 vs HEK-C values. **(D and E)** Down-regulation of AnxA2 in HEK-mGAS cells results in loss of activation of NFκB and β-catenin. **D=** HEK-C/HEK-mGAS cells were transfected with either control or AnxA2-specific siRNA for 48 hours, followed by transfection with either FOPFlash (lane 1, 2) or TOPFlash (lane 3, 4) plasmids. Twenty-four hours after transfection, promoter activity was measured in terms of luciferase units, and data from 6 separate samples/2 experiments are presented. **E=** Cells were transfected with either control or AnxA2-specific siRNA for 48 hours, followed by preparation of nuclear extracts, and processed for measuring binding of activated NFκB in a DNA-binding assay; data from 6 separate samples/2 experiments are presented as mean ± standard error of mean.

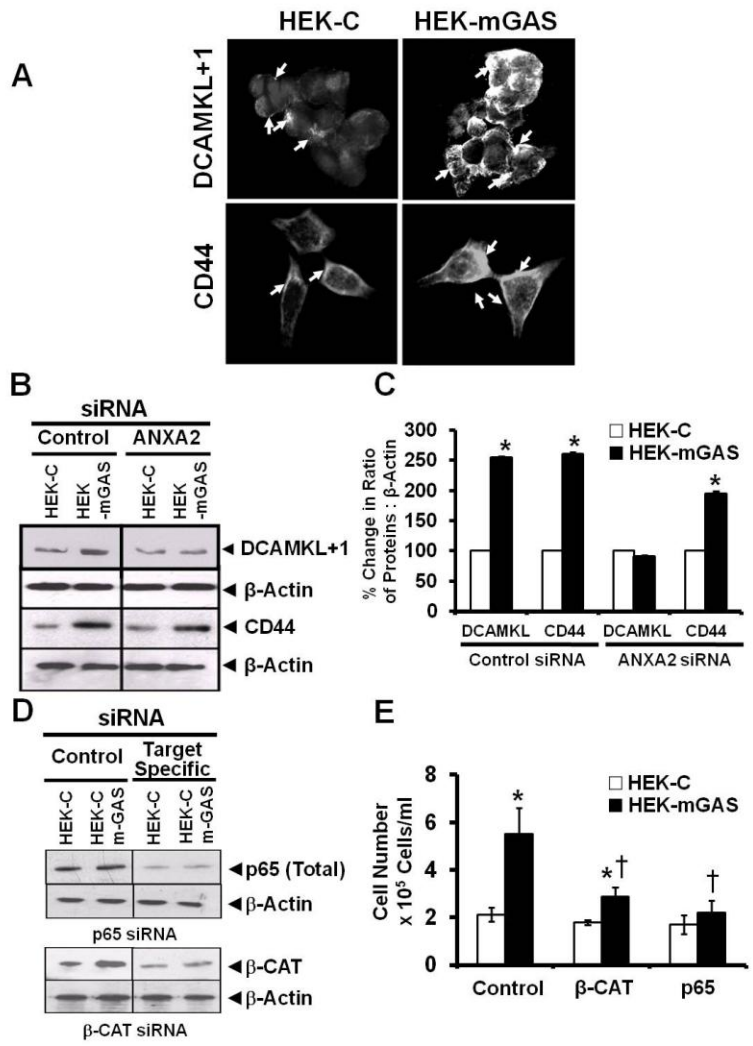

Figure 2.4. (*A*–*E*) Autocrine progastrin up-regulates DCAMKL-1/CD44 in HEK-mGAS vs HEK-C cells in an AnxA2-dependent manner. A= HEK-C/HEK-mGAS cells growing on coverslips were stained for the indicated stem cell marker, as described in legend of **Figure 2.2E**. **B-C=** HEK-C/HEK-mGAS cells were transfected with either control or specific AnxA2 siRNA, followed by preparation of cellular extracts after 48 hours. Lysates were processed for immunoblot analysis, and data from a representative blot from a total of 4 blots/2 experiments are shown in *B*. Data from 4 blots are presented as percent change in the ratio of indicated proteins:β-actin as mean ± standard error of mean in *C*. **P* < .05 vs HEK-C values. **D-E=** Effect of down-regulating β-catenin/p65NF-κB on growth of HEK-C/HEK-mGAS cells. HEK-C/HEK-mGAS cells in culture were transfected with either control or β-catenin/p65 specific siRNA. After 72 hours, cells were either processed for immunoblot analysis **(D)** or counted **(E)**. Cell numbers in 6 separate dishes/experiment were measured and presented as mean ± standard error of mean in *E*. Data presented are representative of 3 similar experiments. **P* < .05 vs corresponding HEK-C values; †*P* < .05 vs corresponding control siRNA values.

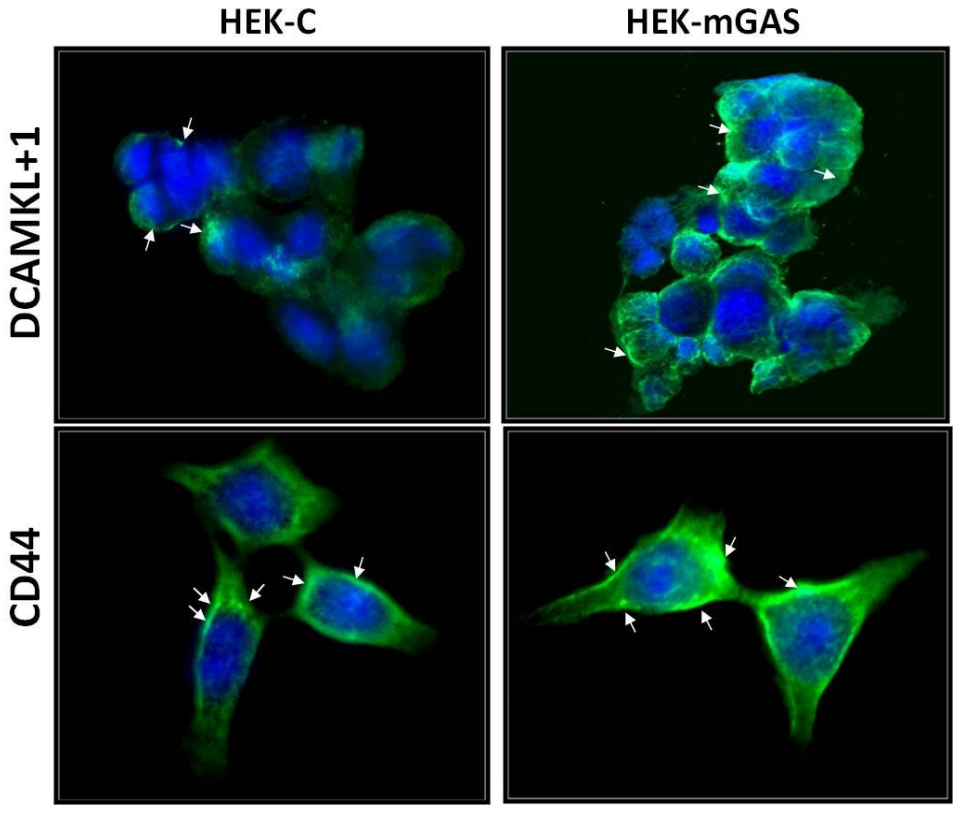

Figure 2.5. Autocrine progastrin up-regulates relative levels of DCAMKL-1/CD44 in HEK-mGAS and HEK-C cells. HEK-C and HEK-mGAS cells growing on coverslips were stained for the indicated stem cell markers, as described in the legend of **Figure 2.2E**. The *bright green fluorescence* in each case represents specific antibody binding to either CD44 or DCAMKL-1 as shown.

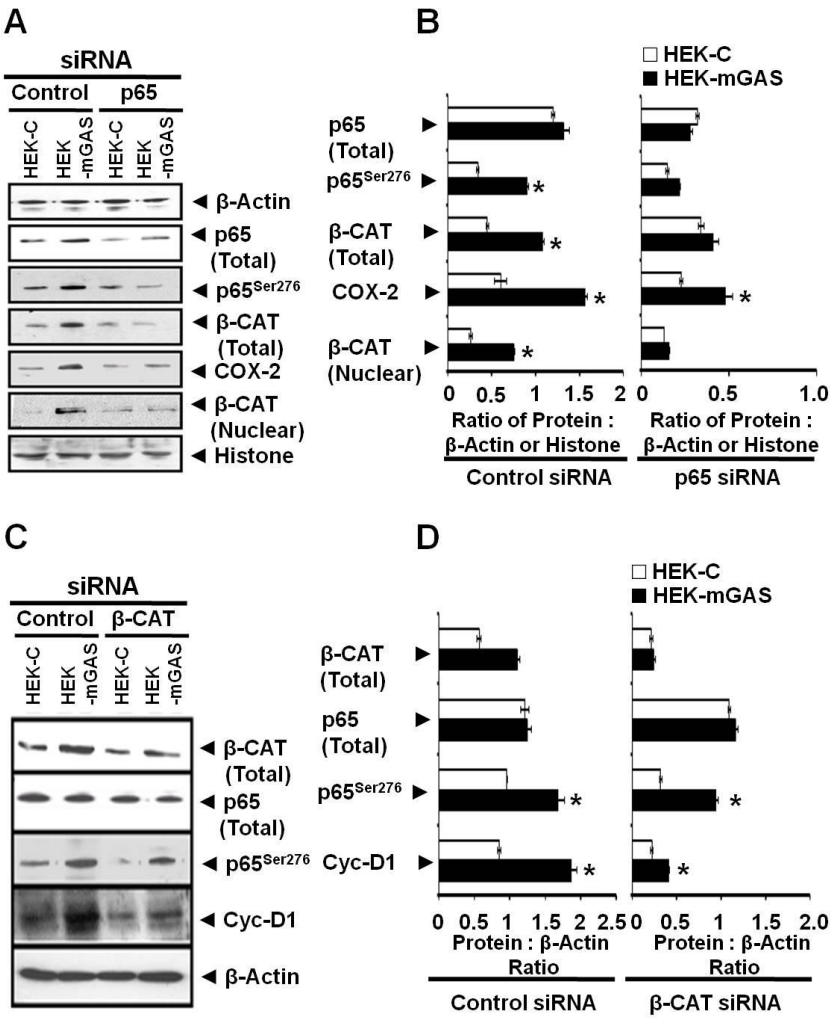

Figure 2.6 (*A*-D) Down-regulation of p65NFκB attenuates β-catenin activation in HEK-mGAS cells. Cells were transfected with either control siRNA or p65NFκB-specific siRNA and processed for immunoblot analysis. Representative blots from a total of 4 blots/2 experiments are presented in **A**. β-actin and histone levels were used as internal controls for cellular/nuclear lysates, respectively. Ratio of indicated proteins to either β-actin (total p65/p65^{276}/total-β-catenin/COX-2) or histone (nuclear β-catenin) are presented as mean ± standard error of mean from all 4 blots in *B*, *left panel*: control siRNA, and *right panel*: p65-specific siRNA. *$P < .05$ vs corresponding HEK-C values. **C-D=** Activation of p65NFκB is independent of β-catenin activation in HEK-mGAS cells. Cells were transfected with either control siRNA or β-catenin-specific siRNA and processed for immunoblot analysis of cellular lysates. β-actin levels were measured as an internal control. Representative blots of a total of 4 blots/2 experiments are presented in **C**. Ratio of indicated proteins:β-actin, determined from densitometric analysis of immunoblot bands, is presented as mean ± standard error of mean of data from all 4 blots in **D** (as described above for **B**). *$P < .05$ vs HEK-C values. β-CAT, β-catenin; Cyc-D1, Cyclin D1.

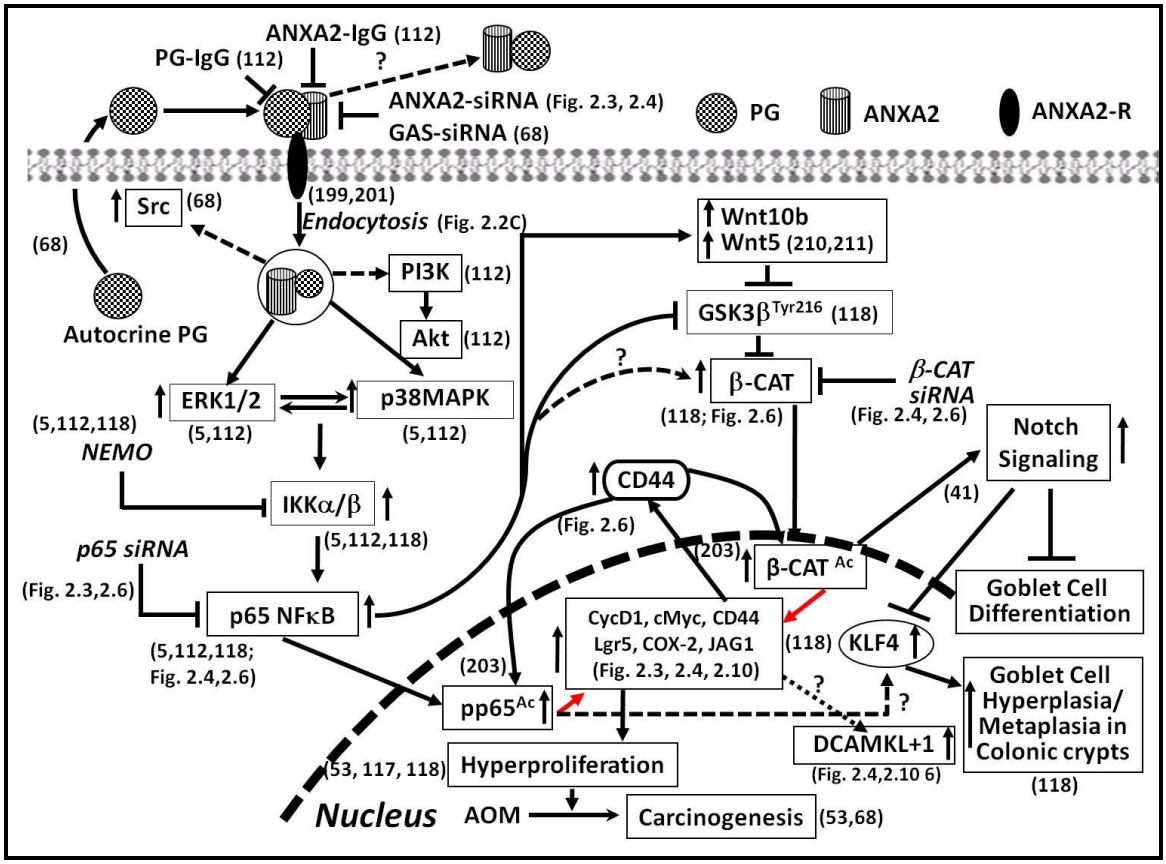

Figure 2.7. Diagrammatic representation of cellular/intracellular mechanisms mediating growth response of target cells to exogenous or autocrine progastrin: role of ANXA2. Based on our previous and current findings, the role of ANXA2 and several signaling molecules/transcription factors/target proteins in mediating the growth effects of endocrine/autocrine progastrin peptides is presented as a diagrammatic model. Relevant data from other investigators is also presented. Reference numbers or figure numbers (current studies) which provide evidence for a role of the indicated molecules (pathways) are shown in parentheses. *Dashed lines* indicate speculative pathway. *Solid lines* indicate experimentally shown in the indicated figure/reference. *T lines* indicate Inhibition of the indicated pathway.

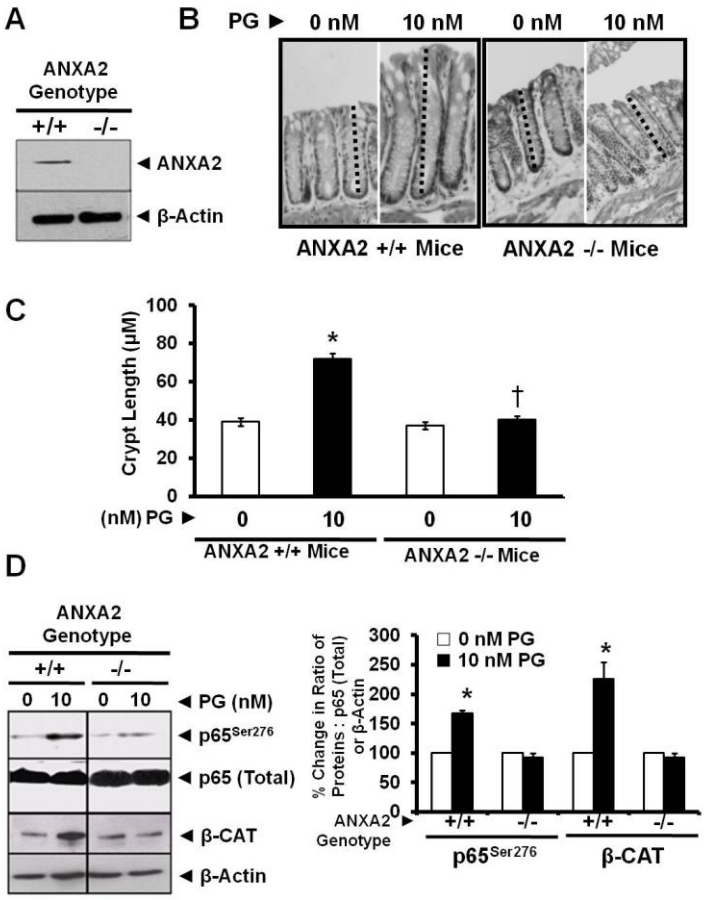

Figure 2.8. ANXA2 expression is required for the growth/signaling effects of progastrin *in vivo*. A= Representative immunoblot data demonstrating absence of AnxA2 expression in colonic crypts of $ANXA2^{-/-}$ mice. **B=** Representative tissue sections from midcolons of $ANXA2^{+/+}$/$ANXA2^{-/-}$ mice, treated with either saline (0 nmol/L) or 10 nmol/L rhPG. *Dashed lines* represent average length of colonic crypts in the indicated mice. **(*C*)** To obtain accurate measurements of colonic crypt lengths, colons were processed for preparation of isolated colonic crypts **(Figure 2.9)**, and lengths were measured as previously described in (5,118). Each bar graph = mean ± standard error of mean of 30–50 isolated crypt lengths from 3 to 5 mice. **P* < .05 vs control (saline treated) mice: †*P* < .05 vs respective $ANXA2^{+/+}$ levels. **D=** Isolated colonic crypts from midcolons of the indicated genotypes were processed for immunoblot analysis. Representative blots of 6–8 blots from 3 to 4 mice are shown in *left panel*. Percent change in the ratio of $p65^{Ser276}$:total p65 and β-catenin:β-actin is shown in *right panel*; each group represents mean ± standard error of mean of data from 3 to 5 separate mice. **P* < .05 vs corresponding control (*0 nmol/L PG*) group.

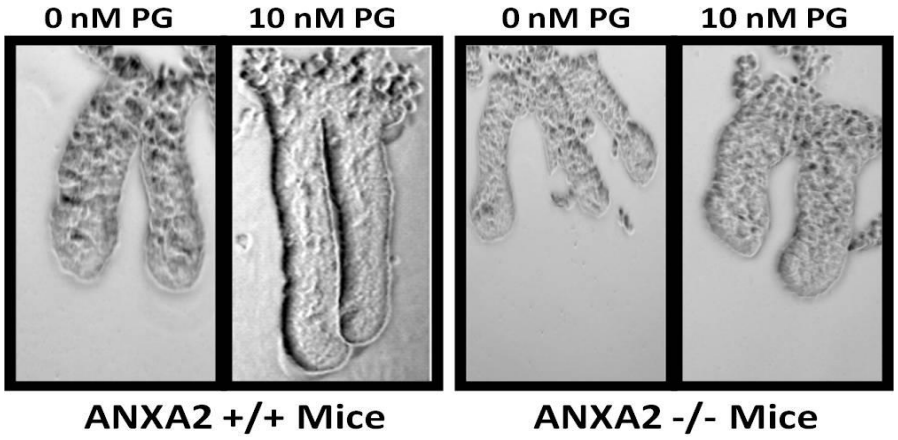

Figure 2.9. Annexin A2 expression is required for measuring an increase in the lengths of isolated colonic crypts in response to progastrin *in vivo*. Using FVB/N mice, we had previously reported that colonic crypts from the proximal colons of the mice were extremely responsive to the growth promoting effects of progastrin (5). However, for reasons unknown, the C57Bl/6J mice do not develop tumors in the proximal colon in response to azoxymethane (175), but mainly develop tumors in the middle and distal portions of the colon. In initial studies, we therefore confirmed growth effects of progastrin on the mid-colons of the C57Bl/6J (C57) mice. For these studies the colons were processed for the preparation of isolated intact colonic crypts, as described previously in (5,118). In the next set of experiments we examined the growth promoting effects of 10nM PG on the colonic crypts of $ANXA2^{+/+}$ and $ANXA2^{-/-}$ mice, as described in the Methods section. Because the mid-colons of the $ANXA2^{+/+}$ mice were most responsive to the growth effects of PG, we chose to measure the lengths of isolated colonic crypts only from the mid-colons of the mice, and representative images of the isolated colonic crypts are presented from the four groups of mice. Data from all the mice in the four groups are presented as bar graphs in **Figure 2.8C**.

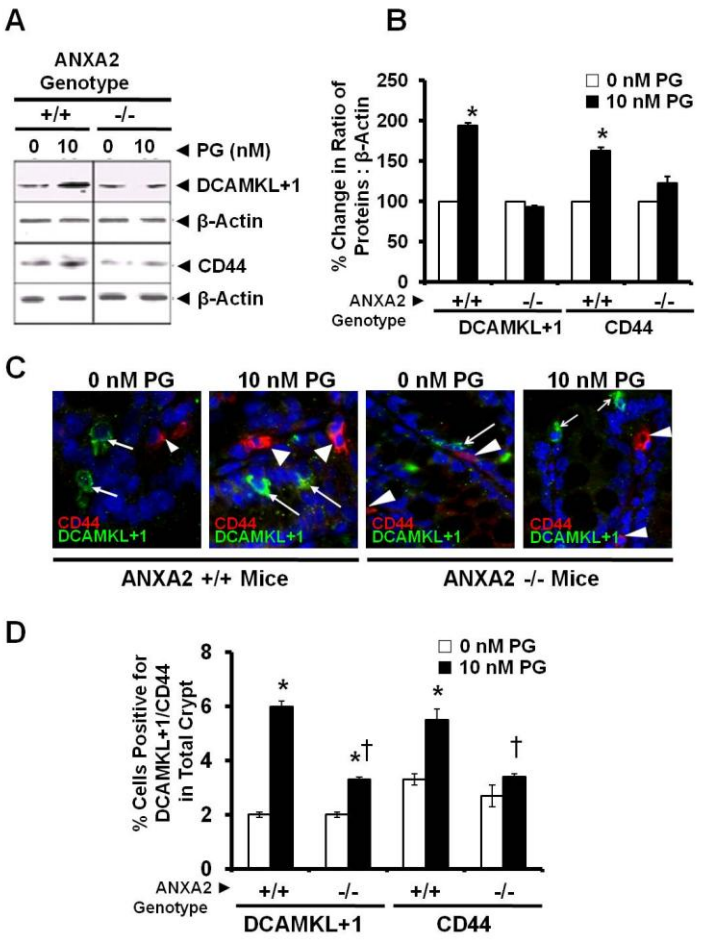

Figure 2.10 (*A-D*). AnxA2 expression is required for stimulatory effect of progastrin on CD44/DCAMKL-1 expression in colonic crypts. Colonic crypts were isolated from the mice and processed for immunoblot analysis as described in **Figure 2.8**. Immunoblots from a representative mouse, of a total of 3–5 mouse blots, are shown in **A**. Immunoblot data from all the mice are presented in *B* as percent change in the ratio of indicated proteins:β-actin. **P* < .05 vs corresponding control (*0 nmol/L PG*) values. **C**= Mouse colon sections from the indicated 4 groups of mice were processed for immunofluorescence staining with either anti-DCAMKL-1 IgG (*green*) or anti-CD44 IgG (*red*) **(Figure 2.11)**. Representative enlarged images from stained colonic crypts of indicated mice are presented in *C*. Relative staining/cell for both DCAMKL-1/CD44 appears to be increased in PG-treated ANXA2$^{+/+}$ colonic crypts, but no significant differences were observed in PG-treated ANXA2$^{-/-}$ mice compared with corresponding controls **(D-C, Figure 2.8)**. The percent cells (within a viewing field at 20x magnification) positive for either DCAMKL-1 or CD44 were counted in 10 sections from 3 to 5 mice. Data are presented as mean ± standard error of mean in *D*. **P* < .05 vs corresponding control mouse sections; †*P* < .05 vs corresponding ANXA2$^{+/+}$ levels.

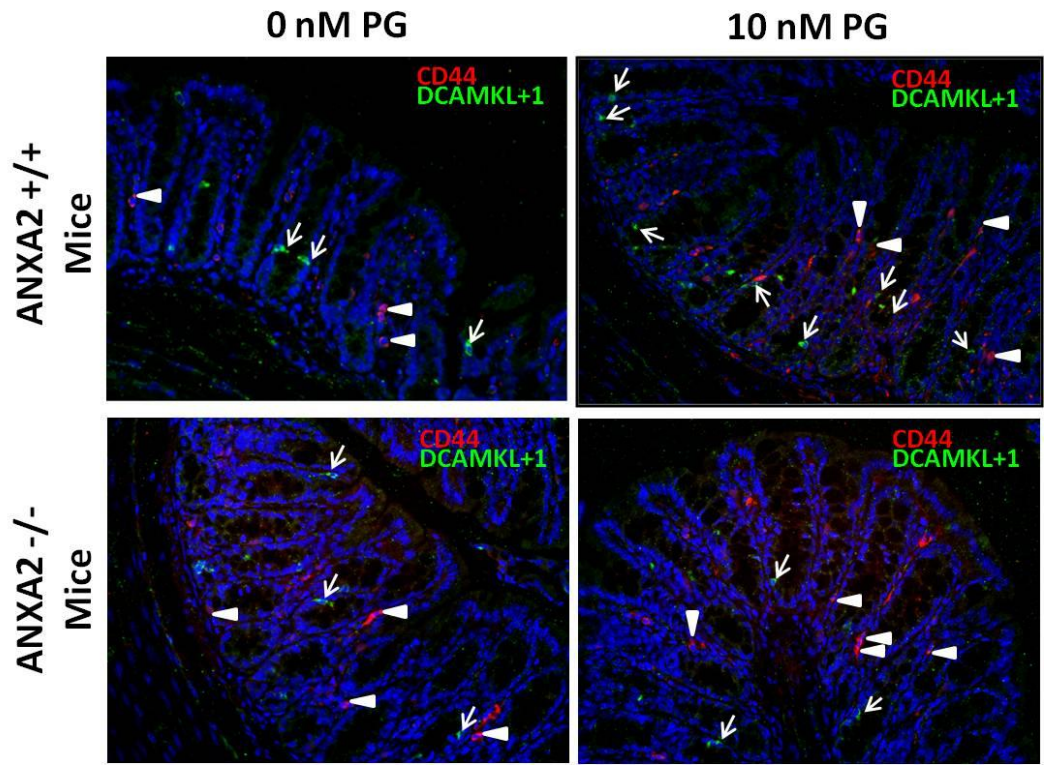

Figure 2.11. AnxA2 expression is required for stimulatory effect of progastrin on CD44/DCAMKL-1 expression in colonic crypts. AnxA2$^{+/+}$/AnxA2$^{-/-}$ mice were treated with either saline (0nM) or 10nM-rhPG. Colons were removed at the time of sacrifice and processed for making tissue sections, as described in Methods. Mouse colon sections from the indicated 4 groups of mice were processed for immunofluorescence staining with either anti-DCAMKL-1-IgG (green) or anti-CD44-IgG (red). Representative images from stained sections of colons from indicated mice are presented at 20x magnification. Enlarged images (60x) from a representative portion of each section, are also presented in **Figure 2.10C**. Red and green staining shows cells staining for CD44 and DCAMKL-1, respectively, along the lengths of the colonic crypts, at 20x. DAPI shows the nucleated cells within the viewing field. As can be seen, the relative staining for CD44 and DCAMKL-1 per cell was highest in progastrin treated ANXA2$^{+/+}$ mice, compared to all other groups. The total number of cells, positive for the two stem/progenitor cell markers, within a viewing field were also the highest in ANXA2$^{+/+}$ mice, compared to all other groups. The quantitative analysis of the data, obtained from these images, are presented in **Figure 2.10**. A curious finding was that while down-regulation of ANXA2 *in vitro* in HEK-mGAS cells did not completely attenuate the increase in CD44 levels in response to autocrine PG **(Fig 2.4C)**, the loss of ANXA2 expression in ANXA2-/- mice resulted in complete attenuation of PG stimulated increase in CD44 levels, *in vivo*. The differences in the relative effects on CD44 levels *in vitro* versus *in vivo* may reflect the fact that CD44 expression was increased robustly *in vitro* in HEK-mGAS cells **(Figure 2.4B-C)**, but was not increased to the same extent in ANXA2+/+ mice in response to PG **(Figure 2.10C-D)**.

2.4 DISCUSSION

Proliferative effects of precursor gastrins (PG/glycine-extended gastrins) are reportedly mediated by novel receptor mechanisms, distinct from cholecystokinin type 1 receptor (CCK_1R)/cholecystokinin type 2 receptor (CCK_2R) *in* vitro (175,115,185,188) and *in vivo* (189,190). Several years ago, our laboratory had identified a 33- to 36-kilodalton protein with high affinity for PG/gastrin peptides (111). Recently, our laboratory discovered that AnxA2 represents the novel p36 "receptor" protein (182). Unlike CCK_2R antibodies, AnxA2-antibodies blocked growth effects of PG on target cells *in vitro* (112,182). In addition, AnxA2 expression was required for the growth effects of PG on colon cancer cells (182). Only proliferative/antiapoptotic effects of PG have been reported (175). Amidated gastrins, however, either stimulate (191) or inhibit (192) growth of target cells in vitro via CCK_2R. Proapoptotic effects of amidated gastrins via CCK_2R have also been reported *in* vivo (191,193); a recent study, however, reported that CCK_2R expression may be required for measuring co-carcinogenic effects of pharmacologic levels of PG on colons of transgenic hGASmice (68).

In the current studies, we demonstrate for the first time that AnxA2 expression is required for activating both NFκB and β-catenin signaling pathways and for the hyperproliferative effect of PG on colonic crypts *in vivo*. Because anti-AnxA2 antibodies block binding of AnxA2 to PG, and significantly attenuate growth effect of exogenous PG on AR42J/IEC-18 cells *in vitro* (112,182), we hypothesized that membrane-associated extracellular AnxA2 is required for growth effects of PG. Presence of extracellular, membrane-associated AnxA2 has been reported on several cancer cells (194-198). Results of our studies, so far, provide further evidence for the presence of membrane-associated AnxA2 on HEK-293 cells and other target cells of PG, suggesting that PG-AnxA2 complexes are rapidly internalized after binding **(Figure 2,2E). (**current

studies, 187). Interestingly, in prostate cancers, cytoplasmic staining of AnxA2 was detected, whereas in benign prostatic glands, AnxA2 was localized to plasma membranes (199) TM601, a 36-amino acid synthetic peptide, specifically binds extracellular AnxA2 on endothelial and tumor cells and was reported to be internalized by proliferating endothelial cells, resulting in neoangiogenesis (197). Paracrine/endocrine PG induces hyperproliferation of proximal colonic crypts associated with internalization of AnxA2, whereas, in the nonresponsive distal crypts, AnxA2 remains localized to plasma membranes (5). Thus, internalization of AnxA2/ligand complexes may represent a hallmark of cells responsive to proliferative agents, such as PG and TM601. Because AnxA2 lacks transmembrane domain(s), mechanisms mediating internalization of AnxA2/PG remain speculative. AnxA2 may be anchored to the cell surface by AnxA2 receptor (200) **(as diagrammatically represented in Figure 2.7)**. Binding of AnxA2 to AnxA2 receptor is reportedly essential for metastasis of prostate cancer cells (201). Knockdown of AnxA2 inhibits metastatic invasion of breast cancer cells (202). It remains to be determined whether AnxA2 receptors play a role in the observed effects of PG.

Activation of both NFκB and β-catenin was required for achieving maximal growth effect of autocrine PG **(Figure 2.4E)**. Whereas p65NFκB activation increased ~2- to 3-fold in response to autocrine PG, COX-2 increased ~6-fold **(Figure 2.3A)**. CD44 amplifies transcriptional activity of p65/β-catenin by up-regulating acetyl-transferase activity of p300, which acetylates β-catenin/p65NFκB (203) **(Figure 2.7)**. Thus, PG mediated nuclear translocation of NFκB/β-catenin, resulting in up-regulation of CD44 **(Figure 2.4A-B)**, may enhance transcriptional activity of NFκB/β-catenin, thus amplifying COX-2 expression. Similarly, in colorectal cancer cells, activation of β-catenin in response to autocrine PG up-regulated stem/progenitor cell markers (CD133/CD44) (183), as well as Jagged1 (Notch-ligand) (41) **(Figure 2.7)**. Accumulating

evidence confirms a critical role of activated p65NFκB in mediating direct growth effects of PG on target cells (112,118,192,204) and current studies. Elevated activation/expression of NFκB/COX-2 is observed in aggressive colorectal cancers (205), which also express PGs (175,176), providing further support for a central role for activated NFκB, downstream of autocrine PG, in cancer growth. Progastrin also up-regulates β-catenin in colon cancer cells, HEK-293-cells, and proximal colonic crypts (41,118,109) and current studies. Results of our previous *in vivo* studies suggest that β-catenin activation may be downstream of activated p65NFκB (5). Our current *in vitro* studies confirm that β-catenin activation is downstream of NFκB **(Figure 2.6A-B)**. However, down-regulation of β-catenin had no effect on levels of activated p65 **(Figure 2.6C-D).** Thus, we demonstrate for the first time that, whereas β-catenin activation is downstream of activated NFκB, p65 activation is independent of β-catenin, in response to direct *in vitro* stimulation with PG **(Figure 2.7)**. Cross talk between IκB kinase (IKK)α/β/NFκB and Wnt signaling pathways has been reported by several investigators (206-208). Activated IKKβ blocks both canonical and noncanonical degradation of β-catenin (209). During morphogenesis of hair follicles, NFκB directly up-regulates Wnt10b (210) **(Figure 2.7**). Wnt5a promoter has conserved NFκB binding sites, and its expression is up-regulated by activated NFκB and other signaling pathways (211) resulting in activation of β-catenin. Our previous *in vivo* studies suggested that down-regulation of IKKα/β/NFκB results in Tyr-phosphorylation of glycogen synthase kinase 3 beta (GSK3β) (and hence deactivation of GSK3β), which can potentially activate β-catenin (118) **(Figure 2.7)**. It remains to be determined whether Tyr-phosphorylation of GSK3β is down-regulated by Wnt10b/Wnt5a in response to PG activated NFκB. DCAMKL-1 is believed to be a marker for quiescent stem cells within intestinal crypts (20,67). In PG overexpressing hGAS mice, a significant increase in DCAMKL-1

expressing colonic crypt cells was reported (68). In the current study, we suggest the novel possibility that AnxA2 expression is required for measuring a significant increase in the cell numbers and relative levels of DCAMKL-1 expression in direct response to PG stimulation *in vitro* and *in vivo*. It remains to be determined whether DCAMKL-1 up-regulation in response to PG is mediated via NFκB and/or β-catenin signaling pathways. In summary, resulted of our studies, presented in this chapter, strongly suggest that AnxA2 expression is required for mediating activation of both p65NFκB and β-catenin *in vitro* and *in vivo* and that both transcriptional factors are required for observing maximal growth effects of PG.

We demonstrated for the first time that AnxA2 expression is required for PG-mediated up-regulation of stem/progenitor cell markers DCAMKL-1 and CD44, in both colonic crypts, *in vivo,* and in an embryonic epithelial cell line, HEK-293 *in vitro*. Given that the over-expression of PG in HEK-mGAS cells resulted in the up-regulation of stem cell expression and in an increase in the proliferative potential of HEK-mGAS cells, I was next interested in examining whether the tumorigenic and metastatic potentials of these cells were also increased. This goal was addressed in chapter 3 wherein athymic nude mouse were used as a model.

CHAPTER 3

PROGASTRIN OVEREXPRESSION IMPARTS TUMORIGENIC/METASTATIC POTENTIAL TO EMBRYONIC EPITHELIAL CELLS: PHENOTYPIC DIFFERENCES BETWEEN TRANSFORMED AND NON-TRANSFORMED STEM CELLS

3.1 INTRODUCTION

Our results, so far, strongly suggest that AnnexinA2 (ANXA2) represents a non-conventional 'receptor' for PG/gastrin peptides (51,112,182), and mediates activation of p65NFκB/β-catenin in response to PG, as presented in the previous chapter (51). Based on the published reports from our laboratory, we already know that ANXA2 expression is required for inducing proliferative/anti-apoptotic effects of PG on target cells *in vitro* (51,112,182). My results in chapter 2, additionally confirmed that ANXA2 mediates proliferative effects of PG on intestinal crypt cells, *in vivo,* as well*,* which were published last year by us (51). We additionally discovered that cell-surface-ANXA2 (CS-ANXA2) mediates endocytotic internalization of PG, which is required for measuring biological effects of PG (51,213).

Our results in chapter 2, as recently reported (51) demonstrated that over-expression of gastrin-cDNA (PG) in HEK293-cells (HEK-mGAS cells) significantly increased activation/expression of NFκBp65/β-catenin, associated with increased proliferation of the cells. As a continuation of these studies, I next examined if the dramatic changes measured in HEK-mGAS cells, in response to autocrine PG, can perhaps increase clonogenic/tumorigenic potential of cells. Our results, as presented in

this chapter, demonstrate for the first time that over-expression of autocrine-PG in embryonic HEK293-cells, imparts tumorigenic/metastatic potential to cells.

Our results in chapter 2, as recently reported (51), also demonstrated a significant increase in the relative expression levels of DCAMKL-1/CD44/ANXA2 in HEK-mGAS vs HEK-C cells; in the studies presented in this chapter, we examined if % cells expressing the indicated markers are also elevated. A critical role of CS-ANXA2 in metastasis of epithelial-cancers has been reported (195,214,215). Since HEK-mGAS cells developed metastatic potential, we examined the possibility if HEK-mGAS derived stem-cells had acquired the ability to co-express CS-ANXA2. We report for the first time that a high % of CS-ANXA2 positive HEK-mGAS cells, co-expressed stem-cell-markers, CD44 and DCAMKL-1, which may represent the transformed phenotype of stem-cells.

Non-adherent cell cultures, select for growth of stem-cells as spheroids (216). Surprisingly, we discovered that HEK-C cells formed well-rounded spheroids with a distinct, rim-like, perimeter encircling the spheroid, while HEK-mGAS cells formed amorphous spheroids, without a distinct rim-like perimeter. Elevated levels of CS-ANXA2 are associated with increased expression of matrixmetalloproteinases (MMPs) and invasion (217). Since we measured high levels of CS-ANXA2/MMPs in HEK-mGAS vs HEK-C cells (current studies), we examined the impact of altering expression levels of CS-ANXA2/ANXA2 on spheroid-morphology. Our results demonstrate that either down-regulation of ANXA2/CS-ANXA2, or enrichment of cells for CS-ANXA2, significantly altered spheroid-morphology, suggesting the novel possibility that phenotypic differences in spheroidal growths may predict tumorigenic/metastatic potential of cells.

3.2 Materials and Methods

In this section, only reagents and methods that have not been described in previous chapters are listed below.

3.2.1 Materials

Antibodies used included anti-GPCR-GPR49 (LGR5) for FACS, anti-Ki67 (Abcam, Cambridge, MA), anti-LGR5/GPR49 for IF (Abgent, San Diego, CA). Recombinant human PG (rhPG) and anti-PG-antibodies were generated in our laboratory as described (115). Anti-immunoglobulin G (IgG), coupled to horseradish peroxidase, were from Amersham. Alexa Fluor-488 and Alexa Fluor-594 coupled secondary IgG were from Invitrogen (Carlsbad, CA). Luciferase reporter plasmids for measuring activation of β-catenin (TOPFlash wild type and FOPFlash mutant) were obtained from Dr. Bert Volgestein (Johns Hopkins, Baltimore, MD). Smart Pool of target-specific small interfering RNA (siRNA) and Non-Targeting (control) siRNA Pool was purchased from Dharmacon (Lafayette, CO). Lentiviral shRNA plasmid for targeting hANXA2 was obtained from Open Biosystems Products, Huntsville, AL**.**

3.2.2 Cell-culture and generation of PG-expressing HEK-mGAS clones

HEK293 and HCT-116 cells, obtained from ATCC, were maintained in DMEM/F12 as described (51,182). Eukaryotic expression plasmid containing full-length coding sequence for triple-double mutant hGAS gene (R57A-R58A, K74A-K75A, R94A-R95A) (53), was transfected into HEK293-cells to create stably-expressing hPG-clones (HEK-mGAS), and confirmed, as described (51). Vector-transfected clones (HEK-C) were used as control.

3.2.3 In vitro growth assays and in vivo tumorigenic/metastatic assays

Cell growth was measured in an MTT (3-4,5-Dimethylthiazol-2-yl) or soft-agar assay (clonogenic growth) as described (114). Cells were inoculated in athymic (SCID/Nude) mice to grow either sub-dermal xenografts, or orthotopic-growths in cecum, or metastatic-growths in liver/lung after intrasplenic-inoculations.

3.2.3.1 Preparation of cells for inoculation into the athymic (SCID/Nude) mice

Sub-confluent cells in cultures were scraped and re-suspended in phosphate buffered saline (PBS) as single cell suspensions. $5x10^6$ cells/100µl PBS were inoculated on right and left flanks of female athymic SCID mice (Harlan Sprague Dawley) for inducing growth of sub-dermal xenografts. Similarly, $5x10^6$ cells were inoculated in the cecum, after making a <1cm vertical incision in the abdomen of the anesthetized mice (by our approved IACUC protocols), followed by suturing the dermis and clipping the skin with wound clips. For intrasplenic inoculations, $2x10^6$ cells/50µl PBS were inoculated in the tip of the spleens, after making a <1cm incision on the dorsal side (left of center, right below the ribs); the incision was sutured and clipped as described above. Mice receiving intrasplenic inoculations were subjected to splenectomy after 24h of inoculation to avoid splenic/peritoneal growths. Majority of mice inoculated with HEK-C clones did not show palpable growths even after 6wks. After 4-6wks from time of inoculation, tumors were harvested, dissected free of host tissue, patted dry and weighed. Where indicated, mice were also inoculated with cells, stably expressing firefly-luciferase (Luc); Luc-expressing tumors were imaged *in vivo*, as described below.

3.2.4 Preparation of lentiviral-plasmids encoding firefly luciferase (Luc)

Plasmid encoding Luc in lentivirus packaging plasmid was generated by amplifying the gene by PCR. The plasmid pFB-Luc (Stratagene; La Jolla, CA) was used as a template for this purpose. Primers used contained the sequences for flanking restriction endonucleases (*Bam*HI and *Apa*I) and the resulting product was ligated into the lentivirus packaging plasmid pLenti6 (Invitrogen; Carlsbad, CA). The resulting pLenti6-Luc construct was confirmed by DNA sequencing in the recombinant core facility at UTMB.

3.2.4.1 Lentivirus preparation

Lentiviruses were generated by transfecting 293FT cells with the ViraPower packaging mix (encodes HIV structural proteins and the glycoprotein of vesicular stomatitis virus) into 293FT cells, together with the firefly packaging plasmids described above. After 2 days viruses were collected in the culture supernatant and concentrated by centrifugation at 35,000 x g in a swinging bucket rotor for 45 minutes at 4 °C. The viral pellet was then resuspended in Dulbeco's PBS to 10^6 particles/ml. The viral titer was determined by serial dilution of virus and by infecting HEK293 cells. Our previous work has shown that 100 cps corresponds to approximately 1 cfu and this correlation was used to estimate titer.

3.2.4.2 Cell infection for establishing Luc stable transfectants

Cells were grown in DMEM medium supplemented with 2.0 mM L-Glutamine (Invitrogen; Calsbad, CA), penicillin/streptomycin (Invitrogen; Carlsbad, CA) and 10% heat-inactivated FBS (HyClone; Logan, UT). The cells were plated at 20% confluence onto 6-well plate. 24h later, virus was added to give a multiplicity of infection of 0.1

(infection rate of 10%). 48h post-infection, cells were split to 10% confluence and the culture medium was replaced with medium containing blasticidin (1.5 ug/mL). The cells were then cultured for 14 additional days, exchanging culture medium every 2 days. During this time most cells died and the remaining drug resistant cells were expanded. Luciferase-expression by cells was confirmed in luciferase assays measured as described (51,112). Briefly, firefly luciferase-activity was measured using Steady-Glo Luciferase Assay Reagent, as recommended by manufacturer (Promega, Madison, WI). The same assay was used to measure luciferase expression in cells transfected with TOP/FOP plasmids, for results presented in **Fig 3.12C.**

3.2.5 In vivo imaging of Luc-expressing tumors

Athymic nude mice were inoculated with HEK-mGAS-Luc cells (generated as described above) for growing either primary sub-dermal xenografts or orthotopic growths in the cecum, as described above. To examine the growth of Luc-expressing cells as either sub-dermal vs orthotopic tumors, mice were injected s.c. with 30mg/kg XenoLight D-Luciferin Potassium Salt substrate (Caliper Life Sciences; Hopkinton, MA) in saline and 15min later *in vivo* Luc activity was visualized using Kodak In-Vivo MS FX PRO Imaging System (Carestream Health, Inc.; Rochester, NY) according to manufacturer suggestions. The *in vivo* imaging of Luc-expressing tumors was conducted after 4-6wks of tumor inoculation to compare the growth of equal number of Luc-expressing cells as either orthotopic or sub-dermal tumors. HEK-mGAS, HEK-C and HCT-116 cells express CS-ANXA2 and bind PG with high-affinity (51,182), followed by internalized (51,213). Based on a previous report (180), we confirmed binding/biological effects of PG26 (26 amino-acids at C-terminal end of PG). PG26-peptide was conjugated to Lys-(5/6-FAM) at N-terminal end (FAM-PG26) by Peptide Core Facility

(http://www.tucf.org). The high relative-binding-affinity of FAM-PG26 for displacing binding of ^{125}I-rhPG to HEK-C cells was confirmed as previously described (115). Internalization of FAM-PG26 was also confirmed in target-cells, as a functional readout (**Fig 3.1A-C**). FAM-PG26 was then used for detecting primary/metastatic tumors as described.

3.2.6 Detection of primary/metastatic tumors in athymic nude mice using FAM-PG26

Mice were inoculated with HEK-mGAS cells for growing as either sub-dermal xenografts or metastatic tumors as described above. 4wks after inoculation, possible homing of FAM-PG26 to primary/metastatic growths was examined to determine if labeled PG26 peptide can potentially be used for diagnosing the presence of primary/metastatic tumors in proof-of-principle experiments. FAM (carboxy-fluorescein) is similar to FITC (fluorescein-isothyosionate) with similar excitation/emission. Mice were injected with 50nM of FAM-PG26 through tail vein, and the appearance of fluorescence at the sub-dermal tumor sites detected in Real Time in anesthetized mice using LT-9500 Illunatool Tunable Lighting System (Lightools Research http://lightools.com/It9500.html). The homing of FAM-PG26 to the tumor site was examined at 5,15,30,60min after tail vein injection. Since the fluorescence from FAM is not very strong, presence of metastatic tumors could not be examined in live animals using the fluorescence illuminator. Thus mice inoculated sub-dermally or intrasplenically (as described above) were sacrificed at an optimal time-period (15min) after tail vein injection with 50nM FAM-PG26, and sub-dermal tumors (from mice inoculated sub-dermally), and liver/lung tissues (from mice inoculated intrasplenically) were dissected

out, washed with chilled PBS in culture dishes and examined directly using the illuminator described above.

3.2.7 Co-immunoprecipitation (Co-IP) of ANXA2 with anti-PG-Antibodies (Abs) from sub-dermal xenografts

Tumors were immediately frozen after removal from mice in liquid nitrogen. The tissues were homogenized in Precellys24 (Breved Bertin Technologies, Biomedical, Miami, FL) at 4ºC, and processed for preparation of cellular lysates, as described previously (115), followed by co-IP of ANXA2 with anti-PG-Abs as described below. The lysates were pre-cleared for non-specific binding by incubating with 5µg of normal rabbit serum for 2h at 4°C, followed by incubating with 50µl sepharose H/C beads for 1h. The lysate was then incubated at 4°C overnight with 5µg of anti-PG monospecific polyclonal antibody (generated in our laboratory as described previously in (115). The bound complex was pulled down with Protein A sepharose beads for 6h at 4°C followed by washing the beads with RIPA buffer. The beads were suspended in 2X SDS sample buffer, boiled and processed for Western Blot analysis for ANXA2 and PG.

3.2.8 Analysis of % cells positive for expression of stem cell markers (DCAMKL-1/LGR5/CD44) and/or ANXA2/CS-ANXA2

Several methods were used to analyze presence of stem cell markers±ANXA2 as diagrammatically presented in **Fig 3.5A**. These methods are described in detail below.

3.2.8.1 Method I: Analysis of labeled-cells cytospun on glass slides

HEK-C and HEK-mGAS cells were cultured in 6-well plates. At ~70% confluency, cells were treated with 0.25% Trypsin-EDTA for ~30s, followed by addition

of growth medium containing 10% serum. Cells were then harvested into 15ml conical tubes, centrifuged at 300g for 5min, followed by two washes with PBS. Cells were finally re-suspended in growth medium containing 1% BSA (Bovine Albumin Serum), and incubated for 1h on a rocking platform with antibodies against either ANXA2, DCAMKL-1, CD44 or LGR5, tagged to a fluorophore (DyLight™ 488 NHS-Ester) (Thermo Scientific, Rockford, IL). The primary antibodies were tagged to fluorophores using the DyLight™ Microscale Antibody Labeling Kit (Thermo Scientific). Cells were washed 3 times with medium containing 1% BSA. Cells were then cytospun at 300g for 5min onto Superfrost®/Plus microscope slides (Fisher Scientific, Pittsburgh, PA) using a Shandon CytoSpin III cytocentrifuge (Cheshire, England). Images were acquired using Zeiss Axioplan epifluorescent microscope (META). Images were analyzed using METAMORPH, v6.0 software (Molecular Devices).

3.2.8.2 Method II: IF analysis of cells growing on cover slips

Cells were grown on glass cover slips in 24-well plates as described previously (51). At ~70% confluency, cells were processed for IF staining as previously described (5,51). Cells were fixed using a 1:1 ratio of acetone:methanol solution at -20˚C for 20 min. Cells were then washed 3x with 1X PBS, and blocked with 5% goat serum for 1h. Cells were then stained with either ANXA2-antibody (1:200), anti-DCAMKL-1-antibody (1:200), anti-CD44-antibody (1:100) or anti-LGR5-antibody (1:100). Excess antibody was washed off, and cells were incubated with either goat anti-rabbit-IgG coupled to Alexa Fluor 488 (for detecting DCAMKL-1 and LGR5) or goat anti-mouse-IgG coupled to Alexa Fluor 594 (for detecting ANXA2 and CD44). Excess antibody was washed off and cells were incubated with 4', 6-diamidino-2-phenylindole (DAPI) for 2 minutes. Cover slips were then mounted onto glass slides using FluorSave™ Reagent

(CALBIOCHEM, La Jolla, CA), and images acquired using Zeiss Axioplan epifluorencent microscope and images analyzed using as described above.

3.2.8.3 Method III: Analysis of cells by FACSorting and FACScan

HEK-C and HEK-mGAS cells were cultured in 6-well plates, and processed for labeling with primary antibodies as described above in Method I. Primary antibody labeled cells were analyzed using either the Becton-Dickinson FACSaria I (for FACSorting) or the LSII Fortessa (for FACScan) (Carlsbad, CA) in the FACS Core Facility at UTMBHealth. In a few experiments, cells FACSorted into 2 distinct populations of CS-ANXA2(+) or CS-ANXA2(-), using anti-ANXA2 antibody, were grown as 3D-spheroids in non-adherent cultures as described below. Cells subjected to FACScan analysis were analyzed for % cells positive for specific markers expressed on the cell surface; co-expression of dual markers on the cell surface was examined by this method.

3.2.9 In Vitro growth of cells as spheroids

HEK-C and HEK-mGAS cells were plated at a density of 5000 cells/well into 24-well ultra low-attachment plates (Costar, Corning NY). Cells were suspended in serum-free media containing DMEM/F12(1:1) + 1% Anti-Anti Antibiotic-Antimycotic' supplemented with B-27 (50X) (all from Invitrogen), epidermal growth factor (EGF) 20ng/ml and fibroblast growth factor (bFGF) (10ng/ml) (both from Sigma-Aldrich, St Louis, MO). Media was changed every 2-3 days and the formation of spheroids monitored daily. Spheroids were imaged at 4x, 10x and 40x using white light microscopy (Nikon Eclipse TS100, Melville, NY).

3.2.10 Processing of spheroids for embedding, sectioning and staining

Spheroids floating in non-adherent cultures, at days 6-14 of growth, were gently washed with PBS and fixed overnight using 10% formalin. Spheroids were then re-suspended in 2% agar gel containing 0.05% sodium azide. Agar gel was allowed to solidify at 4˚C for 20min prior to processing the samples for paraffin embedding and sectioning. Embedding and sectioning was performed in the Research Histopathology Core at UTMBHealth, and the sections were processed for H&E (hemotoxylin and eosin), immunohistochemistry (IHC) and immunofluorescent (IF) staining for specific protein markers (as published previously, 51).

3.2.11 Western Blot (WB) analysis

Cells growing either as 2D-cultures, 3D-spheroids or sub-dermal tumors in mice were harvested and processed for preparing cellular-lysates, followed by electrophorosis and transfer to PVDF-membranes as described (51,182). Blots were cut into horizontal strips containing target or loading-control proteins, and processed for WB (as described previoulsy, 51). Antigen-antibody complexes were detected with chemiluminescent reagent kit (GE Health Care). Membrane-strips containing either target or loading-control proteins were simultaneously exposed to autoradiographic films. Relative band-density on scanned autoradiograms was analyzed using Image J program (rsbweb.nih.gov/ij/download), and expressed as a ratio of β-actin in the corresponding samples.

3.2.12 Transient-transfection of cells with oligonucleotides

HEK-C/HEK-mGAS cells, seeded in 96-well plates were transfected with 5pmol of either DCAMKL-1 or control siRNA using Lipofectamine^{TM} 2000 (Invitrogen), as

described (51). Transfected cells were propagated in normal growth medium containing 10% FCS, and growth examined after 48h in an MTT assay. In a few experiments, pre-transfected cells were washed and transiently-transfected with promoter-reporter-plasmids (TOPFlash or FOPFlash) to measure relative activation of β-catenin, as described (51).

3.2.13 Statistical analysis

Data are presented as mean±SEM of values obtained from 4-8 samples/2-3 experiments. To test for significant differences between means, nonparametric Mann-Whitney test was employed using Statview 4.1 (Abacus Concepts, Inc., Berkeley, CA); *P* values were considered statistically significant if less than 0.05.

3.3 RESULTS

3.3.1 Clonogenic/tumorigenic potential of HEK-mGAS vs HEK-C clones

HEK-mGAS clones were confirmed to stably express full-length PG as previously described (51). Clonogenic growth of HEK-mGAS/HEK-C clones on soft-agar is presented in **Fig 3.2Ai**. Number of colonies formed/dish from HEK-mGAS clones (mGAS1-3) vs an HEK-C clone increased from ~2-fold (1% FCS) to >4-fold (10% FCS) **(Fig 3.2Aii)**. Tumorigenic-potential of cells was examined *in vivo* as described in Methods. Representative sub-dermal tumors from nude mice are shown in **Fig 3.2Bi**. Only 20% mice inoculated with HEK-C cells developed palpable tumors **(Fig 3.2Bii)**, suggesting negligible tumorigenic potential of HEK-C cells, similar to wtHEK293-cells. All mice inoculated with HEK-mGAS/HCT-116 cells formed sub-dermal tumors with almost identical weights **(Fig 3.2Bii-iii)**. Thus overexpression of PG in the background of

HEK293-cells resulted in significantly increasing tumorigenic potential of cells. HEK-mGAS-Luc cells, stably expressing firefly-luciferase, were inoculated orthotopically (ORT) within the cecal wall and imaged as described in Methods **(Fig 3.2Ci)**. Orthotopic-tumors were slightly smaller than sub-dermal tumors (P), but gave rise to metastatic (MET) growths in the liver **(Fig 3.2Ci-ii)**. These results suggest that orthotopic tumors can potentially metastasize, mimicking metastatic spread of *in situ* colorectal-adenocarcinomas (CRC). Intrasplenic inoculation of HEK-mGAS/HEK-mGAS-Luc cells resulted in metastatic lesions in the livers, within 3-4wks of inoculation; representative visual **(Fig 3.2Di)** and bioluminescent **(Fig 3.2Dii)** images of HEK-mGAS/HEK-mGAS-Luc tumors, are shown, respectively. Presence of metastatic-lesions in liver/lung was confirmed by H&E and IF staining **(Fig 3.32A-C)**. Since HEK-mGAS cells express autocrine-PG, both primary (**Fig 3.3Di**) and metastatic-lesions **(Fig 3.3B-E)** were positive for PG staining, while sub-dermal HEK-C tumors were negative **(Fig 3.3Di)**; normal (NOR) livers from mice were negative for PG expression, as expected **(Fig 3.3E).** Co-immunoprecipitation of ANXA2 with PG was confirmed in Western-Blots of sub-dermal HEK-mGAS tumors **(Fig 3.3Dii)**. ANXA2 strongly co-localized with PG in HEK-mGAS metastatic-lesions, confirming metastasis to lungs/liver (**Fig 3.3B-C).**

3.3.2 Primary/metastatic lesions diagnosed with fluorescently-labeled PG

High-affinity-ligands of CS-ANXA2 have been developed to detect tumors (197). Since PG binds CS-ANXA2 with high-affinity (51,112,182), we examined if labeled-PG peptides can detect primary/metastatic-tumors. FAM-PG26, confirmed to be biologically active **(Fig 3.1)**, was used for reasons described in Methods. FAM-PG26, injected intra-tumorally, was retained for ~30min (representative image at 15min shown in **(Fig 3.4Ai).** Tail-vein injection of FAM-PG26 resulted in increasing accumulation of peptide at the

tumor-site from 0-15min followed by a rapid decline; representative images from a single mouse at 0,5,15,30 min, after tail-vein injection of FAM-PG26, are shown in **Fig 3.4Bi**; relative fluorescence-intensity from 3 mice are presented in **Fig 3.4Bii**. HCT116-xenografts also accumulated FAM-PG26 peptide from 0-15min, followed by a rapid decline; representative image at 15min is shown in **Fig 3.4Aii**. Representative images from resected tumors after 15min of tail-vein injection with either FITC (used as control) or FAM-PG26 are shown in **Fig 3.4Ci-ii,** demonstrating focal uptake/retention of labeled-peptide. Metastatic lesions in liver and lung specimens were detected after 15min of FAM-PG26 injection **(Fig 3.4Di-ii)**; once again the lesions were positive for FAM-PG26 up-take in focal areas.

3.3.3 Up-regulation of % cells expressing CS-ANXA2/ANXA2 and stem-cell-markers in HEK-mGAS vs HEK-C cells

Three separate methods (Methods I-III) (described in **Fig 3.5A**) were used to define % cells positive for stem-cell-markers and CS-ANXA2/ANXA2. Representative staining of cells growing on cover slips, for the indicated markers (Method-II) are presented in **Fig 3.6A**. Representative results with FACSorting of cells (Method-III), using antibodies against stem-cell-markers (DCAMKL-1/CD44/LGR5), and ANXA2, are presented in **Fig 3.5B**. Results with all three methods from 2-3 separate experiments are presented as % cells positive for the indicated proteins in **Fig 3.6B**. Percent cells positive for ANXA2/CS-ANXA2 and the indicated stem-cell-marker(s) were significantly increased in HEK-mGAS vs HEK-C cells **(Fig 3.6B; Fig 3.5B)**. Importantly, all three methods gave similar results.

3.3.4 High % of ANXA2 positive cells co-express DCAMKL-1/CD44

IF staining of cells, by Method-II, suggested that significant % of HEK-C/HEK-mGAS cells co-express ANXA2 with a stem cell marker **(Fig 3.7A)**. To further confirm this finding, cells were FACSorted with Anti-ANXA2-Abs, and cells positive (ANXA2+) or negative (ANXA2-) for CS-ANXA2, were stained for stem-cell-markers **(Fig 3.7B)**. HEK-C cells were negative, while HEK-mGAS cells were positive for PG staining, irrespective of ANXA2 status; PG strongly co-localized with ANXA2 in HEK-mGAS ANXA2+ve cells **(Fig 3.7B; Fig 3.8A)**. ANXA2-ve cells stained poorly while ANXA2+ve cells stained strongly for ANXA2 **(Fig 3.7B)**. Staining intensity for LGR5/DCAMKL-1/CD44 was highest in ANXA2(+) HEK-mGAS cells **(Fig 3.7B; Fig 3.8B-C)**. Percent cells co-expressing ANXA2 and a stem-cell-marker, were quantified by FACScanning (as described in Methods), and results are presented in **Fig 3.7C-E**. Significantly higher % of HEK-mGAS cells co-expressed ANXA2 and the indicated stem-cell-marker **(Fig 3.7C)**. Results were recalculated as % ANXA2+ve cells which co-expressed DCAMKL-1/CD44/LGR5; surprisingly almost all ANXA2+ve cells co-expressed CD44 in both HEK-C/HEK-mGAS cells, while a lower % co-expressed DCAMKL-1/LGR5 **(Fig 3.7D)**. Percent cells positive for a stem cell marker along with CS-ANXA2 were also analyzed by FACScan **(Fig 3.7E)**. Once again almost all CD44+ve cells co-expressed CS-ANXA2, while ~50-80% of DCAMKL-1+ve cells co-expressed CS-ANXA2; much lower % of LGR5+ve cells co-expressed CS-ANXA2 **(Fig 3.7E)**. Importantly, significantly higher % of DCAMKL-1/LGR5 positive HEK-mGAS cells co-expressed CS-ANXA2 **(Fig 3.7E),** suggesting that combined expression of these proteins may impact tumorigenic/metastatic potential of cells.

3.3.5 Morphological differences in spheroidal growths of HEK-C/HEK-mGAS cells

Stem cells from normal/cancerous tissues have inherent potential of amplifying and forming spheroidal structures in non-adherent cultures (216,218). Since stem cell populations were significantly up-regulated in HEK-mGAS cells, we examined possible increase in rate of spheroid-formation by HEK-mGAS vs HEK-C cells. Both HEK-C/HEK-mGAS cells formed spheroidal structures at days 5-6, with significant morphological differences **(Fig 3.9A)**. Non-adherent growth of HEK-mGAS cells was more pronounced at initial time-points (24-48h), but appeared to even out by day 6 **(Fig 3.9A)**. HEK-C spheroids appeared well-rounded with a distinct, rim-like, perimeter (arrows), while HEK-mGAS spheroids lacked a distinct, rim-like, perimeter and were more amorphous in shape **(Fig 3.9A)**. Since wtHEK-mGAS spheroids were amorphous and appeared to be less well aggregated, especially at the periphery of the spheroids, we could not process intact HEK-mGAS spheroids for staining. Representative sections of HEK-C spheroids, stained with specific-Abs are presented in **Fig 3.9B**. Surprisingly, DCAMKL-1+ve and LGR5+ve cells were present along the periphery of the spheroids, while CD44(+) cells were present throughout the spheroids. None of the stem cells (positive for CD44/DCAMKL-1), co-expressed ANXA2 in HEK-C spheroids, while clumps of HEK-mGAS spheroids, leftover after processing, co-expressed ANXA2 with CD44/DCAMKL-1 (representative data shown in **Fig 3.10A**). Anti-Ki67-Abs stained HEK-C spheroidal cells both at the periphery and within the spheroids **(Fig 3.9B)**, suggesting proliferating cells are present at the periphery and within the spheroids. DCAMKL-1+ve cells were also observed mainly around the edges of sub-dermal tumors from HEK-mGAS cells **(Fig 3.9B)**, suggesting that stem cell populations may be primarily present along the outer edges of tumors/spheroids **(Fig 3.9B; Fig 3.10B)**. Focal areas of the sub-dermal tumors, derived from HEK-mGAS cells, were also heavily

stained for CD44/ANXA2 by IHC, and the two proteins appeared to be expressed in the same areas **(Fig 3.10C)**; IF staining highlighted significant co-expression of CD44 and ANXA2 in these focal areas at the outer edges of the sub-dermal tumors **(Fig 3.10D)**.

3.3.6 Role of ANXA2 expression on spheroidal growths

We next examined the hypothesis that overexpression of CS-ANXA2/ANXA2 may have resulted in the inability of HEK-mGAS cells to form well-rounded spheroids. HEK-C cells expressing CS-ANXA2 were enriched by FACSorting with anti-ANXA2-Abs. Surprisingly, CS-ANXA2(+) HEK-C cells grew as amorphous-spheroids, while HEK-C cells negative for CS-ANXA2 continued to grow like wtHEK-C cells **(Fig 3.9C)**. Alternatively, HEK-mGAS cells were down-regulated for ANXA2 expression by transiently transfecting the cells with ANXA2-shRNA plasmids. HEK-mGAS cells transfected with control-shRNA developed amorphous-spheroids, while HEK-mGAS cells down-regulated for ANXA2 formed more compact spheroids, which could be processed for sectioning/staining more successfully (**Fig 3.9D**). Importantly, MMP2/7 expression in HEK-mGAS spheroids, down-regulated for ANXA2 expression, was significantly attenuated compared to that in HEK-mGAS spheroids, treated with control-shRNA **(Fig 3.9E)**, suggesting the possibility that ANXA2 may regulate secretion/expression of MMPs.

3.3.7 Relative expression of stem cell markers by HEK-mGAS vs HEK-C cells

Based on our current and previous studies (12), we now know that PG over-expression in HEK-mGAS cells significantly up-regulates relative expression levels of stem cell markers and ANXA2 and activates β-catenin/NFκBp65. It is, however, not known if enhanced expression/activation is maintained in HEK-mGAS cells growing as

spheroids/tumors. Cells growing either as 2D-cultures, 3D-spheroids or xenografts were processed for WB analysis. Representative data from 2-3 experiments are presented in **Fig 3.11A**; % change in the ratio of target proteins/β-actin in HEK-C vs HEK-mGAS samples was determined, wherein the ratios obtained for HEK-C samples was arbitrarily assigned a 100% value (dashed lines in each panel of **Fig 3.11B**). Enhanced expression of DCAMKL-1/LGR5/CD44 and ANXA2/β-catenin/*p*NFκBp65 in HEK-mGAS vs HEK-C cells was similarly increased in cells growing either as monolayer-cultures **(M)**, 3D-spheroids **(S)** or tumors **(T) (Fig 3.11A-B)**. HEK-mGAS cells growing as spheroids/tumors expressed significantly higher levels of PG than cells growing as monolayer-cultures, suggesting the novel possibility that HEK-mGAS cells growing as 3D-structures (*in vitro/in vivo*) may increasingly express endogenous PG.

3.3.8 Down-regulation of DCAMKL-1 attenuates activation of β-catenin and growth of HEK-C/HEK-mGAS cells in culture

Recent reports suggest that DCAMKL-1 may play an important role in growth of cancer cells (73,74). Cells were treated with either DCAMKL-1 siRNA or control siRNA **(Fig7A)**. Even though HEK-C cells expressed low levels of DCAMKL-1 **(Fig 3.6B; Fig 3.11A)**, proliferation of both HEK-C/HEK-mGAS cells was significantly down-regulated in DCAMKL-1 siRNA vs control siRNA treated cells **(Fig 3.12B)**, providing evidence that DCAMKL-1 may play an important role in proliferation of immortalized/transformed HEK293-cells. Surprisingly, activation of β-catenin (measured in a promoter-reporter assay) was also significantly attenuated in DCAMKL-1 siRNA vs control siRNA treated cells; activity of the mutant plasmid (FOP) remained unchanged **(Fig 3.12C)**. These results for the first time suggest that DCAMKL-1, may play a functional role in supporting proliferation of cells, via perhaps facilitating activation of β-

catenin, by as yet unknown mechanisms. Thus a possible cross-talk between stem cell markers and signaling pathways needs to be further examined in relation to proliferation/tumorigenesis of cells.

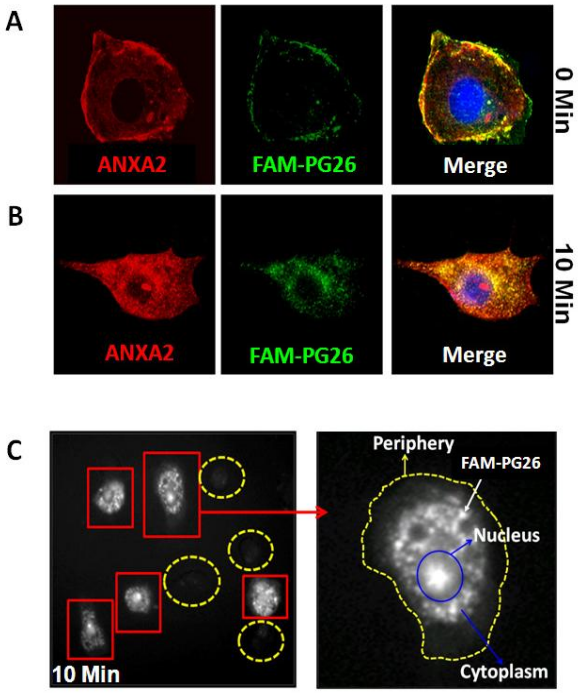

Figure 3.1 (*A-C*): Biological activity of FAM-PG26. We have previously reported specific binding of PG with CS-ANXA2 followed by rapid internalization of the peptide/ANXA2 complexes (5,51,112,182,213), which was required for measuring activation of NFκB/β-catenin in HEK-293 and IEC-18 cells (51,213). Relative binding affinity (RBA) of FAM-PG26 for displacing the binding of ^{125}I-rhPG was determined to be slightly higher than that of rhPG, by our published methods (115) (data not shown). Biological activity of FAM-PG26 was further examined in terms of binding and internalization of the peptide in IEC-18 cells, as previously described (51,213). Briefly, IEC-18 cells were seeded on glass cover slips and grown overnight. Cells were washed with PBS and incubated with 10nM FAM-PG26 for 0 and 10min. Cells were washed with chilled PBS and fixed in acetone:methanol. Immunostaining was done with Anti-PG-Abs and Anti-ANXA2-Abs by our published methods (51). Images were acquired using Carl Zeiss Axioplan epifluorescent microscope. Images were analyzed using METAMORPH, v6.0 software. Representative data, demonstrating binding and strong co-localization of FAM-PG26 with CS-ANXA2 at 0min (**A**), followed by internalization of FAM-PG26 in association with ANXA2 at 10min (**B**) are shown from 1 of 2 similar experiments. Co-localization of FAM-PG26 with ANXA2 appears bright yellow in the merged images (**A,B**). **C**= IEC-18 cells were also subjected to live cell imaging after incubating the cells with FAM-PG26. For live cell imaging, IEC-18 cells were grown overnight in black-well-dishes with transparent bottoms in growth medium containing 10% serum. Cells were washed with chilled PBS and incubated on ice for 20min to remove all serum. FAM-PG26 (10nM) was added in growth medium containing 0.1% serum, and cells moved to 37ºC. Cells were then washed with PBS and fresh medium added to the cells. Within 5-10min of adding FAM-PG26 to the cells, these dishes were transferred to the microscope stage equipped with Real Time imaging capabilities to capture images every 2min (BD Biosciences Pathways, 855, BD Biosciences, San Jose, CA). Representative images at ~10-15min are presented in **C**. Red outlined cells are positive for internalization of PG while yellow circled cells were negative for internalization, perhaps reflecting absence of CS-ANXA2 in these cells.

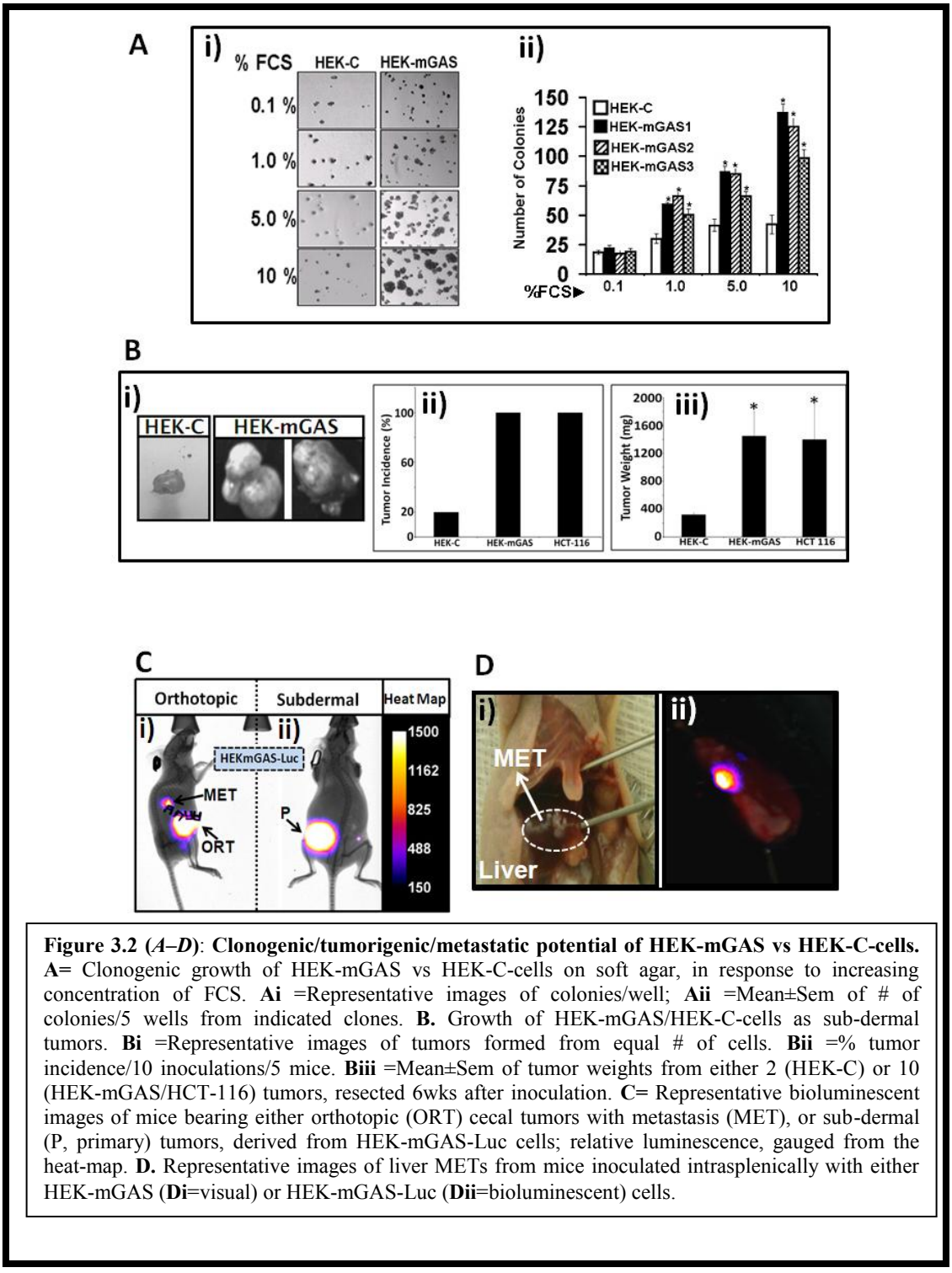

Figure 3.2 (*A–D*): **Clonogenic/tumorigenic/metastatic potential of HEK-mGAS vs HEK-C-cells.** **A=** Clonogenic growth of HEK-mGAS vs HEK-C-cells on soft agar, in response to increasing concentration of FCS. **Ai** =Representative images of colonies/well; **Aii** =Mean±Sem of # of colonies/5 wells from indicated clones. **B.** Growth of HEK-mGAS/HEK-C-cells as sub-dermal tumors. **Bi** =Representative images of tumors formed from equal # of cells. **Bii** =% tumor incidence/10 inoculations/5 mice. **Biii** =Mean±Sem of tumor weights from either 2 (HEK-C) or 10 (HEK-mGAS/HCT-116) tumors, resected 6wks after inoculation. **C=** Representative bioluminescent images of mice bearing either orthotopic (ORT) cecal tumors with metastasis (MET), or sub-dermal (P, primary) tumors, derived from HEK-mGAS-Luc cells; relative luminescence, gauged from the heat-map. **D.** Representative images of liver METs from mice inoculated intrasplenically with either HEK-mGAS (**Di**=visual) or HEK-mGAS-Luc (**Dii**=bioluminescent) cells.

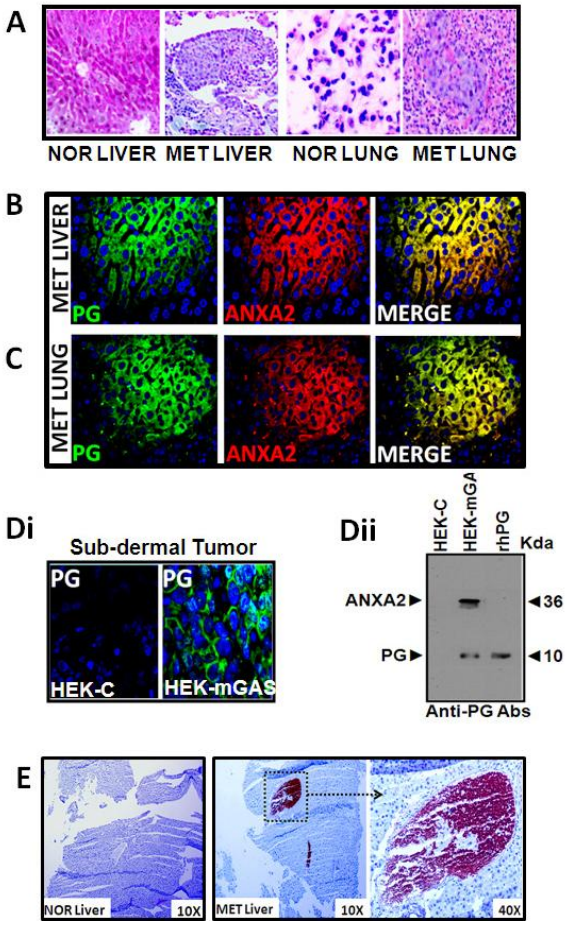

Figure 3.3 (*A-E*): Primary and metastatic tumors from HEK-mGAS-cells are positive for PG. **A**=liver and lung tissues were removed 4wks after intrasplenic inoculation of mice with HEK-mGAS cells and processed for paraffin embedding. Tissue sections from either normal livers and lungs, or tumor sections from metastatic lesions in liver and lungs were processed for H&E staining, and representative sections from either normal (NOR) or metastatic (MET) lesions are shown. **B-C**=liver/lung tissue sections (from **A**), confirmed to contain metastatic lesions, were processed for IF staining with anti-PG-Abs and anti-ANXA2-Abs as described previously (5,51). Representative sections from liver/lung tissues containing Met lesions, from 4 different mice, are presented in **B** (liver) and **C** (lung). **D**=sub-dermal primary tumors, 4wks after inoculation, were resected and processed for paraffin-embedding. Tumor sections (5µm) were processed for IF staining with anti-PG-Abs (**Di**) to confirm the stable expression of PG by HEK-mGAS tumor cells; HEK-C tumors were negative for PG staining as expected. **Dii**=co-immunoprecipitation of ANXA2 with anti-PG-Abs in HEK-C/HEK-mGAS tumors. Tumors were resected from mice as described above, and processed for co-immunoprecipitation of ANXA2 with anti-PG-Abs as described in methods. The Mr of ANXA2 and PG is shown on the right hand side; rhPG (recombinant human PG), was run as a control in lane 3. **E**. Liver tissues were removed 4wks after intrasplenic inoculation of mice with either vehicle control (NOR liver) or with HEK-mGAS cells (MET liver) and processed for paraffin embedding, sectioning and staining with anti-PG-Abs by IHC, as described (5). While no staining was observed in normal livers (as expected), strong staining was observed in the metastatic lesions within the liver. The black outlined box in the middle panel was further enhanced as shown in the right-hand panel.

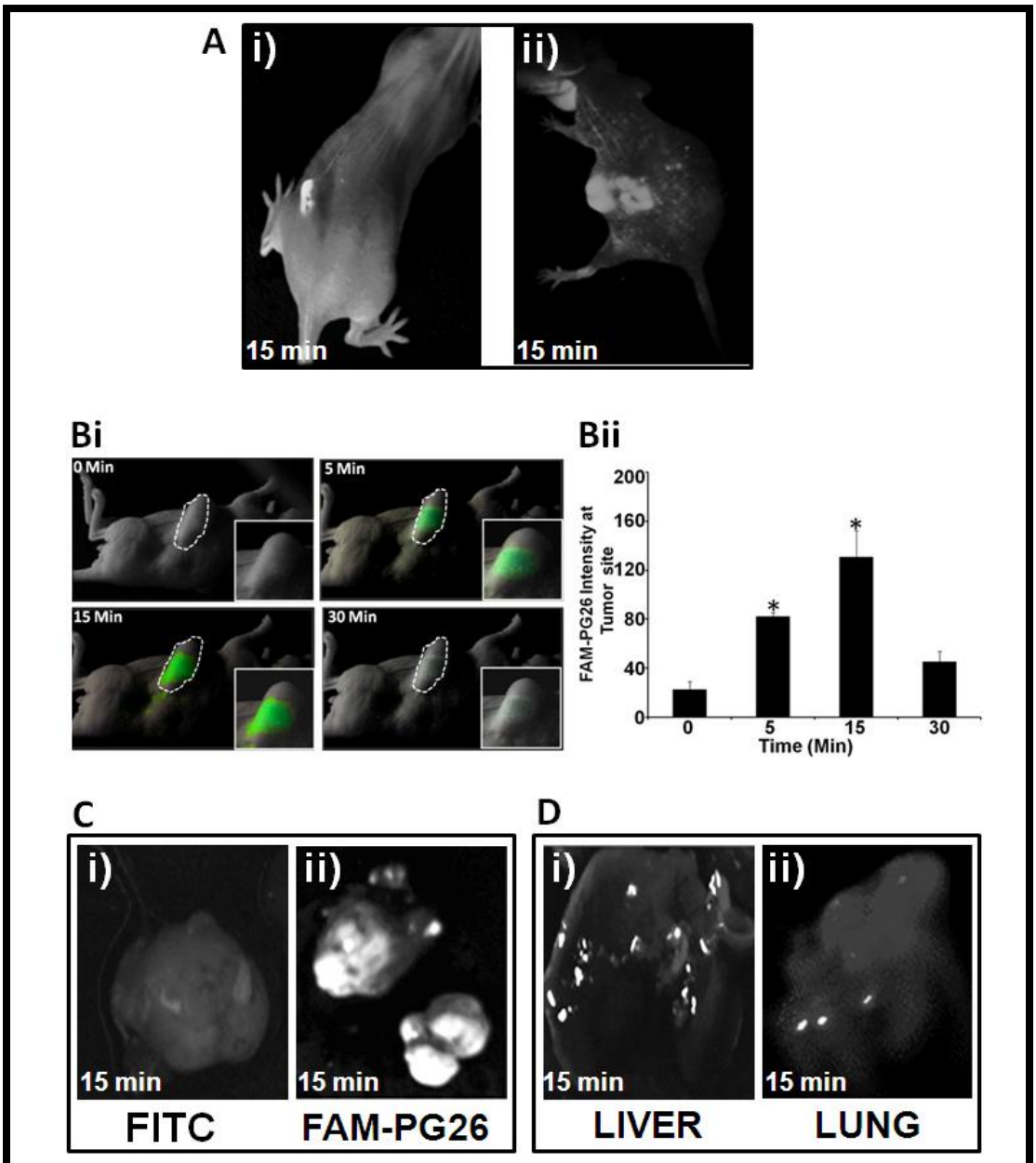

Figure 3.4 (*A–D*): **Detection of primary/metastatic tumors with FAM-PG26.** Fluorescense detection of FAM-PG26 in tumors derived from HEK-mGAS (**Ai,B,C,D**) and HCT-116 (**Aii**) cells. FAM-PG26 was injected either intratumorally (**Ai**) or in tail veins (**Aii,B,Cii,D**). Images were taken after indicated time-points either in intact anesthetized mice (**A,B**) or after resection of tumors/tissues(**C,D**). **(B)** =Time-dependent uptake of FAM-PG26 by sub-dermal tumors. **Bi** = fluorescent images from a representative mouse; **Bii** =Mean±Sem of relative fluorescence intensity at tumor site from 3 mice (described in methods). *=$p<0.05$ vs 0min values. **(Ci,Cii)** =sub-dermal tumors from mice injected with either FITC (**Ci,** control) or FAM-PG26 **(Cii). (D)**=liver/lung samples containing metastatic-lesions from mice injected with FAM-PG-26.

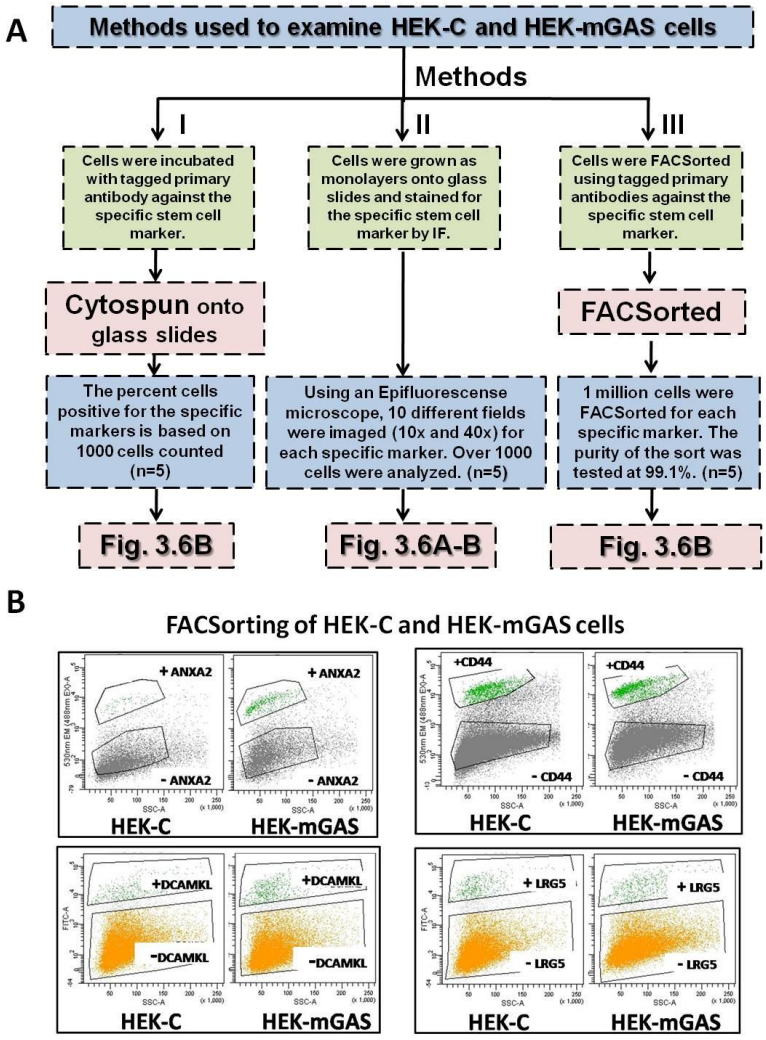

Figure 3.5 (*A-B*). A= Diagrammatic chart describing the 3 methods (I, II, III) that were used to analyze % cells positive for stem-cell-markers (DCAMKL-1, CD44, LGR5) and ANXA2/CS-ANXA2 in HEK-C vs HEK-mGAS-cells. Details for the methods used are described in methods**.** Over 1000 cells were analyzed/experiment for each method, and a total of 2-3 experiments were conducted/method. **B=. Cell populations positive (+) or negative (-) for the indicated proteins analyzed by FACSorting.** HEK-C/HEK-mGAS-cells, fluorescently labeled with specific antibodies against the indicated proteins (as described in Methods) were sorted using the Becton-Dickinson FACSaria I. X-axis of the graphs represents the site scatter (SSC) while the Y-axis represents the fluorescence intensity of the cells. Cells with relatively high intensity (above background levels) were delineated from cells poorly labeled.

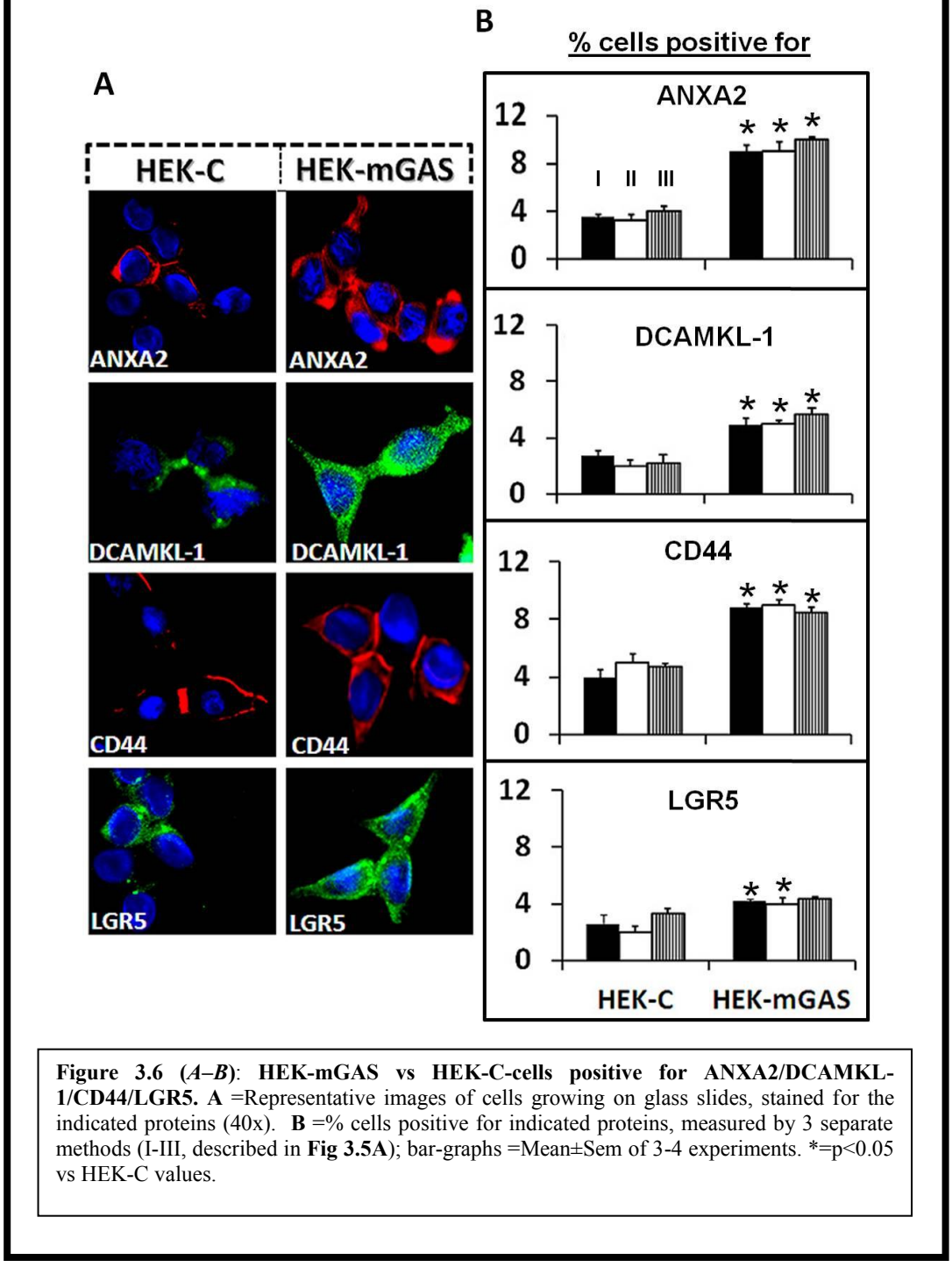

Figure 3.6 (*A–B*): HEK-mGAS vs HEK-C-cells positive for ANXA2/DCAMKL-1/CD44/LGR5. A =Representative images of cells growing on glass slides, stained for the indicated proteins (40x). **B** =% cells positive for indicated proteins, measured by 3 separate methods (I-III, described in **Fig 3.5A**); bar-graphs =Mean±Sem of 3-4 experiments. *=$p<0.05$ vs HEK-C values.

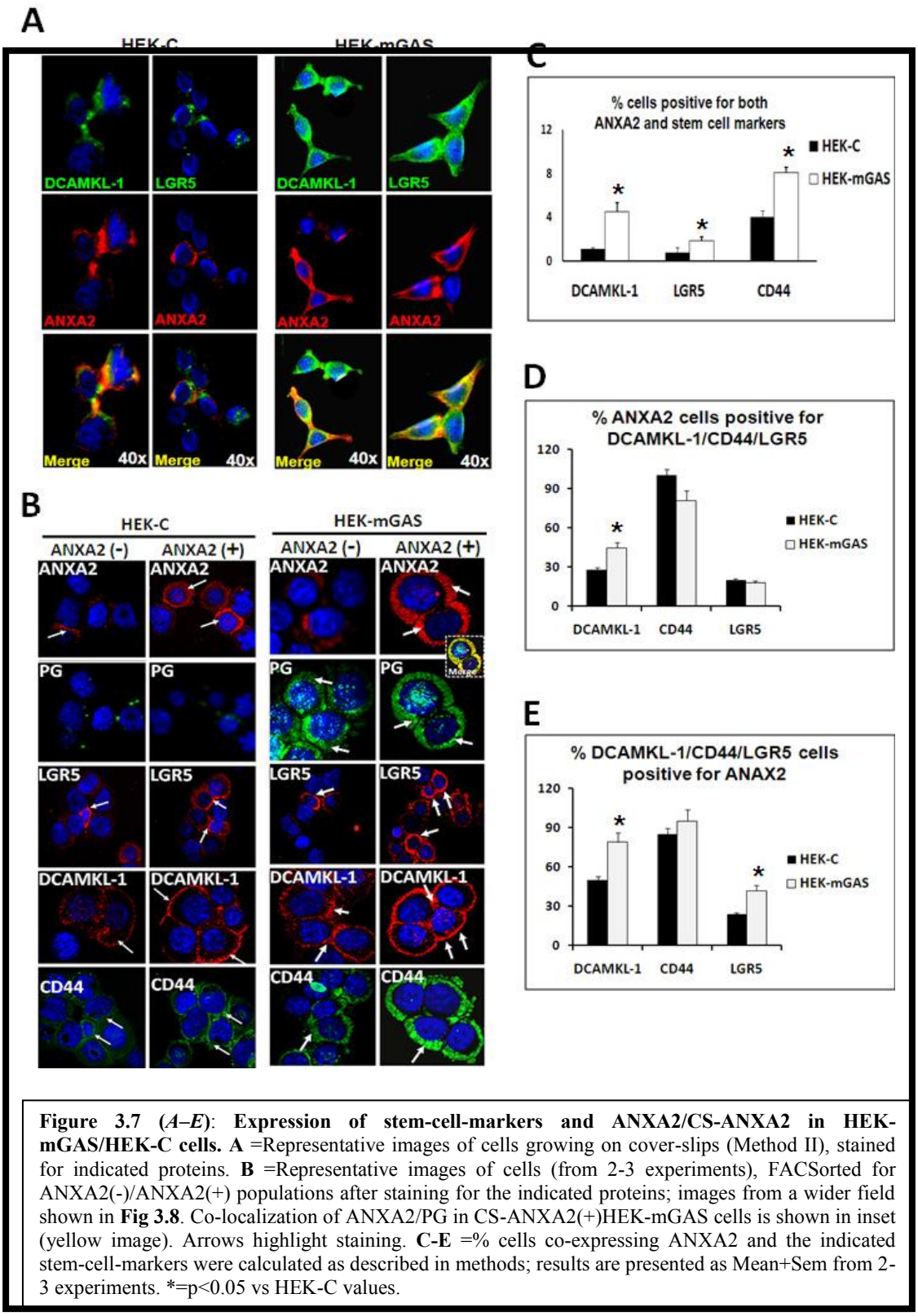

Figure 3.7 (*A–E*): Expression of stem-cell-markers and ANXA2/CS-ANXA2 in HEK-mGAS/HEK-C cells. A =Representative images of cells growing on cover-slips (Method II), stained for indicated proteins. **B** =Representative images of cells (from 2-3 experiments), FACSorted for ANXA2(-)/ANXA2(+) populations after staining for the indicated proteins; images from a wider field shown in **Fig 3.8**. Co-localization of ANXA2/PG in CS-ANXA2(+)HEK-mGAS cells is shown in inset (yellow image). Arrows highlight staining. **C-E** =% cells co-expressing ANXA2 and the indicated stem-cell-markers were calculated as described in methods; results are presented as Mean+Sem from 2-3 experiments. *=p<0.05 vs HEK-C values.

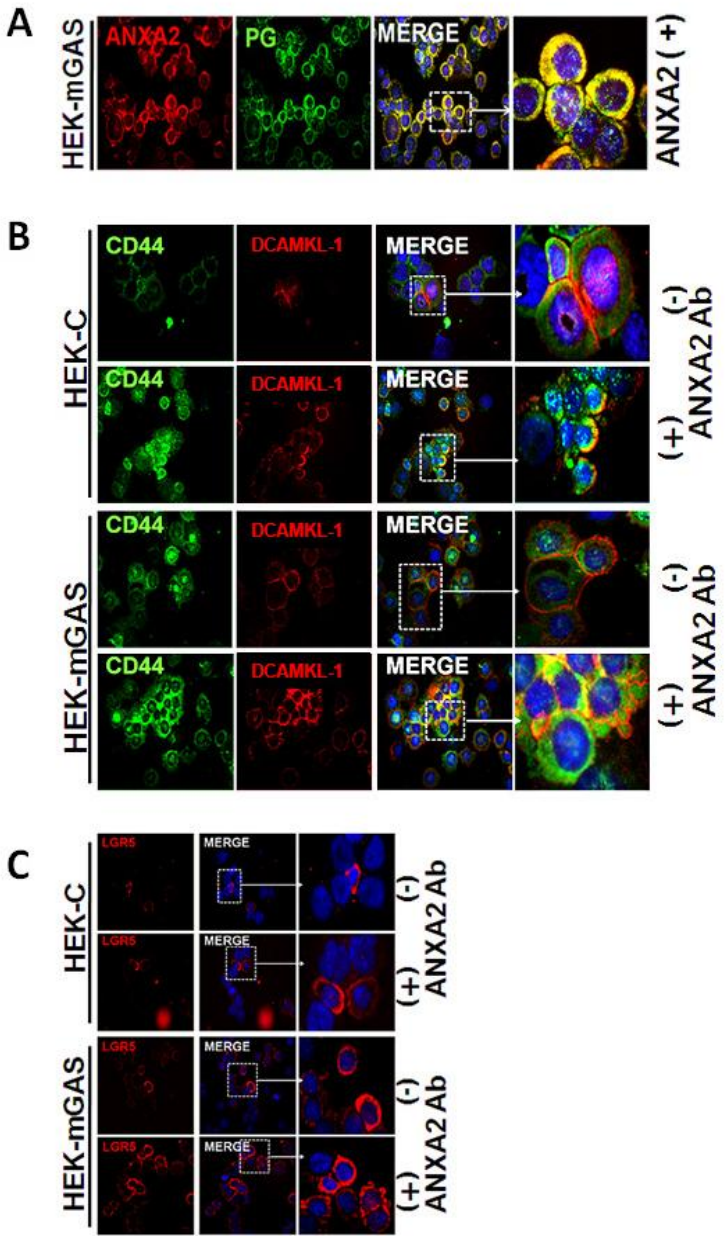

Figure 3.8 (*A-C*): Relative abundance of HEK-mGAS vs HEK-C cells co-expressing ANXA2 with stem-cell-markers. PG expression and co-localization of PG with ANXA2 was confirmed in almost all HEK-mGAS cells, FACSorted to be positive for CS-ANXA2 (**A**). Cells FACSorted to be positive(+) or negative (-) for CS-ANXA2 with anti-ANXA2-Ab (as described in legend of **Fig 3.7**) were processed for IF staining with the indicated stem-cell-markers. Representative data from 1 of 2 separate experiments, demonstrating the extent of co-staining in ANXA2(+) and ANXA2(-) cells for CD44 and DCAMKL-1 (**B**), and for LGR5 (**C**) are shown from HEK-mGAS vs HEK-C cells. As can be seen, ANXA2(+)HEK-mGAS cells had the highest % cells which co-stained for CD44; % cells co-staining with ANXA2 and a stem-cell-marker was in the order of CD44>DCAMKL>LGR5. A high % of cells positive for CS-ANXA2 were also positive for both CD44 and DCAMKL-1 in HEK-mGAS cells (lower-most panel in **B**).

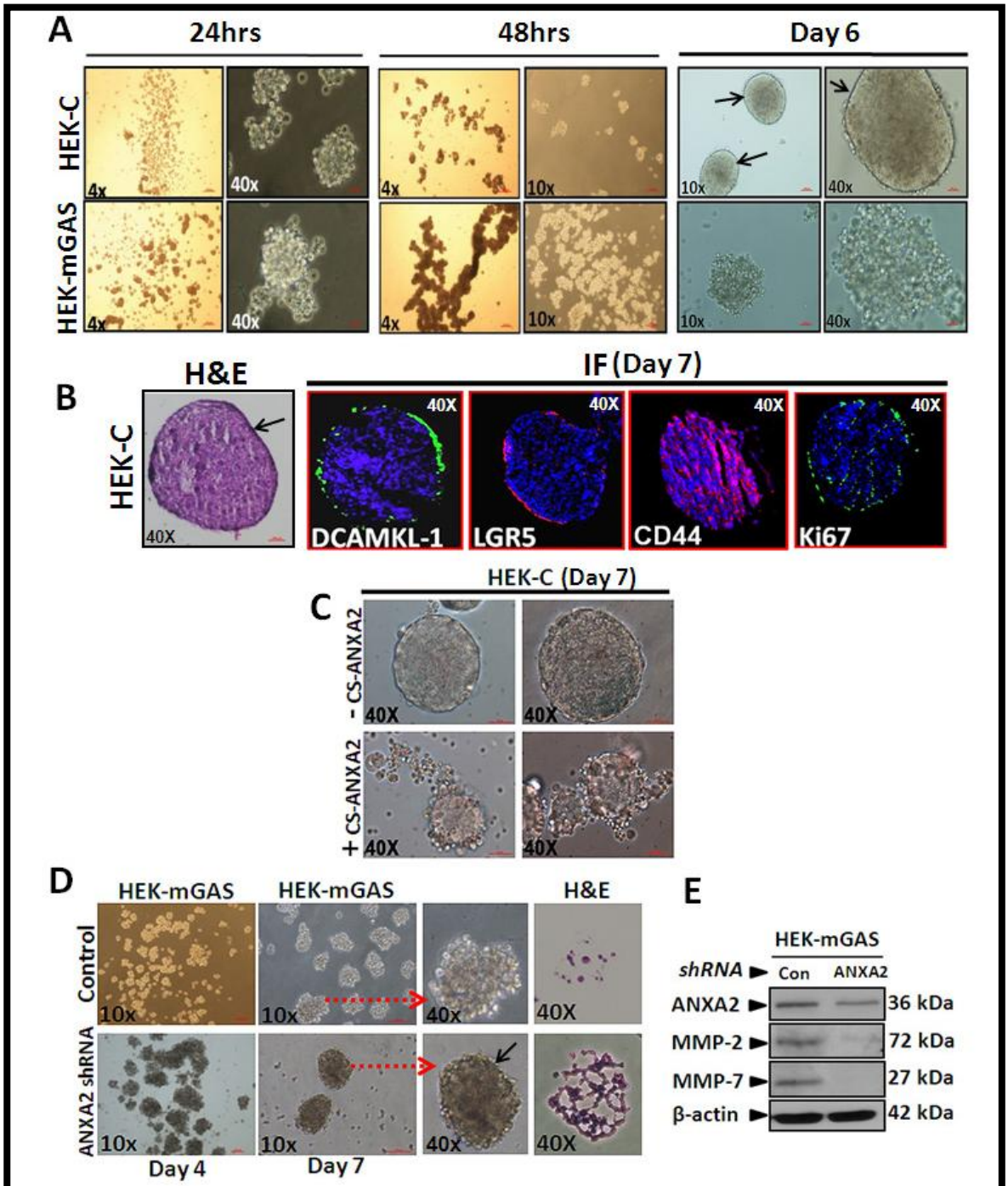

Figure 3.9. (*A–E*): **Morphology of HEK-C/HEK-mGAS spheroids in presence or absence of ANXA2 expression; effect on MMP levels. A**= Cell growth in non-adherent cultures after indicated time-points. **B**=Representative images of H&E/IF stained sections (5µm) from HEK-C-spheroids. **C**=HEK-C-cells, FACSorted for presence(+) or absence(-) of CS-ANXA2, and grown as spheroids, using equal # of cells; representative images at day 7. **D** =Representative images of spheroids from HEK-mGAS-cells, transfected with either control or ANXA2-shRNA plasmids; H&E stained spheroid sections shown in the last panel. Arrows point to enhanced images. **E** =relative levels of indicated proteins by WB analysis of HEK-mGAS-spheroids in **D** (day 7); data is representative of 4 blots from 2 experiments.

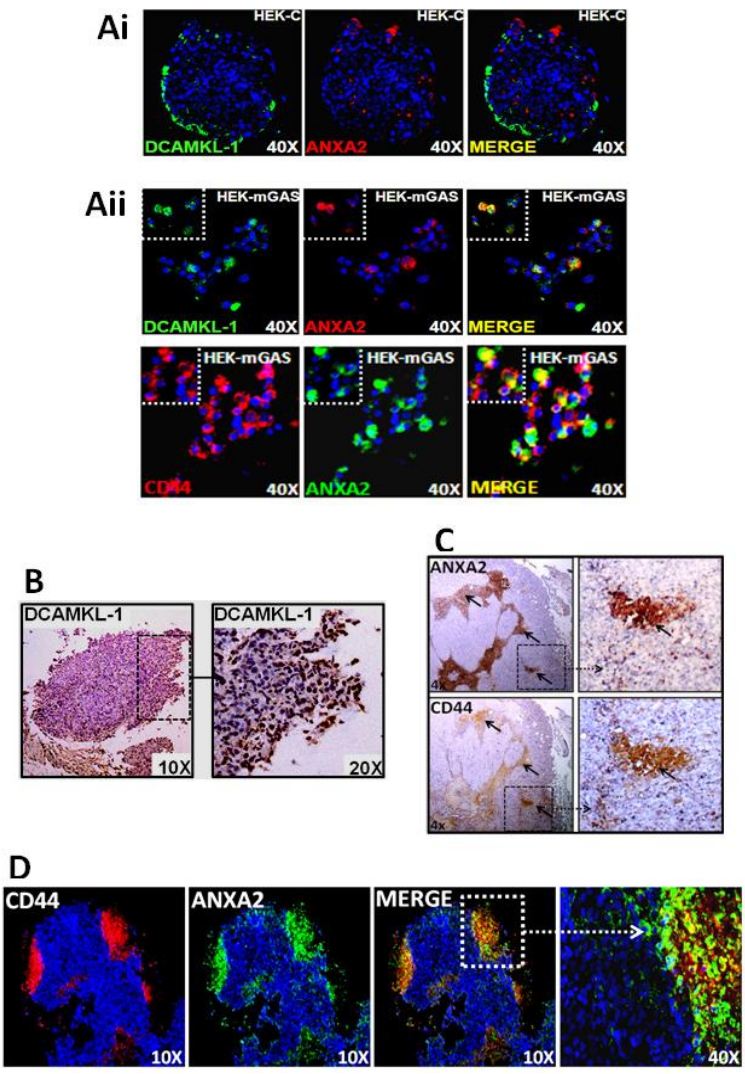

Figure 3.10 (*A-D*): A=Co-expression of ANXA2 and stem-cell-markers, CD44/DCAMKL-1 in HEK-C vs HEK-mGAS spheroids. The HEK-C and HEK-mGAS spheroids were processed as described in methods**.** As described in the text, since the HEK-C-spheroids were compact and surrounded by a perimeter, they remained intact during processing (upper panels), while the HEK-mGAS-spheroids largely disintegrated during processing but clumps of spheroidal cells remained which were processed for staining (lower panels). The sections and clumps of cells were subjected to IF staining for the indicated markers. As can be seen, the HEK-C-spheroidal cells did not co-stain for ANXA2 and the indicated stem cell marker in **Ai**. However, the HEK-mGAS spheroidal cells co-stained for ANXA2 and the indicated stem cell markers in **Aii**. The data presented are representative of >10 sections from 2 separate experiments. **B= IHC staining for DCAMKL-1 in HEK-mGAS tumor sections.** Sub-dermal tumors of HEK-mGAS-cells were processed for staining with anti-DCAMKL-Abs by IHC, as described (5.51). The brown staining for DCAMKL was largely concentrated at the outer edges of the tumors (left hand panel), which could be better observed at a higher magnification (right hand panel). We were unable to stain the sections by IHC for LGR5 using the available anti-LGR5-Abs. **C-D= IHC and IF staining for CD44/ANXA2 in HEK-mGAS tumors.** HEK-mGAS tumor sections were processed as described above and stained for either CD44 or ANXA2, as shown. Data are representative of 6 sections from 3 different mouse tumors. As can be seen, both CD44 and ANXA2 staining was observed in focal areas of the tumor by IHC **(C)**, which was confirmed by IF staining of the sections (**D**); yellow color in merged images suggests co-expression of CD44 and ANXA2 in the indicated focal areas.

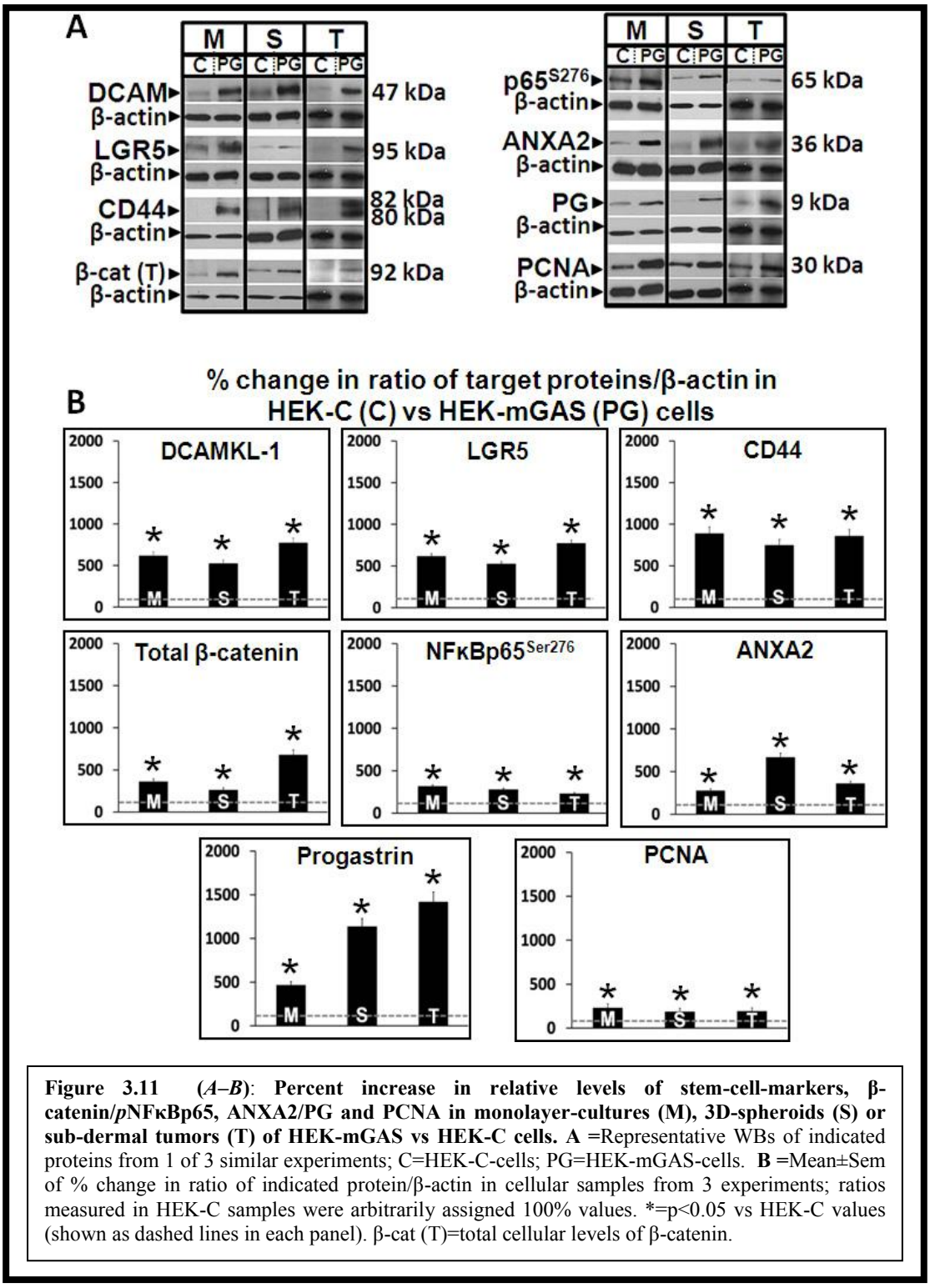

Figure 3.11 (*A–B*): Percent increase in relative levels of stem-cell-markers, β-catenin/*p*NFκBp65, ANXA2/PG and PCNA in monolayer-cultures (M), 3D-spheroids (S) or sub-dermal tumors (T) of HEK-mGAS vs HEK-C cells. A =Representative WBs of indicated proteins from 1 of 3 similar experiments; C=HEK-C-cells; PG=HEK-mGAS-cells. **B** =Mean±Sem of % change in ratio of indicated protein/β-actin in cellular samples from 3 experiments; ratios measured in HEK-C samples were arbitrarily assigned 100% values. *=p<0.05 vs HEK-C values (shown as dashed lines in each panel). β-cat (T)=total cellular levels of β-catenin.

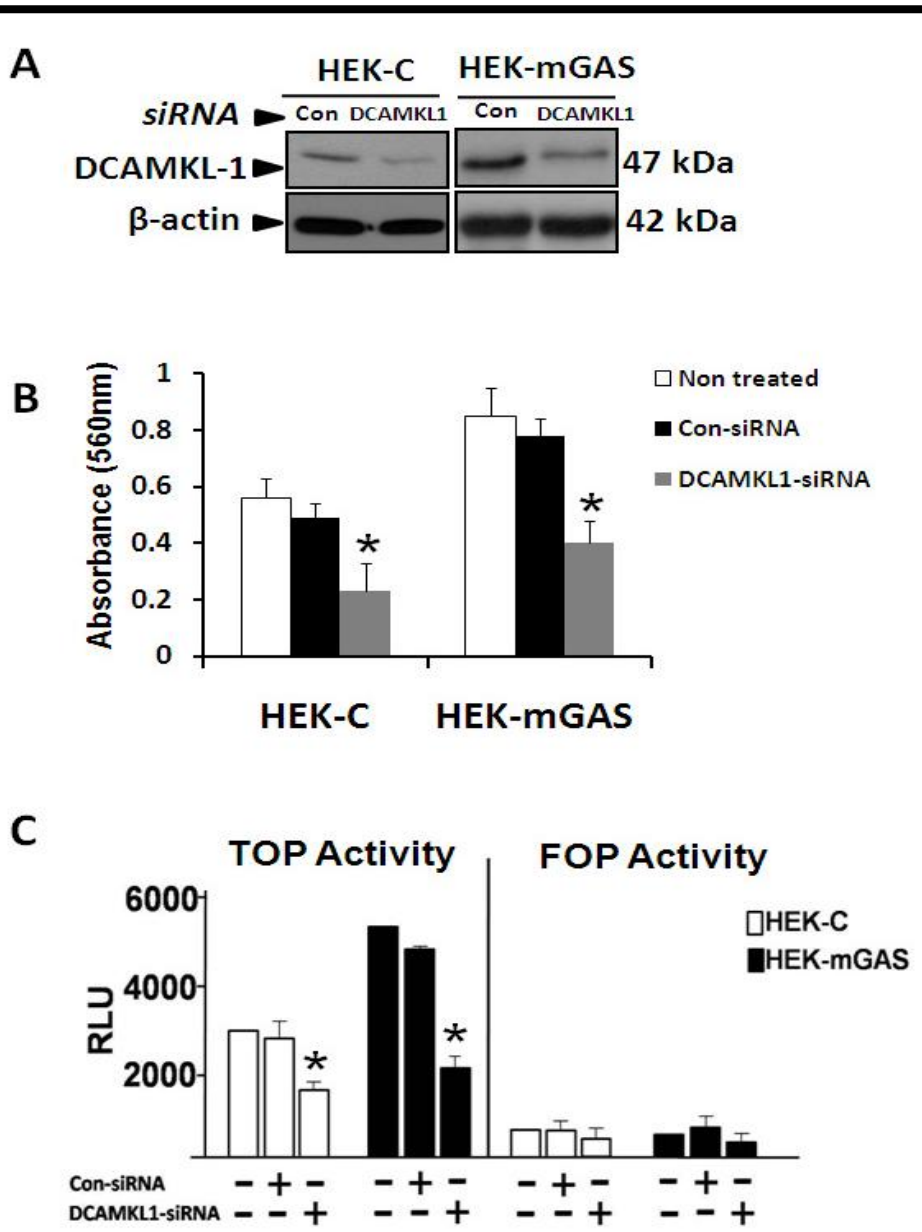

Figure 3.12 (*A–C):* Down-regulation of DCAMKL-1 significantly reduces activation of β-catenin and growth of HEK-C/HEK-mGAS cells. A=representative autoradiogram of WB data from 1 of 3 experiments, demonstrating relative levels of DCAMKL-1 in cells treated with either control (Con) or DCAMKL-1 specific siRNA; β-actin run as a loading control. **B**=growth (in terms of absorbance in an MTT assay) of indicated cells; each bar-graph=Mean±Sem of data from 8 wells/2experiments. **C**=activation of β-catenin (relative luminescence) measured in a reporter-promoter (TOP) assay in indicated cells. Data in bar-graphs=Mean±Sem from 6 samples/2experiments. Cells transiently-transfected with FOP-plasmid served as negative-controls. *=$p<0.05$ vs values measured in control-siRNA treated cells.

3.4 DISCUSSION

In the current studies, we demonstrate for the first time that PG expression in immortalized embryonic cells increases tumorigenic/metastatic potential of these cells. Over-expression of autocrine PG, however, was not effective in transforming immortalized intestinal-epithelial cells (IEC-18), as previously reported by our laboratory (184). It is thus possible that HEK293-cells, unlike IEC18-cells, are positive for an initiating event, and over-expression of PG facilitates transformation of HEK293-cells. Transgenic mice over-expressing PG are at an increased risk for colon-carcinogenesis in response to azoxymethane (53,68,117). Gastrin gene (PG) expression is normally repressed in colonic epithelial-cells, but is increasingly expressed during hyperplastic/adenoma/carcinoma sequence of colon-carcinogenesis (175). It is thus possible that increasing expression of autocrine PG contributes to colon-carcinogenesis of 'initiated' cells; our current findings provide evidence for this novel possibility.

Membrane associated CS-ANXA2, recently discovered as a novel receptor for PG (51,112,182), binds several ligands and is present on endothelial cells/keratinocytes/epithelial cancer cells (195,198,214,215,217,219). Functional significance of CS-ANXA2 in proliferation/metastasis of cancer-cells is becoming increasingly evident (195,198,214,215,217). Progression of pancreatic/breast cancer disease is associated with a switch from cytoplasmic to cell-surface expression of ANXA2 (196,220). Exosomes, secreted by cancer cells, contain ANXA2 (221), and may be the source of CS-ANXA2 and soluble-ANXA2 measured in conditioned-medium/serum of cancer-cells/patients (219,221-223). We also measured 2-3fold

increase in percent cells positive for CS-ANXA2 in HEK-mGAS vs HEK-C cells **(Fig 3.6)**, supporting the notion that wounding/immortalization/oncogenic transformation is conducive to increasing CS-ANXA2 on epithelial cells (196,198,214,215,217,219,220,221,224,current studies).

Radiolabeled peptide-ligands for membrane-receptors are being developed for diagnostic/therapeutic purposes (225). We demonstrate for the first time that iv injected labeled-PG-peptide (FAM-PG26) effectively and specifically homed to primary/metastatic HEK-mGAS/HCT-116 tumors within 5-15min of injection **(Fig 3.4)**. Even though HEK-mGAS/HCT-116 cells over-express autocrine PG (51,114,175,212), high concentrations of FAM-PG26 competed effectively with autocrine PG, perhaps reflecting higher binding-affinity of FAM-PG26 for CS-ANXA2 than PG (213), and/or rapid turnover of CS-ANXA2. Accumulation of FAM-PG26 was localized to focal areas of primary/metastatic tumors **(Fig 3.4)**, which may reflect over-expression of CS-ANXA2 at these sites, as strongly suggested from results with ANXA2 staining of HEK-mGAS xenografts **(Fig 3.10C-D)**. Thus labeled/conjugated molecules with high-affinity for CS-ANXA2 may be useful for diagnosing/treating epithelial cancers.

Several signaling molecules/transcription factors are activated in target-cells in response to PG *in vitro* and *in vivo* (including: Src,PI3K,Akt,JAK2,STAT5/3, ERKs, p38MAPK, NFκB, β-catenin, Jagged1) (5,41,51,118,175,226). ANXA2 mediates signaling and proliferative effects of PG (51,112,1827), and anti-ANXA2-Abs attenuate growth effects of exogenous/autocrine PG on pancreatic/colon-cancer cells (112,182). Current studies additionally demonstrate a significant (3-8fold) increase in relative-levels

of potent transcription-factors (β-catenin/*p*NFκBp65) and stem/progenitor cell markers (DCAMKL-1/LGR5/CD44) in HEK-mGAS vs HEK-C cells, growing either as mono-layer cultures, 3D-spheroids or xenografts in mice **(Fig 3..11)**. Thus cells growing as 3D-structures *in vitro* and *in vivo* maintain parental expression profiles. Surprisingly, ratio of PG expression in HEK-mGAS vs HEK-C cells significantly increased in spheroids/tumors compared to that in mono-layer cultures, suggesting the novel possibility that gastrin gene (PG) expression is up-regulated by factors (stress?) associated with 3D-growths. Percentage of stem/progenitor cells positive for DCAMKL-1/CD44/LGR5 were also significantly increased in HEK-mGAS vs HEK-C cells in the order of CD44>DCAMKL-1>LGR5 **(Fig 3.6)**. The most interesting finding was that almost all CS-ANXA2+ve cells co-expressed CD44 and vice versa **(Fig 3.6D-E)**, suggesting that similar pathways may up-regulate cell-surface expression of CD44/CS-ANXA2.

The smallest CD44-isoform that lacks variant exons (CD44s) is abundantly expressed by normal and cancer cells, while variably glycosylated CD44v-isoforms (CD44v1-v10) are mainly expressed by cancer cells (107). Chondroitin-sulfate/heparin-sulfate modifications enables CD44v-isoforms to bind growth-factors/CS-ANXA2/MMPs (107,227,228), which dictates cellular-functions (migration/growth/survival) of CD44, as evidenced by loss of growth/metastasis of colonic-tumors, treated with anti-CD44v6-antibodies (229). Clustering of CD44 on tumor cells reportedly traps MMPs, which imparts invasive potential to epithelial cancer cells (228). At the same time, CS-ANXA2 expression is critically required for metastasis of

tumors (195,202,214,215,217). CS-ANXA2 on hepatocellular-cancer-cells (HCC) (230), binds CD147-like-proteins resulting in secretion of MMPs and metastasis of HCC cells (217). Thus, CS-ANXA2 plays an equally important role in proliferation/metastasis of cancer-cells, which may be mediated by binding to specific ligands, such as tPA/plasminogen/PG/CD147 (51,182,195,217,202). Since both CS-ANXA2/CD44 appear to up-regulate/activate MMPs (as discussed above), significant increase in MMP2,7 levels in HEK-mGAS vs HEK-C cells **(Fig 3.9E)**, may reflect increased presence of CS-ANXA2/CD44 on cell-surface of HEK-mGAS cells **(Fig 3.7)**. Surprisingly, down-regulation of ANXA2 attenuated MMP2,7 expression in HEK-mGAS cells, by unknown mechanisms, which may have resulted in re-formation of rounded, less amorphous spheroids by HEK-mGAS cells **(Fig 3.9D)**; HEK-C cells, enriched for CS-ANXA2, on the other hand, developed amorphous-spheroids **(Fig 3.9C)**. Based on our current understanding of interactions between CD44/CS-ANXA2/MMPs on tumor cells (as discussed above), it is speculated that loss or gain of CS-ANXA2/MMPs in CD44+ve stem cells may impact metastatic behavior of cancer cells, and dictate morphology of spheroidal growths. In a recent study, down-regulation of LGR5 in CRC-cells reportedly altered expression/distribution of MMPs/CD44, associated with invasion/migration of cells, resulting in formation of amorphous spheroids (87). The above findings support the novel concept that spheroid morphology may reflect tumorigenic/metastatic potential of cells.

Several cell-surface markers have been used to identify colonic CSCs (including CD44,CD133,CD166,LGR5,DCAMKL-1) (73,102). Accumulating evidence suggests

that CD133/CD166 may not be robust markers of cancer stem cells (CSCs) (45). CD44, however, is a strong marker for CSCs with a functional role in CSC biology (45), including cancer-cell migration. Our results additionally suggest that CD44 and CS-ANXA2 may be co-expressed by highly tumorigenic/metastatic cells **(Fig 3.7)**.

Functional role of LGR5 in CSC biology remains unclear. LGR5 expressing cells in small intestine generate structures resembling intestinal crypts *in vitro*, and intestinal tumors can arise from LGR5+ve cells in APC mutant mouse models (218), suggesting LGR5+ve cells may represent intestinal CSCs. Surprisingly, down-regulation of LGR5 enhanced tumorigenesis of CRC cells, while over-expression of LGR5 increased cell-cell adhesion (87). These confounding results provide evidence that LGR5 may be a marker for CRC cells due to increased Wnt activity (supported by current findings); Walker et al (87) speculate that LGR5 may regulate Wnt response and maintain colonic-crypt structures by inhibiting EMT. Since <20% CS-ANXA2+ve cells co-expressed LGR5 **(Fig 3.7)**, presence of CS-ANXA2 does not appear to be linked to expression of LGR5, unlike co-expression of CD44/CS-ANXA2 **(Fig 3.7D-E)**.

We observed that ~50% of CS-ANXA2(+) HEK-mGAS cells co-expressed DCAMKL-1 and >75% DCAMKL-1+ve HEK-mGAS cells co-expressed CS-ANXA2, suggesting a significant linkage between DCAMKL-1/CS-ANXA2 expression **(Fig 3.7D-E)**. DCAMKL-1 is a microtubule-associated kinase and regulates spindle formation and mitotic cell-division in neuroblasts (64). Down-regulation of DCAMKL-1 induces apoptosis in neuroblastoma cells (62). Thus DCAMKL-1 plays an important role in neuroblastoma/neuronal biology. DCAMKL-1 is up-regulated in CRC and down-

regulation of DCAMKL-1 results in growth arrest of tumors (73). Pancreatic cancer stem cells increasingly express DCAMKL-1 and down-regulation of DCAMKL-1 results in loss of c-Myc/Kras and EMT (74), suggesting that DCAMKL-1 may play an important functional role in pancreatic/colorectal cancers. We similarly observed that down-regulation of DCAMKL-1 significantly reduced proliferation of HEK-C/HEK-mGAS cells by ~50-70% **(Fig 3.12B)**, suggesting that DCAMKL-1 is required for maintaining growth of embryonic epithelial-cells as well. Our studies additionally suggest the novel possibility that DCAMKL-1 is required for maintaining β-catenin activation **(Fig 3.12C)**.

DCAMKL-1 expression levels were significantly increased in colonic-crypts of mice in response to elevated levels of circulating PG, resulting in hyperproliferation of colonic-crypts (51). In the current studies, we measured a significant increase in DCAMKL-1+ve cells, co-expressing CS-ANXA2 and/or CD44 in HEK-mGAS cells **(Fig 3.7)**, which may represent a pool of highly tumorigenic/metastatic stem cells.

Interestingly, DCAMKL-1/LGR5 staining cells were present mainly around perimeters of HEK-C spheroids, while CD44+ve cells were present both at the periphery and within the spheroids, resembling Ki67 staining **(Fig 3.9B)**. Co-expression of ANXA2 with DCAMKL-1 was not observed in HEK-C spheroids **(Fig 3.10A)**, resembling the profile seen in normal colonic crypts (51). Processing of HEK-mGAS spheroids resulted in loss of intact structures **(Fig 3.9D)**, but the remaining clumps of HEK-mGAS spheroids co-stained for DCAMKL-1/CD44 **(Fig 3.10A)**, suggesting that the expression profile of transformed HEK-mGAS stem cells observed in 2D-cultures **(Fig 3.7)**, is maintained in 3D-growths of HEK-mGAS cells.

In conclusion, we demonstrate a significant increase in % stem cell populations co-expressing DCAMKL-1/CD44/CS-ANXA2 in PG-overexpressing HEK-mGAS cells, in association with increased expression of MMPs which may contribute to increased tumorigenic/metastatic potential of HEK-mGAS cells and formation of amorphous-spheroids *in vitro*. Since almost all CD44(+) HEK-mGAS cells, growing either as monolayer-cultures/3D- spheroids or xenografts, co-expressed CS-ANXA2 **(Fig 3.7; 3.10A,C,D)**, it is possible that co-expression of CD44/CS-ANXA2 by stem cells may facilitate growth/metastasis of transformed cells, and represent a hallmark (phenotype) of transformed stem cells. Previous and current findings confirm a functional role of DCAMKL-1 for maintaining proliferation of normal/cancer cells; this may be linked to the surprising finding that β-catenin activation is attenuated in cells down-regulated for DCAMKL-1 expression. Since down-regulation of either ANXA2, DCAMKL-1 or CD44 (73,107,182, current studies) attenuates proliferative/tumorigenic/ metastatic potential of transformed/cancer cells, targeting all three factors may provide an efficient approach for diagnosing/treating epithelial-cancers. Based on our findings we also postulate that labeled-ligands, demonstrating high-affinity for CS-ANXA2, may provide a selective tool for diagnosing/treating epithelial-cancers, since a majority of epithelial-cancers over-express CS-ANXA2 at leading edges of the tumors.

One of the main challenges in treating cancer is the inability to differentiate between normal and cancer cells. In the current studies, we demonstrated for the first time a phenotypic difference between non-transformed/normal and transformed/tumorigenic stem cells. Researchers are also focused on identifying stem

cells markers which would enable them to recognize normal versus cancer stem cells. Since our studies with tumorigenic vs non-tumorigenic HEK293 cells strongly suggested significant differences in the phenotype of stem cells positive for DCAMKL-1 and LGR5, in the next set of studies (chapter 4), we investigated the role of DCAMKL-1+ve versus LGR5+ve cancer stem cells, using colon cancer cell lines, and examined phenotypic/proliferative differences, if any, in order to identify the most potent cancer stem cell marker, for purposes of developing targeted therapies against cancer stem cells (chapter 5).

CHAPTER 4

CHARACTERIZATION OF DCAMKL-1 AND LGR5 POSITIVE CELLS IN COLON CANCER STEM CELLS

4.1 INTRODUCTION

Colorectal cancer is one of the most common and leading causes of death in the United States (231). Although several therapies are currently being used to treat this disease, recurrence remains a challenge. It has been speculated that cancer stem cells within the tumors are responsible for the relapse of this disease given their resistant properties to currently available therapies. Cancer stem cells (CSCs) are believed to originate from normal adult stem cells which eventually transform and adopt an aberrant/malignant phenotype. It is therefore important to understand the biology and regulatory molecules which mediate transformation of stem cells from a benign to a malignant phenotype.

In recent years, researchers in this field have focused on identifying markers which would allow for the enrichment of stem cell populations in order to examine these cells in more depth. To date, several normal and cancer stem cell markers have been identified in the small and large intestinal crypts (Table 1.1, Chapter 1), including DCAMKL-1 and LGR5 (20,23).

Within the colonic crypts, DCAMKL-1+ve cells were found to be located at the +4 position and represent the quiescent stem cells (20). In contrast, Lgr5+ve cells were found to be located at the base of the crypts and represent the actively cycling stem cells which are clearly distinct from the +4 positioned cells (76). Both DCAMKL-1 and LGR5 have been shown to be overexpressed in various cancers, including colon cancer (72,84).

However, the specific contributions of DCAMKL-1+ve and LGR5+ve stem cells towards the growth of cancer cells remain unknown. During the course of my investigations, within the past year, it has been reported that down-regulation of DCAMKL-1 in pancreatic and colon cancer xenografts resulted in attenuating the growth of these tumors *in vivo*, suggesting that DCAMKL-1 may play an important role in supporting the growth of cancer cells, and that DCAMKL+ve cancer cells may represent cancer stem cells. This possibility is supported by our findings with HEK-mGAS cells in chapter 3.Therefore, my next goal was to characterize the phenotype of cancer stem cells positive for the two putative stem cell markers and further examine the role of DCAMKL-1 and LGR5 in the growth of colon cancer cells.

To address the above goals, I first established an *in vitro* spheroidal growth assay in our laboratory, which is believed to select for the growth of cancer stem cells as tumorospheres (216), to better mimic the 3D pattern of growth of tumors *in vivo*, as developed by several investigators in this field. The results of the current studies demonstrate that DCAMKL-1 and LGR5 expressing cells are located on the outer periphery of tumorospheres and along the leading edges of the colon cancer xenografts, resembling our findings with transformed HEK-mGAS cells. Our findings also strongly suggest that DCAMKL-1 and LGR5 expressing cells likely represent two distinct stem cell populations with differential proliferative potential, growth patterns and phenotypic characteristics.

In chapter 3, we reported an important role for ANXA2 in the formation of HEK-mGAS tumorospheres. Down-regulation of ANXA2 resulted in the formation of more compact spheroids which revealed an essential role for ANXA2 in the proliferative and tumorigenic potential of HEK-mGAS cells. In this chapter, we similarly examined the role of ANXA2 in the formation of tumorospheres arising from colon cancer cell lines.

The results demonstrated a differential growth pattern of tumorospheres in the presence and absence of ANXA2 expression, and confirm our findings with HEK-mGAs cells, suggesting the novel possibility that cell surface associated AnnexinA2 may play a critical role in the metastatic spread of cancer cells.

4.2 MATERIALS AND METHODS

In this section, only reagents and methods that have not been described in previous chapters are listed below.

4.2.1 Materials

Antibodies used included anti-phospho-p65NF-κB(Ser^{536}), anti-phospho-β-catenin (Ser^{552}) (Cell Signaling Technology, Danvers, MA), anti-phospho-β-catenin(Tyr^{142}) (Abcam, Cambridge, MA), anti-active caspase-3 (Millipore, Temecula, CA).

4.2.2 Cell Culture

HCT-116, DLD-1 and HT-29 cells were purchased from the American Tissue Culture Collection (ATCC) (Manassas, VA) and maintained in DMEM medium as described in Chapters 2 and 3.

4.2.3 Cell Viability Assay

4.2.3.1 Method 1

HCT-116 cells were grown either as monolayers or tumorospheres. Cells were stained using trypan blue and viability was measured using the Cellometer^{TM} Auto T4 (Nexcelom Bioscience, Lawrence, MA).

4.2.3.2 Method 2

Dissociated monolayers or tumorospheres cells were cytospun at 300g for 5min onto Superfrost®/Plus microscope slides (Fisher Scientific, Pittsburgh, PA) using a Shandon CytoSpin III cytocentrifuge (Cheshire, England). Cells were then fixed and stained for the apoptotic marker activated caspase-3 by IF following the same methods described in Chapters 2 and 3.

4.2.4 In vitro growth of cells as primary and secondary spheroids

HCT-116, DLD-1 and HT-19 cells were plated at a density of 5000 cells/well respectively into 24-well ultra low-attachment plates (Costar, Corning NY). Cells were maintained as described in Chapter 3. The growth of secondary spheroids was performed by dissociating the first generation of primary tumorospheres into single cells. The single cells were then replated in a low-attachment plate using and maintained as described in Chapter 3.

4.2.5 Processing of spheroids for embedding, sectioning and staining

As described in Chapter 3.

4.2.6 Immunofluorescent (IF) staining

As described in Chapters 2 and 3.

4.2.7 Western Blot (WB) analysis

As described in Chapters 2 and 3.

4.2.8 Analysis of cells by FACScaning and FACSorting

As described in Chapter 3.

4.2.9 Statistical analysis

Data are presented as mean±SEM of values obtained from 6 samples/3 experiments. To test for significant differences between means, nonparametric Mann-Whitney test was employed using Statview 4.1 (Abacus Concepts, Inc., Berkeley, CA); *P* values were considered statistically significant if less than 0.05.

4.3 RESULTS

4.3.1 Expression of stem-cell-markers, DCAMKL-1, CD44 and LGR5 in HCT-116 colon cancer cells

In chapter 3, we learnt that the expression pattern of stem cell markers, DCAMKL-1, CD44 and LGR5 in a non-tumorigenic human embryonic cell line (HEK-C) was significantly different than that of isogenic cell line (HEK-mGAS) which was rendered tumorigenic due to overexpression of progastrin (PG). Since a majority of colon cancers express autocrine PG (175), we examined if human colon cancer cell lines have a similar stem cell phenotype as HEK-mGAS cells. A human colon cancer cell line (HCT-116) was chosen, since our laboratory has demonstrated that growth of the cells/xenografts is dependent on autocrine expression of progastrin (114). Relative expression of DCAMKL-1, CD44 and LGR5 was examined in HCT-116 cells by western

blot analysis (**Fig 4.1Ai)**. Ratios of target proteins to loading control, β-actin, are presented as a bar graph **(Fig 4.1Aii)**. The results confirmed significant expression of DCAMKL-1, CD44 and LGR5 in HCT-116 cells. We next investigated the localization of the three markers in HCT-116 cells, growing as monolayers in 2D cultures. HCT-116 cells were stained by IF for DCAMKL-1, CD44 and LGR5. DAPI was used to stain the nucleus (**Fig 4.1B).** Our results demonstrated that all three stem cell markers were present on the cell membranes of the cells, as expected, since all three are known to have extracellular and transmembrane domains. To further examine the stem cells, HCT-116 cells were FACSorted with labeled primary antibodies against DCAMKL-1, CD44 or LGR5, and analyzed for % cells positive or negative for the specific markers. The quantitative graphs demonstrated a clean separation between the positive (top green) and negative (bottom grey) cell populations **(Fig 4.1Ci)**. The % cells positive for the specific markers is presented as a bar graph **(Fig 4.1Cii)**, and demonstrated that 2.7%, 1.9% and 2% of HCT-116 cells were positive for DCAMKL-1, CD44 and LGR5 respectively. Thus the % cells positive for the three stem cell markers ranged from 1-3% which is in conformity with the expected range of stem cell populations, reinforcing the validity of using DCAMKL-1, CD44 and LGR5 as cancer stem cell markers.

4.3.2 Optimization of an in vitro assay for growing tumorospheres from colon cancer cells

The formation of tumorospheres *in vitro* is a well established assay which selects for the growth of stem cells. *In vitro* monolayer cell cultures do not simulate well the *in vivo* 3D growths of tumors (232). Spheroidal assays provide a 3D *in vitro* model which mimics morphological conditions, as seen in tumors *in vivo.* The number of cells required to form tumorospheres vary from 10-20000 and is contingent on various factors including

cell type and media additives (232). Therefore, our goal was to optimize an assay which would allow for the growth of colon cancer cells as tumorospheres, in a reasonable time period. HCT-116 cells were plated in low-attachment 24-well plates at different concentrations (50, 100, 500, 1000, 2000, 5000, 10000 and 20000 cells/well respectively)**.** The growths of the tumorospheres were imaged at 24 hours, day 7 and day 10. Our results demonstrated that HCT-116 cells grew tumorospheres with a well defined outer perimeter (resembling a basement membrane) in approximately 8-10 days **(Fig 4.2A).** The size of the tumorospheres reflected plating cell density. For example, 5000-20000 cells/well formed significantly larger spheroids (300-500µm) compared to 50-2000 cells/well (100-200µm). Furthermore, the increases in cell density lead to an increase in number of tumorospheres, as expected **(Fig 4.2B).** On an average, plating of 10,000 HCT-116 cells/well lead to the formation of 30 tumorospheres within 7days. Secondary spheroids have been reported to have higher % of stem cells (233). The expectation is that "non-stem cell" populations remaining in culture in the first generation of spheroidal growths would be eliminated, to examine this possibility; we next examined the growth of secondary versus primary tumorospheres. HCT-116 primary tumorospheres were dissociated into single cells and re-plated in low-attachment plates, to allow for the growth of secondary spheroids. Cells were plated at a density of 50, 100, 500, 1000, 2000, 5000, 10000 and 20000 cells/well respectively. The formation of secondary tumorospheres was imaged at 24 hours, 72 hours and at day 4 **(Fig 4.2C).** Our results revealed that secondary tumorospheres grew at a faster rate than primary tumorospheres. The formation of secondary spheroids at 72 hours was equivalent to that of the primary tumorospheres at day 10. These results confirm the notion that stem cell populations are enriched as a result of selection during growth of primary spheroids, and thus give rise to faster growing secondary tumorospheres. The size and number of secondary

tumorospheres also increased as the cell density increased, which is consistent with the findings with primary tumorospheres (**Fig 4.1A).** Apart from the rate of tumorosphere formation, no significant differences were observed in the morphology of primary versus secondary tumorospheres. To confirm these findings, a cell viability assay was performed on cells arising from both primary and secondary tumorospheres. Primary and secondary spheroids were dissociated into single cells and stained with trypan blue. The dissociated secondary tumorosphere cells were 98% viable compared to 91% viability of dissociated primary tumorosphere cells **(Fig 4.2D)**. Dissociated primary and secondary tumorospheres cells were cytospun onto glass slides and stained by IF for the apoptotic marker, activated caspase-3. DAPI was used to stain the nucleus. No significant staining for activated caspase-3 was observed, suggesting the lack of apoptotic cell death in tumorospheres formed from cancer stem cells, in the time frame of our studies. On the other hand organoids formed from primary normal colonic crypt stem cells, grow and differentiate rapidly, and undergo apoptotic death (234), as observed by us in related studies (unpublished data from our lab). These findings confirmed that primary and secondary tumorospheres formed from colon cancer stem cells are viable and functional entities which can be used in further studies.

4.3.3 Differential growth of tumorospheres from colon cancer cell lines as a reflection of PG expression

In chapter 3, we demonstrated differences in the spheroidal growths of HEK-C versus HEK-mGAS cells. HEK-C spheroids grew more compact tumorospheres with a well defined perimeter, whereas HEK-mGAS spheroids grew amorphous spheroids. The differential morphology observed was believed to be due to over-expression of progastrin which rendered HEK-mGAS cells tumorigenic and metastatic. Therefore, we examined

spheroidal growth of colon cancer cell lines, expressing different levels of progastrin. DLD-1 is a colorectal adenocarcinoma cell line which expresses high levels of progastrin similar to HCT-116 cell line (235). In contrast, HT-29 is a human colon adenocarcinoma grade II cell line which expresses low levels of progastrin (235). DLD-1, HCT-116 and HT-29 cells were grown as primary tumorospheres at a density of 10000 cells/well. Spheroids were imaged at 4x and zoomed insets are shown **(Fig 4.3A)**. DLD-1, HCT-116 and HT-29 cells formed primary tumorospheres, but at different rates, and could be observed at days 4, 6 and 11, respectively, for the three cells lines **(Fig 4.3A).** Cells expressing higher levels of progastrin (DLD-1 and HCT-116) formed tumorospheres at a faster rate compared to HT-29 cells expressing much lower levels of PG. These results suggest that autocrine expression of growth factors, such as PG, likely up-regulates stem cell populations (as supported by our findings in chapters 2 and 3), resulting in differences in rate of tumorosphere formation.

4.3.4 Morphological/cellular features of tumorospheres, formed from colon cancer cell lines

During the process of our investigations, several laboratories have examined the gross morphology of the tumorospheres formed from colon cancer cell lines (236, 237). Our results confirm many of their findings; however the morphology of tumorospheres grown from different colon cancer cell lines has not been examined. Additionally, cellular features of the tumorospheres, and specific localization of molecular markers has not been examined in sufficient detail. Our laboratory developed a method for fixing and embedding intact tumorospheres in paraffin. Sections were stained by H&E and images taken at 20x magnification. The spheroids from HCT-116 and DLD1 cells were well rounded with a well defined perimeter; in contrast to HT-29 spheroids which were

slightly asymmetrical **(Fig 4.3B)**. Thus in the case of cancer cell lines, unlike embryonic cells, higher expression of autocrine PG did not result in formation of amorphous spheroids, but only appeared to impact the rate of spheroid formation.

Next the localization of stem cell markers in the colon cancer tumorospheres was investigated. Tumorospheres were processed and stained by IF for the specific stem cell markers. DCAMKL-1 and LGR5 positive cells were expressed on the outer edge of the spheroids whereas CD44 positive cells were scattered throughout the entire sphere including the outer layer of cells **(Fig 4.3C)**. These results are consistent with the findings in Chapter 3 and reiterate the notion that DCAMKL-1+ve and LGR5+ve cells may represent stem cells whereas CD44+ve cells likely represent progenitor stem cells. In chapter 2, we demonstrated that overexpression of progastrin in HEK-mGAS cells lead to up-regulation of NFκBp65 and β-catenin signaling molecules. The results were associated with a significant increase in the expression of stem cell markers, and the resultant increase in proliferative potential of HEK-mGAS cells. In the current studies, we investigated the localization of cells, up-regulated for activated NFκBp65 and stabilized β-catenin, in relation to cells positive for proliferative versus apoptotic markers in HCT-116 tumorospheres. HCT-116 cells were grown as tumorospheres and stained by IF for the expression of phosphorylated (activated) NFκBp65 and total/activated β-catenin. Total β-catenin and activated *p*β-catenin (Ser^{552}) were exclusively expressed in the peripheral layer of cells. In contrast, *p*β-catenin (Tyr^{142}), activated via the non-canonical pathway, was expressed in cells throughout the sphere **(Fig 4.4A)**. Activated *p*p65NFκB^{s276} and *p*p65NFκB^{s536} was also surprisingly expressed by cells throughout the entire core and perimeter of the sphere **(Fig 4.4B)**, suggesting that the activation of NFkBp65 may be a ubiquitous and perhaps unique feature of cancer stem cells growing as tumorospheres, which needs to be further

examined. Since DCAMKL+ve and LGR5+ve cells were located primarily at the periphery of the spheroids along with cells positive for NFκB, β-catenin and proliferation markers, it is possible that these stem cells represent initiating stem cells, which perhaps give rise to all other cells, including progenitor cells (positive for CD44), which move inwards and form the bulk of the spheroidal structures.

It has been reported that the outer peripheral layer of cells in tumorospheres are actively proliferating whereas the inner core cells are slightly necrotic (232). To confirm these reports, we investigated the localization of apoptotic and proliferative cells within the HCT-116 tumorospheres by IF staining. Our data revealed that apoptotic cells were indeed located within the core of the sphere as depicted by the IF staining for activated caspases-3 (green) **(Fig 4.4C).** In contrast, cells positive for the proliferation marker Ki67 (green) and PCNA (red) were exclusively expressed on the perimeter of the spheroids **(Fig 4.4D)**, which coincidence with the findings of several other studies.

4.3.5 Phenotype of DCAMKL-1+ve and Lgr5+ve cells in colon cancer cell lines

Our results in chapters 2 and 3 demonstrated that HEK-293 cells, over-expressing progastrin, were rendered more proliferative, tumorigenic and metastatic. These changes in phenotype were associated with increased co-expression of DCAMKL-1/CD44 with CS-ANXA2 by transformed stem cells in HEK-mGAs cells, which were not observed in non-transformed, HEK-C cells. Since both DCAMKL-1 and LGR5 mark stem cells, one of my goals was to examine if the phenotype of DCAMKL-1+ve cells was significantly different from that of LRG5+ve cells, and if these differences impacted growth patterns of the two stem cell populations.

Therefore, we examined whether cancer stem cells co-expressing DCAMKL-1 with CD44 were also positive for PCNA, by IF staining. Results in **Fig 4.5A** confirmed

that cells co-expressing DCAMKL-1 and CD44 were proliferating **(Fig 4.5B)**, confirming their stem/progenitor cell status. In contrast, cells positive for LGR5 seldom co-expressed CD44 and were not as strongly positive for PCNA **(Fig 4.5B)**. Therefore, even though LGR5 is a target protein of the Wnt signaling pathway, it may not always represent the proliferating pool of stem cells, since the Wnt pathway may not be the main driver of proliferation in colon cancer cells, which are genotypically wildtype for both APC and β-catenin (238,239). HCT-116 cells are wildtype for the Wnt pathway. A major driving force in the case of colon cancer cell lines, such as HCT-116, is their mismatch repair (MMR) deficient genotype (240) and their expression of autocrine PG (241, 242), which may explain our findings in Fig 5.

Since tumorospheres possess heterogeneity similar to tumors xenografts *in vivo* (232), we additionally examined expression pattern of DCAMKL-1 and LGR5 in HCT-116 xenografts. HCT-116 cells were grown *in* vivo as xenografts and processed/ stained by IHC for DCAMKL-1 and LGR5. Images were taken at 4x, 10x and 20x. DCAMKL-1 was highly expressed at leading edges of the tumor **(Fig 4.5C-top panel)**, just as we had observed with HEK-mGAs xenografts in Chapter 3. The latter findings are consistent with the notion that stem cells remain in close proximity to peripheral regions of the tumors, allowing contact with signals from the host/microenvironment. Similarly, LGR5 expression was exclusively observed on the outer edges of the tumor **(Fig 4.5C-bottom panel)**, albeit at lower levels compared to DCAMKL-1, which may reflect the genotype of HCT-116 cells, as discussed above. Importantly these results once again confirm our previous findings that DCAMKL-1 and LGR5 positive cancer stem cells represent different population of cells, in both tumorospheres and tumors, despite their postulated function as stem cell markers, which may reflect the molecular/mutant signature of the cells.

We next determined the % cells which were positive for DCAMKL-1 and/or LGR5. Cells were FACScanned and analyzed for % cells positive for DCAMKL-1 and/or LGR5. As illustrated in **Fig 4.6A**, 3.4% of HCT-116 cells were positive for LGR5, 3.3% HCT-116 cells were positive for DCAMKL-1 and only 0.4% were positive for both DCAMKL-1 and LGR5. These results once again reiterated our findings that the majority of DCAMKL-1+ve and Lgr5+ve cancer stem cells represent distinct population of cells. However, a small minority of cells co-expressed DCAMKL-1 and LGR5, which is unique to transformed/colon cancer cells and different from the pattern we and others have observed in normal colonic crypt cells (20, 23) and non-transformed HEK-C cells (51, and chapter 3). It is possible that normal/non-transformed cells do not co-express the extracellular domain of the two stem cell markers simultaneously and/or do not process the stem cell markers completely within the same cells, based on specific cues from the normal niche of colonic crypts (as described in Fig 1.10 in chapter 1). Cancer cells, on the hand lose the normal cues, and hence may have the potential to co-express the stem cell markers within the same cell population. These and other possibilities need to be further examined in future studies.

4.3.6 Differences in growth of DCAMKL-1+ve and LGR5+ve cells as tumorospheres

Our results so far strongly suggest that the majority of cancer stem cells are positive for either DCAMKL-1 or LGR5. Therefore we next examined whether the growth pattern of these cells as tumorospheres, was also different. HCT-116 cells were FACSorted into pure populations, expressing the extracellular domain of either DCAMKL-1 or LGR5, the enriched cells were grown *in vitro* as tumorospheres and imaged at imaging at 24, 48, and 72 hrs and finally at day 7. DCAMKL-1+ve cells grew larger and faster tumorospheres compared to Lgr5+ve cells, which appeared to form very

few aggregates **(Fig 4.6Bi)**. This stark difference in the potential to form and grow tumorospheres may be due to the co-expression of CD44/CS-ANXA2 by DCAMKL-1+ve cells, which may be required for formation/aggregation of cells as tumorospheres; this is based on the findings in chapter 3 which demonstrate that CS-ANXA2 may be playing a critical role in motility and invasive properties of stem cells. Surprisingly, Lgr5-ve cells grew compact tumorospheres at a much faster rate than LGR5+ve cells, while DCAMKL–ve cells were the least aggressive of all other populations **(Fig 4.6Bi)**. These surprising findings may be due to the presence of DCAMKL-1+ve cells within the Lgr5-ve population, as confirmed by us **(Fig 4.7Diii)**. The absence of tumorosphere formation by DCAMKL-ve cells even by day 7 can be appreciated from images presented in **Fig 4.6Bii**. Importantly, LGR5-ve cells had formed large intact spheroids by day 7, while LGR5+ve cells remained loosely aggregated **(Fig 4.6Bii),** once again suggesting that the genotype and phenotype of the two cell populations is likely very different, and needs to be examined in future studies.

Possible differences in the phenotype of DCAMKL-1 and LGR5 cells were further examined. Cells FACSorted for either DCAMKL-1 or LGR5 were cytospun and stained by IF for DCAMKL-1, CD44, LGR5 and PCNA. Images were taken at 10x and 40x magnification. DCAMKL-1+ve cells significantly co-stained with CD44 **(Fig 4.7Ai)** and PCNA **(Fig 4.7Bi)** compared to DCAMKL-1-ve cells which did not express CD44 **(Fig 4.7Aii)** or PCNA **(Fig 4.7Bii)**. Lgr5+ve cells, unlike DCAMKL-1+ve cells, did no co-stain with CD44 **(Fig 4.7Ci)** or PCNA **(Fig 4.7Di)**. Surprisingly, Lgr5-ve cells expressed CD44 **(Fig 4.7Cii)** and PCNA **(Fig 4.7Dii).** The data reaffirms our findings in **(Fig 4.5Bi-ii)** which illustrated co-expression of DCAMKL-1 with CD44, but a relative absence of co-expression of LGR5 with CD44 in HCT-116 tumorospheres. Next, we examined if LGR5-ve cells expressed DCAMKL-1, which may explain the co-

expression of CD44 with LGR5-ve cells in **Fig 4.7Diii**. Our results confirmed that about 50% of LGR5-ve cells were positive for DCAMKL-1 which may likely explain the rapid growth rate of Lgr5-ve cells as tumorospheres *in vitro* (**Fig 4.6Bi-ii***)*. The % cells co-expressing DCAMKL-1/CD44/PCNA vs LGR5/CD44/PCNA was analyzed (**Fig 4.7Ei-ii)**, and demonstrated that 87% and 91% of DCAMKL-1 cells co-stained with CD44 and 91% PCNA, respectively. However, only 7% of DCAMKL-1-ve cells co-stained with CD44 and 9% with PCNA (**Fig 4.7Ei)**. However, only 8% and 11% of LGR5+ve cells co-stained with CD44 and PCNA, respectively, while 75% and 87% of Lgr5-ve cells co-stained with CD44 and PCNA, respectively (**Fig 4.5Eii)**, resembling the profile of DCAMKL-1+ve cells. These results suggest that DCAMKL-1+ve and Lgr5-ve cells may represent the same population of stem cells, which significantly co-express CD44 and are highly proliferative. These novel findings may explain the rapid formation of tumorospheres from DCAMKL+ve and LGR5-ve cells while both LGR5+ve and DCAMKL-ve cells are much less potent towards formation of tumorospheres (**Fig 4.6Bi-ii**). It is thus possible that co-expression of CD44 by stem cells may dictate proliferative and tumorosphere formation potential of the cells.

4.3.7 Role of ANXA2 expression on spheroidal growths of colon cancer cell lines

Results with the transformed embryonic cells in chapter 3, demonstrated that over-expression of cell-surface ANXA2 (CS-ANXA2) may lead to de-stablization of spheroids, resulting in the formation of 'amorphous' structures. Down-regulation of ANXA2, on the other hand, resulted in attenuation of MMP levels and in the formation of more compact HEK-mGAS spheroids. We therefore examined if ANXA2 has a similar role in the formation of tumorospheres from colon cancer cell lines. ANXA2 expression was confirmed in HCT-116 cells by Western blot analysis **(Fig 4.8A)**. HCT-116

tumorospheres were down-regulated for ANXA2 expression by transiently transfecting the cells with ANXA2-shRNA plasmids. HCT-116 tumorospheres, transfected with control-shRNA, formed less well rounded tumorospheres by Day 2, while HCT-116 tumorospheres, treated with ANXA2-shRNA, formed more compact rounded spheroids **(Fig 4.8Bi);** down-regulation of ANXA2 was confirmed by western blot **(Fig 4.8Bii)**. However, by Day 7, both control and ANXA2-shRNA treated spheroids had formed compact spheroids, which may reflect the loss of transiently transfected shRNA in the spheroids. In future studies, the role of ANXA2 will be examined by transfecting the spheroids with viral particles expressing shRNA, which are being prepared by us in the laboratory.

4.3.8 High % of CS-ANXA2 positive cells co-express DCAMKL-1, CD44 and LGR5

Based on our findings in chapter 3 and results presented above, we further examined the % CS-ANXA2+ve cells, which are also expressing stem cell markers DCAMKL-1, CD44 and LGR5. HCT-116 cells were FACSorted using Anti-ANXA2-Abs. The % cells positive for CS-ANXA2 was measured as 3.6% of the total cell population **(Fig 4.8C).** CS-ANXA2+ve and CS-ANXA2-cells were stained by IF for the specific stem cell markers. Enrichment and separation of CS-ANXA2+ve cells from CS-ANXA2-ve cells was confirmed by IF staining for ANXA2 **(Fig 4.8D)**. A high % of CS-ANXA2+ve cells co-expressed DCAMKL-1, CD44 and LGR5, while CS-ANXA2-ve cells were not positive for the indicated stem cell markers **(Fig 4.8D)**. These results mimic our findings with HEK-mGAS cells as presented in chapter 3, suggesting that an increased co-expression of CS-ANXA2 with stem cell markers may be a hallmark of transformation, which likely impacts tumorigenic and metastatic potential of colon cancer cells as well. An important difference between transformed embryonic cells and colon

cancer cells, however, was that CS-ANXA2 also co-localized with LGR5 in colon cancer cells (**Fig 4.8D**), while transformed embryonic cells did not demonstrate this feature (Fig 4B, chapter 3). The later findings further suggest the novel possibility that co-expression of stem cell markers DCAMKL-1/CD44 with CS-ANXA2, may represent a common phenotype of all epithelial cancer stem cells, which could be used for diagnosing circulating cancer stem cells; our laboratory has completed preliminary studies developing this diagnostic assay (243), and a patent has been filed ("Diagnosis of Benign and cancerous growths by measuring circulating tumor stem cells and serum annexinA2", final patent application number D6987 UTMB-SING-P-10B, filed on June 29th 2011). In future studies, I will further analyze the % colon cancer cells which co-express CS-ANXA2 with either DCAMKL-1,CD44 and LGR5, as a function of tumorigenic and metastatic potential of the cells, and examine the effect of chemotherapeutic modalities on the co-expression profiles, which may serve as a means to diagnose therapeutic efficacy in the clinic.

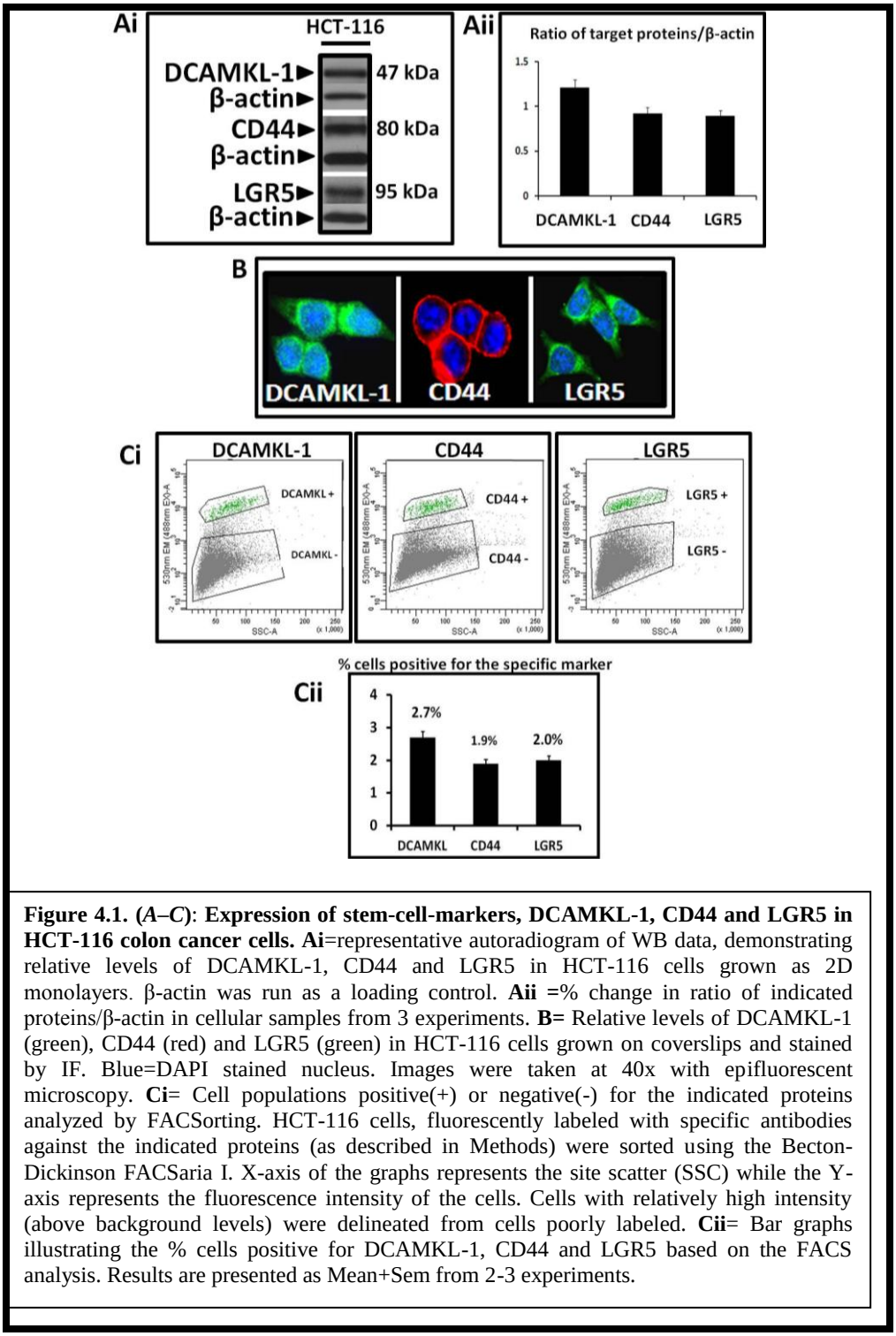

Figure 4.1. (*A–C*): **Expression of stem-cell-markers, DCAMKL-1, CD44 and LGR5 in HCT-116 colon cancer cells. Ai**=representative autoradiogram of WB data, demonstrating relative levels of DCAMKL-1, CD44 and LGR5 in HCT-116 cells grown as 2D monolayers. β-actin was run as a loading control. **Aii** =% change in ratio of indicated proteins/β-actin in cellular samples from 3 experiments. **B=** Relative levels of DCAMKL-1 (green), CD44 (red) and LGR5 (green) in HCT-116 cells grown on coverslips and stained by IF. Blue=DAPI stained nucleus. Images were taken at 40x with epifluorescent microscopy. **Ci**= Cell populations positive(+) or negative(-) for the indicated proteins analyzed by FACSorting. HCT-116 cells, fluorescently labeled with specific antibodies against the indicated proteins (as described in Methods) were sorted using the Becton-Dickinson FACSaria I. X-axis of the graphs represents the site scatter (SSC) while the Y-axis represents the fluorescence intensity of the cells. Cells with relatively high intensity (above background levels) were delineated from cells poorly labeled. **Cii**= Bar graphs illustrating the % cells positive for DCAMKL-1, CD44 and LGR5 based on the FACS analysis. Results are presented as Mean+Sem from 2-3 experiments.

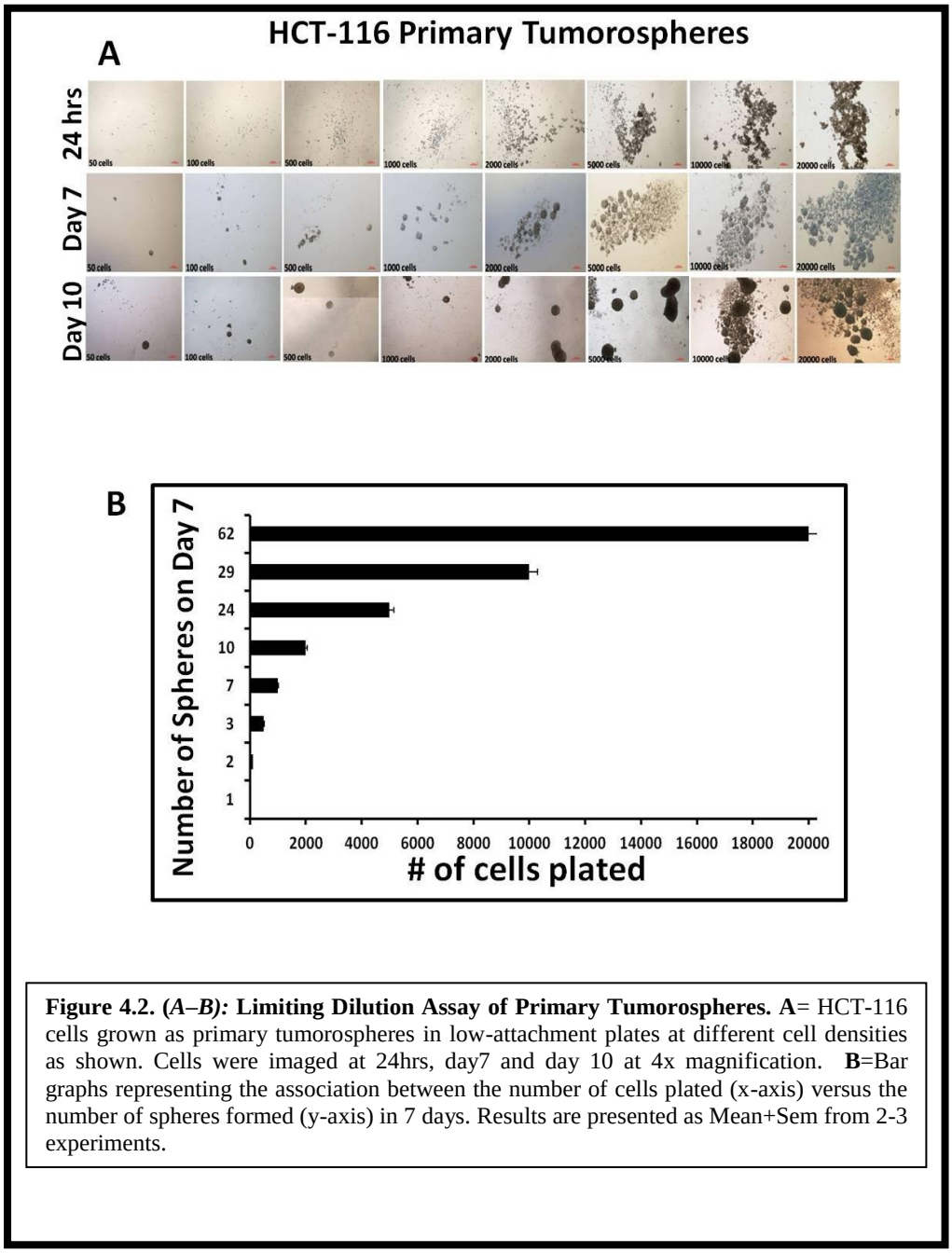

Figure 4.2. (*A–B*): Limiting Dilution Assay of Primary Tumorospheres. A= HCT-116 cells grown as primary tumorospheres in low-attachment plates at different cell densities as shown. Cells were imaged at 24hrs, day7 and day 10 at 4x magnification. **B**=Bar graphs representing the association between the number of cells plated (x-axis) versus the number of spheres formed (y-axis) in 7 days. Results are presented as Mean+Sem from 2-3 experiments.

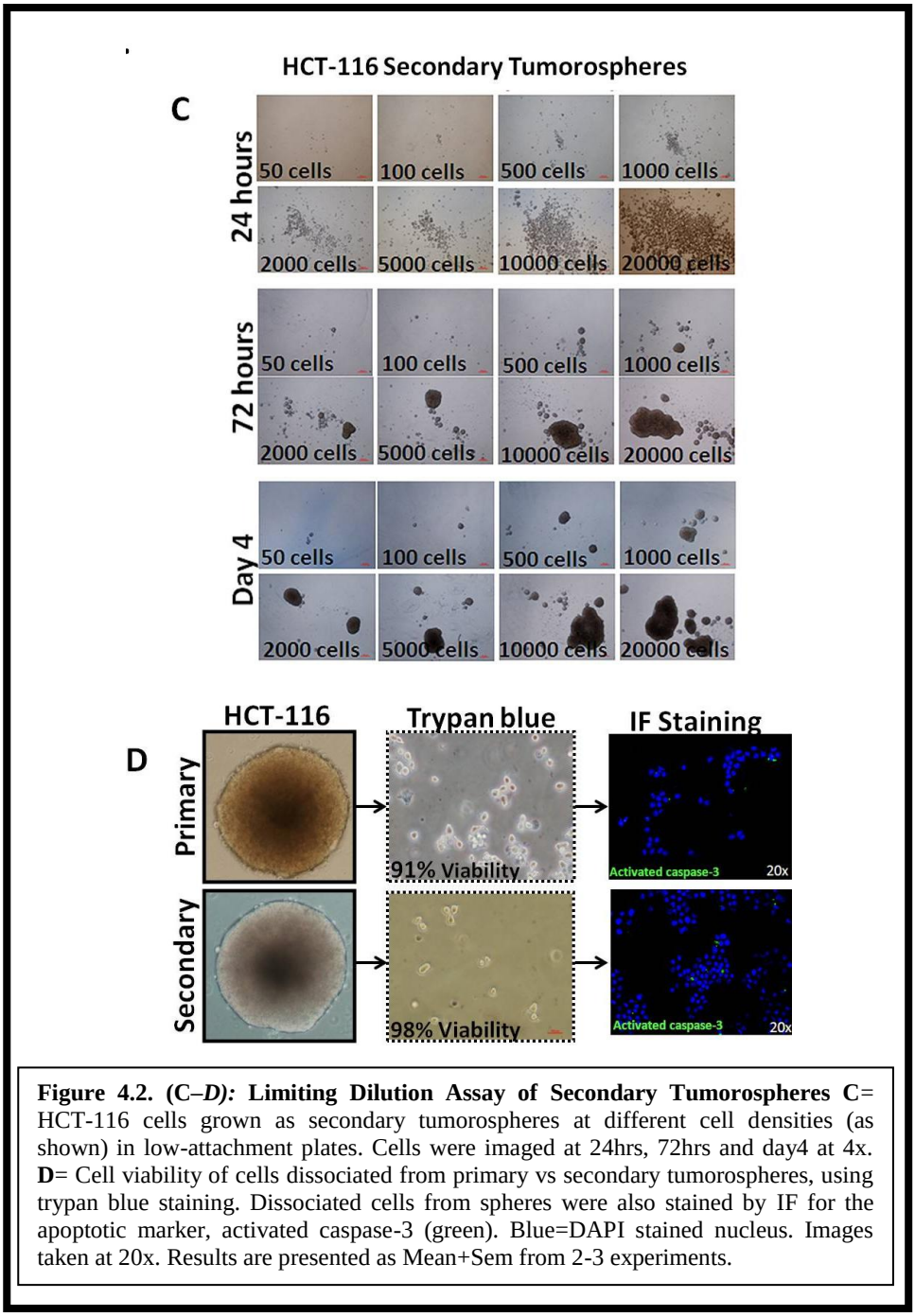

Figure 4.2. (C–*D*): Limiting Dilution Assay of Secondary Tumorospheres C= HCT-116 cells grown as secondary tumorospheres at different cell densities (as shown) in low-attachment plates. Cells were imaged at 24hrs, 72hrs and day4 at 4x. **D**= Cell viability of cells dissociated from primary vs secondary tumorospheres, using trypan blue staining. Dissociated cells from spheres were also stained by IF for the apoptotic marker, activated caspase-3 (green). Blue=DAPI stained nucleus. Images taken at 20x. Results are presented as Mean+Sem from 2-3 experiments.

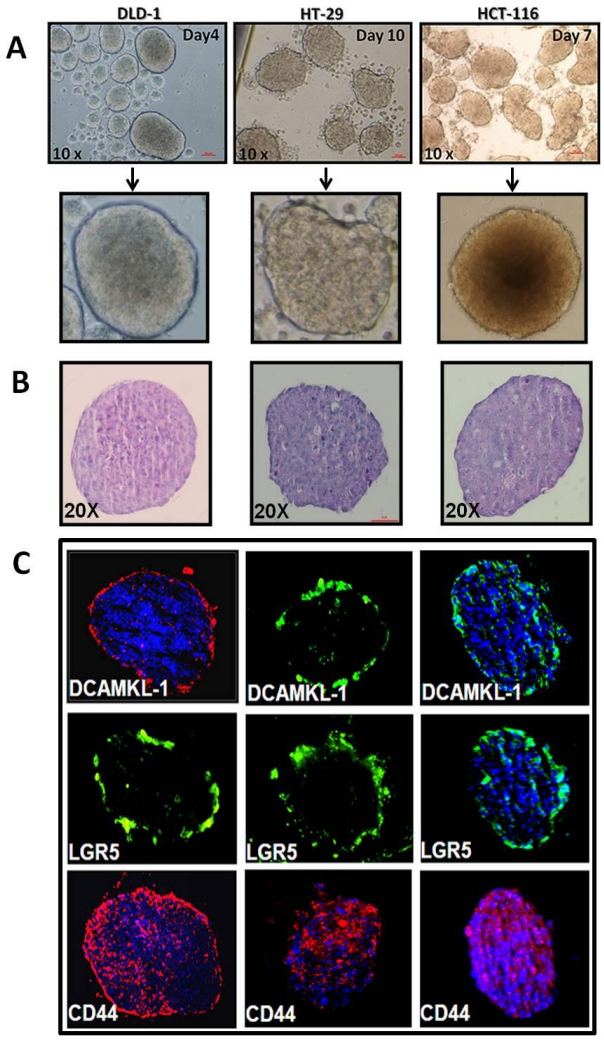

Figure 4.3. (*A–C):* Morphological/cellular features of tumorospheres formed from colon cancer cell lines. A= Equal number of DLD-1, HT-29 and HCT-116 cells were grown as primary tumorospheres. Images were taken at days 4, 6 and 10 respectively at 4x. Representative tumorospheres (zoomed in) are shown. **B**= H&E staining from a representative section (5µm) of fixed and processed tumorospheres from all 3 colon cancer cell lines. **C**= IF stained sections, for stem cell markers DCAMKL-1, CD44 and LGR5, from representative tumorospheres of the three colon cancer cell lines. Blue=DAPI stained nucleus. Images were taken at 20x.

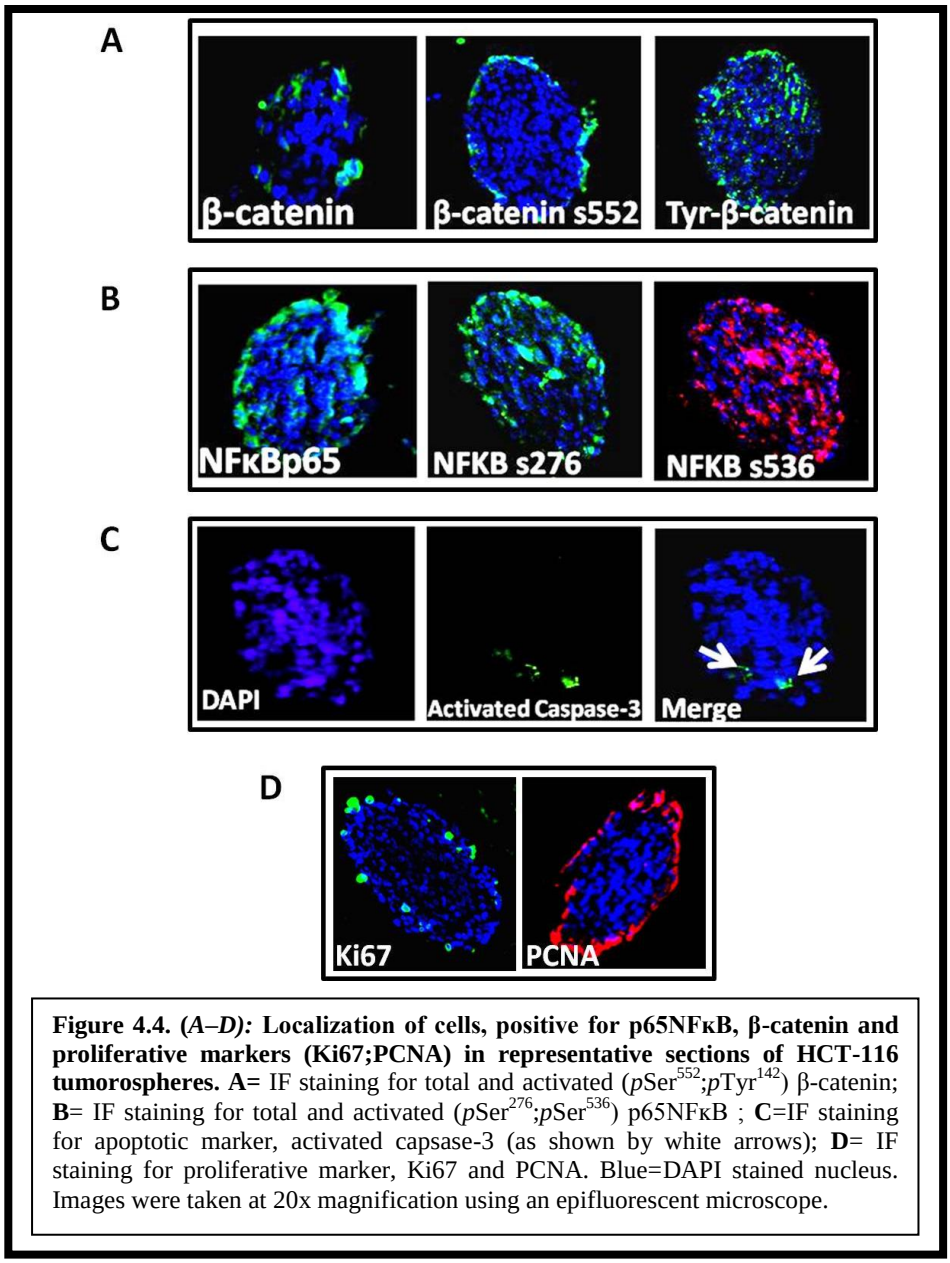

Figure 4.4. (*A–D):* Localization of cells, positive for p65NFκB, β-catenin and proliferative markers (Ki67;PCNA) in representative sections of HCT-116 tumorospheres. A= IF staining for total and activated (pSer^{552};pTyr^{142}) β-catenin; **B**= IF staining for total and activated (pSer^{276};pSer^{536}) p65NFκB ; **C**=IF staining for apoptotic marker, activated capsase-3 (as shown by white arrows); **D**= IF staining for proliferative marker, Ki67 and PCNA. Blue=DAPI stained nucleus. Images were taken at 20x magnification using an epifluorescent microscope.

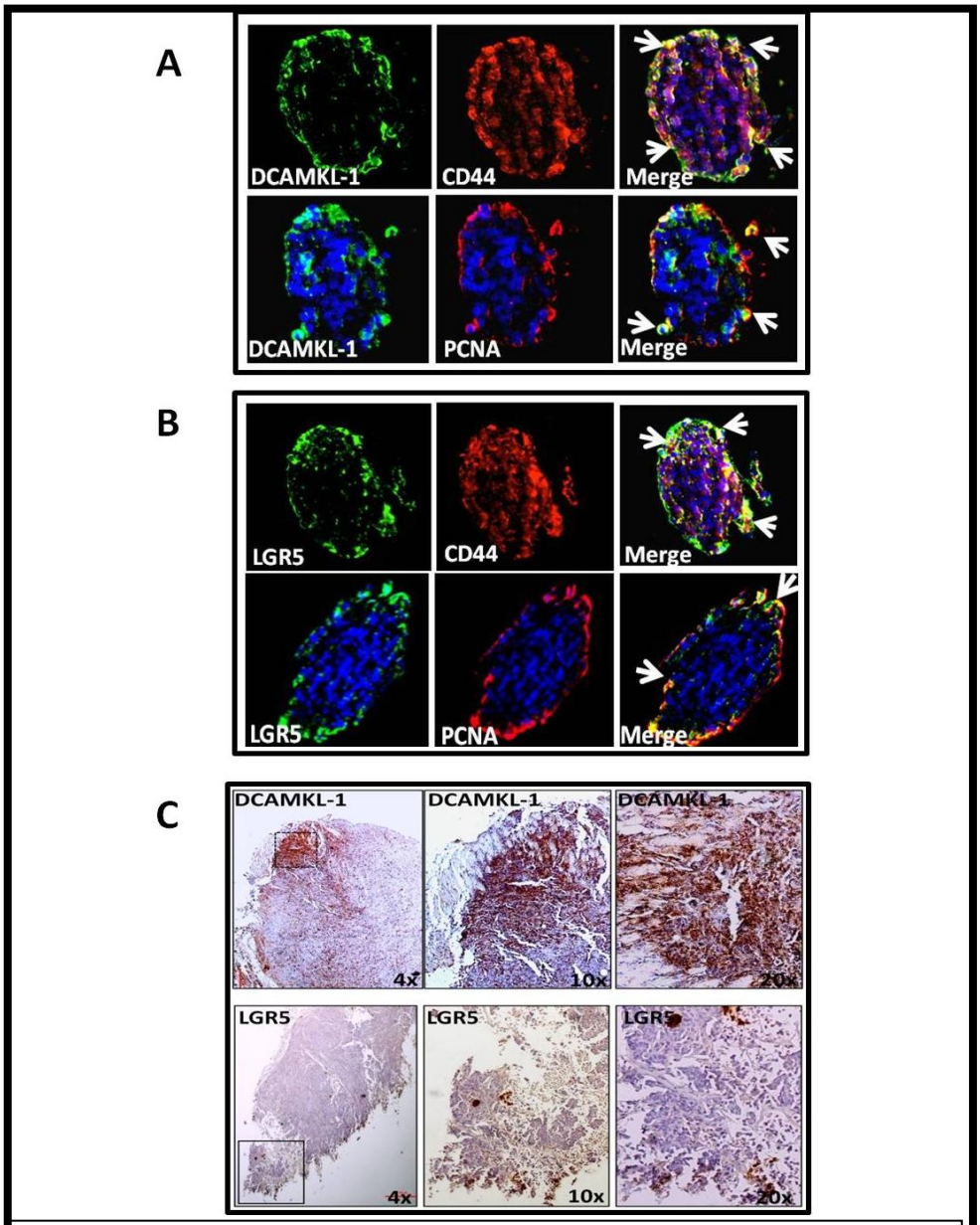

Figure 4.5. (*A–C):* Co-Localization of DCAMKL-1(A) or LGR5 (B) positive stem cells with either CD44 or PCNA, in representative sections of HCT-116 spheres. A-B=IF staining for observing co-expression of the indicated markers are shown in merged images. Co-localization is depicted by white arrows. Images were taken at 20x magnification. Blue=DAPI stained nucleus**. C**= Representative sections (4-5µm) from HCT-116 tumor xenografts were stained by immunohistochemistry for either DCAMKL-1 or LGR5, as shown. Images in the left hand panels were taken at 4x. Insets were further imaged at 10x or 20x as shown in the middle and right hand panels, respectively.

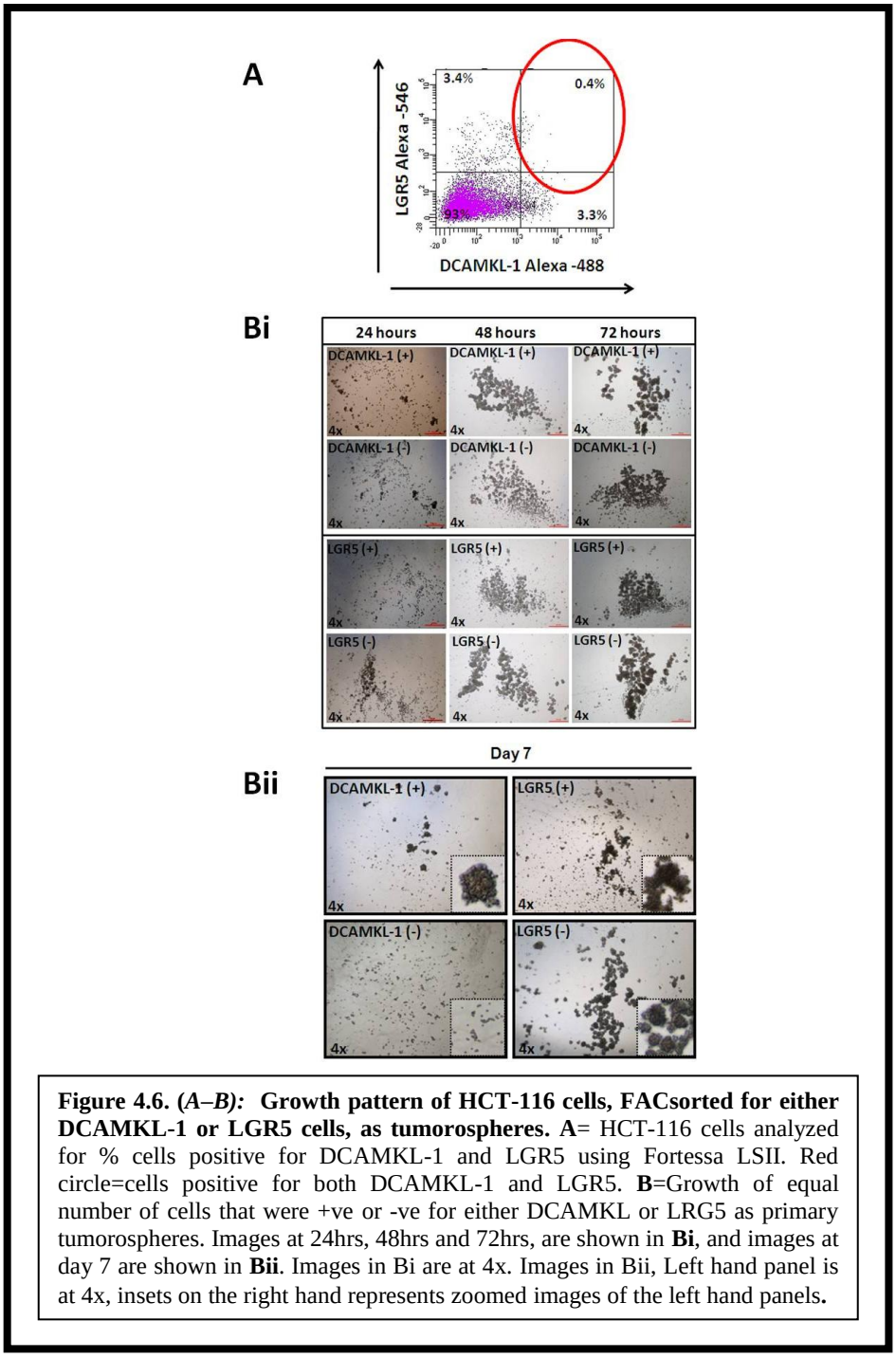

Figure 4.6. (*A–B):* Growth pattern of HCT-116 cells, FACsorted for either DCAMKL-1 or LGR5 cells, as tumorospheres. A= HCT-116 cells analyzed for % cells positive for DCAMKL-1 and LGR5 using Fortessa LSII. Red circle=cells positive for both DCAMKL-1 and LGR5. **B**=Growth of equal number of cells that were +ve or -ve for either DCAMKL or LRG5 as primary tumorospheres. Images at 24hrs, 48hrs and 72hrs, are shown in **Bi**, and images at day 7 are shown in **Bii**. Images in Bi are at 4x. Images in Bii, Left hand panel is at 4x, insets on the right hand represents zoomed images of the left hand panels**.**

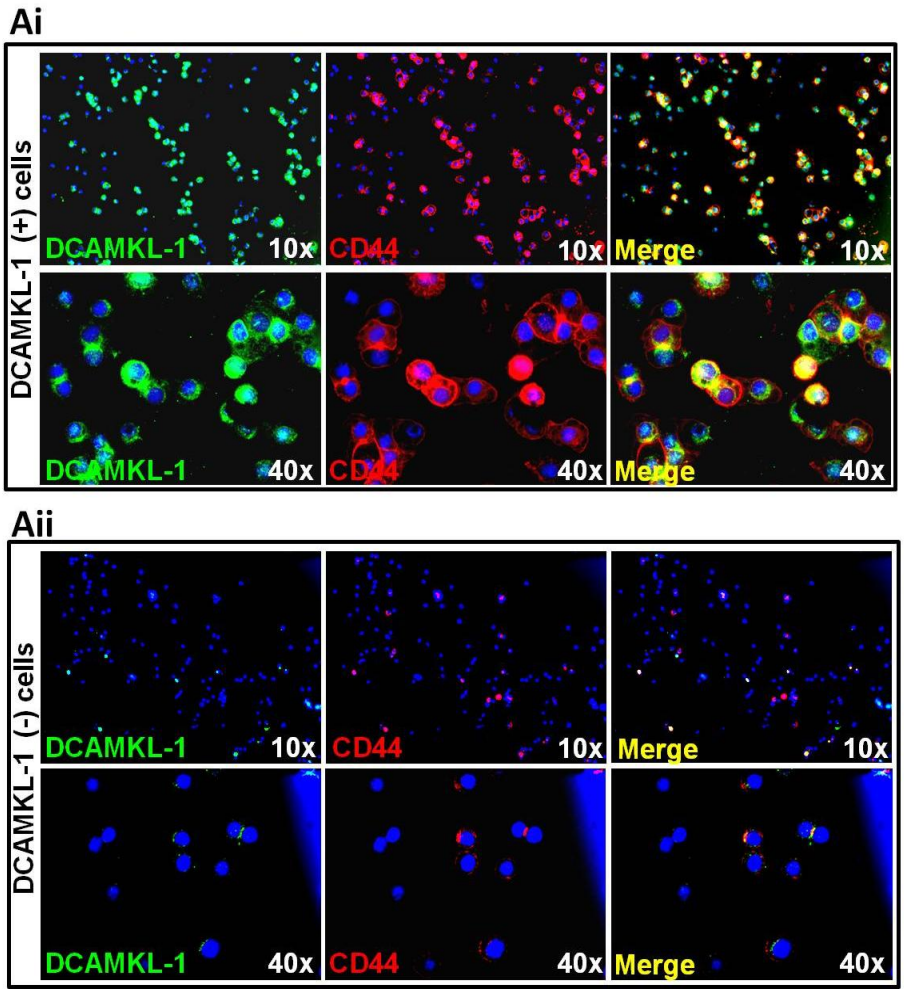

Figure 4.7. (*Ai-ii):* Co-expression of DCAMKL-1(+/-) cells and CD44 in colon cancer cells. Ai-ii=HCT-16 cells FACSorted for the stem cell marker DCAKML-1. DCAMKL-1(+/-) cells were cytopsun and stained by IF for DCAMKL-1 (green) and CD44 (red). Blue=DAPI stained nucleus. Images were taken at 10x and 40x. Yellow color in the merged images suggests co-localization of DCAMKL-1 and CD44 in the cells. The data presented are representative of >10 sections from 2 separate experiments

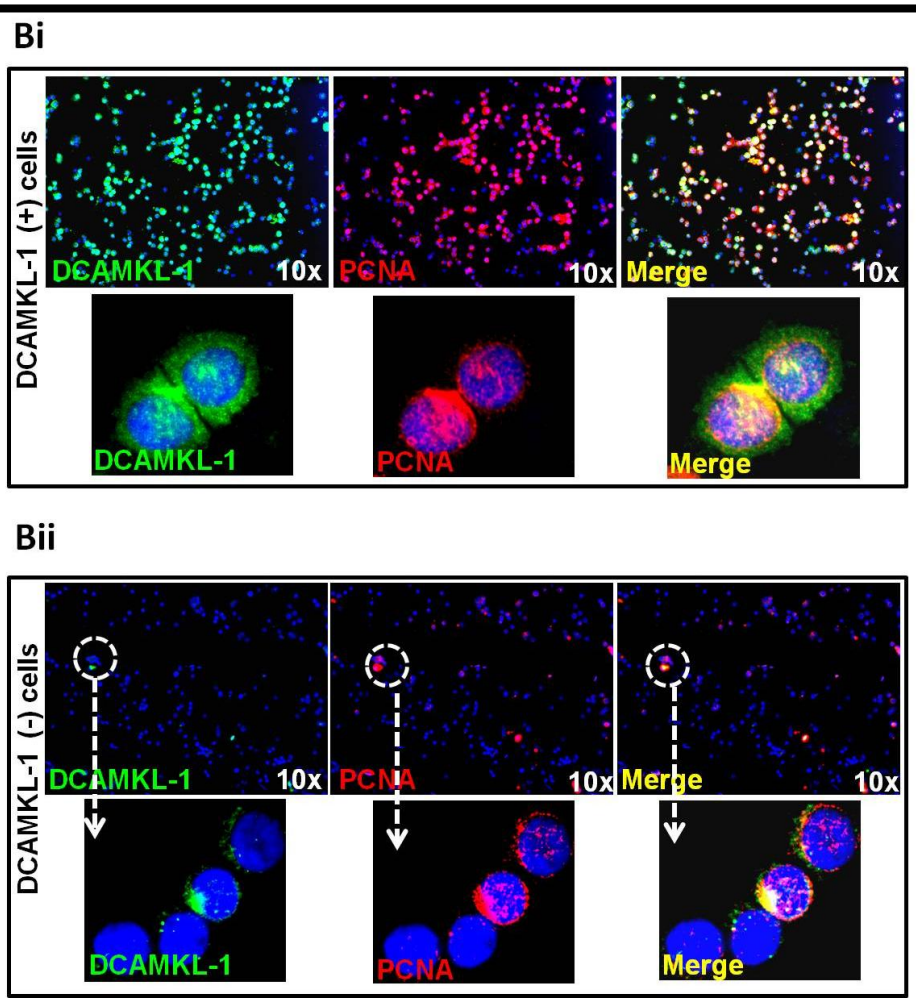

Figure 4.7. (*Bi-ii):* Proliferative potential of DCAMKL-1+ve versus DCAMKL-1-ve cells in HCT-116 cells. Bi-ii= DCAMKL-1(+/-) cells were cytopsun and stained by IF for stem cell marker DCAMKL-1 (green) and proliferative marker PCNA (red). Blue=DAPI stained nucleus. Images were taken at 10x and cells depicted by the white dotted circles were digitally enhanced as marked by white dotted arrows. Yellow color in the merged images suggests co-localization of DCAMKL-1 and PCNA in the cells. The data presented are representative of >10 sections from 2 separate experiments.

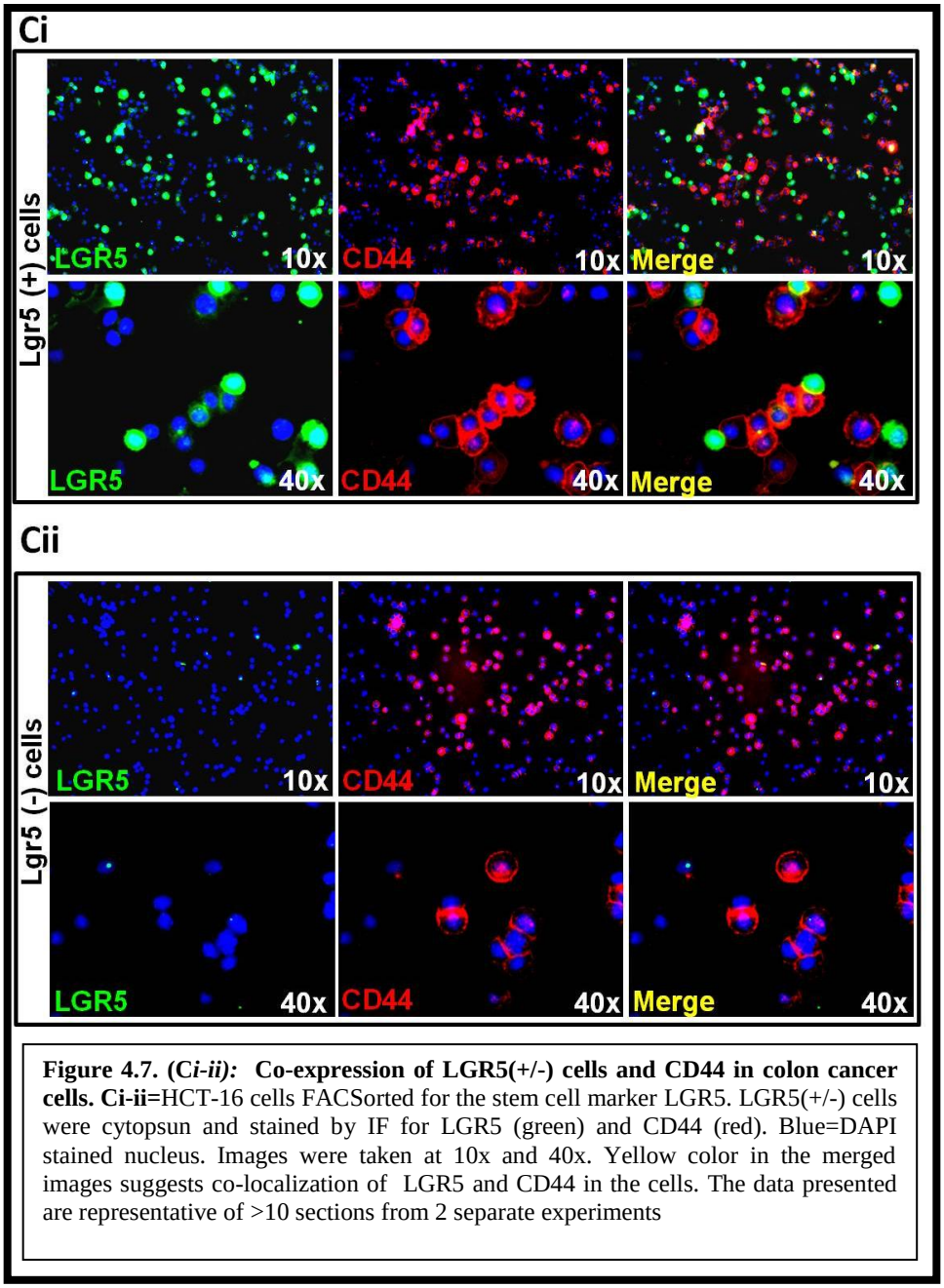

Figure 4.7. (C*i-ii):* Co-expression of LGR5(+/-) cells and CD44 in colon cancer cells. Ci-ii=HCT-16 cells FACSorted for the stem cell marker LGR5. LGR5(+/-) cells were cytopsun and stained by IF for LGR5 (green) and CD44 (red). Blue=DAPI stained nucleus. Images were taken at 10x and 40x. Yellow color in the merged images suggests co-localization of LGR5 and CD44 in the cells. The data presented are representative of >10 sections from 2 separate experiments

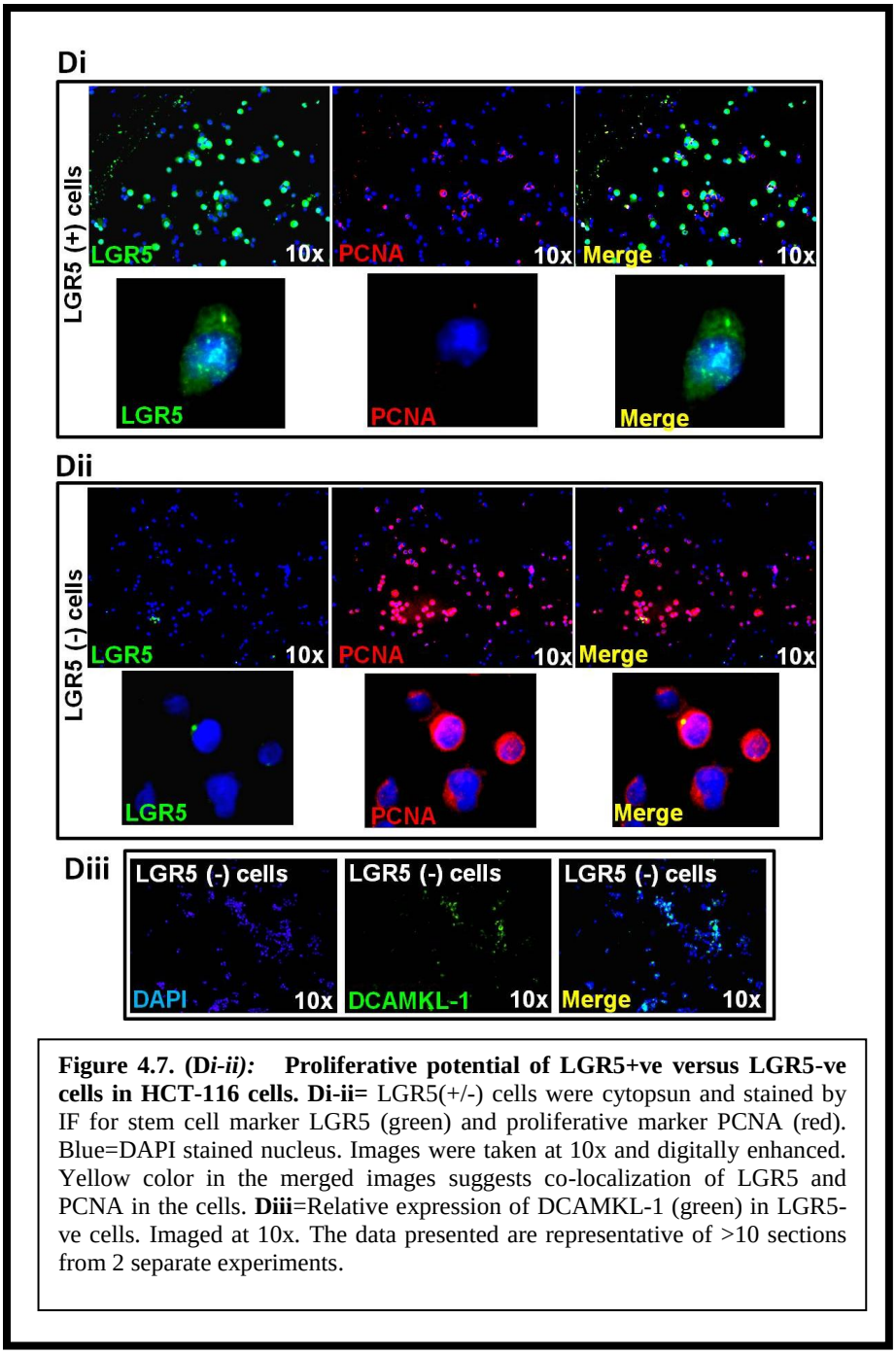

Figure 4.7. (D*i-ii):* **Proliferative potential of LGR5+ve versus LGR5-ve cells in HCT-116 cells. Di-ii=** LGR5(+/-) cells were cytopsun and stained by IF for stem cell marker LGR5 (green) and proliferative marker PCNA (red). Blue=DAPI stained nucleus. Images were taken at 10x and digitally enhanced. Yellow color in the merged images suggests co-localization of LGR5 and PCNA in the cells. **Diii**=Relative expression of DCAMKL-1 (green) in LGR5-ve cells. Imaged at 10x. The data presented are representative of >10 sections from 2 separate experiments.

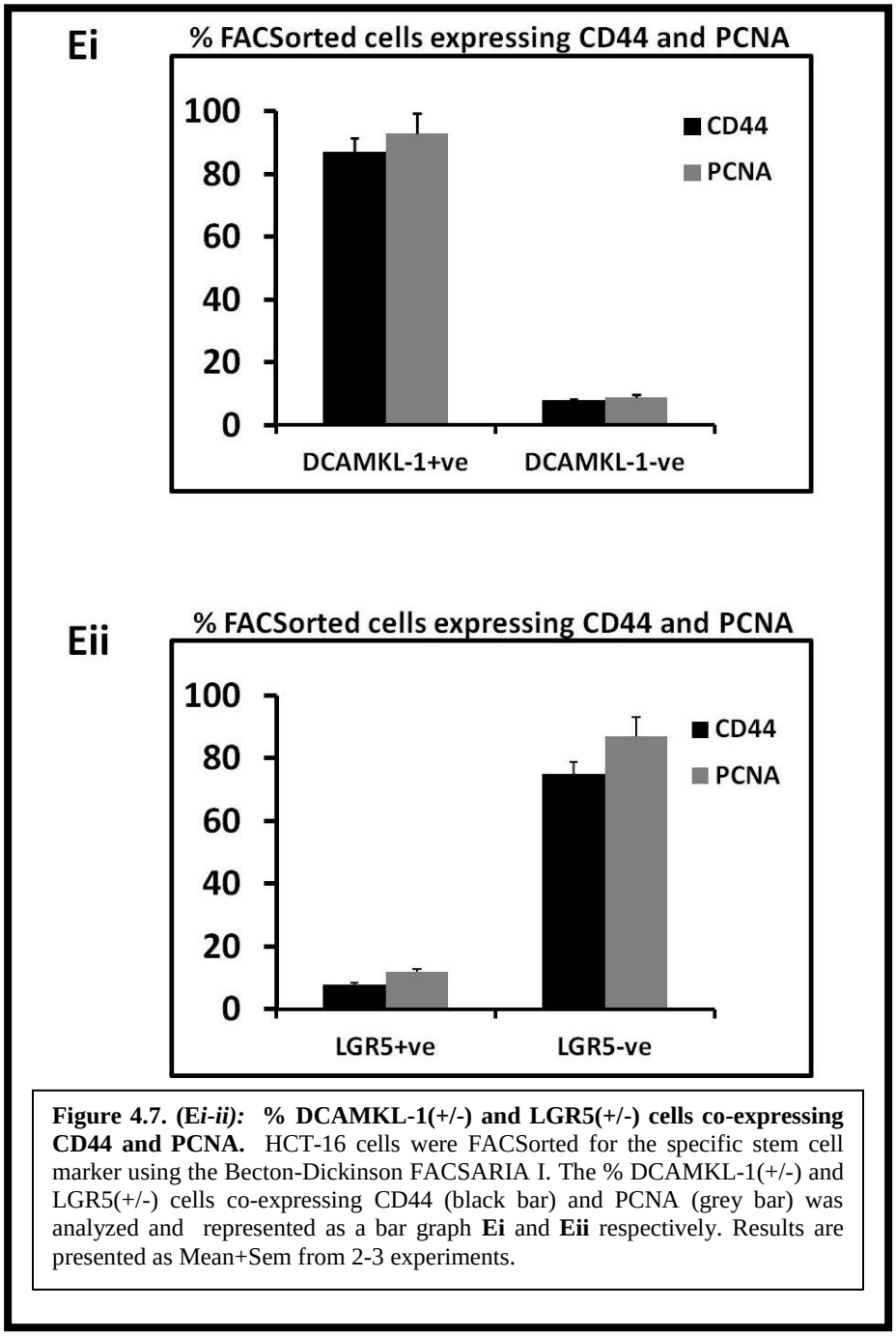

Figure 4.7. (E*i-ii):* % DCAMKL-1(+/-) and LGR5(+/-) cells co-expressing CD44 and PCNA. HCT-16 cells were FACSorted for the specific stem cell marker using the Becton-Dickinson FACSARIA I. The % DCAMKL-1(+/-) and LGR5(+/-) cells co-expressing CD44 (black bar) and PCNA (grey bar) was analyzed and represented as a bar graph **Ei** and **Eii** respectively. Results are presented as Mean+Sem from 2-3 experiments.

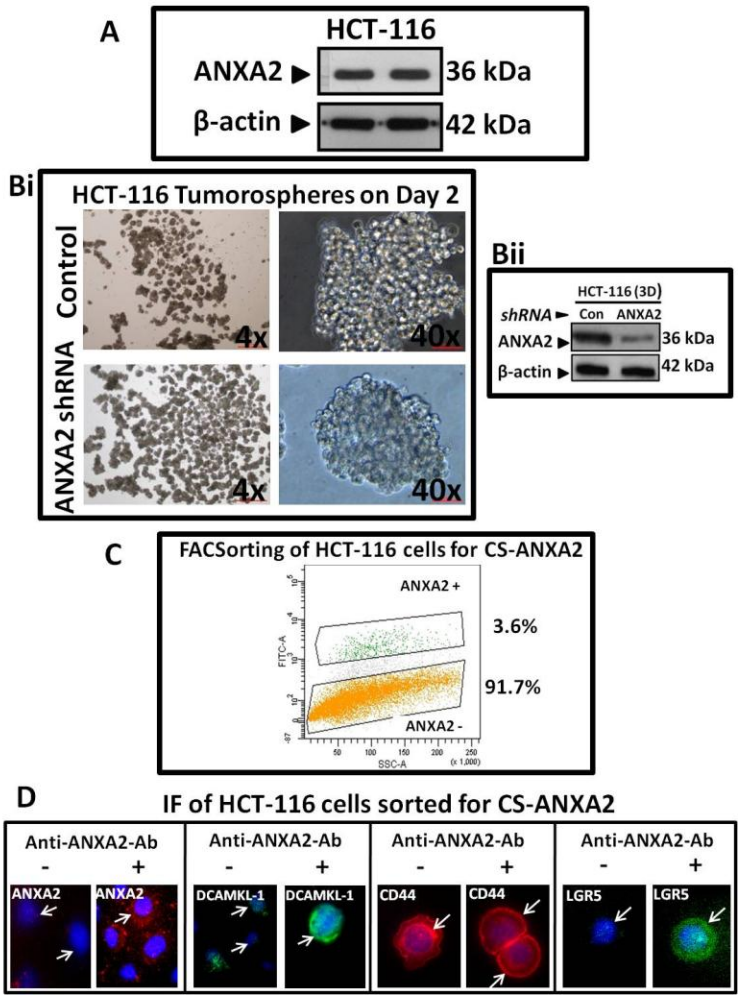

Figure 4.8. (*A-D):* Role of Annexin A2 in the formation of tumorospheres from colon cancer cell lines. A= Representative immunoblot illustrating the relative expression of ANXA2 in HCT-116 cells bby WB analysis. β-actin was run as a loading control. **Bi**= Representative images of spheroids from HCT-116 cells, transfected with either control or ANXA2-shRNA plasmids. Images were taken at 4x and 40x at day 2. **Bii**= Representative immunoblot illustrating the relative expression of ANXA2 in HCT-116 spheres transfected with control vs ANXA2-shRNA, by WB analysis. **C**= Representative graph illustrating FACSorting analysis of HCT-116 cells positive(+) and negative (-) for CS-ANXA2. HCT-116 cells fluorescently labeled with anti-ANXA2-Ab were sorted using the Becton-Dickinson FACSAria I. X-axis of the graph represent the side scatter (SSC) while the y-axis represent the fluorescence intensity of the cells. Cells with relatively high intensity (above background levels) were delineated in green vs cells with low intensity (orange). **D=** Representative images of HCT-116 cells, FACSorted for ANXA2(-) /ANXA2(+) populations and cytospun onto glass slides. Cells were stained by IF for the relative expression of stem cell markers DCAMKL-1 (green), CD44 (red),LGR5(green) and ANXA2/CS-ANXA2 (red). Images were taken at 40x. Blue=DAPI stained nucleus.

4.4 DISCUSSION

Results presented in this chapter demonstrate that DCAMKL-1+ve and LGR5+ve cells represent two distinct cancer stem cell populations, which are characterized by differences in proliferative potential, spheroidal growth patterns and expression profiles for CD44/CS-ANXA2/PCNA.

DCAMKL-1, CD44 and LGR5 expression levels have been shown to be significantly increased in colon cancer tumors, and are increased with progression of the disease (72,88,84). In the above studies, we confirmed the presence of all three stem cell markers in HCT-116 colon cancer cell line. Cells positive for the specific markers ranged from 1-3% of the total cell population, which is in conformity with the range of stem cell populations in tumors **(Fig 4.1)**.

It has been reported that normal stem cells (NSCs) can potentially form organoid-like structures *in vitro*, which differentiate into specialized cell types representing the organ of origin (234), as confirmed by me in preliminary studies with colonic crypt stem cells (data not shown). In contrast, cancer stem cells (CSCs), grown as spheroids result in the formation of compact spheroidal structures which are held together by a basement membrane (244, 232), as confirmed by us with HEK-mGAS and colon cancer cells (chapters 3 and 4). In preliminary studies, we have demonstrated that the well defined peripheral membrane, surrounding HCT-116 spheroids is composed of collagen IV and several other matrix proteins (data not shown). Importantly, the cancer cell spheroids appeared to be solid with relative absence of differentiated features within the time frame of our studies. It is expected that long term growth in culture, resulting in very large spheroidal structures, may eventually result in cell death and necrosis of inner most cells, reflecting lack of nutrition (as observed in my preliminary studies).

The size of the spheroids varied when plating low versus high concentrations of cells **(Fig 4.2A-C)**. It is possible, that the increase in cell density, leads to the formation of numerous small spheroids which aggregate with one another to form even larger structures. It has also been reported that a single stem cell is capable of forming an entire sphere (245); therefore the correlation between tumorosphere size and cell density may merely be caused by an increase in the census of cancer stem cells within the population. Unlike the normal stem cells, CSCs are highly proliferative and shown to be continuously motile (246), which may explain the rapid sphere formation observed when plating high versus low cell densities.

From our studies in Chapter 3, we learnt that over-expression of PG in HEK-mGAS cells led to formation of 'amorphous' spheroids compared to control HEK-C cells, which formed compact spheroids. We also demonstrated that HEK-mGAS cells had become significantly more proliferative and tumorigenic compared to HEK-C cells. We speculated that these differences in growth patterns may reflect either over-expression of PG in HEK-mGAS cells or transformation of normal/non-transformed cells into a tumorigenic/transformed phenotype. In here, we examined the growth of 3 different colon cell lines, HCT-116, HT-29 and DLD-1, as tumorospheres. Our data demonstrate that all 3 cell lines grew tumorospheres **(Fig 4.3A)**; however cells expressing higher levels of PG, such as DLD-1 and HCT-116, formed tumorospheres more rapidly compared to HT-29 cells expressing low levels of PG (235). It is also possible that HT-29 cells may have a lower census of stem cells compared to HCT-116 and DLD-1 cells, which need to be examined in future studies. Thus, tumorigenic potential, number of stem cells and expression of autocrine factors such as PG, may likely dictate the morphology and number of spheroids formed from a cell line in a given time.

We recently reported the distinct localization of DCAMKL-1 and CD44

expressing cells in normal colonic crypts, and demonstrated that cell populations expressing these stem/progenitor cell markers are significantly increased in colonic crypts of mice in response to PG (51 and chapter 3). Other investigators have also reported DCAMKL-1+ve cells in intestinal crypts at +4 position and have demonstrated DCAMKL-1 expression in colonic tumors 20, 72). Unlike DCAMKL-1, LGR5+ve cells have been reported at the base of intestinal crypts (76), confirming that the two stem cell populations are separate and distinct from each other in normal intestinal crypts. We now demonstrate that DCAMKL+ve and LGR5+ve stem cells similarly represent different population of cancer stem cells, as observed in HEK-mGAS (chapter 3) and HCT-116 cells **(Fig 4.6A)**. However, a very small % of colon cancer stem cells may be co-expressing both stem cell markers (**Fig 4.6A**), which is a novel finding, the significance of which needs to be further examined.

Our results in Chapter 3, demonstrated that DCAMKL-1 and LGR5+ve cells were localized at the periphery of spheroids formed from non-transformed immortalized HEK-C cells, while CD44 was localized at both the perimeter and within the spheroids. However, we were unable to determine the localization of stem cell markers in tumorospheres formed from transformed HEK-mGAS cells, as the spheroids were relatively unstable and dissociated easily when processed. We were, however, successful in localizing DCAMKL-1, LGR5 and CD44 +ve cells in tumorospheres formed from colon cancer cell lines, which represents a new finding of my studies. We confirmed that DCAMKL-1 and LGR5 +ve cells were indeed localized on the outer peripheral layer of spheroids, while CD44 was expressed throughout the spheroids (**Fig 4.3C**), as we had observed in the case of HEK-C cells, suggesting that this pattern of distribution of stem cell populations may represent a common feature of all spheroids. DCAMKL-1, CD44 and LGR5 were also found to be localized at the leading edges of HCT-116 xenografts

(Fig 4.5C), which is similar to the recent findings of other investigators (81, 247), suggesting that stem cells may have a propensity of growing at invasive ends, to support tumor growth.

The outer peripheral layer of tumorospheres has been reported to be actively proliferating, while cells in the inner core were shown to be necrotic (232). At the same time, previous reports suggest that DCAMKL-1 marks quiescent stem cell populations whereas LGR5 marks actively cycling stem cells in normal intestinal crypts (67). However, proliferative potential of DCAMKL-1 and LGR5 positive cancer stem cells has remained unknown so far. Our findings with HCT-116 cells strongly suggest that DCAMKL-1+ve cells, co-expressing PCNA, may be significantly more proliferative than LGR5+ve cells, which did not co-stain with PCNA as well **(Fig 4.5B, 4.7Aii).** This important finding co-tails with our findings that cancer stem cells enriched for DCAMKL-1 grew tumorospheres rapidly while LGR5+ve cells were not as effective **(Fig 4.6Bi-ii)**, and suggests that the properties of DCAMKL+ve cancer stem cells may be quite different from that of DCAMKL+ve normal stem cells, which needs to be further explored.

Our results with colon cancer cell lines further confirmed our findings with HEK-mGAS cells that, DCAMKL-1+ve cells co-express CD44, while LGR5+ve cells are less likely to co-express CD44 **(Fig 4.7Ai, Ci)**. Knockdown of CD44 is known to inhibit cell proliferation/invasion of cancer cells, and induces apoptosis of colon cancer cell lines (248). Thus our results with HEK-mGAS and HCT-116 colon cancer cells, strongly suggest that the increased proliferative potential of these cells may be due to co-expression of CD44 with stem cell marker DCAMKL-1, which maybe a hallmark of tumorigenecity

A novel finding of our studies was that HCT-116 cells, enriched for DCAMKL-1, grew larger tumorospheres more rapidly, compared to LGR5+ve cells which did not grow spheroids as well, and seemed to remain dormant for a while in non-adherent cultures **(Fig 4.6Bi-ii)**.

In a recent study, it was reported that silencing of LGR5 expression surprisingly promoted tumorigenesis by up-regulating the Wnt signaling pathway and the epithelial-mesenchymal pathway (87). Reducing the expression of LGR5 in colon cancer cells resulted in the formation of amorphous spheroids, increased cell migration, increased cell motility and rearrangement of cell surface proteins such as CD44 (87). Thus, our results demonstrating that LGR5-ve cells grow larger spheroids than LGR5+ve cells (**Fig 4.6Bii**), are in agreement with the findings of Walker et al. 2011 (87), as described above. The above findings may be explained by our novel observations that CD44 and DCAMKL-1 are co-expressed by a significant population of LGR5-ve cells **(Fig 4.7Aii, Cii, Diii)**, which appears to be conducive to proliferation and growth of cancer stem cells as tumorospheres.

The role of CD44 in the growth and metastasis of colon cancer cell lines has been reported by many investigators (249, 103). A recent study demonstrated that displacement of CD44 from a single focal point to a uniform distribution throughout the cell membrane results from of the expression of MMPs in colon cancer cells, which apparently leads to CD44 shedding and increased migration/invasion of the cells (87). However, another recent study suggests that CD44 is expressed at focal adhesion points in invading cancer cells (250). In future studies, I will examine the specific role of CD44 in dictating growth/invasive effects on DCAMKL+ve and LGR5-ve cancer stem cell populations.

The activation of NFκB and β-catenin signaling pathways has been reported to play a critical role in regulating the proliferative potential of colon cancer cells (118,251). In chapter 2, our studies demonstrated that the down-regulation of p65NFKB or β-catenin significantly reduced proliferation of HEK-mGAS cells (51). Elevated levels p65NFβB or β-catenin resulted in the increased expression of stem cell markers DCAMKL-1 and CD44 in HEK-mGAS cells and colonic crypts in response to PG (51). The localization of cells expressing the two potent transcriptional factors in tumorospheres has not been reported. We demonstrate for the first time that cells positive for p65NFKB and β-catenin are located along the periphery of the tumorospheroids **(Fig 4.4A-B)**. Given that the cancer stem cells expressing DCAMKL-1 and LGR5 were also localized along the periphery of the tumorospheres, it is possible that cancer stem cells may be activated for p65NFKB and/or β-catenin. CD44 is known to activate p65NFKB signaling pathway (252), and our laboratory has reported that activated p65NFkB can up-regulate β-catenin stablization via non-canonical pathway (118), resulting in proliferation of target cells. Since our data strongly suggest that DCAMKL-1+ve colon cancer stem cells co-express CD44 and are highly proliferative, compared to LGR5+ve cells, it is possible that p65NFκB and/or β-catenin expressing cells observed at the periphery of the tumorospheres represent DCAMKL+ve cells and not LGR5+ve cells. At the same time, we now know that LGR5 is a target gene of β catenin (87), suggesting that LGR5+ve cells should also be positive for activated (nuclear) β-catenin. There are thus many unanswered questions that arise from our novel findings, which need to be further investigated in future studies.

We have previously reported that AnnexinA2 plays a critical role in mediating growth effects of PG on normal and cancerous cell lines (51,112,182), via facilitating endocytotic internalization of PG in target cells (187). Results in chapter 3 additionally

suggest that presence of CS-ANAX2 may impact mobility of cells, resulting in the formation of 'amorphous' spheroids from HEK-mGAS cells; this newly discovered function of CS-ANXA2 is quite separate from its role as a receptor for PG, and appears to be linked to the increased expression of MMPs by transformed/cancer cells. In order to confirm a possible role of ANXA2 in impacting morphology of tumorospheres, as a function of MMPs, we repeated the experiments with HCT-116 cells. Down-regulation of ANXA2 in HCT-116 cells, resulted in the formation of more compact spheroids compared to the control HCT-116 spheroids, confirming our findings with HEK-mGAS cells. These results confirm a possible role of ANXA2 in dictating the morphology of spheroidal growths. CS-ANXA2 has been reported to be overexpressed in several cancers including colon cancers (182), and accumulating literature strongly suggests a critical role of CS-ANXA2 in the invasive potential of cancer cells (as discussed in chapter 3). Transformed HEK-mGAS cells co-expressed DCAMKL-1/CD44/CS-ANXA2, while non-transformed HEK-C cells rarely co-expressed these three proteins. This finding demonstrated for the first time a significant difference in the expression profiles of stem cells from normal/non-transformed versus transformed/tumorigenic cells. Our results with HCT-116 cells confirmed that colon cancer stem cells, co-express as well CS-ANXA2 and CD44 with DCAMKL-1; however unlike transformed embryonic cells, colon cancer stem cells co-expressed CS-ANXA2 and CD44 with LGR5 also, albeit at much lower frequency compared to co-expression with DCAMKL-1. The latter findings suggest that cancer stem cells may have differences in the specific phenotypes, depending on tissue of origin.

In summary, DCAMKL-1 and LGR5+ve cancer stem cells represent two distinct cell populations, similar to that reported for normal colonic epithelial cells. DCAMKL-1+ve cancer stem cells form tumorospheres more rapidly than LGR5+ve cancer stem

cells, which may reflect the co-expression of CD44/CS-ANXA2 and MMPs by DCAMKL+ve cells. A surprising finding was that LGR5-ve cells were almost as potent as DCAMKL+ve cells in a tumorosphere bioassay, which likely reflects the expression of DCAMKL-1/CD44 by the LGR5-ve cell populations. ANXA2 expression was associated with a slight loss in spheroidal structures formed from colon cancer stem cells, which may reflect the expression of MMPs in cells expressing CS-ANXA2. Thus co-expression of CD44 and CS-ANXA2 by DCAMKL+ve stem cells may impart a more tumorigenic phenotype to cancer stem cells, which could be used as a diagnostic/prognostic feature of cancer cells/tumors.

CHAPTER 5

COMBINATORY EFFECTS OF CURCUMIN ± SIRNA DCAMKL-1 ON COLON CANCER STEM CELLS *IN VITRO* AND *IN VIVO*: NOVEL TREATMENT STRATEGY

5.1 INTRODUCTION

The ultimate goal in the field of cancer is to treat the disease and prevent its recurrence. Although several therapies, such as chemotherapy and radiation, are currently available for treating cancers, they lack the ability to differentiate between normal and cancer cells, and hence elicit many side effects on normal cells functions. Moreover, currently available treatment strategies target solely the bulk of the rapidly proliferating tumor cells, without eliminating the subpopulation of cancer stem cells, thus resulting in tumor relapse. To address these issues, researchers are developing novel therapies which not only use of non-toxic drugs but are also aimed at directly targeting cancer stem cells, in hopes of preventing tumor recurrence of the disease.

Curcumin is a natural dietary pigment which is currently being used as a chemotherapeutic agent for treating colorectal cancers (253). This non-toxic compound exerts anti-inflammatory, anti-proliferative and anti-tumorigenic effects on cancer cells (154,155), as reported by our laboratory as well (155) hence, a perfect candidate for our studies.

DCAMKL-1 is a microtubule-associated protein kinase which is overexpressed in various tumors types including colorectal cancers (72). In chapters 3 and 4, we demonstrated that DCAMKL-1+ve cancer stem cells, may represent a population of

transformed stem cells which are highly proliferative and may be involved metastasis of the cells. It has been reported that down-regulation of DCAMKL-1 in colon cancer cells decreases proliferative potential of tumors, resulting in growth arrest of the tumors (73).

In the current studies, we examined the effects of curcumin±siRNA DCAMKL-1 on the growth HCT-116 cells grown as either2D monolayer cell cultures, 3D- spheroids or 3D tumor xenografts. Our results show that colon cancer cells/xenografts treated with curcumin demonstrate autophagic cell death, which appears to be regulated by the ERK1/2 pathway. However, curcumin alone did not completely eliminate cancer stem cells, after curcumin treatment was discontinued, resulting in reformation of tumorospheres. DCAMKL-1 siRNA, on the hand, mainly resulted in activation of apoptotic cell death resulting in a significant reduction in tumor growth. Combination of curcumin+siRNA DCAMKL-1 synergistically increased autophagic and apoptotic cell death of colon cancer cells/xenografts, *in vitro* and *in vivo* respectively; the reduction in tumor growth in response to treatment with the combined regimen was significantly higher than that observed with the individual agents. It is thus postulated, that the combined regimen of curcumin+siRNA DCAMKL-1 will be a more specific and non-toxic method for eradicating cancer stem cells populations and reduce the tumor growth.

5.2 MATERIALS AND METHODS

In this section, only reagents and methods that have not been described in previous chapters are listed below.

5.2.1 Materials

Antibodies used, include anti-phospho-MEK1/2(Ser$^{217/221}$), anti-phospho-p38MAPK(Thr ^{180}/Tyr^{182}) anti-Oct-4, anti-Sox2, anti-Nanog, anti-LC3 A/B (Cell Signaling Technology, Danvers, MA), anti-ALDH1A1 (Abcam, Cambridge, MA). Curcumin was purchased from Sigma-Aldrich (St. Louis, MO) and dissolved in dimethyl sulfoxide (DMSO). 3-Methyladenine (3-MA) (Sigma-Aldrich, St. Louis, MO), a PI3K/autophagy inhibitor was kindly supplied to us by Dr. Jackson laboratory, *utmb*Health. Smart Pool of target-specific small interfering RNA (siRNA) and Non-Targeting (control) siRNA Pool were purchased from Dharmacon (Lafayette, CO).

5.2.2 Cell Culture

HCT-116 cells were originally purchased from the American Tissue Culture Collection (ATCC) (Manassas, VA). Cells were maintained in DMEM as Described in Chapters 2, 3 and 4.

5.2.3 Cell Viability and Cell Proliferation Assays

HCT-116 cells were grown either as monolayers (2D) or spheroids (3D) in a 96-well plate. Cells were treated with either DMSO (Control) or Curcumin (25µM) or Non-Targeting siRNA (control) or siRNA against DCAMKL-1 (100nM). These concentrations were optimal effective concentration based on preliminary studies performed with increasing concentrations of the agents. After 48 hours, cells were stained with trypan blue and cell viability was measured as described in chapter 4. Cell proliferation was examined and methods are described in chapter 4.

5.2.4 In vitro growth of cells as spheroids

As described in Chapter 3.

5.2.5 Processing of spheroids for embedding, sectioning and staining

As described in Chapter 3.

5.2.6 Immunofluorescent (IF) staining

As described in Chapter 2.

5.2.7 Western Blot (WB) analysis

As described in Chapter 2.

5.2.8 Transient-transfection of cells with oligonucleotides

As described in Chapter 3.

5.2.9 Animal Studies

5.2.9.1 Inoculation of cells into the athymic (SCID/Nude) mice

At 70% confluency, HCT-116 cells grown as monolayers were scraped and re-suspended in phosphate buffered saline (PBS) as single cell suspensions. $4x10^6$ cells/100µl PBS were inoculated on right and left flanks of female athymic SCID mice (Harlan Sprague Dawley) for inducing growth of sub-dermal xenografts..

5.2.9.2 Treatment of sub-dermal xenografts

3 weeks post-injection, xenografts were visible on both sides of the flanks of the athymic nude mice and ready for treatment. Tumors were injected every 2 days with

either DMSO (Control) or Curcumin (100μM) or Non-Targeting siRNA (control) or siRNA against DCAMKL-1 (100nM) or with both Curcumin (100μM) and siRNA against DCAMKL-1 (100nM) combined. In my preliminary studies, I first confirmed that the doses used were optimal for observing inhibitory effects *in vivo*. Each treatment was injected into 6 tumors in 3 mice/group. Tumor growth was measured every 2 days with calipers. Tumor volume was measured in millimeters by using the formula $(L \times W^2)/2$ where L=length and W=width. Mice were sacrificed 5 weeks after the first day of treatment. Tumors were removed and weighed, half of the sample was frozen for western blot analysis and the other half was fixed for IF/IHC analysis immediately.

5.2.10 Statistical analysis

Data are presented as mean±SEM of values obtained from 6 separate tumors obtained from 3 mice/treatment group. To test for significant differences between means, nonparametric Mann-Whitney test was employed using Statview 4.1 (Abacus Concepts, Inc., Berkeley, CA); *P* values were considered statistically significant if less than 0.05.

5.3 RESULTS

5.3.1 Effects of curcumin on colon cancer stem cells grown in vitro as tumorospheres

Our goal is to develop novel therapies which can directly target cancer stem cells and prevent tumor relapse. In chapter 4, we established an *in vitro* assay which selects for the growth of stem cells as tumorospheres. In the current studies, we used this assay to examine the effect of the non-toxic agent curcumin on cancer stem cells. HCT-116 cells were seeded into a 24-well low-attachment plate at a density of 10000cells/well. At day 7, tumorospheres formed with a well defined perimeter. On day 8, tumorospheres were

treated with either DMSO (control), or 10µM curcumin or 25µM curcumin for 48 hours. Images were taken at 4x and 10x magnifications. Our results demonstrated that DMSO (control) had no morphological effect on tumorospheres **(Fig 5.1Ai-top row)**. In contrast, treatment with 10µM curcumin reduced and slightly disintegrated the spheroids as can be seen by the necrotic cores of the spheroids in H&E stained sections **(Fig 5.1Ai-middle row)**. Treatments with 25µM curcumin resulted in the complete disintegration of the spheroids, and only residual cells were observed in H&E stained sections **(Fig 5.1Ai-bottom row)**. Time lapse images examining the effects of curcumin on spheroids is shown in **Fig 5.1Aii**, wherein HCT-116 tumorospheres were treated with either control or 25µM curcumin at 24hrs and 48hrs. The number of spheroids decreased to only 25% after treatment with 25µM curcumin, whereas the numbers of spheroids did not change in control and 10µM curcumin treated spheres as shown in the bar graphs **(Fig 5.1B)**. This suggests that although treatment with 10µM curcumin slightly affected the growth and morphology of the spheroids, 25µM curcumin represented an optimal concentration for observing significant disintegration of the spheroids *in vitro*. Higher doses of curcumin were only slight more effective (data not shown). Next, we examined the effects of curcumin on the morphology of spheroids formed from colon cancer cells, in a time dependent manner. HCT-116 spheroids were treated with 25µM curcumin for 0hrs, 24hrs, 48hrs and 72hrs; the spheroids were then processed and sections stained by H&E (**Fig 5.1C**). Our results demonstrated that curcumin gradually disintegrated the spheroids, from 24hrs to 72hrs. We also noted curcumin that the treated spheroids had hollow empty structures within a ring of cells, which may perhaps represent an autophagic response.

We next examined whether curcumin induced cell death in spheroids or just in the disintegration of spheroids. HCT-116 cells were treated with or without curcumin were examined by western blot analysis, for the relative expression of the apoptotic marker

activated caspase-3. Treated spheroids were also analyzed by IF for the apoptotic marker. Our results demonstrated elevated expression of activated caspases-3 in HCT-116 spheroids treated with curcumin, compared to control spheroids, **(Fig 5.1Di-ii**). These results confirm that curcumin activates apoptotic death of cancer cells, even though only 30% of cells stained for activated caspases-3 (**Fig 5.1Dii**). However, as noted in **Fig 5.1B**, even after treating HCT-116 spheroids with an optimal dose of curcumin, approximately 50 spheroids still remained, suggesting that curcumin may not be sufficient for eliminating cancer stem cells, which are known to be precursors of spheroidal growths.

5.3.2 Curcumin induces an autophagic response in colon cancer tumorospheres

Several studies have reported the formation of inclusion structures (hollow empty structure) in cells/tumors upon activation of autophagy (254,255). In the current study, similar structures were observed in curcumin treated spheroids. Curcumin has been reported to induce autophagy in various cancer cells, including colon cancer cells (171). We therefore examined if the hollow structures represent autophagosomes-like structures. HCT-116 spheroids were treated with curcumin for 0, 24, 48 and 72hrs; the spheroids were then processed and stained by IF with DAPI. The results demonstrated that at 0hrs, spheroids cells were highly compact and uniform (**Fig 5.2A**). The first appearance of the hollow structures were noted at 24hrs, and increased at 48hrs. However by 72hrs, the structures were no longer visible and cells were completely dissociated (**Fig 5.2A**), suggesting that an autophagy-like phenomenon may have been activated within the first 48 hours of curcumin treatment.

Control and curcumin HCT-116 treated spheroids were also stained by IF for the autophagic marker LC3 and proliferation marker PCNA. The results demonstrated an

absence of autophagic activity in control spheroids, wherein the proliferating cells were exclusively expressed on the perimeter of the spheroids (**Fig 5.2B-top panel**), similar to our findings in chapters 3 and 4. In contrast, HCT-116 spheroids treated with curcumin for 48hrs demonstrated significant increase in LC3 expression, wherein LC3+ve cells were expressed around the hollow structures **(Fig 5.2B-bottom panel)**; presence of LC3 was confirmed by western blot (**Fig 5.2C**). The presence of LC3+ve cells around the hollow structures strongly suggests that curcumin induces autophagy. Interestingly, PCNA+ve cells in curcumin treated spheroids were now present in the core of the spheroids rather than the perimeter as observed in the control spheroids **(Fig 5.2B-bottom panel)**, suggesting the possibility that curcumin-induced autophagy may represent an survival mechanism in an effort to rescue the damaged cells from possible induction of ROS (a known effect of curcumin in cancer cells (260).

5.3.3 Mechanism mediating inhibitory effects of curcumin on colon cance xenografts

Effects of curcumin were examined on colon cancer cells growing as xenografts *in vivo* using athymic nude mice as described in chapter 3. Two weeks after inoculating $1x10^{\wedge 6}$ colon cancer cells in each flank of the mice, tumor growth visible under the naked skin were injected with increasing concentrations of curcumin in 50µL of saline containing < 0.1% DMSO. Our preliminary data indicated that doses less than 100µM were not effective, we therefore used 100µM as an optimal dose and injected the mice once every 3 days for 5 weeks. Control mice received an equal number of injections with the vehicle alone. Our results demonstrated a significant reduction in the growth of tumors treated with curcumin compared to controls (**Fig 5.3A-B**). Interestingly, curcumin treated tumors appeared to have necrotic lesions within their cores (**Fig 5.3A**). Tumor

weights and volumes were measured and are illustrated as bar graphs (**Fig 5.3B**). Curcumin treated tumors weighed an average of 1.05g versus 1.46g for the control tumors (**Fig 5.3Bi**). Tumor volumes were measured weekly with calipers. Control tumors grew to an average volume of $1072mm^3$ compared to curcumin treated tumors which only grew to $655mm^3$ **(Fig 5.3Bii)**, demonstrating a ~ 40% decrease in tumor weight and tumor volume in response to curcumin treatment.

Tumor samples were processed and sections stained by H&E. Our data demonstrated the formation of similar hollow structures in curcumin treated tumors, but not in the control tumor sections (**Fig 5.3C**), suggesting presence of autophagy. HCT-116 tumors sections were stained by IF for autophagic marker LC3 and proliferative marker PCNA. In the control, very few cells were positive for LC3 and did not co-localize with PCNA **(Fig 5.3Ci)**. In contrast, in curcumin treated tumors, LC3+ve cells were significantly increased and lined the hollow structures **(Fig 5.3Cii)**. Interestingly, PCNA+ve cells were also found to line these structures; PCNA did not co-localize with LC3 in the same cells **(Fig 5.3Cii)**. Our findings suggest that the cells undergoing autophagy (LC3+ve), in response to curcumin, are not being rescued, since these cells were not positive for PCNA. It is thus speculated that the LC3+ve cells may be undergoing autophagic death in the absence of cell rescue. It is possible that ROS induced by curcumin in cancer cells, at the concentrations used in our current study, is too massive, resulting in failed cell rescue/survival by inducing an autophagic mechanism which results in cell death (260).

5.3.4 Effects of curcumin on stem/pluripotent cell markers in colon cancer cells

Curcumin was reported to be an effective drug to treat cancer as it decreases the resistance of cancer stem cells to currently used therapies (256). The stemness potency is known to be regulated by proteins used as stem/pluripotent markers. Therefore, we examined the effects of curcumin on the expression of a representable set of markers in HCT-116 colon cancer cells. Cells were grown either as 2D-monolayers, 3D-spheroids or 3D-xenografts and analyzed by western blot analysis for relative expression of stem cell markers (DCAMKL-1, CD44, LGR5, ALDH1) and pluripotent markers (Nanog, Sox-2 and Oct-4). Our results demonstrated that curcumin significantly decreased the expression of both stem and pluripotent markers in monolayer cell cultures **(M)**, 3D-spheroids **(S)**, and tumors **(T)**; representative data from 3 experiments are presented in **(Fig 5.4A).** The % change in the ratios of target proteins/β-actin in HCT-116 control versus curcumin treated cells were measured, wherein the ratios obtained from the control samples were arbitrarily assigned a 100% value **(Fig 5.4B).** Our findings confirmed that curcumin significantly reduced the relative expression levels of the indicated markers in HCT-116 cells. However, the noted reduction was less than 100%, suggesting that curcumin by itself may not be sufficient for completely eradicating stem cell population positive for the stem/pluripotent markers.

5.3.5 Effects of curcumin on the expression of NFκB and β-catenin in colon cancer cells

In chapters 2 and 3, we demonstrated that overexpression of progastrin in HEK-mGAS cells up-regulated activation of NFκBp65 and β-catenin, and significantly increased the relative expression of stem cells markers, associated with increased proliferation of HEK-mGAS cells. Similarly, in chapter 3, we discovered that DCAMKL-

1+ve and LGR5+ve cells also co-express NFκB, β-catenin and proliferation markers. Curcumin is a well known inhibitor of NFκB pathway as shown by several investigators including our laboratory (155,257). We therefore examined if curcumin similarly inhibits activation of NFκBp65 and β-catenin in HCT-116 cells grown either as 2D-monolayers, 3D-spheroids or 3D-xenografts. Relative levels of total and activated NFκBp65 and β-catenin are presented in **(Fig 5.5A)**. The % change in control versus curcumin treated samples are shown **(Fig 5.5B)** Our results demonstrated that curcumin treatment decreased the expression of total β-catenin, activated *p*β-catenin (Ser^{552}) and, *p*β-catenin (Tyr^{142}), as well as the expression of total and activated *p*p65NFκB^{s276} and *p*p65NFκB^{s536} in HCT-116 cells grown as monolayers **(M)**, 3D-spheroids **(S)** and tumors **(T) (Fig 5.5A-B)**. The inhibitory effects of curcumin on p65NFκB and β-catenin pathways were also demonstrated by IF staining **(Fig 5.5C)**. Since both NFκB and β-catenin are essential factors in cell survival and proliferation, we showed that the reduction in NFκB and β-catenin levels in response to curcumin resulted in the loss of viability and proliferative treated HCT-116 cells (**Fig 5.5D-E**).

5.3.6 Curcumin induced autophagy is regulated by ERKs expression in colon cancer cells

The role of ERK pathway in nutrient deprivation-induced autophagy has been well documented in cancer cells (258). However, the role of ERK pathway in curcumin-induced autophagy remains ill-defined. We therefore examined whether expression of ERKs, in colon cancer cells, mediates autophagy in response to curcumin. HCT-116 cells grown either as 2-D monolayers, 3-D spheroids or xenografts were treated with or without curcumin and analyzed by western blot analysis for relative levels of ERK1/2, *p*pMAPK38 and activated caspase-3. Representative data from 3 experiments are

presented in **(Fig 5.6Ai-ii)**. The % change of target proteins/β-actin in HCT-116 control versus curcumin treated cells were measured, wherein the ratios obtained for the control samples were arbitrarily assigned a 100% value as depicted in the bar graphs **(Fig 5.6B)**. The results demonstrated a significant decrease in ERK1/2 and *p*p38MAPK levels (**Fig 5.6Ai)**, and an increase in activated caspase-3 levels **(Fig 5.6Aii)** in HCT-116 cells treated with curcumin for 48hrs.

To examine the role of ERKs in autophagy, HCT-116 monolayer cells were treated with curcumin for 0hrs, 24hrs, 36hrs and 48hrs. Levels of ERK1/2, activated caspase-3 and LC3 were measured by western blot. The results demonstrated that ERK1/2 levels remained unchanged at from 0hrs to 36 hrs, but significantly decreased by 48 hrs **(Fig 5.6C)**. In contrast, levels of activated caspase-3 gradually increased from 0hrs to 48 hours, with the lowest levels observed at 0hrs and highest at 48 hours **(Fig 5.6C)**. No expression of LC3 was noted at 0hrs; however, elevated LC3 expression was observed from 24 to 36hrs and then decreased by 48 hours (**Fig 5.6C**). The results lead us to speculate that autophagy is activated within the first 24 hours as a cell survival mechanism; however the long lasting deleterious effects of curcumin eventually down-regulates ERKs 48hrs, triggering a death signal, since cancer cells may be too damaged to be rescued, hence undergo autophagic death.

5.3.7 Curcumin induced autophagy is an anticancer response and not a protective mechanism of cancer cells

In cancer cells autophagy is usually suppressed, however, it can be activated in response to various anticancer therapeutic drugs including curcumin (170). It has been reported that curcumin suppresses tumor growth by inducing autophagy in various cancers (173,174). However, it is not known if curcumin-induced autophagy in cancer

cells represents a survival mechanism or a cell death mechanism. To examine this question, we used 3-methylalanine (3-MA), an inhibitor of autophagy. HCT-116 were treated with or without curcumin in the presence or absence of 3-MA. In the absence of 3-MA viability and proliferative potential of curcumin treated HCT-116 cells was decreased by ~50% as shown in **Fig 5.6Di-ii**. However, in the presence of 3-MA (2mM), viability and proliferative potential of curcumin treated cells were decreased by only ~25% as shown in **Fig 5.6Di-ii**, suggesting that curcumin induced autophagy is likely required for promoting cell death. Thus, curcumin induced autophagy in cancer cells may represent an anti-tumor effect and not a protective effect.

5.3.8 Curcumin treatment is insufficient in preventing tumor relapse in colon cancers

In **Fig 5.1B**, our results show that the total number of tumorospheres decreased from 200 to 50 spheroids. We also observed that curcumin reduced cell viability and cell proliferation by ~50% compared to the control cells **(Fig 5.5D-E)** and did not completely eradicate the expression of stem/pluripotent markers. These findings suggest that curcumin alone may not be sufficient to target cancer stem cells and prevent tumor relapse. To further confirm this possibly, HCT-116 cells were grown as tumorospheres and treated with either control (DMSO) or 25µM curcumin once every 2 days for 3 weeks *in vitro*. Primary tumorospheres were then collected, dissociated and reseeded to form secondary spheroids in fresh media with no curcumin. Our results demonstrated that cells originating from control non-treated spheroids (group 1) formed secondary tumorospheres within 4 days which increased in numbers through day 45 **(Fig 5.7A)**. In contrast, cells originating from curcumin treated primary spheroids (group 2) showed no growth at day 4, however secondary spheroids were visible by day 30 which grew larger

by day 45 **(Fig 5.7A)**. Viability of cells within the secondary spheroids was measured as shown in (**Fig 5.7B**). Cells in group 1 (control) were 80-90% viable at all days examined compared to cells in group 2 (curcumin treated) which were only 25%, 52% and 63% viable on days 4, 30 and 45, respectively **(Fig 5.7B)**. We also examined the expression of stem cell markers, DCAMKL-1 and LGR5, in both groups by western blot analysis. Our results demonstrated that relative levels of DCAMKL-1 and LGR5 remained unchanged at days 4 and day 30 in group 1 samples **(Fig 5.7Ci)**, whereas in group 2, relative levels of DCAMKL-1 and LRG5 were significantly reduced on day 4 which gradually continued to increase by day 45 (**Fig 5.7Cii**). Based on these results, I speculate that curcumin is ineffective in eradicating all the cancer stem cells and thus results in regrowth of tumorospheres, resembling relapse of the disease.

5.3.9 Effects of DCAMKL-1 down-regulation on colon cancer stem cells in vitro

It has been reported that stem cell marker DCAMKL-1 is over-expressed in various tumor types including colorectal cancers and that its down-regulation inhibits cell proliferation and induces tumor growth arrest (72,73). We therefore examined the effects of down-regulating DCAMKL-1 in colon cancer cells *in vitro.* Initially, we examined the viability and proliferative potential of HCT-116 cells in response to treatment with either control or DCAMKL-1 siRNA for 48hrs. Cells treated with control siRNA remained 95-100% viable both in the floating and attached cell population in monolayer cultures. In contrast, cells treated with DCAMKL-1 siRNA were only ~ 48% viable in both floating and attached cells **(Fig 5.8A)**. Proliferative potential of cells treated with DCAMKL-1 siRNA was ~50% of that observed with cells treated with control siRNA **(Fig 5.8B)**. DCAMKL-1 siRNA treated cells were confirmed to be significantly down-regulated for DCAMKL-1 expression by western blot analysis **(Fig 5.8C)**. Expression levels CD44,

LGR5 and PCNA were also significantly reduced in cells treated with DCAMKL-1 siRNA (**Fig 5.8D**). Our findings thus demonstrate for the first time that DCAMKL-1 may be playing a functional role in maintaining the proliferation of cancer cells by perhaps regulating expression levels of LGR5 and CD44.

In our chapter 3vstudies with HEK-C/HEK-mGAS cells, we observed that loss of DCAMKL-1 expression resulted in loss of β-catenin activation. Therefore, I examined the effects of DCAMKL-1 siRNA on activation of β-catenin in HCT-116 cells using a reporter promoter assay as described in chapters 2 and 3. Our results, with HCT-116 cells, confirmed our findings with HEK-293 cells, demonstrating a significant decrease in the activation of β-catenin in response to DCAMKL-1 siRNA **(Fig 5.8E)**. The latter data was confirmed by IF staining for total and activated β-catenin levels as shown in **(Fig 5.8F)**. Based on these results, I conclude that DCAMKL-1 likely plays an important role in the proliferation of cells by perhaps facilitating activation of β-catenin by an as yet undefined mechanism.

5.3.8 Effects of DCAMKL-1 siRNA the growth of tumorospheres and xenografts derived from HCT-116 colon cancer cells

HCT-116 tumorospheres were treated either with control or siRNA DCAMKL-1 (100nM) for 48 hours. Our results demonstrated that compact spheroids with well defined perimeters were formed from cells treated with control siRNA **(Fig 5.9Ai)**. In contrast, spheroids treated with DCAMKL-1 siRNA were reduced in size and disintegrated **(Fig 5.9Ai)**. Spheroids treated with DCAMKL-1 siRNA were confirmed to be down-regulated for DCAMKL-1 expression by western blot analysis (**Fig 5.9Aii**).

.We next examined the effects of DCAMKL-1 siRNA on the growth of xenografts *in vivo*. Xenografts were grown as described above and injected either control

or DCAMKL-1 siRNA once every 2 days for a total of 4 weeks as described above for curcumin treatment. Tumors treated with DCAMKL-1 siRNA significantly decreased in size compared to tumor treated with control siRNA **(Fig 5.9B)**. The weights and volumes of the tumors, at sacrifice, were also significantly reduced in response to DCAMKL-1 siRNA compared to the controls **(Fig 5.9Ci-ii)**. These findings once again confirm that DCAMKL-1 is not only a stem cell marker but appears to play an important role in maintaining proliferative potential of tumor cells.

The effects of DCAMKL-1 siRNA were next examined on the relative expression levels of stem/pluripotent markers by western blot analysis. As expected, significantly lower levels of stem cells markers (DCAMKL-1, CD44, LGR5, ALDH1) and pluripotent markers (Nanog, Sox-2,Oct-4) was significantly decrease in samples treated with DCAMKL-1 siRNA versus control siRNA **(Fig 5.9Di-ii)**. Thus these results suggest that DCAMKL-1 play an important role directly or indirectly in maintaining pluripotency of cancer stem populations.

Our studies demonstrated that autophagic death may explain the inhibitory effects of curcumin on tumor growth. We therefore examined if DCAMKL-1 siRNA can similarly induce autophagic death of tumor cells. Surprisingly, DCAMKL-1 siRNA did not induce expression of LC3 and there were no hollow structures **(Figs 5.9E and 5.13Ciii)** as observed with curcumin treatment **(Fig 5.13Cii**). However, relative levels of activated caspase-3 were significantly increased in tumor samples treated with DCAMKL-1 siRNA **(Figs 5.12A and 5.13Diii)**. These results suggest the novel possibility that while curcumin induces autophagic/apoptotic death, loss of DCAMKL-1 primarily induces apoptotic death of cancer cells.

5.3.9 Combined effects of curcumin+siRNA DCAMKL-1 on colon cancer cells in vitro

HCT-116 tumorospheres were treated with either control vehicle containing <0.1% DMSO, or 25μM curcumin±100nM siRNA DCAMKL-1. The combined regimens of curcumin+DCAMKL-1 siRNA were significantly more potent than either agent alone towards inhibiting the growth and disintegration of spheroids, as illustrated in (**Fig 5.10A).** The proliferative potential of HCT-116 cells growing as monolayer cultures was also significantly decreased by ~50%, 45% and 80% in response to curcumin, DCAMKL-1 siRNA or both curcumin+DCAMKL-1 siRNA, respectively (**Fig 5.10B**). Similarly, relative expression of activated NFκBp65 and total β-catenin were more potently reduced in cells treated with the combined regimens **(Fig 5.10C).** Interestingly, relative expression levels of DCAMKL-1 were further reduced in response to the combined regimen vs DCAMKL-1 siRNA alone, which may likely be due to the inhibitory effects of curcumin itself on the expression of DCAMKL-1 **(Fig 5.10C)**. These findings suggest that combined regimen of curcumin+siRNA DCAMKL-1 is more efficient than either alone, in targeting cancer stem cells or in decreasing proliferative potential of the cells.

5.3.10 Combinatory effects of curcumin+ siRNA DCAMKL-1 on xenografts in vivo

Tumors were generated and treated as described above with either the control vehicle, 100μM curcumin, 100nM siRNA DCAMKL-1 or both curcumin+siRNA Our results demonstrated that the combined treatment was more potent than the single agent in reducing tumor size and volumes as shown in **Fig 5.11A-C**. The results thus demonstrate that while curcumin or DCAMKL-1 siRNA alone decreased the size of the tumors by ~ 35% and 68% respectively, the combined regimen decrease by ~ 82% in the time frame of our studies. Based on these studies, I concluded that the combined regimen

of curcumin and DCAMKL-1 siRNA may be highly effective in attenuating the growth of the tumor, which may perhaps result in complete eradication.

5.3.11 Effects of curcumin+siRNA DCAMKL-1 on stem/pluripotent cells markers and proliferative/apoptotic potential on colon cancers

Tumor xenografts were treated (described above in section 5.3.10) and processed for measuring the relative expression of indicated stem cell and pluripotent markers **(Fig 5.12A)**. Once again the combined regimen was most potent in reducing the relative expression levels of the indicted stem/pluripotent markers compared to the individual agents **(Fig 5.12A)**. Similarly relative levels of activated NFκB and total β-catenin were most significantly reduced in response to the combined treatments **(Fig 5.12)**. Even though DCAMKL-1 siRNA alone did not induce expression of LC3, in combination with curcumin the expression of LC3 was synergistically increased beyond levels measured with curcumin alone **(Fig 5.12A).** In addition, curcumin or DCAMKL-1 siRNA treatments alone significantly up-regulated the expression of activated caspase-3, while the combined regimen synergistically increased activation of caspase-3 by several fold **(Fig 5.12A).** These results once again demonstrate that the combined regimen is significantly more potent than the individual agents against tumor growth, likely because the combined regimen synergistically increases both autophagic and apoptotic death.

5.3.12 Effects of curcumin±DCAMKL-1 siRNA on the localization of stem cell markers in vivo

Our results in chapter 3 and 4, demonstrated that tumorigenesis or transformation of HEK-293 cells was associated cells with co-expression of CD44 with DCAMKL-1+ve stem cells. We therefore examined if treatment with curcumin±DCAMKL-1 siRNA can

potentially alter the phenotype of cancer stem cells. HCT-116 xenografts treated with curcumin±DCAMKL-1 siRNA were processed and stained by IF for indicated markers as shown in **(Fig 5.13)**. We observed cells co-expressing DCAMKL-1 and CD44 at the leading edge of the control tumors (**Fig 5.13Ai**). In contrast, DCAMKL-1 was expressed around the hollow/autophagic structures in curcumin treated tumors, while significantly reduced staining of CD44 was present at the edges of these tumors **(Fig 5.13Aii**). Surprisingly, in tumors treated with either siRNA DCAMKL-1 or curcumin+DCAMKL-1 siRNA, we did not observe any expression of DCAMKL-1 or CD44 (**Fig 5.13Aiii-iv)**. Our results suggest that the tumorigenic phenotype of co-expression of DCAMKL-1/CD44 is lost upon treatment with combined regimen, thus supporting our hypothesis that the combined regiment may more effectively target cancer stem cells.

Co-staining of LGR5 and CD44 was also observed at the edges of the control tumors **(Fig 5.13Bi)**. Curcumin treatment resulted in the expression of LGR5 exclusively around the hollow structures and CD44 was no longer present at the edges of the tumors. However CD44 staining was observed towards the center core of the tumor, which was largely necrotic, suggesting that CD44 staining may be present within infiltrating cells (**Fig 5.13Bii**). In tumors down-regulated for DCAMKL-1, staining for LGR5 and CD44 was significantly reduced but still co-stained on the leading edge of the tumor (**Fig 5.13Biii**). In tumors treated with curcumin+DCAMKL-1 siRNA, staining for LGR5 and CD44 was significantly reduced at the edges of the tumors but some staining was seen within the core (**Fig 5.13Biv**). These results once again demonstrate that that the tumorigenic phenotype of co-expression of LGR5/CD44 was abolished upon treatment of the combined regimen.

In order to localize autophagic versus apoptotic cells in relation to proliferating cells, we stained tumor sections for LC3, activated-capase-3 and PCNA. Control tumors

were negative for LC3 staining, while cells positive for PCNA were present along the edge of the tumors (**Fig 5.13Ci**). In curcumin treated tumors, cells positive for either LC3 or PCNA were localized around the hollow structures; the cells however did not co-express LC3 and PCNA (**Fig 5.13Cii**). The latter results suggest that autophagy in response to curcumin does not represent a cell survival mechanism but rather a cell death mechanism. Interestingly, tumors down-regulated for DCAMKL-1 were negative for LC3 and PCNA staining (**Fig 5.13Ciii**); once again confirming that down-regulation of DCAMKL-1 siRNA does induce autophagy. However, tumors treated with curcumin+siRNA DCAMKL-1 were positive for LC3 staining around the autophagic structures but remains negative for PCNA staining (**Fig 5.13Civ)**. Our results confirm that curcumin induces an autophagic response whereas loss of DCAMKL-1 siRNA attenuated cell proliferation.

We next examined localization of activated caspase-3 and PCNA. Our results demonstrated that PCNA+ve cells were located at the outer edge of the control tumors with absence of apoptotic cell (**Fig 5.13Di**). In curcumin treated tumors, apoptotic cells were mainly located at the leading edge of the tumors and also observed within the core of the tumors, unrelated to PCNA staining (**Fig 5.13Dii)**. In tumors down-regulated for DCAMKL-1, significant staining for activated caspase-3 was observed at the edge of the tumors and a few cells within the core; PCNA staining was not observed as described above (**Fig 5.13Diii)**. In tumors treated with curcumin+siRNA DCAMKL-1, very few proliferative cells were observed, while a significant increase in apoptotic cells was observed (**Fig 5.13Div)**. Based on our results so far, I speculate that curcumin treatment likely activates autophagy as a mean to rescue cells, however it fails and activates a cell death mechanism, including apoptotic cell death.

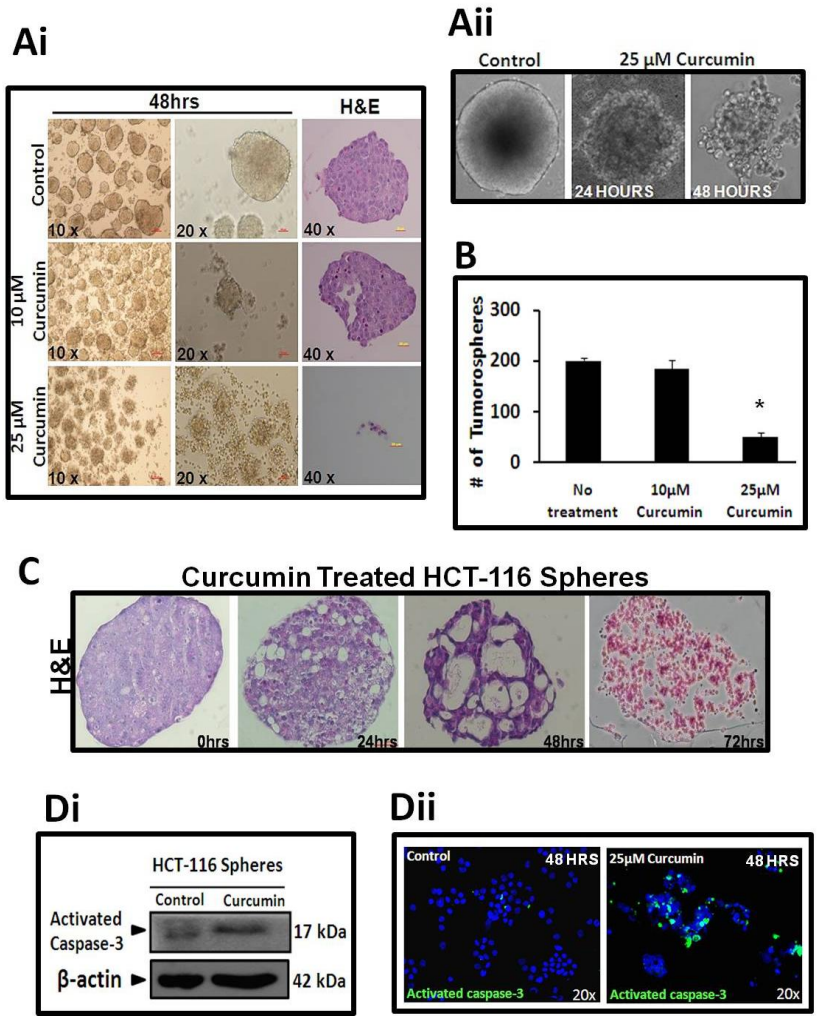

Figure 5.1. ***(A-D)***: **Effects of curcumin on the growth of colon cancer tumorospheres**. **Ai**= Representative images of HCT-116 cells grown as tumorospheres were treated either with no curcumin, 10µM curcumin or 25 µM curcumin for 48 hrs. Images were taken at 10x and 20x. H&E staining of the tumorospheres were imaged at 40x magnification. **Aii**= Representative time lapse images of HCT-116 spheres treated with 25 µM curcumin at 0hrs, 24hrs and 48hrs. **B**= Representative bar graph of number of tumorospheres remaining in response to no curcumin, 10µM curcumin or 25 µM curcumin ater 48 hrs. **C**= H&E stainings illustrating the time lapse effects of curcumin on HCT-116 tumorospheres at 0hrs, 24hrs, 48hrs and 72 hrs. Images were taken at 20x magnification. **Di**= Representative autoradiogram of western blot data demonstrating relative levels of apoptotic marker activated caspase-3 in HCT-116 control vs 25µM curcumin spheres, β-actin was run as a loading control. **Dii**= IF staining illustrating the relative levels of activated caspase-3 in HCT-116 dissociated cells arising from control or 25µM curcumin treated spheres for 48 hrs. Blue= nucleus stained with DAPI. Images were taken at 20x with epifluorescent microscopy. **P* < .05 vs corresponding HCT-116 control values.

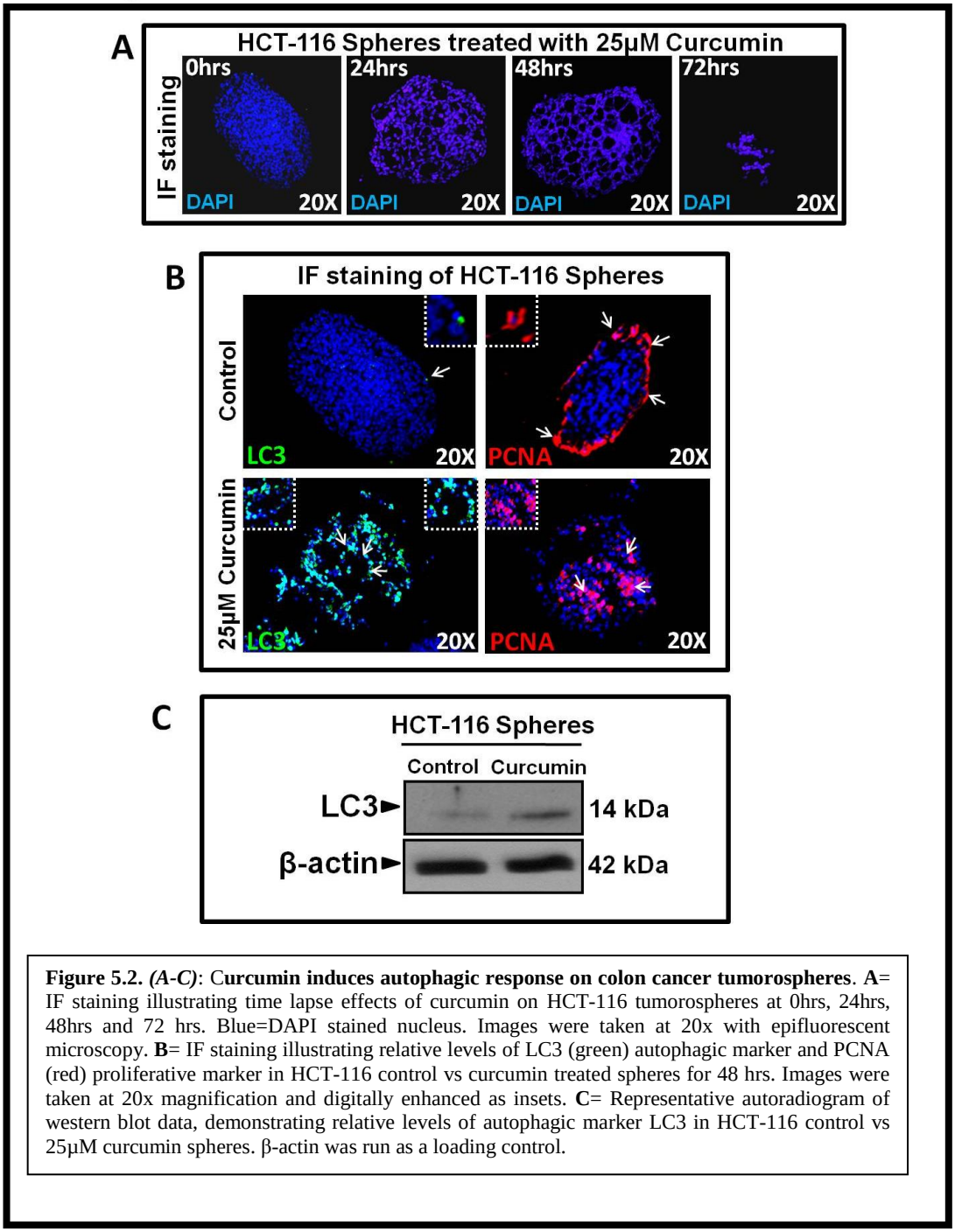

Figure 5.2. ***(A-C)***: C**urcumin induces autophagic response on colon cancer tumorospheres**. **A**= IF staining illustrating time lapse effects of curcumin on HCT-116 tumorospheres at 0hrs, 24hrs, 48hrs and 72 hrs. Blue=DAPI stained nucleus. Images were taken at 20x with epifluorescent microscopy. **B**= IF staining illustrating relative levels of LC3 (green) autophagic marker and PCNA (red) proliferative marker in HCT-116 control vs curcumin treated spheres for 48 hrs. Images were taken at 20x magnification and digitally enhanced as insets. **C**= Representative autoradiogram of western blot data, demonstrating relative levels of autophagic marker LC3 in HCT-116 control vs 25µM curcumin spheres. β-actin was run as a loading control.

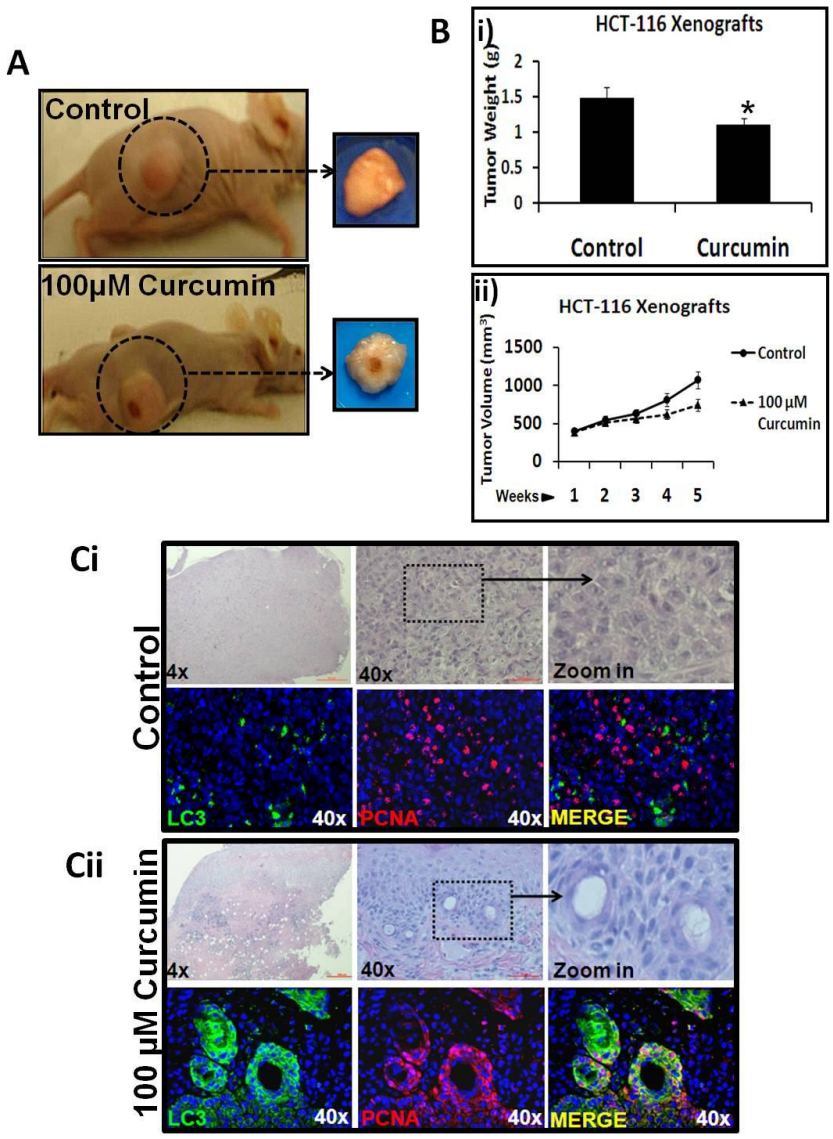

Figure 5.3. ***(A-C)***: C**urcumin reduced colon cancer tumor growth by inducing autophagy**. **A**= Representative images of HCT-116 xenografts grown sub-dermally in the flanks of athymic nude mice, treated with either control or 100µM curcumin for 5 weeks as noted by the dotted circle. Palpable tumors are marked by circles and removed tumors are depicted by dotted arrows. **Bi**= Representative bar graph illustrating final tumor weights of extracted HCT-116 xenografts treated with either control or 100µM curcumin. **Bii=** Representative bar graph illustrating final tumor volume of HCT-116 xenografts treated with either control or 100µM curcumin measured weekly over a period of 5 weeks. **Ci-ii**= H&E staining of the control and curcumin xenografts taken at 4x, 40x and digitally enhanced. IF staining illustrating relative levels of LC3 (green) autophagic marker and PCNA (red) proliferative marker in HCT-116 control vs curcumin treated xenografts. Images were taken at 40x magnification and merged. **P* < .05 vs corresponding HCT-116 control values.

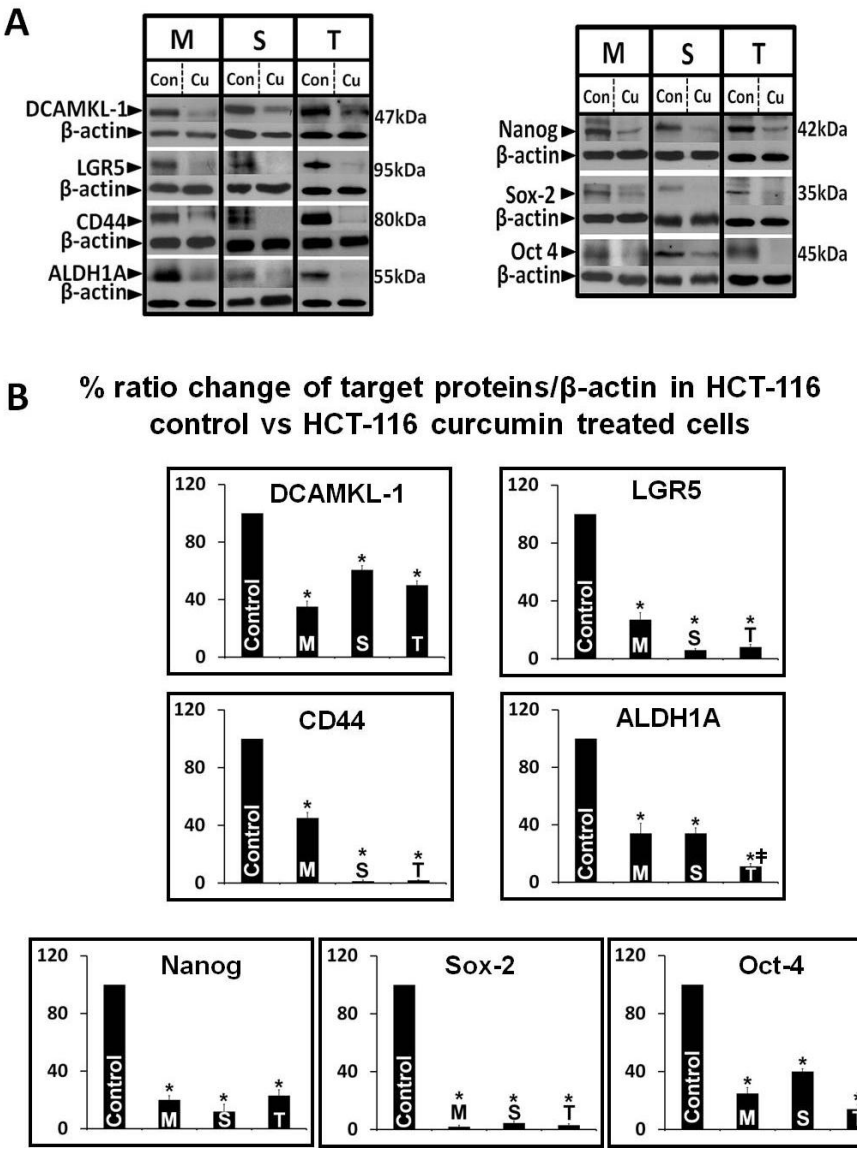

Figure 5.4 (*A*–*B*): **Percent decrease in relative levels of stem cell and pluripotent markers in monolayer-cultures (M), 3D-spheroids (S) or sub-dermal tumors (T) in HCT-116 curcumin versus control treated cells. A** =Representative WBs of indicated proteins from 1 of 3 similar experiments; Con=HCT-116 control treated cells; Cu=HCT-116 curcumin treated cells. **B** =Mean±Sem of % change in ratio of indicated protein/β-actin in cellular samples from 3 experiments; ratios measured in HCT-116 control samples were arbitrarily assigned 100% values. *=p<0.05 vs HCT-116 control values (shown as the first bar in the graphs in each panel).

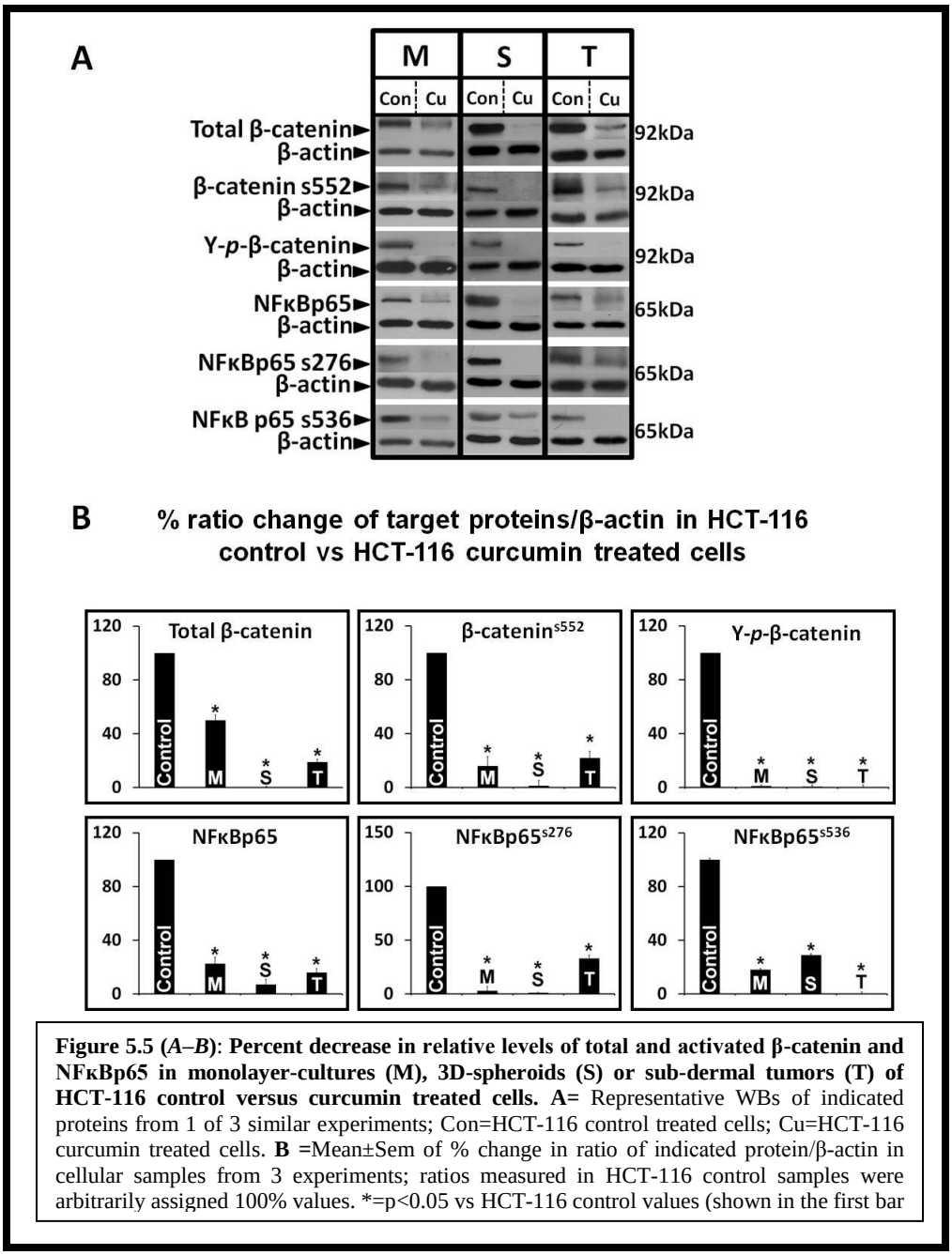

Figure 5.5 (*A*–*B*): **Percent decrease in relative levels of total and activated β-catenin and NFκBp65 in monolayer-cultures (M), 3D-spheroids (S) or sub-dermal tumors (T) of HCT-116 control versus curcumin treated cells. A=** Representative WBs of indicated proteins from 1 of 3 similar experiments; Con=HCT-116 control treated cells; Cu=HCT-116 curcumin treated cells. **B =**Mean±Sem of % change in ratio of indicated protein/β-actin in cellular samples from 3 experiments; ratios measured in HCT-116 control samples were arbitrarily assigned 100% values. *=p<0.05 vs HCT-116 control values (shown in the first bar

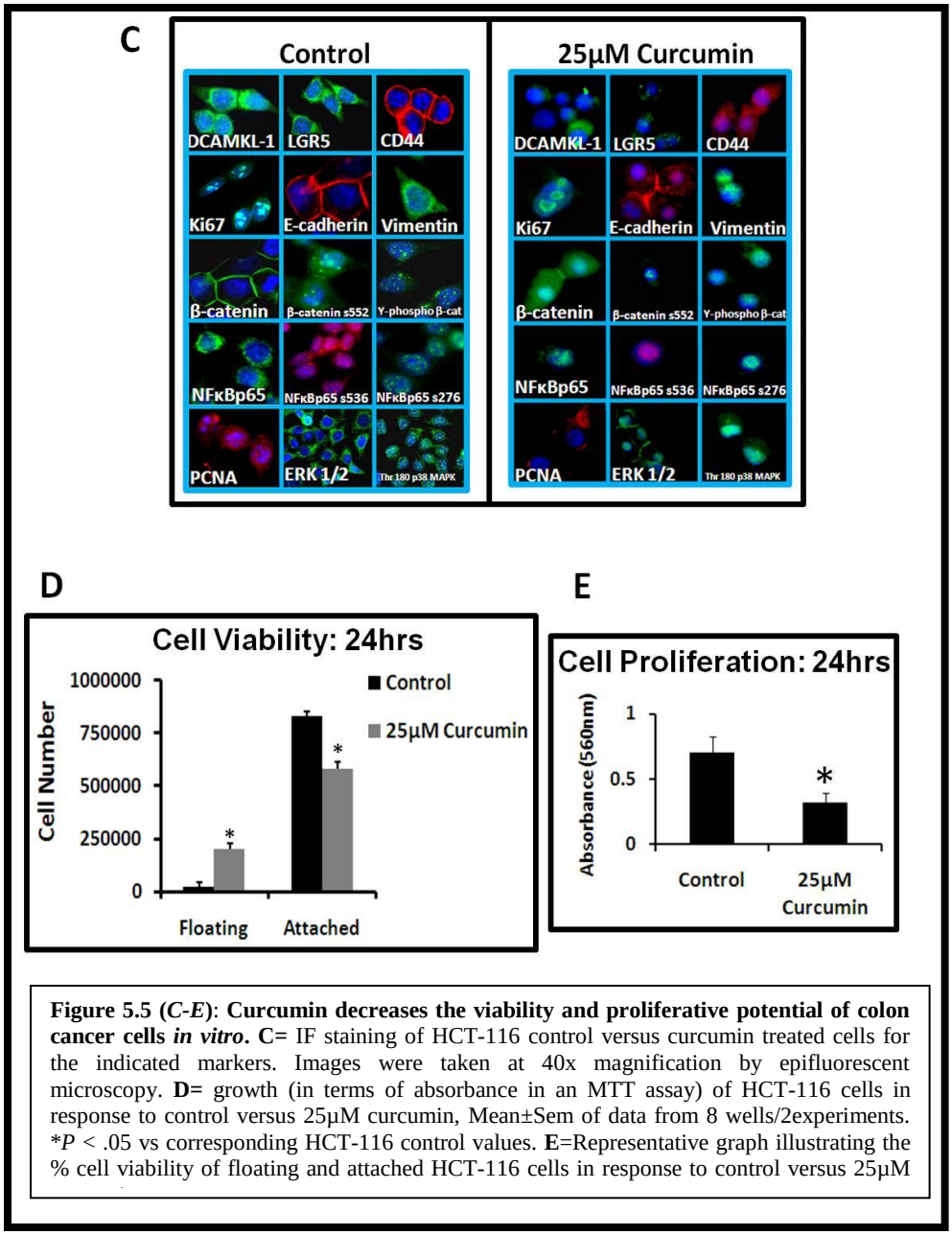

Figure 5.5 (*C-E*): **Curcumin decreases the viability and proliferative potential of colon cancer cells *in vitro*. C=** IF staining of HCT-116 control versus curcumin treated cells for the indicated markers. Images were taken at 40x magnification by epifluorescent microscopy. **D=** growth (in terms of absorbance in an MTT assay) of HCT-116 cells in response to control versus 25µM curcumin, Mean±Sem of data from 8 wells/2experiments. **P* < .05 vs corresponding HCT-116 control values. **E**=Representative graph illustrating the % cell viability of floating and attached HCT-116 cells in response to control versus 25µM

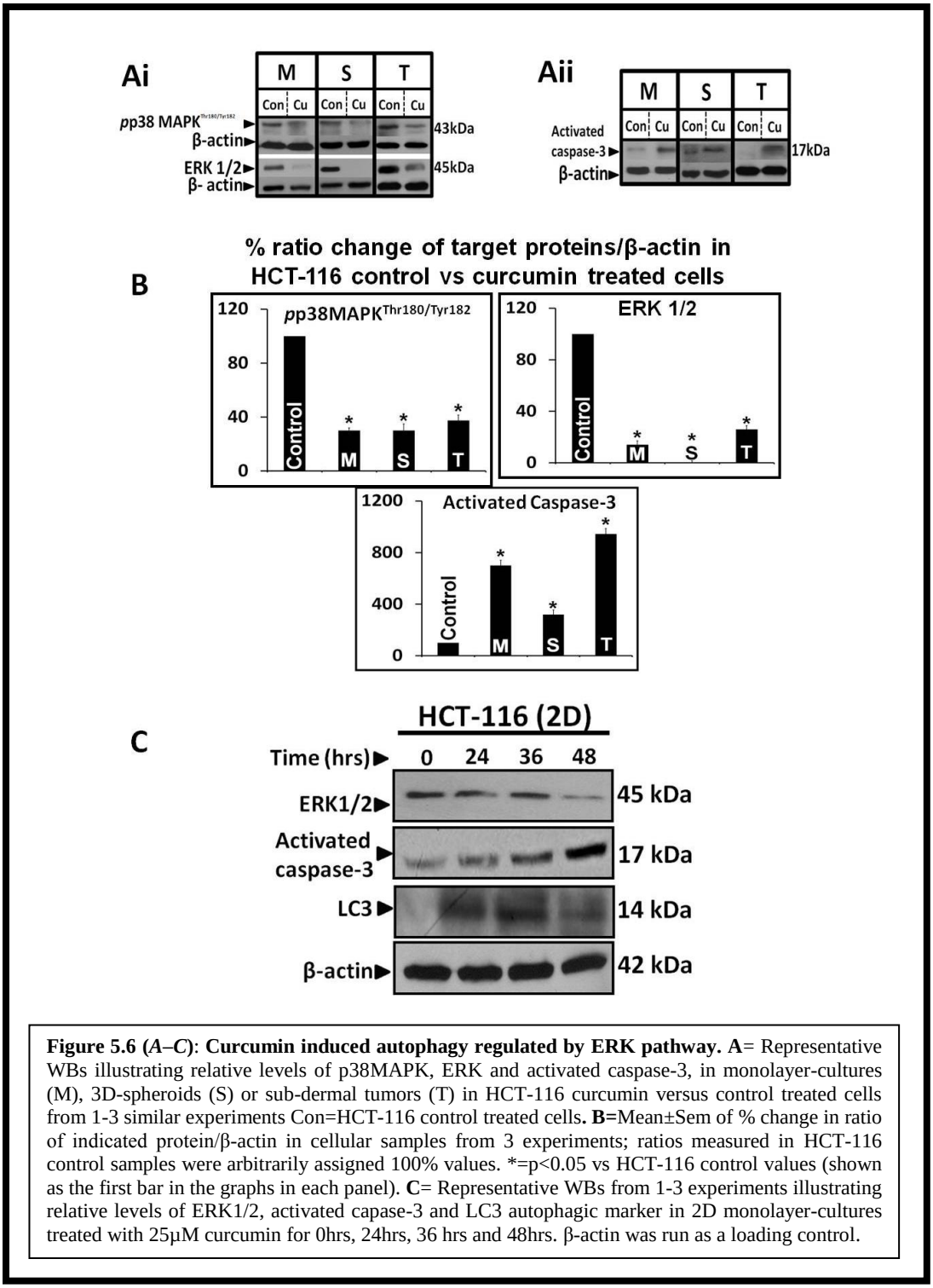

Figure 5.6 (*A*–*C*): **Curcumin induced autophagy regulated by ERK pathway. A**= Representative WBs illustrating relative levels of p38MAPK, ERK and activated caspase-3, in monolayer-cultures (M), 3D-spheroids (S) or sub-dermal tumors (T) in HCT-116 curcumin versus control treated cells from 1-3 similar experiments Con=HCT-116 control treated cells**. B=**Mean±Sem of % change in ratio of indicated protein/β-actin in cellular samples from 3 experiments; ratios measured in HCT-116 control samples were arbitrarily assigned 100% values. *=$p<0.05$ vs HCT-116 control values (shown as the first bar in the graphs in each panel). **C**= Representative WBs from 1-3 experiments illustrating relative levels of ERK1/2, activated capase-3 and LC3 autophagic marker in 2D monolayer-cultures treated with 25μM curcumin for 0hrs, 24hrs, 36 hrs and 48hrs. β-actin was run as a loading control.

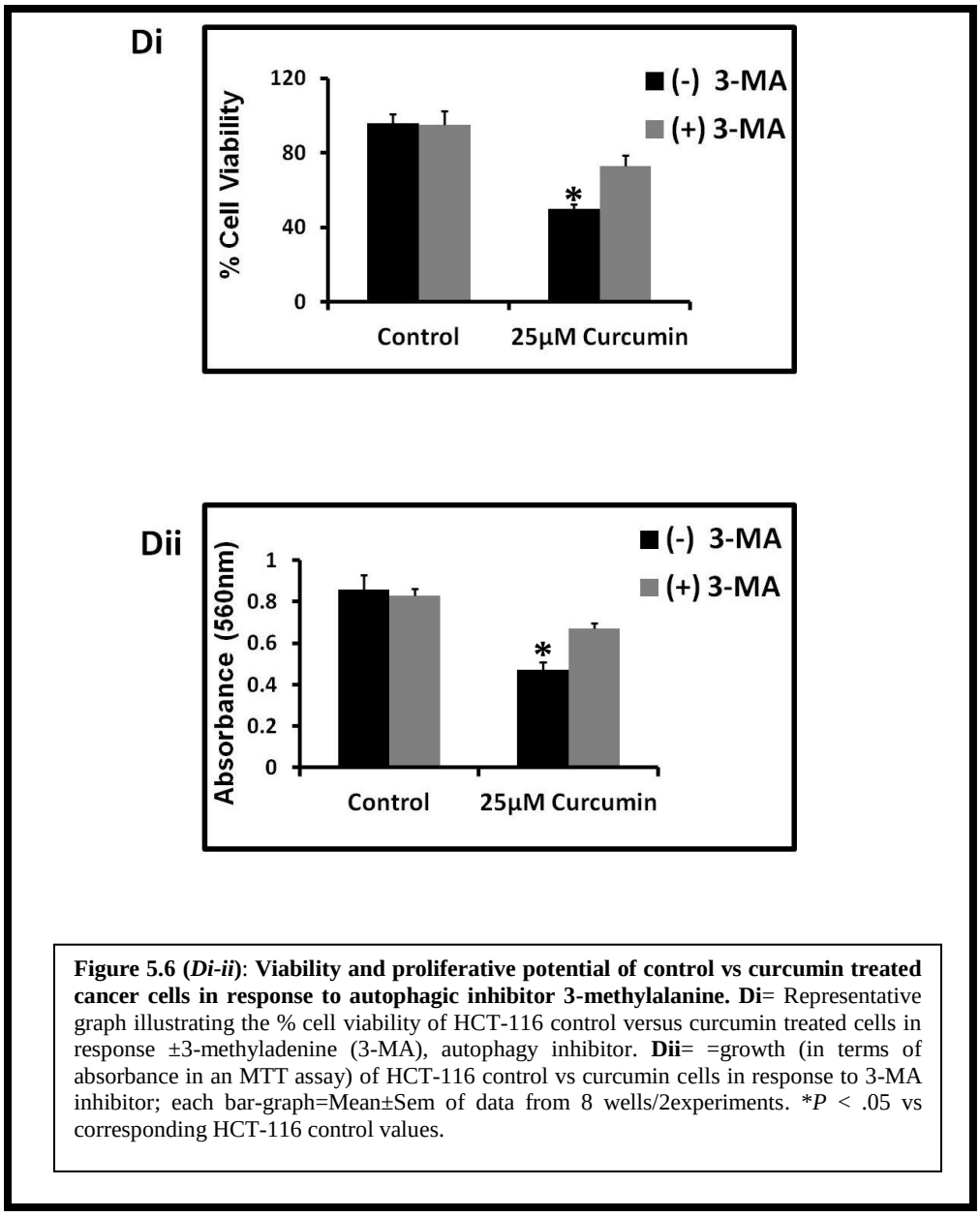

Figure 5.6 (*Di-ii*): **Viability and proliferative potential of control vs curcumin treated cancer cells in response to autophagic inhibitor 3-methylalanine. Di**= Representative graph illustrating the % cell viability of HCT-116 control versus curcumin treated cells in response ±3-methyladenine (3-MA), autophagy inhibitor. **Dii**= =growth (in terms of absorbance in an MTT assay) of HCT-116 control vs curcumin cells in response to 3-MA inhibitor; each bar-graph=Mean±Sem of data from 8 wells/2experiments. **P* < .05 vs corresponding HCT-116 control values.

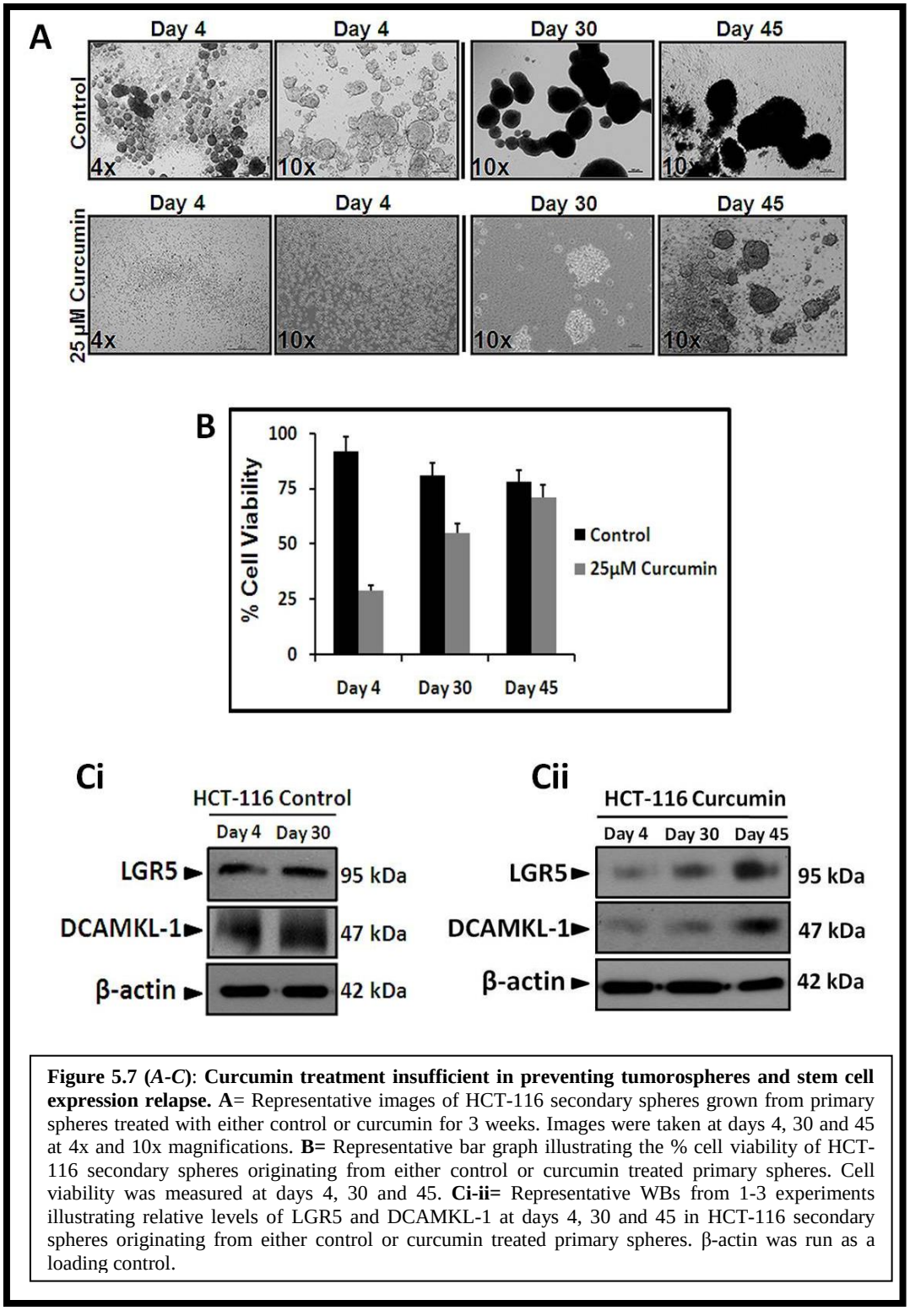

Figure 5.7 (*A*-*C*): **Curcumin treatment insufficient in preventing tumorospheres and stem cell expression relapse. A**= Representative images of HCT-116 secondary spheres grown from primary spheres treated with either control or curcumin for 3 weeks. Images were taken at days 4, 30 and 45 at 4x and 10x magnifications. **B=** Representative bar graph illustrating the % cell viability of HCT-116 secondary spheres originating from either control or curcumin treated primary spheres. Cell viability was measured at days 4, 30 and 45. **Ci-ii=** Representative WBs from 1-3 experiments illustrating relative levels of LGR5 and DCAMKL-1 at days 4, 30 and 45 in HCT-116 secondary spheres originating from either control or curcumin treated primary spheres. β-actin was run as a loading control.

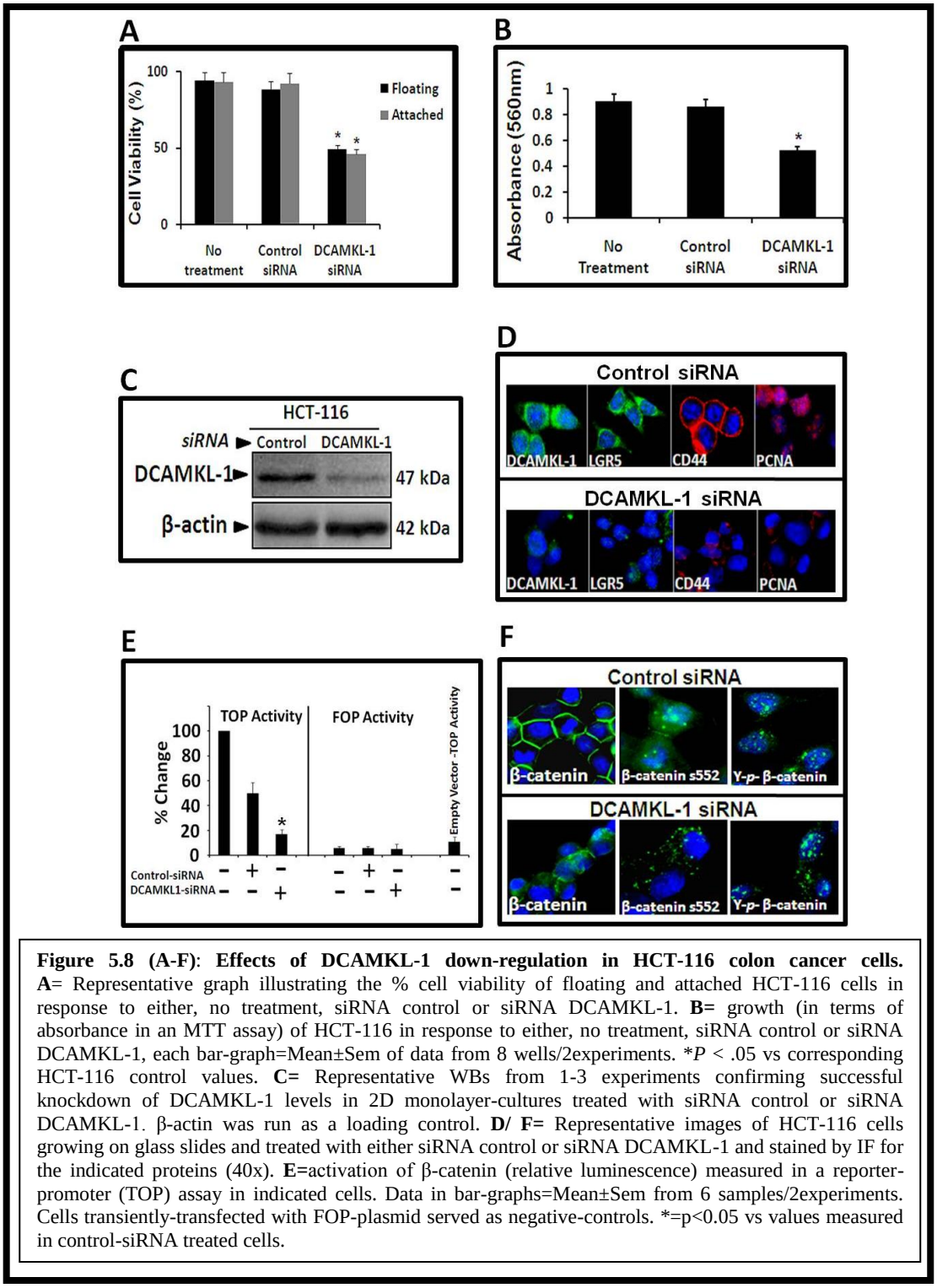

Figure 5.8 (A-F): **Effects of DCAMKL-1 down-regulation in HCT-116 colon cancer cells. A**= Representative graph illustrating the % cell viability of floating and attached HCT-116 cells in response to either, no treatment, siRNA control or siRNA DCAMKL-1. **B=** growth (in terms of absorbance in an MTT assay) of HCT-116 in response to either, no treatment, siRNA control or siRNA DCAMKL-1, each bar-graph=Mean±Sem of data from 8 wells/2experiments. **P* < .05 vs corresponding HCT-116 control values. **C=** Representative WBs from 1-3 experiments confirming successful knockdown of DCAMKL-1 levels in 2D monolayer-cultures treated with siRNA control or siRNA DCAMKL-1. β-actin was run as a loading control. **D/ F=** Representative images of HCT-116 cells growing on glass slides and treated with either siRNA control or siRNA DCAMKL-1 and stained by IF for the indicated proteins (40x). **E=**activation of β-catenin (relative luminescence) measured in a reporter-promoter (TOP) assay in indicated cells. Data in bar-graphs=Mean±Sem from 6 samples/2experiments. Cells transiently-transfected with FOP-plasmid served as negative-controls. *=p<0.05 vs values measured in control-siRNA treated cells.

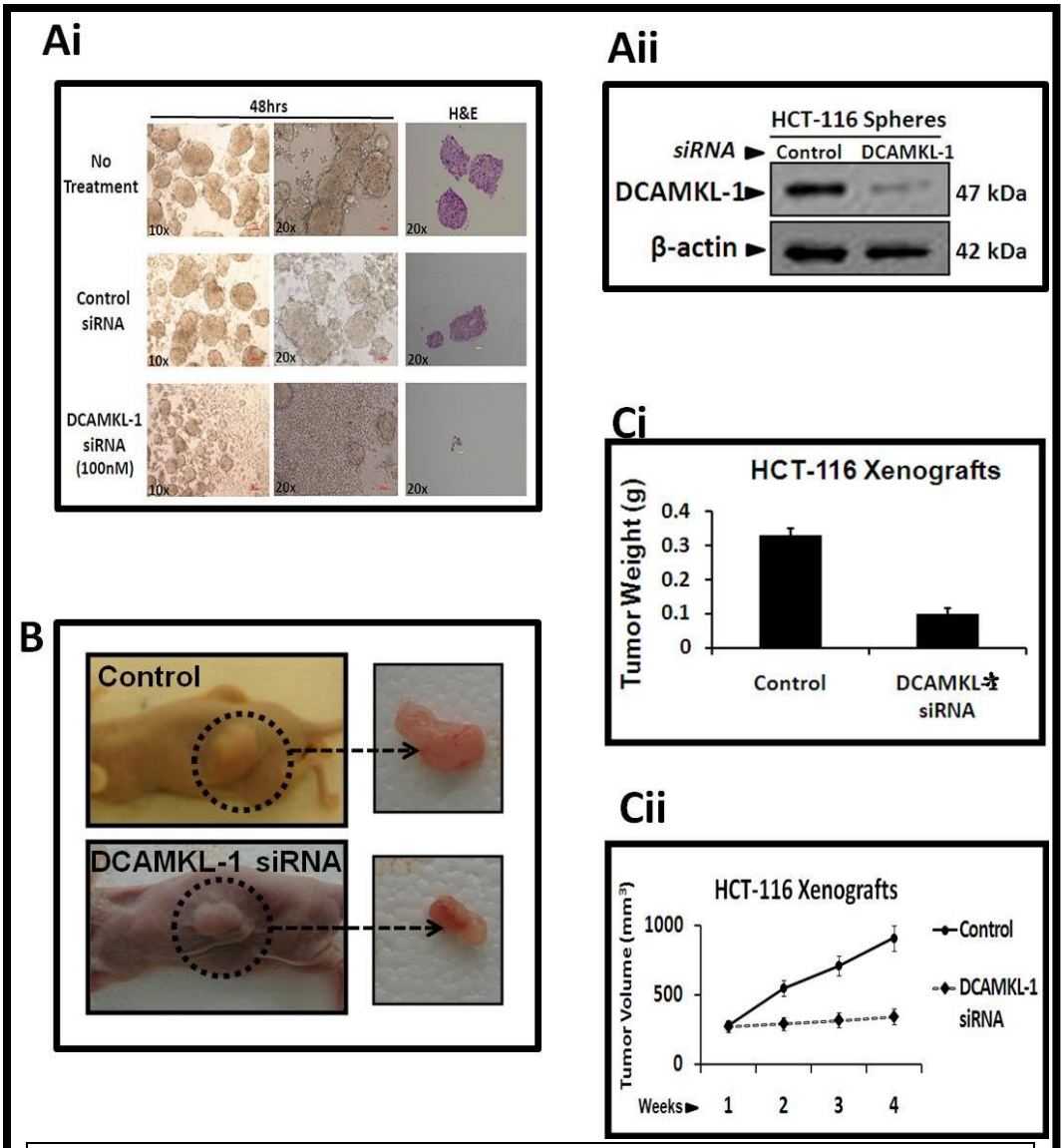

Figure 5.9. ***(A-C)***: **DCAMKL-1 down-regulation decreases the growth of colon cancer tumorospheres and xenografts**. **Ai**=HCT-116 cells grown as tumorospheres were treated with either no treatment, siRNA control or siRNA DCAMKL-1 for 48 hrs. Images were taken at 10x and 20x magnifications. H&E staining of the tumorospheres were imaged at 20x magnification. **Aii**= Representative WB confirming successful knockdown DCAMKL-1 levels in 3D spheres treated with siRNA control or siRNA DCAMKL-1. β-actin run as a loading control. **B**= Representative images of HCT-116 xenografts grown sub-dermally in the flanks of athymic nude mice,, treated with siRNA control or siRNA DCAMKL-1 for every 2 days for 4 weeks as noted by the dotted circle. Excised tumors are also shown as delineated by the dotted arrows. **Ci**= Representative bar graph illustrating final tumor weights of extracted HCT-116 xenografts treated with siRNA control versus siRNA DCAMKL-1. **Cii=** Representative bar graph illustrating final tumor volume of HCT-116 xenografts treated with siRNA control versus siRNA DCAMKL-1, measured weekly over a period of 4 weeks. *=$p<0.05$ vs values measured in control-siRNA treated cells.

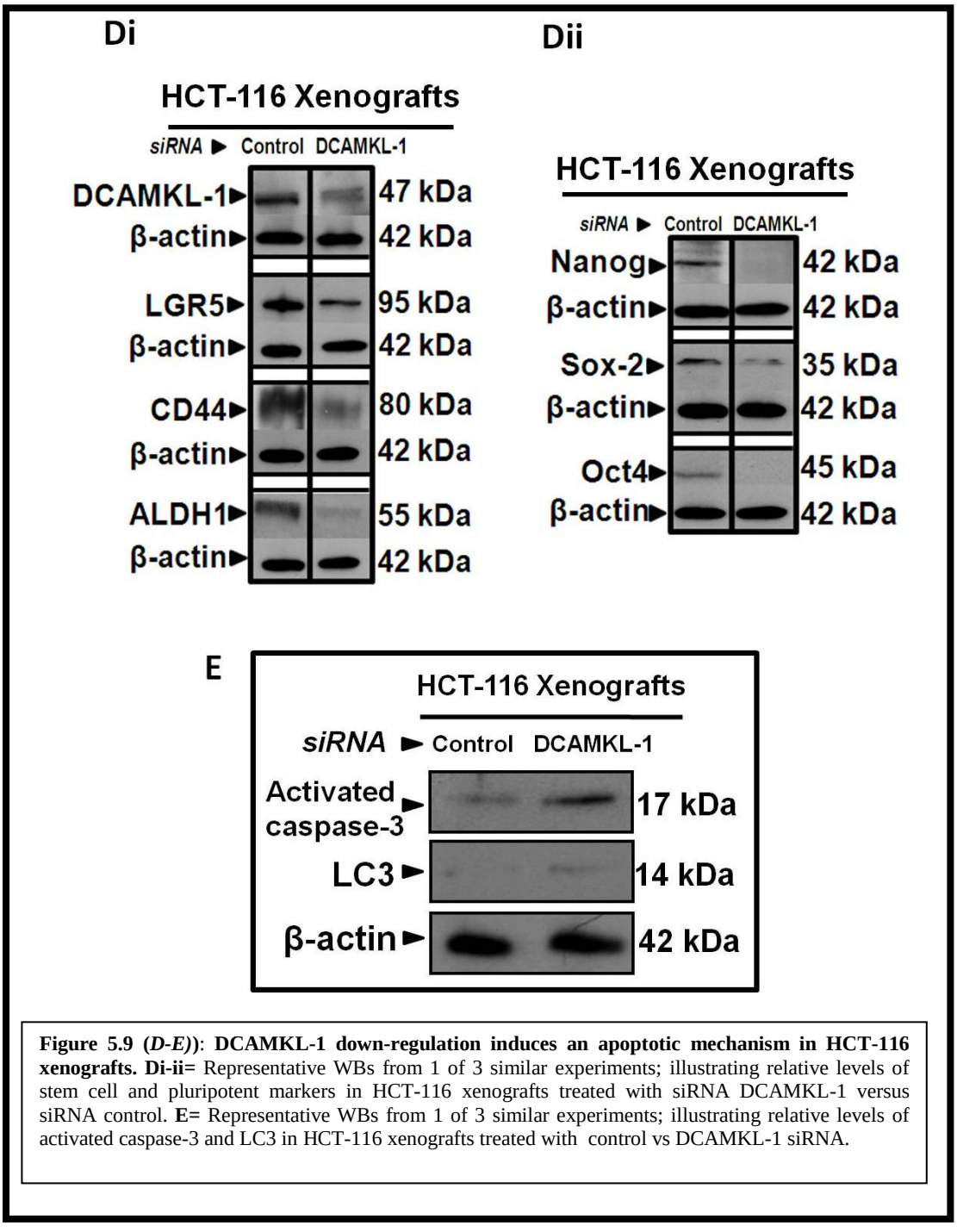

Figure 5.9 (*D-E)*): **DCAMKL-1 down-regulation induces an apoptotic mechanism in HCT-116 xenografts. Di-ii=** Representative WBs from 1 of 3 similar experiments; illustrating relative levels of stem cell and pluripotent markers in HCT-116 xenografts treated with siRNA DCAMKL-1 versus siRNA control. **E=** Representative WBs from 1 of 3 similar experiments; illustrating relative levels of activated caspase-3 and LC3 in HCT-116 xenografts treated with control vs DCAMKL-1 siRNA.

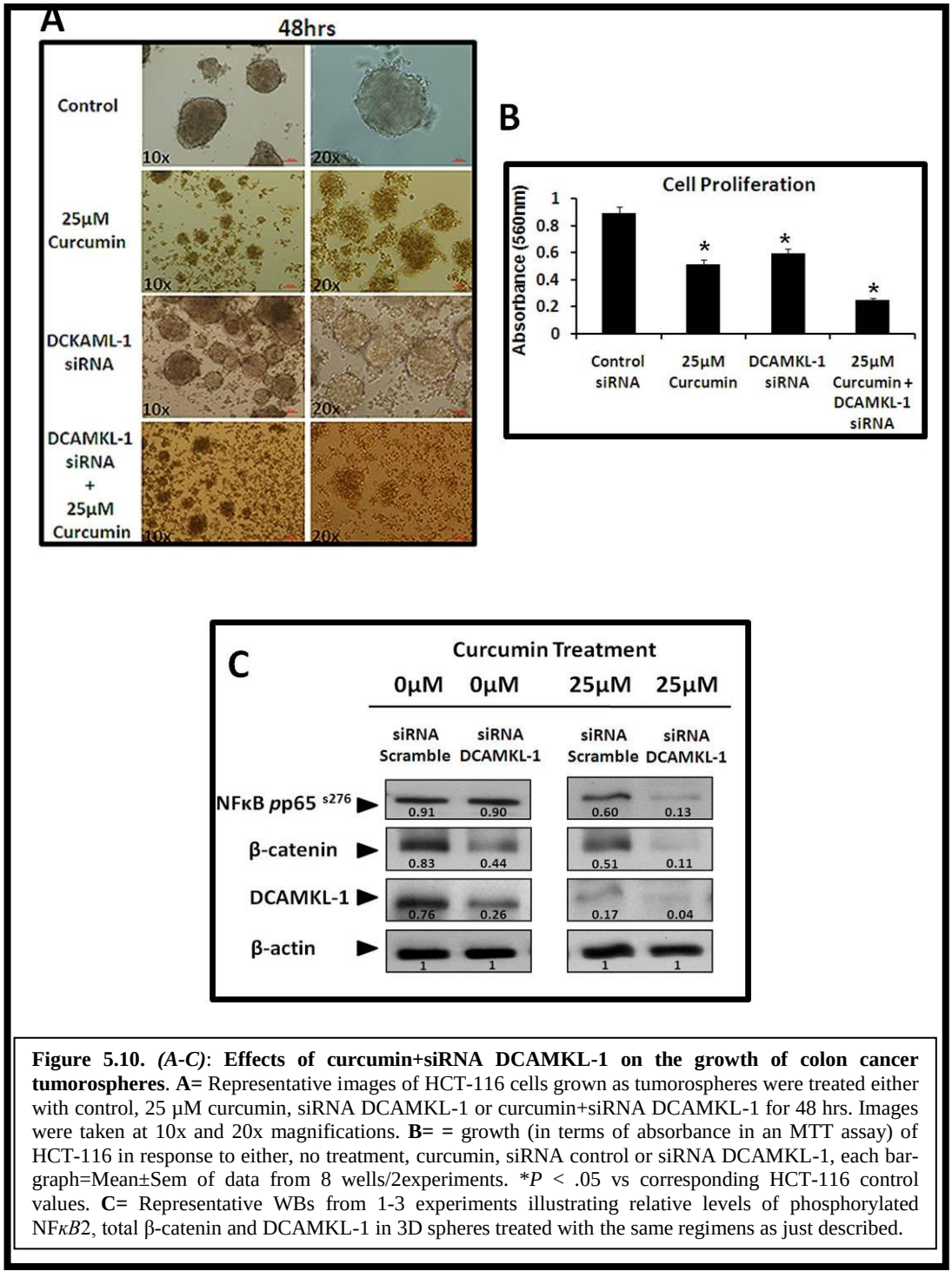

Figure 5.10. ***(A-C)***: **Effects of curcumin+siRNA DCAMKL-1 on the growth of colon cancer tumorospheres**. **A=** Representative images of HCT-116 cells grown as tumorospheres were treated either with control, 25 μM curcumin, siRNA DCAMKL-1 or curcumin+siRNA DCAMKL-1 for 48 hrs. Images were taken at 10x and 20x magnifications. **B= =** growth (in terms of absorbance in an MTT assay) of HCT-116 in response to either, no treatment, curcumin, siRNA control or siRNA DCAMKL-1, each bar-graph=Mean±Sem of data from 8 wells/2experiments. **P* < .05 vs corresponding HCT-116 control values. **C=** Representative WBs from 1-3 experiments illustrating relative levels of phosphorylated NF*κB*2, total β-catenin and DCAMKL-1 in 3D spheres treated with the same regimens as just described.

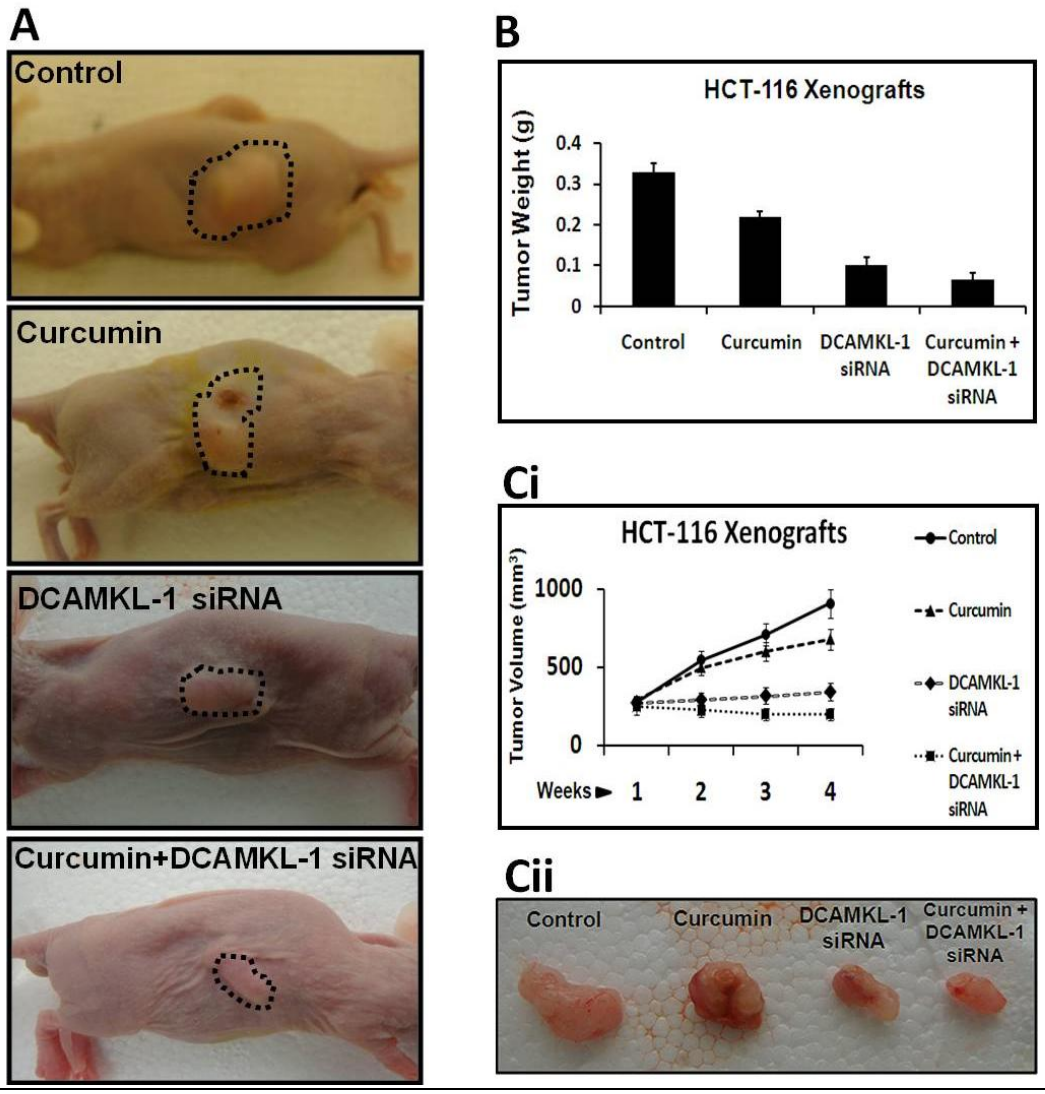

Figure 5.11. ***(A-C)***: **Curcumin±DCAMKL-1 siRNA significantly decreases the growth of colon cancer tumorospheres and xenografts**. **A=** Representative images of HCT-116 xenografts grown sub-dermally in the flanks of athymic nude mice, treated with control, 100μM curcumin, siRNA control or 100nM siRNA DCAMKL-1 for every 2 days for 4 weeks as noted by the dotted circle. Excised tumors are also shown as delineated by the dotted arrows. **Bi**= Representative bar graph illustrating final tumor weights of extracted HCT-116 xenografts treated with the above regimens. **Bii=** Representative bar graph illustrating final tumor volume of HCT-116 xenografts treated with the above regimens, measured weekly over a period of 4 weeks. **C**= Representative image comparing the growth of HCT-116 xenografts treated with control vs curcumin vs siRNA control vs siRNA DCAMKL-1. *=$p<0.05$ vs values measured in control treated cells.

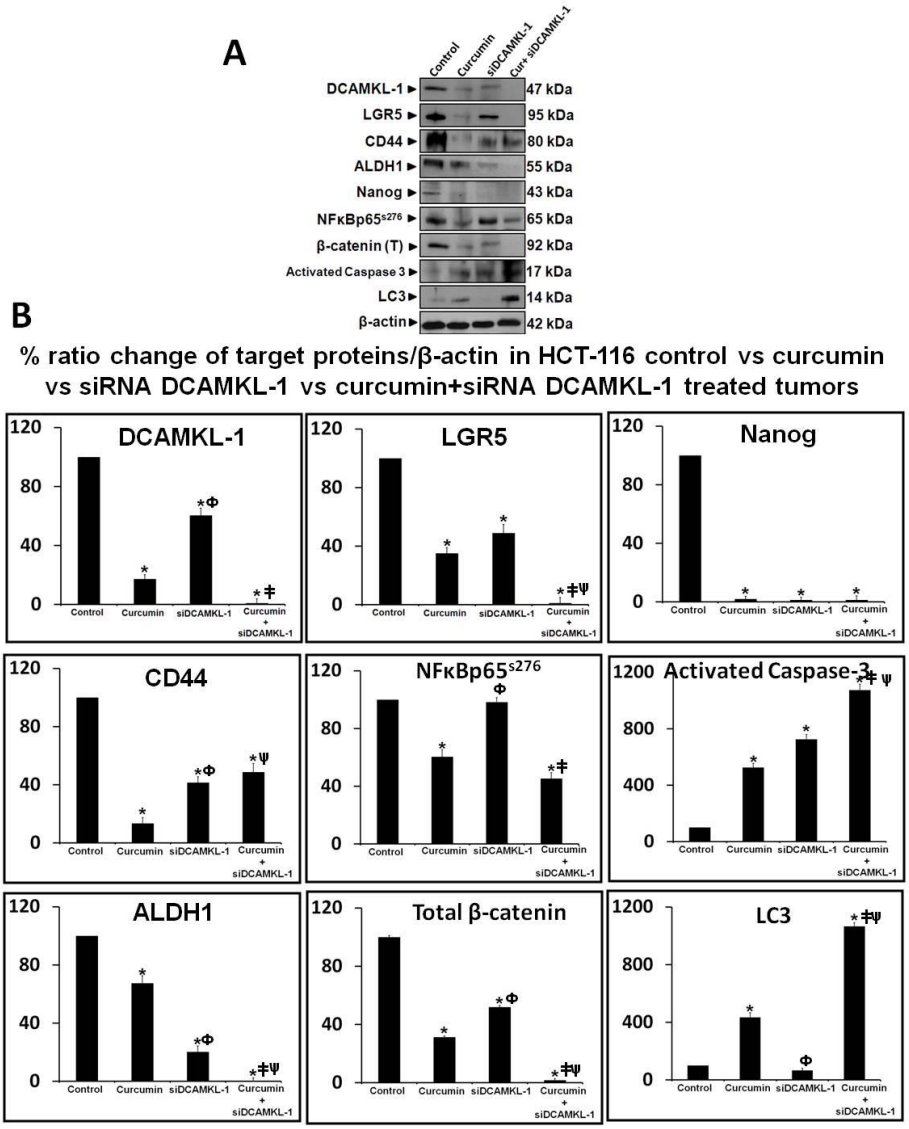

Figure 5.12 (*A*–*B*): **Comparative effects of curcumin±siRNA DCAMKL-1 on the relative levels of stem/pluripotent markers, NFκB/β-catenin and autophagic/apoptotic pathways in HCT-116 xenografts. A=** Representative WBs of indicated proteins from 1 of 3 similar experiments; **B=**Mean±Sem of % change in ratio of indicated protein/β-actin in cellular samples from 3 experiments; ratios measured in HCT-116 control samples were arbitrarily assigned 100% values. *=p<0.05 vs HCT-116 control values (shown in the first bar of each graph panel). Ψ =p<0.05 vs HCT-116 curcumin values; Φ=p<0.05 vs HCT-116 curcumin treated cells; ǂ =p<0.05 vs HCT-116 siRNA DCAMKL-1 treated cells.

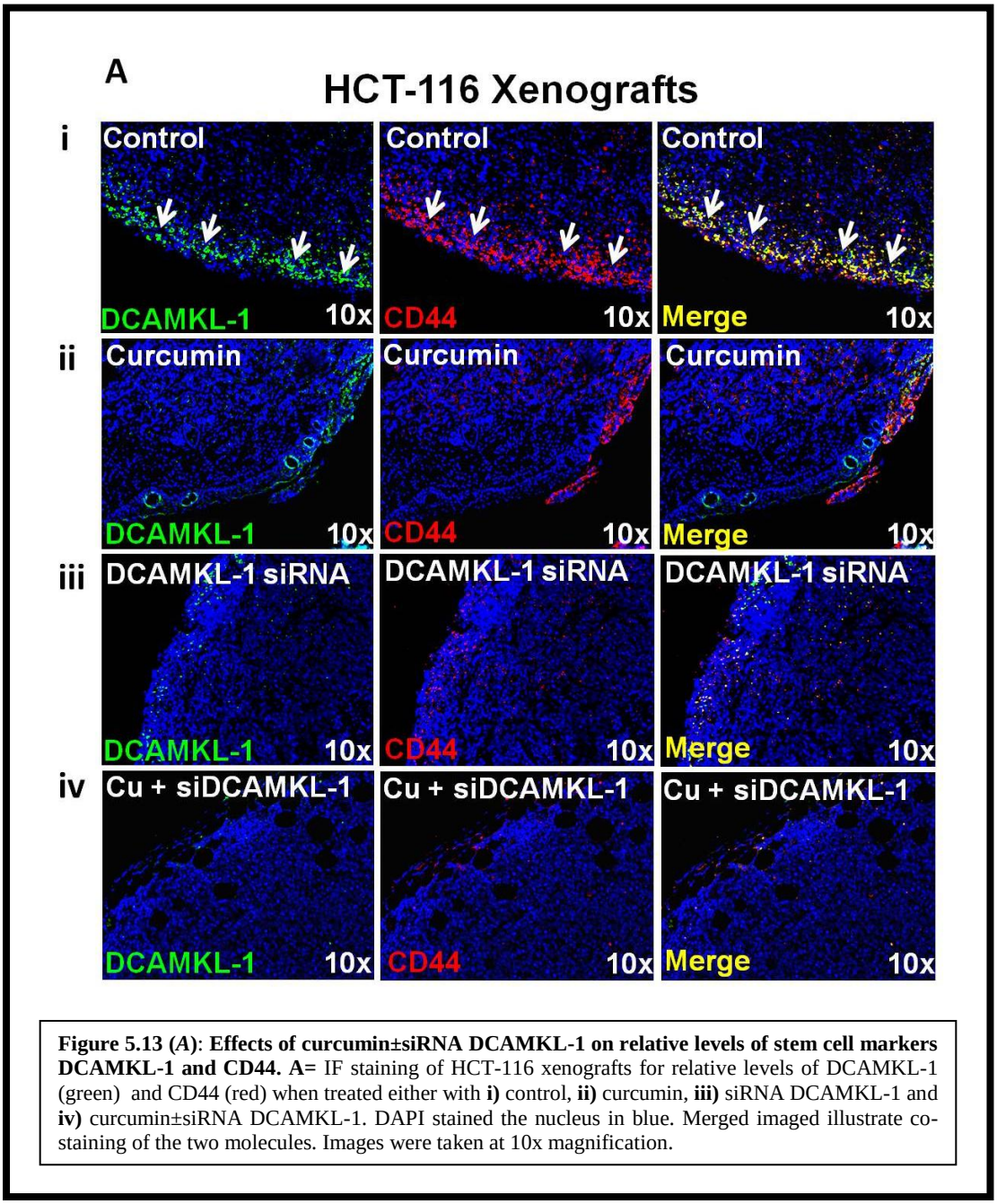

Figure 5.13 (*A*): **Effects of curcumin±siRNA DCAMKL-1 on relative levels of stem cell markers DCAMKL-1 and CD44. A=** IF staining of HCT-116 xenografts for relative levels of DCAMKL-1 (green) and CD44 (red) when treated either with **i)** control, **ii)** curcumin, **iii)** siRNA DCAMKL-1 and **iv)** curcumin±siRNA DCAMKL-1. DAPI stained the nucleus in blue. Merged imaged illustrate co-staining of the two molecules. Images were taken at 10x magnification.

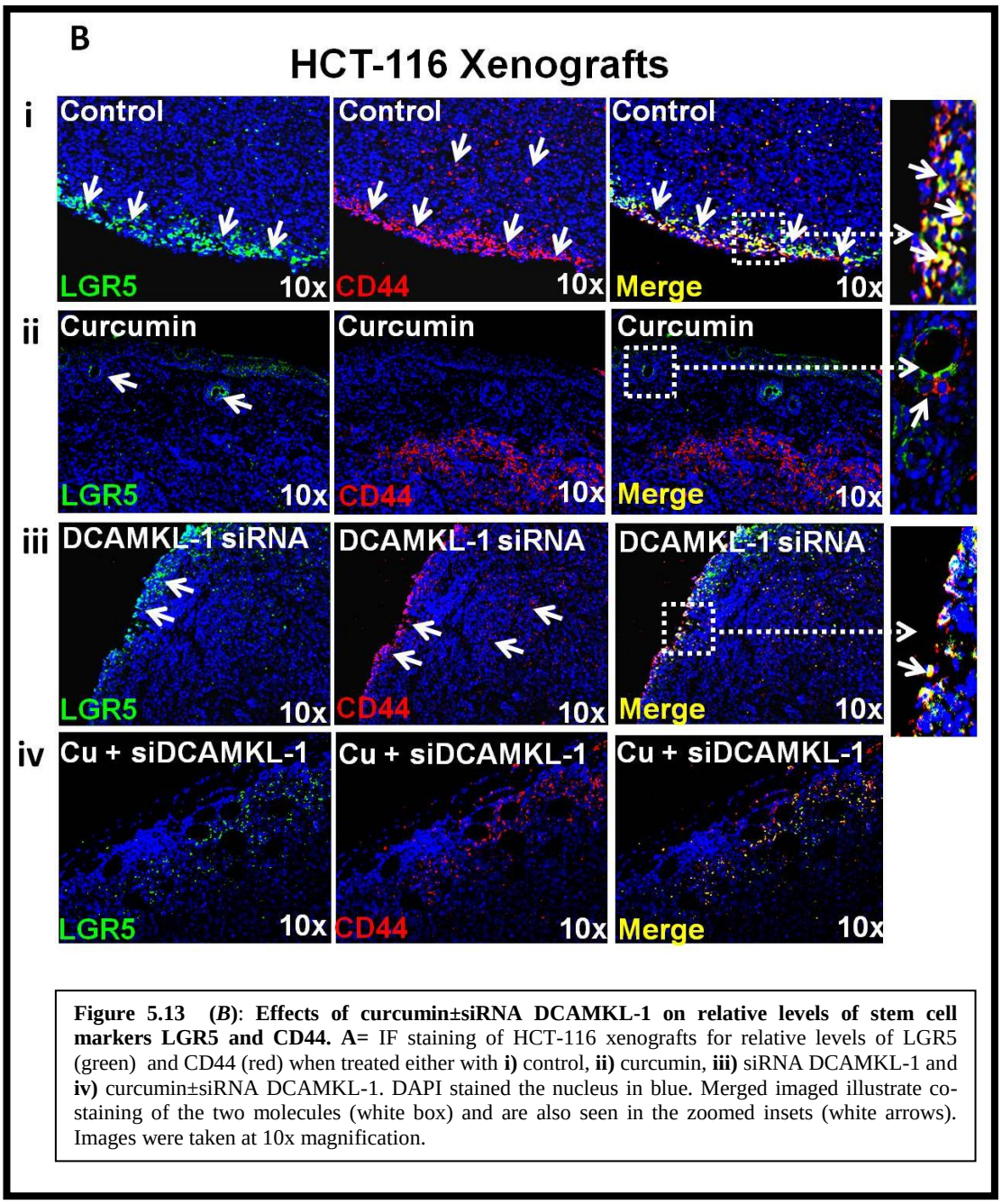

Figure 5.13 (*B*): Effects of curcumin±siRNA DCAMKL-1 on relative levels of stem cell markers LGR5 and CD44. A= IF staining of HCT-116 xenografts for relative levels of LGR5 (green) and CD44 (red) when treated either with **i)** control, **ii)** curcumin, **iii)** siRNA DCAMKL-1 and **iv)** curcumin±siRNA DCAMKL-1. DAPI stained the nucleus in blue. Merged imaged illustrate co-staining of the two molecules (white box) and are also seen in the zoomed insets (white arrows). Images were taken at 10x magnification.

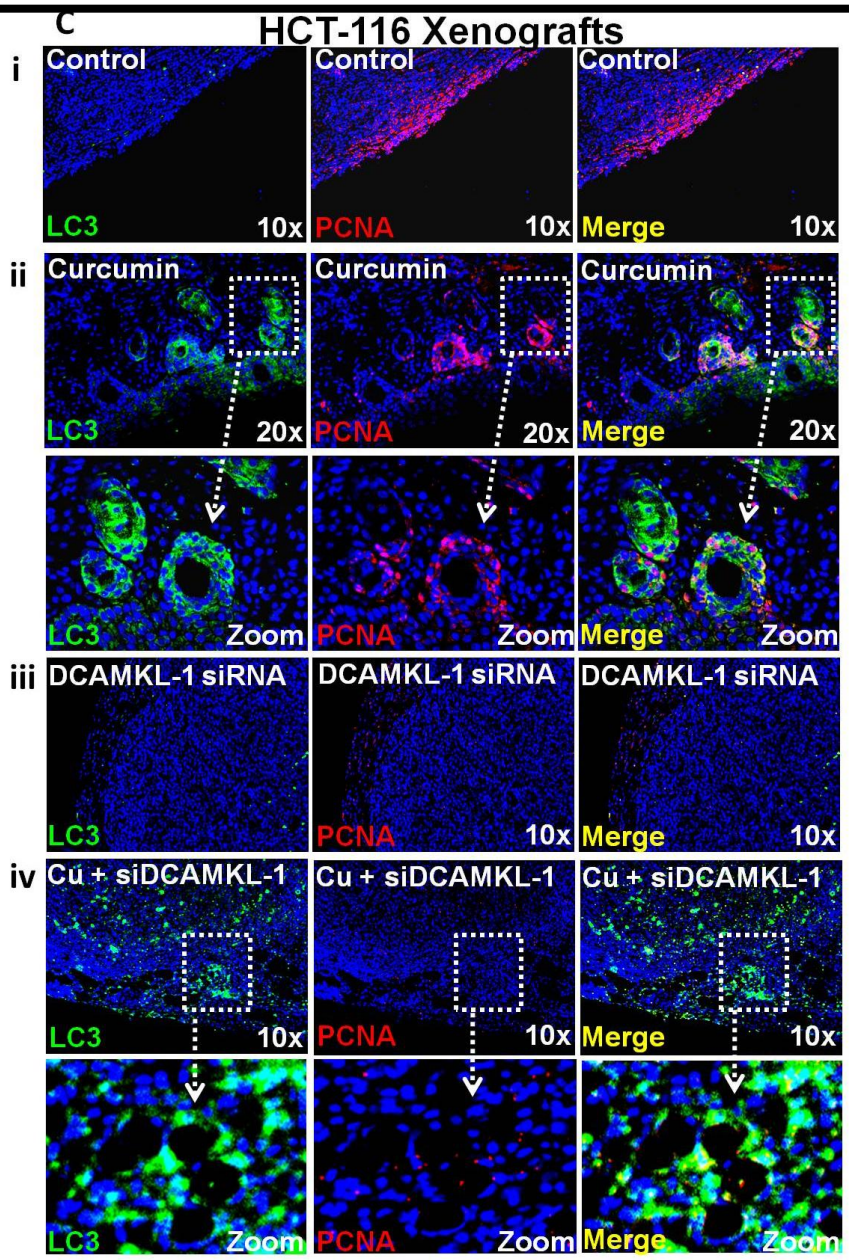

Figure 5.13 (*C*): Effects of curcumin±siRNA DCAMKL-1 on relative levels of autophagic and proliferative markers. A= IF staining of HCT-116 xenografts for relative levels of LC3 (green) and PCNA (red) when treated either with **i)** control, **ii)** curcumin, **iii)** siRNA DCAMKL-1 and **iv)** curcumin±siRNA DCAMKL-1. DAPI stained the nucleus in blue. Merged imaged illustrate co-staining of the two molecules (white box) and are also seen in the zoomed insets (white arrows). Images were taken at 10x magnification and digitally enhanced.

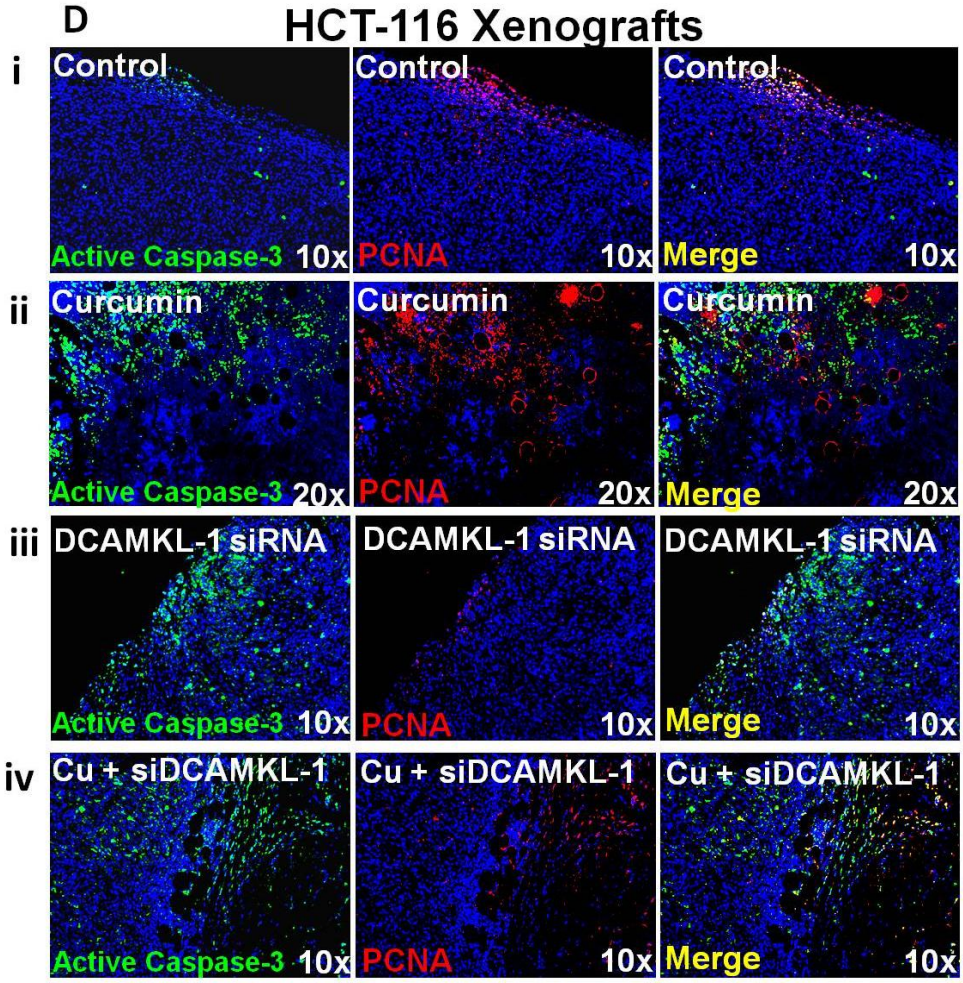

Figure 5.13 (*D*): Effects of curcumin±siRNA DCAMKL-1 on relative levels of apoptotic and proliferative markers. A= IF staining of HCT-116 xenografts for relative levels of activated caspase-3 (green) and PCNA (red) when treated either with **i)** control, **ii)** curcumin, **iii)** siRNA DCAMKL-1 and **iv)** curcumin±siRNA DCAMKL-1. DAPI stained the nucleus in blue. Merged imaged illustrate co-staining of the two molecules. Images were taken at 10x magnification.

5.4 DISCUSSION

Results presented in this chapter demonstrated that the combined treatment with curcumin+ DCAMKL-1 siRNA synergistically increases both autophagic and apoptotic death of colon cancer cells/xenografts, resulting in a more potent reduction of tumor growth and stem cell expression compared to that achieved with the individual agent. A major finding was that the inhibitory effects of the two agents were mediated by separate cell death mechanisms.

Treatment of colon cancer spheroids with curcumin resulted in the disintegration of tumorospheres, with formation of hollow structures within the spheroids **(Fig 5.1A-C).** Curcumin has been reported to induce autophagy in cancer cells (171,173,259). The hollow structures observed by us were lined by cells positive for the autophagic marker, LC3, suggesting that these structures may represent an autophagic response to curcumin. The significant loss in cell viability/proliferation and the growth of spheroids/tumors, in response to curcumin, was only partial (50-60-%), and re-growth of curcumin treated spheroids was observed (resembling relapse), suggesting that curcumin alone may not eradicate cancer stem cells.

In normal cells, autophagy is activated as a rescue/cell survival mechanism; however, in cancer cells this mechanism has been described as a double edged sword inducing either cell survival or cell death at any given time (171,259,260). Autophagy is usually suppressed in cancer cells, and has been shown to be inversely correlated with malignant phenotype of tumor cells (170,173,174). However, in response to dietary

agents, such as curcumin, cancer cells activate autophagic mechanisms (170). We investigated whether curcumin induced autophagy in colon cancer cells was activated as a protective and/or anti-tumor mechanism, resulting in cell death. Our results demonstrated that inhibition of autophagy, increased viability and proliferative potential of colon cancer cells **(Fig 5.6D)**, suggesting that curcumin-induced autophagy is activated as an anticancer response and not as a rescue effort by cancer cells, by perhaps activating autophagic Type II cell death mechanism.

Curcumin has been reported to down regulate critical growth stimulating/oncogenic pathways in cancer cells, including the NFκB pathway (155,163,261), which sensitizes the cells/tumors to a more potent inhibitory response to chemotherapy/radiation (256, 264, 265). Since cancer stem cells are likely the major cause of relapse of the disease, we examined possible inhibitory effects of curcumin on cancer stem cell populations. We found that curcumin decreased relative levels of stem/pluripotent cell markers, associated with a significant loss in activation of potent transcription factors, p65NFκB/β-catenin, (**Figs 5.4 and 5.5**), known to be critically required for maintaining growth potential of colon cancer cells (257). Previous studies form many labs, including ours, has demonstrated that curcumin directly targets p65NFκB and β-catenin signaling pathways resulting in tumor growth arrest (257, 262, 263). Our results further suggest that curcumin can also target cancer stem cells, which may explain the significant loss in the growth of tumors/spheroids in response to curcumin.

Autophagy in cancer cells has been reported to be regulated by mTOR/Akt pathway (171). Curcumin has additionally been reported to inhibit the ERK/Akt/mTOR pathways in several cancers (171,264,266). The loss of ERK expression in cancer cells has been reported to inhibit curcumin-induced autophagy and activate apoptosis (171). We therefore further examined whether ERK expression was involved in the activation of autophagy and/or apoptosis in colon cancer cells, in response to curcumin. Our results demonstrated that autophagy was activated within first 24 hours of curcumin treatment, believed to represent survival mechanism in cancer cells, in the absence of activation of apoptotic pathways at this time point (**Fig 5.6C**). However, by 48hrs, activation of ERK was completely inhibited, resulting in cell death, once again suggesting that cell death in response to curcumin is likely activated by both an autophagy Type II cell death mechanism and apoptosis (**Fig 5.6A-C**). Our results strongly suggest that activation of ERK mediated pathways (including downstream activation of NFκB (5,112), in response to curcumin, may likely regulate autophagy/apoptosis of colon cancer cells.

Results in Chapter 3 showed that transformed stem cells co-express DCAMKL-1 and CD44. Our results in the current chapter demonstrate that co-expression of DCAMKL-1 and CD44 was attenuatted in curcumin treated xenografts compared to controls **(Fig 5.13A)**, suggesting once again that curcumin may indeed target cancer stem cells, resulting in the loss of 'stemness' of colon cancer cells.

DCAMKL-1 is a microtubule-associated kinase over-expressed in various cancers including colorectal cancers (72). Down-regulation of DCAMKL-1 in HEK-C/HEK-mGAS cells significantly reduced proliferative proliferation of the cells, suggesting that

DCAMKL-1 is required for maintaining growth of immortalized embryonic epithelial-cells (Chapter 3). In the current chapter we examined whether DCAMKL-1 was essential in the growth of colon cancer cells as well. Our results demonstrate that DCAMKL-1 expression is similarly required for maintaining proliferative potential of colon cancer cells/tumors **(Fig 5.8 and 5.9)**. DCAMKL-1 was also shown to be required for maintaining β-catenin activation in colon cancer cells (**Fig 5.8E-F**). However, down-regulation of DCAMKL-1expression in colon cancer cells was also only partially effective as curcumin alone, and resulted in reducing the expression levels of stem/pluripotent cell markers by ~ 60% , suggesting that treatment with siRNA DCAMKL-1 may also not be sufficient for eradicating cancer stem cells. It is possible that since siRNAs are generally not effective in completely down-regulating expression levels of a target mRNA for any length of time, due to their transient effects, sustained expression of RNAi via stable transfection with DCAMKL-1-shRNA, may likely improve the loss of cancer stem cells. We are currently in the process of encapsulating lentiviral expressing DCAMKL-shRNA plasmids in nanoparticles to determine if sustained targeting of DCAMKL-1 expression will be more effective in eradicating cancer stem cells.

Since treatment with single agents, curcumin or DCAMKL-1 siRNA, was insufficient for eradicating cancer stem cells (**Figs 5.7 and 5.8**), we examined if the combined regimen of the two agents will be more effective. Several investigators have reported the use of curcumin in combination with chemotherapeutic drugs as a novel approach to treat cancer (163, 266). It is believed that while curcumin sensitizes cancer

cells by reducing oncogenic pathways, as discussed above, chemotherapeutic drugs become more effective at cancer cell kill at lower doses, thus reducing toxicity to normal cells (163, 262). To further improve on the strategy of sparing normal cells while targeting cancer stem cells more potently, we examined effects of combining curcumin+DCAMKL-1 siRNA. Both these agents are likely to be non-toxic to normal cells, and were expected to enhance inhibitory effects on colon cancer cells. Our results demonstrate that the combined regimen was extremely effective. This may be due to the fact that while curcumin induced Type II autophagic death, co- treatment with DCAMKL-1 siRNA synergistically augmented both apoptotic and autophagic death mechanisms, resulting in significantly increasing loss of tumor growth and almost complete loss in pluripotency of cancer stem cells **(Figs 5.12 and 5.13C).**

In future studies, I will examine if the combined regimen is effective in eradicating relapse of the disease, and if the combined regimen has minimal effects on normal cell function. Since normal stem cells are also positive for DCAMKL-1, it is possible that targeting DCAMKL-1 with a more effective strategy of nanoparticle delivery of DCAMKL-1-shRNA may reduce restitution of normal colonic crypts. However, in normal colonic crypts, LGR5 plays a more significant role in the maintenance of crypt structure (23). Thus loss of DCAMKL-1+ve normal stem cells may not have any significant, long lasting, deleterious effects on normal colonic functions, while cancer stem cells, on the other hand, may be eradicated. We are currently conducting experiments with a colon carcinogenesis model using transgenic mice, developed in our laboratory (5,117,118), to examine some of these important questions. I

am also contributing to studies in which our laboratory is examining the signature of circulating colon cancer stem cells, which are believed to be the seeds of metastatic growths. Our studies so far suggest that circulating cancer stem cells also co-express CS-ANXA2 with stem cell markers, DCAMKL-1/CD44, while LGR5 stem cells are not measured in circulation to the same extent in mice and humans bearing human cancer metastatic growths (243). Thus targeting DCAMKL-1 rather than LGR5 may prove to be a specific treatment for colon cancer stem cells, while sparing normal growth of small and large intestinal crypts **(Fig 1.10)**.

Our studies, with patient samples, also demonstrate that DCAMKL-1 is co-expressed with CD44 in the majority of adenomas and adenocarcinoms, unlike corresponding normal colonic mucosa from the same patients (223), suggesting that the phenotype of co-expressing the two stem cell markers (DCAMKL-1/CD44) may be an early event during colon carcinogenesis in humans, and may represent the phenotype of colon cancer stem cells. We have submitted a patent application based on these novel findings, which is currently in review by the patent office.

CHAPTER 6

CONCLUSION

6.1 SUMMARY

The major goal of my dissertation was to examine mechanisms by which progastrins up-regulate growth of colonic cells, and to learn about the stem cell populations in normal and cancer cells, with a long term aim to develop effective inhibitory strategies against colon cancer stem cells. To achieve my major goal, studies were conducted to examine the following: 1) the role of ANXA2 in mediating the proliferative/anti-apoptotic effects of PG on target cells and in regulation of stem cell populations, 2) the role of over-expressing autocrine PG on tumorigenic and metastatic potential of embryonic HEK-293 cells and to examine the phenotypic differences between non-transformed and transformed stem cell using non-tumorigenic (HEK-C) and tumorigenic (HEK-mGAS) isogenic cells 3) the phenotypic/proliferative differences between DCAMKL+ve and LGR5+ve colon cancer stem cells, and 4) the inhibitory effects of curcumin±DCAMKL-siRNA on colon cancer cells *in vitro* and *in vivo.*

My results revealed that 1) ANXA2 mediates the growth effects of PG on target cells (including colonic epithelial cells), *in vitro* and *in vivo,* associated with up-regulation of stem/progenitor cell markers, 2) transformed stem cells, unlike normal stem cells, co-express CS-ANXA2 with stem cell markers DCAMKL-1/CD44, 3) DCAMKL-1+ve cells are significantly more proliferative than either DCAMKL-1-ve or LGR5+ve stem cells, and 4) combination of curcumin + siRNA-DCAMKL-1, effectively attenuates

growth of colon-cancer-cells *in vitro* and *in vivo*, by synergistically augmenting autophagic/apoptotic cell-death mechanisms.

6.2 FUTURE GOALS

Immediate Goals: As a result of my studies several additional intriguing questions have arisen, and will need to be answered in the future. For example, it remains to be determined if up-regulation of DCAMKL-1 in response to PG, is mediated via NFκB and/or β-catenin signaling pathways. Our studies suggested that a minute % of colon cancer stem cells were positive for DCAMKL-1 and LGR5; it remains to be determined if these cells represent a more tumorigenic phenotype. It also remains to be determined whether CD44 and/or CS-ANXA2 mediate the growth and invasive effects on DCAMKL+ve cancer stem cell populations, and if down-regulating LGR5/CD44 in combination with curcumin may exert a more pronounced inhibitory effect on tumor growth compared to siRNA DCAMKL-1+curcumin.

Long term Goals: To understand the mechanisms by which DCAMKL-1 functions as a critical stem cell marker and identify factors which regulate its activities (ligands).

6.3 CLINICAL RELEVANCE

The identification of unique cancer stem cell markers is critical as it will allow for the development of novel therapeutic approaches which are aimed at directly targeting these cells. Once these markers have been identified, antibodies or antagonists tagged to a drug may be used to directly target cancer stem cells, within primary/metastatic tumors

and/or in circulation. Furthermore, it is important to develop novel therapies that are non-toxic, which are specific to cancer cells and spare normal cells. Currently, curcumin is being tested in Phase II clinical trials for treatment of colorectal cancers. Curcumin, however, is not likely to be completely effective as a therapeutic agent by itself, and is proposed to be used for sensitizing the cancer cells to more effective treatment with chemotherapeutic drugs. Based on my studies, it may be possible to use a non-toxic sensitizer, such as curcumin in combination with targeted therapies, which target cancer stem cells, and spare normal functions.

LITERATURE CITED

1. Subramaniam D, Ramalingam S, Houchen CW, Anant S. Cancer stem cells: a novel paradigm for cancer prevention and treatment. Mini Rev Med Chem. 2010;10:359-371.

2. Milla PJ. Advances in Understanding Colonic Function. J Pediatr Gastroenterol Nutr. 2009;48:S43-S45.

3. Roberts, A. *The Complete Human Body: The Definitive Visual Guide*. 1st Edition ed. New York: DK Publishing, 2010.

4. Lindblom A. Different mechanisms in the tumorigenesis of proximal and distal colon cancers. Curr Opin Oncol. 2001;13:63-69.

5. Umar S, Sarkar S, Cowey S, Singh P. Activation of NF-kappaB is required for mediating proliferative and antiapoptotic effects of progastrin on proximal colonic crypts of mice, in vivo. Oncogene. 2008;27:5599-5611.

6. Papailiou J, Bramis KJ, Gazouli M, Theodoropoulos G. Stem cells in colon cancer. A new era in cancer theory begins. Int J Colorectal Dis. 2011;26:1-11.

7. Montgomery RK, Shivdasani RA. Prominin1 (CD133) as an intestinal stem cell marker: promise and nuance. Gastroenterology. 2009;136:2051-2054.

8. Ponder BA, Schmidt GH, Wilkinson MM, Wood MJ, Monk M, Reid A. Derivation of mouse intestinal crypts from single progenitor cells. Nature. 1985;313:689-691.

9. Endo Y, Sugimura H, Kino I. Monoclonality of normal human colonic crypts. Pathol Int. 1995;45:602-604.

10. McDonald SA, Preston SL, Lovell MJ, Wright NA, Jankowski JA. Mechanisms of disease: from stem cells to colorectal cancer. Nat Clin Pract Gastroenterol Hepatol. 2006;3:267-274.

11. Kosinski C, Li VS, Chan AS, Zhang J, Ho C, Tsui WY, Chan TL, Mifflin RC, Powell DW, Yuen ST, Leung SY, Chen X. Gene expression patterns of human colon tops and basal crypts and BMP antagonists as intestinal stem cell niche factors. PNAS. 2007;104:15418-15423.

12. D'Angelo RC, Wicha MS. Stem cells in normal development and cancer. Prog Mol Biol Transl Sci. 2010;95:113-158.

13. Reya T, Clevers H. Wnt Signaling in stem cells and cancer. Nature. 2005;434:843-850.

14. Ricci-Vitiani L, Fabrizi E, Palio E, De Maria R. Colon cancer stem cells. J Mol Med (Berl). 2009;87:1097-1104.

15. Reya T, Morrison SJ, Clarke MF, Weissman IL. Stem Cells, cancer, and cancer stem cells. Nature. 2001;414:105-111.

16. Boman BM, Wicha MS, Fields JZ, Runquist OA. Symmetric division of cancer stem cells. A key mechanism in tumor growth that should be targeted in future therapeutic approaches. Clin Pharmacol Ther. 2007;81:893-899.

17. Farag N, Delbanco T, Strewler GJ. Update: A 64-year-old woman with primary hyperparathyroidism. JAMA. 2008;300:2044-2045.

18. Potten CS, Loeffler M. Stem cells: attributes, cycles, spirals, pitfalls and uncertainties. Lessons for and from the crypt. Development. 1990;110(4):1001-1020.

19. Gordon JI, Schmidt GH, Roth KA. Studies of intestinal stem cells using normal, chimeric, and transgenic mice. FASEB J. 1992;6:3039-3050.

20. May R, Riehl TE, Hunt C, Sureban SM, Anant S, Houchen CW. Identification of a Novel Putative Gastrointestinal Stem Cell and Adenoma stem cell marker, Doublecortin and CaM Kinase-Like-1, following Radiation Injury and in Adenomatous Polyposis Coli/Multiple Intestinal Neoplasia Mice. Stem Cells. 2008;26:630-637.

21. Scoville DH, Sato T, He XC, Li L. Current view: intestinal stem cells and signaling. Gastroenterology. 2008;134:849-864.

22. Quante M, Wang TC. Stem cells in gastroenterology and hepatology. Nat Rev Gastroenterol & Hepatol. 2009;6:724-737.

23. Barker N, van Es JH, Kuipers J, Kujala P, van den Born M, Cozijnsen M, Haegebarth A, Korving J, Begthel H, Peters PJ, Clevers H. Identification of stem cells in small intestine and colon by marker gene Lgr5. Nature. 2007;449:1003-1008.

24. van der Flier LG, Clevers H. Stem cells, Self-Renewal, and differentiation in the intestinal epithelium. Annu Rev Physiol. 2009;71:241-260.

25. Willis ND, Przyborski SA, Hutchison CJ, Wilson RG. Colonic and colorectal cancer stem cells: progress in the search for putative biomarkers. J Anat. 2008;213:59-65.

26. Sato M, Ahnen DJ. Regional variability of colonocyte growth and differentiation in the rat. Anat Rec. 1992;233:409-414.

27. Yen TH, Wright NA. The Gastrointestinal Tract Stem Cell Niche. Stem Cell Rev. 2006;2:203-212.

28. Shanmugathasan M, Jothy S. Apoptosis, anoiksis and their relevance to the pathobiology of colon cancer. Pathol Int. 2000;50:273-279.

29. Spradling A, Drummond-Barbosa D, Kai T. Stem cells find their niche. Nature. 2001;414:98-104.

30. Umar S. Intestinal stem cells. Curr Gastroenterol Rep. 2010;12:340-348.

31. Moore KA, Lemischka IR. Stem Cells and Their Niches. Science. 2006;311:1880-1884.

32. Pinto D, Clevers H. Wnt, stem cells and cancer in the intestine. Bio Cell. 2005;97:185-196.

33. Katoh M. Networking of WNT, FGF, Notch, BMP, and Hedgehog signaling pathways during carcinogenesis. Stem Cell Rev. 2007;3:30-38.

34. Medema JP, Vermeulen L. Microenvironmental regulation of stem cells in intestinal homeostasis and cancer. Nature. 2011;474:318-326.

35. Van der Flier LG, Sabates-Bellver J, Oving I, Haegebarth A, De Palo M, Anti M, Van Gijn ME, Suijkerbuijk S, Van de Wetering M, Marra G, Clevers H. The Intestinal Wnt/TCF Signature. Gastroenterology. 2007;132:628-632.

36. Fearon ER, Vogelstein B. A genetic model for colorectal tumorigenesis. Cell. 1990; 61:759-767.

37. Shih IM, Yu J, He TC, Vogelstein B, Kinzler KW.The beta-catenin binding domain of adenomatous polyposis coli is sufficient for tumor suppression. Cancer Res. 2000;60:1671-1676.

38. Katoh M, Katoh M. WNT antagonist, DKK2, is a Notch signaling target in intestinal stem cells: augmentation of a negative regulation system for canonical WNT signaling pathway by the Notch-DKK2 signaling loop in primates. Int J Mol Med. 2007;19:197-201.

39. Katoh M, Katoh M. WNT signaling pathway and stem cell signaling network. Clin Cancer Res. 2007;13:4042-4045.

40. Miyamoto S, Rosenberg DW. Role of Notch signaling in colon homeostasis and carcinogenesis. Cancer Sci. 2011;102:1938-1942.

41. Pannequin J, Bonnans C, Delaunay N, Ryan J, Bourgaux JF, Joubert D, Hollande F. The Wnt Target Jagged-1 Mediates the Activation of Notch Signaling by Progastrin in Human Colorectal Cancer Cells. Cancer Res. 2009;69:6065-6073.

42. Varnat F, Siegl-Cachedenier I, Malerba M, Gervaz P, Ruiz i Altaba A. Loss of WNT-TCF addiction and enhancement of HH-GLI1 signalling define the metastatic transition of human colon carcinomas. EMBO Mol Med. 2010;2:440-457.

43. Varnat F, Siegl-Cachedenier I, Malerba M, Gervaz P, Ruiz i Altaba A. Loss of WNT-TCF addiction and enhancement of HH-GLI1 signalling define the metastatic transition of human colon carcinomas. EMBO Mol Med. 2010;2:440-457.

44. Vogelstein B, Fearon ER, Hamilton SR, Kern SE, Preisinger AC, Leppert M, Nakamura Y, White R, Smits AM, Bos JL. Genetic alterations during colorectal-tumor development. N Engl J Med. 1988;319:525-532.

45. Powell, S M, Zilz, N, Beazer-Barclay, Y, Bryan, T M, Hamilton, S R, Thibodeau, SN, Vogelstein, B and Kinzler, K W. APC mutations occur early during colorectal tumorigenesis. Nature. 1992;359:235-237.

46. Ricci-Vitiani L, Pagliuca A, Palio E, Zeuner A, De Maria R. Colon cancer stem cells. Gut. 2008;57:538-548.

47. Salama P, Platell C. Colorectal Cancer Stem Cells. ANZ J Surg. 2009;79:697-702.

48. Miller SJ, Lavker RM, Sun T. Interpreting epithelial cancer biology in the context of stem cells: tumor properties and therapeutic implications. Biochimica et Biophysica Acta. 2005;1756:25-52.

49. Neureiter D, Herold C, Ocker M. Gastrointestinal cancer- only a deregulation of stem cell differentiation. Int J Mol Med. 2006;17:483-489.

50. Umar S, Sellin JH, Morris AP. Murine colonic mucosa hyperproliferation. II. PKC-beta activation and cPKC-mediated cellular CFTR overexpression. Am J Physiol Gastrointest Liver Physiol. 2000;278:G765-774.

51. Sarkar S, Swiercz R, Kantara C, Hajjar KA, Singh P. Annexin A2 mediates up-regulation of NF-κB, β-catenin, and stem cell in response to progastrin in mice and HEK-293 cells. Gastroenterology. 2011;140:583-595.

52. Cobb S, Wood T, Tessarollo L, Velasco M, Given R, Varro A, Tarasova N, Singh P. Deletion of functional gastrin gene markedly increases colon carcinogenesis in response to azoxymethane in mice. Gastroenterology. 2002;123:516-530.

53. Cobb S, Wood T, Ceci J, Varro A, Velasco M, Singh P. Intestinal expression of mutant and wild-type progastrin significantly increases colon carcinogenesis in response to azoxymethane in transgenic mice. Cancer. 2004;100:1311-1323.

54. Ricci-Vitiani L, Lombardi DG, Pilozzi E, Biffoni M, Todaro M, Peschle C, De Maria R. Identification and expansion of human colon-cancer-initiating cells. Nature. 2007;445:111-115.

55. Eramo A, Lotti F, Sette G, Pilozzi E, Biffoni M, Di Virgilio A, Conticello C, Ruco L, Peschle C, De Maria R. Identification and expansion of the tumorigenic lung cancer stem cell population. Cell Death Differ. 2008;15:504-514.

56. Peng S, Maihle NJ, Huang Y. Pluripotency factors Lin28 and Oct4 identify a sub-population of stem cell-like cells in ovarian cancer. Oncogene. 2010;29:2153-2159.

57. Zou J, Yu XF, Bao ZJ, Dong J. Proteome of human colon cancer stem cells: a comparative analysis. World J Gastroenterol. 2011;17:1276-1285.

58. O'Brien CA, Pollett A, Gallinger S, Dick JE. A human colon cancer cell capable of initiating tumour growth in immunodeficient mice. Nature. 2007;445:106-110.

59. Todaro M, Francipane MG, Medema JP, Stassi G. Colon cancer stem cells: promise of targeted therapy. Gastroenterology. 2010;138:2151-2162.

60. Lin PT, Gleeson JG, Corbo JC, Flanagan L, Walsh CA. DCAMKL1 encodes a protein kinase with homology to doublecortin that regulates microtubule polymerization. J Neurosci. 2000;20:9152-9161.

61. Burgess HA, Reiner O. Cleavage of doublecortin-like kinase by calpain releases an active kinase fragment from a microtubule anchorage domain. J Biol Chem. 2001;276:36397-36403.

62. Verissimo CS, Molenaar JJ, Meerman J, Puigvert JC, Lamers F, Koster J, Danen EH, van de Water B, Versteeg R, Fitzsimons CP, Vreugdenhil E. Silencing of the microtubule-associated proteins doublecortin-like and doublecortin-like kinase-long induces apoptosis in neuroblastoma cells.Endocr Relat Cancer. 2010;17:399-414.

63. Omori Y, Suzuki M, Ozaki K, Harada Y, Nakamura Y, Takahashi E, Fujiwara T. Expression and chromosomal localization of KIAA0369, a putative kinase structurally related to Doublecortin. J Hum Genet. 1998;43:169-177.

64. Shu T, Tseng HC, Sapir T, Stern P, Zhou Y, Sanada K, Fischer A, Coquelle FM, Reiner O, Tsai LH. Doublecortin-like kinase controls neurogenesis by regulating mitotic spindles and M phase progression. Neuron. 2006;49:25-39.

65. Koizumi H, Higginbotham H, Poon T, Tanaka T, Brinkman BC, Gleeson JG. Doublecortin maintains bipolar shape and nuclear translocation during migration in the adult forebrain. Nat Neurosci. 2006;9:779-786.

66. Zhang Y, Huang X. Investigation of doublecortin and calcium/calmodulin-dependent protein kinase-like-1-expressing cells in the mouse stomach. J Gastroenterol Hepatol. 2010;25:576-82.

67. May R, Sureban SM, Hoang N, Riehl TE, Lightfoot SA, Ramanujam R, Wyche JH, Anant S, Houchen CW. Doublecortin and CaM Kinase-like-1 and Leucine-Rich-Repeat-Containing G-Protein-Coupled Receptor Mark Quiescent and Cycling Intestinal Stem Cells, Respectively. Stem Cells. 2009;27:2571–2579.

68. Jin G, Ramanathan V, Quante M, Baik GH, Yang X, Wang SW, Tu S, Gordon SA, Pritchard DM, Varro A, Shulkes A, Wang T. Inactivating cholecystokinin-2 receptor inhibits progastrin-dependent colonic crypt fission, proliferation, and colorectal cancer in mice. J Clin Invest 2009;119:2691-2701.

69. Potten CS, Booth C, Tudor GL, Booth D, Brady G, Hurley P, Ashton G, Clarke R, Sakakibara S, Okano H. Identification of a putative stem cell and early lineage marker: musashi-1. Differentiation. 2003;71:28-41.

70. Kikuchi M, Nagata H, Watanabe N, Watanabe H, Tatemichi M, Hibi T. Altered expression of a putative progenitor cell marker DCAMKL1 in the rat gastric

mucosa in regeneration, metaplasia and dysplasia. BMC Gastroenterol. 2010;10:65.

71. Mwangi SM, Srinivasan S. DCAMKL-1: a new horizon for pancreatic progenitor identification.Am J Physiol Gastrointest Liver Physiol. 2010;299:G301-302.

72. Sureban SM, May R, Mondalek FG, Qu D, Ponnurangam S, Pantazis P, Anant S, Ramanujam RP, Houchen CW. Nanoparticle-based delivery of siDCAMKL-1 increases microRNA-144 and inhibits colorectal cancer tumor growth via a Notch-1 dependent mechanism. J Nanobiotechnology. 2011;9:40.

73. Sureban SM, May R, Ramalingam S, Subramaniam D, Natarajan G, Anant S, Houchen CW. Selective blockade of DCAMKL-1 results in tumor growth arrest by a Let-7a MicroRNA-dependent mechanism. Gastroenterology. 2009;137:649-659.

74. Sureban SM, May R, Lightfoot SA, Hoskins AB, Lerner M, Brackett DJ, Postier RG, Ramanujam R, Mohammed A, Rao CV, Wyche JH, Anant S, Houchen CW. DCAMKL-1 regulates epithelial-mesenchymal transition in human pancreatic cells through a miR-200a-dependent mechanism. Cancer Res. 2011;71:2328-2338.

75. Barker N, van de Wetering M, Clevers H. The intestinal stem cell. Genes Dev. 2008;22:1856-1864.

76. Barker N, Ridgway RA, van Es JH, van de Wetering M, Begthel H, van den Born M, Danenberg E, Clarke AR, Sansom OJ, Clevers H. Crypt stem cells as the cells-of-origin of intestinal cancer. Nature. 2009;457:608-611.

77. Haegebarth A, Clevers H. Wnt signaling, lgr5, and stem cells in the intestine and skin. Am J Pathol. 2009;174:715-721.

78. Sato T, Vries RG, Snippert HJ, van de Wetering M, Barker N, Stange DE, van Es JH, Abo A, Kujala P, Peters PJ, Clevers H. Single Lgr5 stem cells build crypt-villus structures in vitro without a mesenchymal niche. Nature. 2009;459:262-265.

79. Barker N, Huch M, Kujala P, van de Wetering M, Snippert HJ, van Es JH, Sato T, Stange DE, Begthel H, van den Born M, Danenberg E, van den Brink S, Korving J, Abo A, Peters PJ, Wright N, Poulsom R, Clevers H. Lgr5(+ve) stem cells drive self-renewal in the stomach and build long-lived gastric units in vitro. Cell Stem Cell. 2010;6:25-36.

80. McClanahan T, Koseoglu S, Smith K, Grein J, Gustafson E, Black S, Kirschmeier P, Samatar AA. Identification of overexpression of orphan G protein-coupled receptor GPR49 in human colon and ovarian primary tumors. Cancer Biol Ther. 2006;5:419-426.

81. Takahashi H, Ishii H, Nishida N, Takemasa I, Mizushima T, Ikeda M, Yokobori T, Mimori K, Yamamoto H, Sekimoto M, Doki Y, Mori M. Significance of Lgr5(+ve) cancer stem cells in the colon and rectum. Ann Surg Oncol. 2011;18:1166-1174.

82. Kleist B, Xu L, Li G, Kersten C. Expression of the adult intestinal stem cell marker Lgr5 in the metastatic cascade of colorectal cancer. Int J Clin Exp Pathol. 2011;4:327-335.

83. Becker L, Huang Q, Mashimo H. Immunostaining of Lgr5, an intestinal stem cell marker, in normal and premalignant human gastrointestinal tissue. ScientificWorldJournal. 2008;8:1168-1176.

84. Uchida H, Yamazaki K, Fukuma M, Yamada T, Hayashida T, Hasegawa H, Kitajima M, Kitagawa Y, Sakamoto M. Overexpression of leucine-rich repeat-containing G protein-coupled receptor 5 in colorectal cancer. Cancer Sci. 2010;101:1731-1737.

85. von Rahden BH, Kircher S, Lazariotou M, Reiber C, Stuermer L, Otto C, Germer CT, Grimm M. LgR5 expression and cancer stem cell hypothesis: clue to define the true origin of esophageal adenocarcinomas with and without Barrett's esophagus? J Exp Clin Cancer Res. 2011;30:23.

86. Morita H, Mazerbourg S, Bouley DM, Luo CW, Kawamura K, Kuwabara Y, Baribault H, Tian H, Hsueh AJ. Neonatal lethality of LGR5 null mice is associated with ankyloglossia and gastrointestinal distension. Mol Cell Biol. 2004;24:9736-9743.

87. Walker F, Zhang HH, Odorizzi A, Burgess AW. LGR5 is a negative regulator of tumourigenicity, antagonizes Wnt signalling and regulates cell adhesion in colorectal cancer cell lines. PLoS One. 2011;6:e22733.

88. Wielenga VJ, Smits R, Korinek V, Smit L, Kielman M, Fodde R, Clevers H, Pals ST. Expression of CD44 in Apc and Tcf mutant mice implies regulation by the WNT pathway. Am J Pathol. 1999;154:515-523.

89. Wielenga VJ, van der Neut R, Offerhaus GJ, Pals ST. CD44 glycoproteins in colorectal cancer: expression, function, and prognostic value. Adv Cancer Res. 2000;77:169-187.

90. Zeilstra J, Joosten SP, Dokter M, Verwiel E, Spaargaren M, Pals ST. Deletion of the WNT Target and Cancer Stem Cell Marker CD44 in Apc(Min/+) Mice Attenuates Intestinal Tumorigenesis. Cancer Res. 2008;68:3655-3661.

91. Al-Hajj M, Wicha MS, Benito-Hernandez A, Morrison SJ, Clarke MF. Prospective identification of tumorigenic breast cancer cells. Proc Natl Acad Sci U S A. 2003;100:3983-3988.

92. Kim H, Yang XL, Rosada C, Hamilton SR, August JT. CD44 expression in colorectal adenomas is an early event occurring prior to K-ras and p53 gene mutation. Arch Biochem Biophys. 1994;310:504-507.

93. Nagabhushan M, Pretlow TG, Guo YJ, Amini SB, Pretlow TP, Sy MS. Altered expression of CD44 in human prostate cancer during progression.Am J Clin Pathol. 1996;106:647-651.

94. Li C, Heidt DG, Dalerba P, Burant CF, Zhang L, Adsay V, Wicha M, Clarke MF, Simeone DM. Identification of pancreatic cancer stem cells. Cancer Res. 2007;67:1030-1037.

95. Prince ME, Sivanandan R, Kaczorowski A, Wolf GT, Kaplan MJ, Dalerba P, Weissman IL, Clarke MF, Ailles LE. Identification of a subpopulation of cells with cancer stem cell properties in head and neck squamous cell carcinoma. Proc Natl Acad Sci U S A. 2007;104:973-978.

96. Dalerba P, Dylla SJ, Park IK, Liu R, Wang X, Cho RW, Hoey T, Gurney A, Huang EH, Simeone DM, Shelton AA, Parmiani G, Castelli C, Clarke MF. Phenotypic characterization of human colorectal cancer stem cells. Proc Natl Acad Sci U S A. 2007;104:10158-10163.

97. Kopp R, Fichter M, Schalhorn G, Danescu J, Classen S. Frequent expression of the high molecular, 673-bp CD44v3,v8-10 variant in colorectal adenomas and carcinomas. Int J Mol Med. 2009;24:677-683.

98. Subramaniam V, Vincent IR, Gardner H, Chan E, Dhamko H, Jothy S. CD44 regulates cell migration in human colon cancer cells via Lyn kinase and AKT phosphorylation. Exp Mol Pathol. 2007;83:207-215.

99. Subramaniam V, Vincent IR, Gilakjan M, Jothy S. Suppression of human colon cancer tumors in nude mice by siRNA CD44 gene therapy. Exp Mol Pathol. 2007;83:332-340.

100. Morin PJ, Sparks AB, Korinek V, Barker N, Clevers H, Vogelstein B, Kinzler KW. Activation of beta-catenin-Tcf signaling in colon cancer by mutations in beta-catenin or APC. Science. 1997;275:1787-1790.

101. Du L, Wang H, He L, Zhang J, Ni B, Wang X, Jin H, Cahuzac N, Mehrpour M, Lu Y, Chen Q. CD44 is of functional importance for colorectal cancer stem cells. Clin Cancer Res. 2008;14:6751-6760.

102. Kemper K, Grandela C, Medema JP. Molecular identification and targeting of colorectal cancer stem cells. Oncotarget. 2010;1:387-395.

103. Su YJ, Lai HM, Chang YW, Chen GY, Lee JL. Direct reprogramming of stem cell properties in colon cancer cells by CD44. EMBO J. 2011;30:3186-3199.

104. Patel BB, Yu Y, Du J, Levi E, Phillip PA, Majumdar AP. Age-related increase in colorectal cancer stem cells in macroscopically normal mucosa of patients with adenomas: a risk factor for colon cancer. Biochem Biophys Res Commun. 2009;378:344-347.

105. Huh JW, Kim HR, Kim YJ, Lee JH, Park YS, Cho SH, Joo JK. Expression of standard CD44 in human colorectal carcinoma: association with prognosis. Pathol Int. 2009;59:241-246.

106. Levi E, Misra S, Du J, Patel BB, Majumdar AP. Combination of aging and dimethylhydrazine treatment causes an increase in cancer-stem cell population of rat colonic crypts. Biochem Biophys Res Commun. 2009;385:430-433.

107. Misra S, Heldin P, Hascall VC, Karamanos NK, Skandalis SS, Markwald RR, Ghatak S. Hyaluronan-CD44 interactions as potential targets for cancer therapy. FEBS J. 2011;278:1429-1443.

108. Smith K, Patel O, Lachal S, Jennings I, Kemp B, Burgess J, Baldwin G, Shulkes A. Production, secretion, and biological activity of the C-terminal flanking peptide of human progastrin. Gastroenterology. 2006;131:1463-1474.

109. Pannequin J, Delaunay N, Buchert M, Surrel F, Bourgaux JF, Ryan J, Boireau S, Coelho J, Pélegrin A, Singh P, Shulkes A, Yim M, Baldwin GS, Pignodel C, Lambeau G, Jay P, Joubert D, Hollande F. Beta-catenin/Tcf-4 inhibition after

progastrin targeting reduces growth and drives differentiation of intestinal tumors. Gastroenterology. 2007;133:1554-1568.

110. Baldwin GS, Casey A, Mantamadiotis T, McBride K, Sizeland AM, Thumwood CM. PCR cloning and sequence of gastrin mRNA from carcinoma cell lines. Biochem Biophys Res Commun. 1990;170:691-697.

111. Chicone L, Narayan S, Townsend CM Jr, Singh P. The presence of a 33-40 KDa gastrin binding protein on human and mouse colon cancer. Biochem Biophys Res Commun. 1989;164:512-519.

112. Rengifo-Cam W, Umar S, Sarkar S, Singh P. Antiapoptotic effects of progastrin on pancreatic cancer cells are mediated by sustained activation of nuclear factor-{kappa}B. Cancer Res. 2007;67:7266-7274.

113. Baldwin GS, Shulkes A. Gastrin, gastrin receptors and colorectal carcinoma. Gut. 1998;42:581-584.

114. Singh P, Owlia A, Varro A, Dai B, Rajaraman S, Wood T. Gastrin gene expression is required for the proliferation and tumorigenicity of human colon cancer cells. Cancer Res. 1996;56:4111-4115.

115. Singh P, Lu X, Cobb S, Miller BT, Tarasova N, Varro A, Owlia A. Progastrin1-80 stimulates growth of intestinal epithelial cells in vitro via high-affinity binding sites. Am J Physiol Gastrointest Liver Physiol. 2003;284:G328-339.

116. Wu H, Owlia A, Singh P. Precursor peptide progastrin(1-80) reduces apoptosis of intestinal epithelial cells and upregulates cytochrome c oxidase Vb levels and synthesis of ATP. Am J Physiol Gastrointest Liver Physiol. 2003;285:G1097-1110.

117. Singh P, Velasco M, Given R, Varro A, Wang TC. Progastrin expression predisposes mice to colon carcinomas and adenomas in response to a chemical carcinogen. Gastroenterology. 2000;119:162-171.

118. Umar S, Sarkar S, Wang Y, Singh P. Functional cross-talk between beta-catenin and NFkappaB signaling pathways in colonic crypts of mice in response to progastrin. J Biol Chem. 2009;284:22274-22284.

119. Black WJ, Stagos D, Marchitti SA, Nebert DW, Tipton KF, Bairoch A, Vasiliou V. Human aldehyde dehydrogenase genes: alternatively spliced transcriptional variants and their suggested nomenclature. Pharmacogenet Genomics. 2009;19:893-902.

120. Ginestier C, Hur MH, Charafe-Jauffret E, Monville F, Dutcher J, Brown M, Jacquemier J, Viens P, Kleer CG, Liu S, Schott A, Hayes D, Birnbaum D, Wicha MS, Dontu G. ALDH1 is a marker of normal and malignant human mammary stem cells and a predictor of poor clinical outcome. Cell Stem Cell. 2007;1:555-567.

121. Huang EH, Hynes MJ, Zhang T, Ginestier C, Dontu G, Appelman H, Fields JZ, Wicha MS, Boman BM. Aldehyde dehydrogenase 1 is a marker for normal and malignant human colonic stem cells (SC) and tracks SC overpopulation during colon tumorigenesis. Cancer Res. 2009;69:3382-3389.

122. Sanders MA, Majumdar AP. Colon cancer stem cells: implications in carcinogenesis.
Front Biosci. 2011;16:1651-1662.

123. Deng S, Yang X, Lassus H, Liang S, Kaur S, Ye Q, Li C, Wang LP, Roby KF, Orsulic S, Connolly DC, Zhang Y, Montone K, Bützow R, Coukos G, Zhang L. Distinct expression levels and patterns of stem cell marker, aldehyde dehydrogenase isoform 1 (ALDH1), in human epithelial cancers. PLoS One. 2010;5:e10277.

124. Lin L, Liu Y, Li H, Li PK, Fuchs J, Shibata H, Iwabuchi Y, Lin J. Targeting colon cancer stem cells using a new curcumin analogue, GO-Y030. Br J Cancer. 2011;105:212-220.

125. Jaenisch R, Young R. Stem cells, the molecular circuitry of pluripotency and nuclear reprogramming. Cell. 2008;132:567-582.

126. Chen X, Vega VB, Ng HH. Transcriptional regulatory networks in embryonic stem cells. Cold Spring Harb Symp Quant Biol. 2008;73:203-209.

127. Okumura-Nakanishi S, Saito M, Niwa H, Ishikawa F. Oct-3/4 and Sox2 regulate Oct-3/4 gene in embryonic stem cells. J Biol Chem. 2005;280:5307-5317.

128. Ben-Porath I, Thomson MW, Carey VJ, Ge R, Bell GW, Regev A, Weinberg RA. An embryonic stem cell-like gene expression signature in poorly differentiated aggressive human tumors. Nat Genet. 2008;40:499-507.

129. Bae KM, Su Z, Frye C, McClellan S, Allan RW, Andrejewski JT, Kelley V, Jorgensen M, Steindler DA, Vieweg J, Siemann DW. Expression of pluripotent stem cell reprogramming factors by prostate tumor initiating cells. J Urol. 2010;183:2045-2053.

130. Bapat SA, Mali AM, Koppikar CB, Kurrey NK. Stem and progenitor-like cells contribute to the aggressive behavior of human epithelial ovarian cancer. Cancer Res. 2005;65:3025-3029.

131. Saiki Y, Ishimaru S, Mimori K, Takatsuno Y, Nagahara M, Ishii H, Yamada K, Mori M. Comprehensive analysis of the clinical significance of inducing pluripotent stemness-related gene expression in colorectal cancer cells. Ann Surg Oncol. 2009;16:2638-2644.

132. Boer B, Kopp J, Mallanna S, Desler M, Chakravarthy H, Wilder PJ, Bernadt C, Rizzino A. Elevating the levels of Sox2 in embryonal carcinoma cells and embryonic stem cells inhibits the expression of Sox2:Oct-3/4 target genes. Nucleic Acids Res. 2007;35:1773-1786.

133. Meng HM, Zheng P, Wang XY, Liu C, Sui HM, Wu SJ, Zhou J, Ding YQ, Li JM. Overexpression of nanog predicts tumor progression and poor prognosis in colorectal cancer. Cancer Biol Ther. 2010 Feb 16;9.

134. Kong D, Li Y, Wang Z, Sarkar FH. Cancer Stem Cells and Epithelial-to-Mesenchymal Transition (EMT)-Phenotypic Cells: Are They Cousins or Twins? Cancers (Basel). 2011;3:716-729.

135. Atlasi Y, Mowla SJ, Ziaee SA, Bahrami AR. OCT-4, an embryonic stem cell marker, is highly expressed in bladder cancer. Int J Cancer. 2007;120:1598-1602.

136. Kim RJ, Nam JS. OCT4 Expression Enhances Features of Cancer Stem Cells in a Mouse Model of Breast Cancer. Lab Anim Res. 2011;27:147-152.

137. Chen Z, Xu WR, Qian H, Zhu W, Bu XF, Wang S, Yan YM, Mao F, Gu HB, Cao HL, Xu XJ. Oct4, a novel marker for human gastric cancer. J Surg Oncol. 2009;99:414-419.

138. Cheng L, Sung MT, Cossu-Rocca P, Jones TD, MacLennan GT, De Jong J, Lopez-Beltran A, Montironi R, Looijenga LH. OCT4: biological functions and clinical applications as a marker of germ cell neoplasia. J Pathol. 2007;211:1-9.

139. Tysnes BB. Tumor-initiating and -propagating cells: cells that we would like to identify and control. Neoplasia. 2010;12:506-515.

140. Kashyap V, Rezende NC, Scotland KB, Shaffer SM, Persson JL, Gudas LJ, Mongan NP. Regulation of stem cell pluripotency and differentiation involves a mutual regulatory circuit of the NANOG, OCT4, and SOX2 pluripotency

transcription factors with polycomb repressive complexes and stem cell microRNAs. Stem Cells Dev. 2009;18:1093-1108.

141. Hochedlinger K, Yamada Y, Beard C, Jaenisch R. Ectopic expression of Oct-4 blocks progenitor-cell differentiation and causes dysplasia in epithelial tissues. Cell. 2005;121:465-477.

142. Niwa H. How is pluripotency determined and maintained? Development. 2007;134:635-646.

143. Chen YC, Hsu HS, Chen YW, Tsai TH, How CK, Wang CY, Hung SC, Chang YL, Tsai ML, Lee YY, Ku HH, Chiou SH. Oct-4 expression maintained cancer stem-like properties in lung cancer-derived CD133-positive cells. PLoS One. 2008;3:e2637.

144. Tsukamoto T, Mizoshita T, Mihara M, Tanaka H, Takenaka Y, Yamamura Y, Nakamura S, Ushijima T, Tatematsu M. Sox2 expression in human stomach adenocarcinomas with gastric and gastric-and-intestinal-mixed phenotypes. Histopathology. 2005;46:649-658.

145. Rodriguez-Pinilla SM, Sarrio D, Moreno-Bueno G, Rodriguez-Gil Y, Martinez MA, Hernandez L, Hardisson D, Reis-Filho JS, Palacios J. Sox2: a possible driver of the basal-like phenotype in sporadic breast cancer. Mod Pathol. 2007;20:474-481.

146. Silva J, Barrandon O, Nichols J, Kawaguchi J, Theunissen TW, Smith A. Promotion of reprogramming to ground state pluripotency by signal inhibition. PLoS Biol. 2008;6:e253.

147. Takayanagi N, Ikuta Y, Anakura T. A case of advanced colon cancer with marked response to combination chemotherapy with 5-FU, low dose CDDP, and leucovorin. Gan To Kagaku Ryoho. 1997;24:357-360.

148. Stein A, Hiemer S, Schmoll HJ. Adjuvant therapy for early colon cancer: current status. Drugs. 2011;71:2257-2275.

149. Bayoudh L, Afrit M, Daldoul O, Zarrad M, Boussen H. Trastuzumab (herceptine) in medical therapy in breast cancer. Tunis Med. 2012;90:6-12.

150. Seshacharyulu P, Ponnusamy MP, Haridas D, Jain M, Ganti AK, Batra SK. Targeting the EGFR signaling pathway in cancer therapy. Expert Opin Ther Targets. 2012;16:15-30.

151. Khosravi-Shahi P, Cabezón-Gutiérrez L. Antiangiogenic drugs in the treatment of advanced epithelial ovarian cancer. Anticancer Agents Med Chem. Jan 19, 2012.

152. Conley SJ, Gheordunescu E, Kakarala P, Newman B, Korkaya H, Heath AN, Clouthier SG, Wicha MS. Antiangiogenic agents increase breast cancer stem cells via the generation of tumor hypoxia. Proc Natl Acad Sci U S A. Jan 23, 2012.

153. Ammon HP, Wahl MA: Pharmacology of Curcuma longa. Planta Med 1991;57: 1–7.

154. Hatcher H, Planalp R, Cho J, Torti FM, Torti SV. Curcumin: from ancient medicine to current clinical trials. Cell Mol Life Sci. 2008;65:1631-1652.

155. Singh P, Sarkar S, Umar S, Rengifo-Cam W, Singh AP, Wood TG. Insulin-like growth factors are more effective than progastrin in reversing proapoptotic effects of curcumin: critical role of p38MAPK. Am J Physiol Gastrointest Liver Physiol. 2010;298:G551-562.

156. Rao CV, Rivenson A, Simi B, Reddy BS. Chemoprevention of colon cancer by dietary curcumin. Ann N Y Acad Sci. 1995;768:201-204.

157. Carroll RE, Benya RV, Turgeon DK, Vareed S, Neuman M, Rodriguez L, Kakarala M, Carpenter PM, McLaren C, Meyskens FL Jr, Brenner DE. Phase IIa clinical trial of curcumin for the prevention of colorectal neoplasia. Cancer Prev Res (Phila). 2011;4:354-364.

158. Shehzad A, Wahid F, Lee YS. Curcumin in cancer chemoprevention: molecular targets, pharmacokinetics, bioavailability, and clinical trials. Arch Pharm (Weinheim). 2010;343:489-99.

159. Sa G, Das T. Anti cancer effects of curcumin: cycle of life and death. Cell Div. 2008;3:14.

160. Wilken R, Veena MS, Wang MB, Srivatsan ES. Curcumin: A review of anti-cancer properties and therapeutic activity in head and neck squamous cell carcinoma. Mol Cancer. 2011;10:12.

161. Sen GS, Mohanty S, Hossain DM, Bhattacharyya S, Banerjee S, Chakraborty J, Saha S, Ray P, Bhattacharjee P, Mandal D, Bhattacharya A, Chattopadhyay S, Das T, Sa G.J. Curcumin Enhances the Efficacy of Chemotherapy by Tailoring p65NFκB-p300 Cross-talk in Favor of p53-p300 in Breast Cancer. Biol Chem. 2011;286:42232-42247.

162. Bhattacharyya A, Mandal D, Lahiry L, Sa G, Das T. Black tea protects immunocytes from tumor-induced apoptosis by changing Bcl-2/Bax ratio. Cancer Lett. 2004;209:147-154.

163. Yu Y, Kanwar SS, Patel BB, Nautiyal J, Sarkar FH, Majumdar AP. Elimination of Colon Cancer Stem-Like Cells by the Combination of Curcumin and FOLFOX. Transl Oncol. 2009;2:321-328.

164. Patel VB, Misra S, Patel BB, Majumdar AP. Colorectal cancer: chemopreventive role of curcumin and resveratrol. Nutr Cancer. 2010;62:958-67.

165. Høyer-Hansen M, Jäättelä M. Autophagy: an emerging target for cancer therapy. Autophagy. 2008;4:574-580.

166. Tanida I, Ueno T, Kominami E. LC3 conjugation system in mammalian autophagy. Int J Biochem Cell Biol. 2004;36:2503-2518.

167. Kuma A, Matsui M, Mizushima N. LC3, an autophagosome marker, can be incorporated into protein aggregates independent of autophagy: caution in the interpretation of LC3 localization.Autophagy. 2007;3:323-328.

168. Cherra SJ 3rd, Kulich SM, Uechi G, Balasubramani M, Mountzouris J, Day BW, Chu CT. Regulation of the autophagy protein LC3 by phosphorylation. J Cell Biol. 2010;190:533-539.

169. Yang Z, Klionsky DJ. An overview of the molecular mechanism of autophagy. Curr Top Microbiol Immunol. 2009;335:1-32.

170. Ogier-Denis E, Codogno P. Autophagy: a barrier or an adaptive response to cancer. Biochim Biophys Acta. 2003;1603:113-128.

171. Aoki H, Takada Y, Kondo S, Sawaya R, Aggarwal BB, Kondo Y. Evidence that curcumin suppresses the growth of malignant gliomas in vitro and in vivo through induction of autophagy: role of Akt and extracellular signal-regulated kinase signaling pathways. Mol Pharmacol. 2007;72:29-39.

172. Yu L, Strandberg L, Lenardo MJ. The selectivity of autophagy and its role in cell death and survival. Autophagy. 2008;4:567-573.

173. Jia YL, Li J, Qin ZH, Liang ZQ. Autophagic and apoptotic mechanisms of curcumin-induced death in K562 cells. J Asian Nat Prod Res. 2009;11:918-928.

174. O'Sullivan-Coyne G, O'Sullivan GC, O'Donovan TR, Piwocka K, McKenna SL.

Curcumin induces apoptosis-independent death in oesophageal cancer cells. Br J Cancer. 2009;101:1585-95.

175. Rengifo-Cam W, Singh P. Role of progastrins and gastrins and their receptors in GI and pancreatic cancers: targets for treatment. Curr Pharm Des 2004;10,2345-2358.

176. Grabowska A M, Watson S A. Role of gastrin peptides in carcinogenesis. Cancer Lett. 2007;257:1-15.

177. Baldwin GS, Hollande F, Yang Z, Karelina Y, Paterson A, Strang R, Fourmy D, Neumann G, Shulkes A. Biologically active recombinant human progastrin(6-80) contains a tightly bound calcium ion. J Biol Chem 2001;276:7791-7796.

178. Wang TC, Koh TJ, Varro A, Cahill RJ, Dangler CA, Fox JG, Dockray GJ. Processing and proliferative effects of human progastrin in transgenic mice. J Clin Invest. 1996;98:1918-1929.

179. Wu H, Owlia A, Singh P. Precursor peptide progastrin reduces apoptosis of intestinal epithelial cells and upregulates cytochrome c oxidase Vb levels and synthesis of ATP. Am. J. Physiol. 2003;285:G1097-G1110.

180. Ottewell PD, Varro A, Dockray GJ, Kirton CM, Watson AJ, Wang TC, Dimaline R, Pritchard DM. COOH-terminal 26-amino acid residues of progastrin are sufficient for stimulation of mitosis in murine colonic epithelium in vivo. Am J Physiol. 2005;288:G541-G549.

181. Stepan VM, Krametter DF, Matsushima M, Todisco A, Delvalle J, Dickinson CJ. Glycine-extended gastrin regulates HEK cell growth. Am. J Physiol. 1999;277:R572-R581.

182. Singh P, Wu H, Clark C, Owlia A. AnnexinII binds progastrin and gastrin-like peptides, and mediates growth factor effects of autocrine and exogenous gastrins on colon cancer and intestinal-epithelial-cells. Oncogene. 2007;26:425-440.

183. Ferrand A, Sandrin MS, Shulkes A, Baldwin GS. Expression of gastrin precursors by CD133-positive colorectal cancer cells is crucial for tumour growth. Biochim Biophys Acta. 2009;1793:477-488.

184. Singh P, Sarkar S, Umar S, Rengifo-Cam W, Singh AP, Wood TG. Insulin-like growth factors are more effective than progastrin in reversing proapoptotic effects of curcumin: critical role of p38MAPK. Am J Physiol 2010;298:G551-G562.

185. Singh P, Owlia A, Espeijo R, Dai B. Novel gastrin receptors mediate mitogenic effects of gastrin and processing intermediates of gastrin on Swiss 3T3 fibroblasts. Absence of detectable cholecystokinin (CCK)-A and CCK-B receptors. J Biol Chem. 1995;270:8429-8438.

186. Jacovina AT, Deora AB, Ling Q, Broekman MJ, Almeida D, Greenberg CB, Marcus AJ, Smith JD, Hajjar KA. Homocysteine inhibits neoangiogenesis in mice through blockade of annexin A2-dependent fibrinolysis. J Clin Invest. 2009;119:3384-3394.

187. Sarkar S, Kantara C, Singh P. Clathrin mediates endocytosis of Progastrin and activates MAPKs; Role of cell surface AnnexinA2. Am J Physiol Gastrointest Liver Physiol. Jan 12, 2012.

188. Beales IL, Ogunwobi O. Glycine-extended gastrin inhibits apoptosis in Barrett's oesophageal and oesophageal adenocarcinoma cells through JAK2/STAT3 activation. J Mol Endocrinol. 2009;42:305-318.

189. Dubeykovskiy A, Nguyen T, Dubeykovskaya Z, Lei S, Wang TC. Flow cytometric detection of progastrin interaction with gastrointestinal cells. Regul. Pept. 2008;151:106-114.

190. Przemeck SM, Varro A, Berry D, Steele I, Wang TC, Dockray GJ, Pritchard DM. Hypergastrinemia increases gastric epithelial susceptibility to apoptosis. Regul Pept. 2008;146:147-156.

191. Song DH, Rana B, Wolfe JR, Crimmins G, Choi C, Albanese C, Wang TC, Pestell RG, Wolfe MM. Gastrin-induced gastric adenocarcinoma growth is mediated through cyclin D1. Am J Physiol. 2003;285:G217–G222.

192. Sebens Müerköster S, Rausch AV, Isberner A, Minkenberg J, Blaszczuk E, Witt M, Fölsch UR, Schmitz F, Schäfer H, Arlt A. Apoptosis-inducing effect of gastrin on colorectal cancer cells relates to an increased IEX-1 expression mediating NF-kappaB inhibition. Oncogene. 2008;27:1122-1134.

193. Cui G, Takaishi S, Ai W, Betz KS, Florholmen J, Koh TJ, Houghton J, Pritchard DM, Wang TC. Gastrin-induced apoptosis contributes to carcinogenesis in the stomach. Lab Invest. 2006; 86:1037-1051.

194. Ortiz-Zapater E, Peiró S, Roda O, Corominas JM, Aguilar S, Ampurdanés C, Real FX, Navarro P. Tissue plasminogen activator induces pancreatic cancer cell proliferation by non-catalytic mechanism that requires extracellular signal-

regulated kinase 1/2 activation through epidermal growth factor receptor and annexin A2. American J. Pathology. 2007;170:1573-1584.

195. Díaz VM, Hurtado M, Thomson TM, Reventós J, Paciucci R. Specific interaction of tissue-type plasminogen activator (t-PA) with annexinII on the membrane of pancreatic cancer cells activates plasminogen and promotes invasion *in vitro.* Gut. 2004;53:993-1000.

196. Sharma MC, Sharma M. Role of annexinII in angiogenesis and tumor progression: a potential therapeutic target. Curr Pharm Des. 2007;13:3568-3575.

197. Kesavan K, Ratliff J, Johnson EW, Dahlberg W, Asara JM, Misra P, Frangioni JV, Jacoby DB. AnnexinA2 is a molecular target for TM601, a peptide with tumor-targeting and anti-angiogenic effects. J Biol Chem. 2010;285:4366-4374.

198. Singh P. Role of Annexin-II in GI cancers: interaction with gastrins/progastrins. Cancer Lett. 2007;252:19-35.

199. Inokuchi J, Narula N, Yee DS, Skarecky DW, Lau A, Ornstein DK, Tyson DR. AnnexinA2 positively contributes to malignant phenotype and secretion of IL-6 in DU145 prostate cancer cells. Int J Cancer. 2009;124:68-74.

200. Lu G, Maeda H, Reddy SV, Kurihara N, Leach R, Anderson JL, Roodman GD. Cloning and characterization of annexin-II receptor on human marrow stromal cells. J Biol Chem. 2006;281:30542-30550.

201. Shiozawa Y, Havens AM, Jung Y, Ziegler AM, Pedersen EA, Wang J, Wang J, Lu G, Roodman GD, Loberg RD, Pienta KJ. AnnexinII/annexinII-receptor axis regulates adhesion, migration, homing, and growth of prostate cancer. J Cell Biochem. 2008;105:370-380.

202. Ling Q, Jacovina AT, Deora A, Febbraio M, Simantov R, Silverstein RL, Hempstead B, Mark WH, Hajjar KA. AnnexinII regulates fibrin homeostasis and neoangiogenesis in vivo. J Clin Invest. 2004;113:38-48.

203. Bourguignon LY, Xia W, Wong G. Hyaluronan-CD44 interaction with protein kinase C(epsilon) promotes oncogenic signaling by stem cell marker Nanog and the Production of microRNA-21, leading to down-regulation of tumor suppressor protein PDCD4, anti-apoptosis, and chemotherapy resistance in breast tumor cells. J Biol Chem. 2009;284: 2657-2671.

204. Subramaniam D, Ramalingam S, May R, Dieckgraefe BK, Berg DE, Pothoulakis C, Houchen CW, Wang TC, Anant S. Gastrin-mediated interleukin-8 and

cyclooxygenase-2 gene expression: differential transcriptional and posttranscriptional mechanisms. Gastroenterology. 2008;134:1070-1082.

205. Pancione M, Forte N, Sabatino L, Tomaselli E, Parente D, Febbraro A, Colantuoni V. Reduced beta-catenin and peroxisome proliferator-activated receptor-gamma expression levels are associated with colorectal cancer metastatic progression: correlation with tumor-associated macrophages, cyclooxygenase 2, and patient outcome. Hum Pathol. 2009;40:714-725.

206. Albanese C, Wu K, D'Amico M, Jarrett C, Joyce D, Hughes J, Hulit J, Sakamaki T, Fu M, Ben-Ze'ev A, Bromberg JF, Lamberti C, Verma U, Gaynor RB, Byers SW, Pestell RG. IKKalpha regulates mitogenic signaling through transcriptional induction of cyclin D1 via Tcf. Mol Biol Cell. 2003;14:585-599.

207. Cho HH, Song JS, Yu JM, Yu SS, Choi SJ, Kim DH, Jung JS. Differential effect of NF-kappaB activity on beta-catenin/Tcf pathway in various cancer cells. FEBS Lett. 2008;582:616-622.

208. Lamberti C, Lin KM, Yamamoto Y, Verma U, Verma IM, Byers S, Gaynor RB. Regulation of beta-catenin function by the IkappaB kinases. J Biol Chem. 2001;276:42276-42286.

209. Carayol N, Wang CY. IKKalpha stabilizes cytosolic beta-catenin by inhibiting both canonical and non-canonical degradation pathways. Cell Signal. 2006;18:1941-1946.

210. Zhang Y, Tomann P, Andl T, Gallant NM, Huelsken J, Jerchow B, Birchmeier W, Paus R, Piccolo S, Mikkola ML, Morrisey EE, Overbeek PA, Scheidereit C, Millar SE, Schmidt-Ullrich R. Reciprocal requirements for EDA/EDAR/NF-kappaB and Wnt/beta-catenin signaling pathways in hair follicle induction. Dev Cell. 2009;17:49-61.

211. Katoh M, Katoh M. Integrative genomic analyses of CXCR4: transcriptional regulation of CXCR4 based on TGFbeta, Nodal, Activin signaling and POU5F1, FOXA2, FOXC2, FOXH1, SOX17, and GFI1 transcription factors. Int J Mol Med. 2009;23:763-769.

212. Smith JP, Verderame MF, Ballard EN, Zagon IS. Functional significance of gastrin gene expression in human cancer-cells. Regul Pept. 2004;117:167-173.

213. Sarkar S and Singh P. Endosomal translocation of progastrin/AnnexinII is required for measuring activation of p38MAPK/ERK/NFκBp65 in IEC-18 cells. Gastroenterology. 2009;138(Supplement-1):S-1987.

214. Sharma M, Ownbey RT, Sharma MC. Breast cancer cell-surface annexinII induces cell migration and neoangiogenesis via tPA dependent plasmin generation. Exp Mol Pathol. 2010;88:278-86.

215. Zheng L, Foley K, Huang L, Leubner A, Mo G, Olino K, Edil BH, Mizuma M, Sharma R, Le DT, Anders RA, Illei PB, Van Eyk JE, Maitra A, Laheru D, Jaffee EM. Tyrosine 23 phosphorylation-dependent cell-surface localization of annexinA2 is required for invasion and metastases of pancreatic cancer. PLoS One. 2011;6:e19390.

216. Dontu G, Abdallah WM, Foley JM, Jackson KW, Clarke MF, Kawamura MJ, Wicha MS. In vitro propagation and transcriptional profiling of human mammary stem/progenitor cells. Genes Dev. 2003;17:1253-1270.

217. Zhao P, Zhang W, Tang J, Ma XK, Dai JY, Li Y, Jiang JL, Zhang SH, Chen ZN. Annexin II promotes invasion and migration of human hepatocellular-carcinoma-cells in vitro via its interaction with HAb18G/CD147. Cancer Sci. 2010;101:387-395.

218. Barker N, Clevers H. Leucine-rich repeat-containing G-protein-coupled receptors as markers of adult stem cells. Gastroenterology. 2010;138:1681-96.

219. Ma AS, Bel DJ, Mittal AA, Harrison HH. Immunocytochemical detection of extracellular-annexinII in cultured human skin keratinocytes and isolation of annexinII isoforms enriched in extracellular pool. J Cell Sci. 1994;107:1973-1984.

220. Esposito I, Penzel R, Chaib-Harrireche M, Barcena U, Bergmann F, Riedl S, Kayed H, Giese N, Kleeff J, Friess H, Schirmacher P. Tenascin-C and annexinII expression in the process of pancreatic carcinogenesis. J Pathol. 2006;208:673-685.

221. Valapala M, Vishwanatha JK. Lipid raft endocytosis and exosomal transport facilitate extracellular trafficking of AnnexinA2. J Biol Chem. 2011; 286:30911-30925.

222. Ji NY, Park MY, Kang YH, Lee CI, Kim DG, Yeom YI, Jang YJ, Myung PK, Kim JW, Lee HG, Kim JW, Lee K, Song EY. Evaluation of annexin II as a potential serum-marker for hepatocellular-carcinoma using a sandwich ELISA method. Int J Mol Med. 2009; 24:765-771.

223. Sarkar S, Maxwell CA, Kantara C, Luthra G, Singal A, Qui S, Bauer V, Okorodudu A, and Singh P. AnnexinA2 is increasingly expressed and released into serum of patients positive for colonic growths in relation to disease progression: Diagnostic implications. Gastroenterology. 2011;140 (Supplement-1):S-341.

224. Patchell BJ, Wojcik KR, Yang TL, White SR, Dorscheid DR. Glycosylation and annexinII cell-surface translocation mediates airway epithelial wound repair. Am J Physiol 2007; 293:L354-363.

225. Brumlik MJ, Daniel BJ, Waehler R, Curiel DT, Giles FJ, Curiel TJ.. Trends in immunoconjugate and ligand-receptor based targeting development for cancer therapy. Expert Opin Drug Deliv. 2008;5:87-103.

226. Ferrand A, Bertrand C, Portolan G, Cui G, Carlson J, Pradayrol L, Fourmy D, Dufresne M, Wang TC, Seva C. Signaling pathways associated with colonic mucosa hyperproliferation in mice overexpressing gastrin-precursors. Cancer Res. 2005;65:2770-2777.

227. McVoy LA, Kew RR. CD44 and annexinA2 mediate C5a chemotactic cofactor function of vitamin D binding protein. J Immunol. 2005;175:4754-4760.

228. Yu Q, Stamenkovic I. Localization of matrix-metalloproteinase-9 to cell-surface provides mechanism for CD44-mediated tumor invasion. Genes Dev. 1999;13:35-48.

229. Reeder JA, Gotley DC, Walsh MD, Fawcett J, Antalis TM. Expression of antisense CD44-variant6 inhibits colorectal tumor metastasis and tumor growth in a wound environment. Cancer Res. 1998;58:3719-3726.

230. Longerich T, Haller MT, Mogler C, Aulmann S, Lohmann V, Schirmacher P, Brand K. AnnexinA2 as a differential diagnostic marker of hepatocellular-tumors. Pathol Res Pract. 2011;207:8-14.

231. Saif MW, Chu E. Biology of colorectal cancer. Cancer J. 2010;16:196-201.

232. Ivascu A, Kubbies M. Rapid generation of single-tumor spheroids for high-throughput cell function and toxicity analysis. J Biomol Screen. 2006;11:922-932.

233. Rajasekhar VK, Studer L, Gerald W, Socci ND, Scher HI. Tumour-initiating stem-like cells in human prostate cancer exhibit increased NF-κB signalling. Nat Commun. 2011;2:162.

234. Sato T, van Es J, Snippert H, Stange D, Vries R, van den Born M, Barker N, Shroyer N, van de Wetering M, Clevers H. Paneth cells constitute the niche for Lgr5 stem cells in intestinal crypts. Nature. 2011;469:415-418.

235. Wu H, Rao G, Dai B, Singh P. Autocrine gastrins in colon cancer cells Up-regulate cytochrome c oxidase Vb and down-regulate efflux of cytochrome c and activation of caspase-3. J Biol Chem. 2000;275:32491-32498.

236. Fang DD, Kim YJ, Lee CN, Aggarwal S, McKinnon K, Mesmer D, Norton J, Birse CE, He T, Ruben SM, Moore PA. Expansion of CD133(+) colon cancer cultures retaining stem cell properties to enable cancer stem cell target discovery. Br J Cancer. 2010;102:1265-1275.

237. Kanwar SS, Yu Y, Nautiyal J, Patel BB, Majumdar AP. The Wnt/beta-catenin pathway regulates growth and maintenance of colonospheres. Mol Cancer. 2010;9:212.

238. Heinen C, Richardson D, White R, Groden J. Microsatellite instability in colorectal adenocarcinoma cell lines that have full-length adenomatous polyposis coli protein.
Cancer Res. 1995;55:4797-4799.

239. Ilyas M, Tomlinson I, Rowan A, Pignatelli M, Bodmer W. Beta-catenin mutations in cell lines established from human colorectal cancers. Proc Natl Acad Sci U S A. 1997;94:10330-10334.

240. Lengauer C, Kinzler KW, Vogelstein B. DNA methylation and genetic instability in colorectal cancer cells. Proc Natl Acad Sci U S A. 1997;94:2545-2550.

241. Singh P, Dai B, Wu H, Owlia A. Role of autocrine and endocrine gastrin-like peptides in colonic carcinogenesis. Curr Opin Gastroenterol. 2000;16:68-77.

242. Singh P, Xu Z, Dai B, Rajaraman S, Rubin N, Dhruva B. Incomplete processing of progastrin expressed by human colon cancer cells: role of noncarboxyamidated gastrins. Am J Physiol. 1994;266:G459-468.

243. Kantara C, Sarkar S, Maxwell C, Ullrich R, and Singh P. Detection of circulating tumor cells (CTCs) in mice, using cancer stem cell (CSC) markers and a novel cell surface marker, AnnexinA2. Proceedings of the American Association of Cancer Research, 2012. Abstract #2378.

244. Fan X, Ouyang N, Teng H, Yao H. Isolation and characterization of spheroid cells from the HT29 colon cancer cell line. Int J Colorectal Dis. 2011;26:1279-1285.

245. Vermeulen L, Todaro M, de Sousa Mello F, Sprick M, Kemper K, Perez Alea M, Richel D, Stassi G, Medema J. Single-cell cloning of colon cancer stem cells reveals a multi-lineage differentiation capacity. Proc Natl Acad Sci U S A. 2008;105:13427-13432.

246. Harless W. Cancer treatments transform residual cancer cell phenotype. Cancer Cell Int. 2011;11:1.

247. Silva IA, Bai S, McLean K, Yang K, Griffith K, Thomas D, Ginestier C, Johnston C, Kueck A, Reynolds R, Wicha M, Buckanovich R. Aldehyde dehydrogenase in combination with CD133 defines angiogenic ovarian cancer stem cells that portend poor patient survival. Cancer Res. 2011;71:3991-4001.

248. Park Y, Huh J, Lee J, Kim H. shRNA against CD44 inhibits cell proliferation, invasion and migration, and promotes apoptosis of colon carcinoma cells. Oncol Rep. 2012;27:339-346.

249. Bendardaf R, Algars A, Elzagheid A, Korkeila E, Ristamäki R, Lamlum H, Collan Y, Syrjänen K, Pyrhönen S. Comparison of CD44 expression in primary tumours and metastases of colorectal cancer. Oncol Rep. 2006;16:741-746.

250. Wang Y, McNiven M. Invasive matrix degradation at focal adhesions occurs via protease recruitment by a FAK-p130Cas complex. J Cell Biol. 2012;196:375-385.

251. Deng J, Miller S, Wang H, Xia W, Wen Y, Zhou B, Li Y, Lin S, Hung M. Beta-catenin interacts with and inhibits NF-kappa B in human colon and breast cancer. Cancer Cell. 2002;2:323-334.

252. Zhang J, Yamada O, Kida S, Matsushita Y, Yamaoka S, Chagan-Yasutan H, Hattori T. Identification of CD44 as a downstream target of noncanonical NF-κB pathway activated by human T-cell leukemia virus type 1-encoded Tax protein. Virology. 2011;413:244-252.

253. Bansal SS, Goel M, Aqil F, Vadhanam MV, Gupta RC. Advanced drug delivery systems of curcumin for cancer chemoprevention. Cancer Prev Res (Phila). 2011;4:1158-1171.

254. Kraft C, Peter M, Hofmann K. Selective autophagy: ubiquitin-mediated recognition and beyond. Nat Cell Biol. 2010;12:836-841.

255. Ichimura Y, Kumanomidou T, Sou YS, Mizushima T, Ezaki J, Ueno T, Kominami E, Yamane T, Tanaka K, Komatsu M. Structural basis for sorting mechanism of p62 in selective autophagy. J Biol Chem. 2008;283:22847-22857.

256. Nautiyal J, Kanwar SS, Yu Y, Majumdar AP. Combination of dasatinib and curcumin eliminates chemo-resistant colon cancer cells. Mol Signal. 2011;6:7.

257. Bharti AC, Donato N, Singh S, Aggarwal BB. Curcumin (diferuloylmethane) down-regulates the constitutive activation of nuclear factor-kappa B and IkappaBalpha kinase in human multiple myeloma cells, leading to suppression of proliferation and induction of apoptosis. Blood. 2003;101:1053-1062.

258. Pattingre S, Bauvy C, Codogno P. Amino acids interfere with the ERK1/2-dependent control of macroautophagy by controlling the activation of Raf-1 in human colon cancer HT-29 cells. J Biol Chem. 2003 May 9;278:16667-16674.

259. Tsuchihara K, Fujii S, Esumi H. Autophagy and cancer: dynamism of the metabolism of tumor cells and tissues. Cancer Lett. 2009;278:130-138.

260. White E, DiPaola RS. The double-edged sword of autophagy modulation in cancer. Clin Cancer Res. 2009;15:5308-5316.

261. Yan G, Graham K, Lanza-Jacoby S. Curcumin enhances the anticancer effects of trichostatin a in breast cancer cells. Mol Carcinog. Jan 30, 2012.

262. Hartojo W, Silvers AL, Thomas DG, Seder CW, Lin L, Rao H, Wang Z, Greenson JK, Giordano TJ, Orringer MB, Rehemtulla A, Bhojani MS, Beer DG, Chang AC. Curcumin promotes apoptosis, increases chemosensitivity, and inhibits nuclear factor kappaB in esophageal adenocarcinoma.Transl Oncol. 2010;3:99-108.

263. Narayan S. Curcumin, a multi-functional chemopreventive agent, blocks growth of colon cancer cells by targeting beta-catenin-mediated transactivation and cell-cell adhesion pathways. J Mol Histol. 2004;35:301-307.

264. Aggarwal BB, Shishodia S. Molecular targets of dietary agents for prevention and therapy of cancer. Biochem Pharmacol. 2006;71:1397-1421.

265. Abuzeid WM, Davis S, Tang AL, Saunders L, Brenner JC, Lin J, Fuchs JR, Light E, Bradford CR, Prince ME, Carey TE. Sensitization of head and neck cancer to cisplatin through the use of a novel curcumin analog. Arch Otolaryngol Head Neck Surg. 2011;137:499-507.

266. Beevers CS, Li F, Liu L, Huang S. Curcumin inhibits the mammalian target of rapamycin-mediated signaling pathways in cancer cells. Int J Cancer. 2006;119:757-764.

267. Cheng AL, Hsu CH, Lin JK, Hsu MM, Ho YF, Shen TS, Ko JY, Lin JT, Lin BR, Ming-Shiang W, Yu HS, Jee SH, Chen GS, Chen TM, Chen CA, Lai MK, Pu YS, Pan MH, Wang YJ, Tsai CC, Hsieh CY. Phase I clinical trial of curcumin, a chemopreventive agent, in patients with high-risk or pre-malignant lesions. Anticancer Res. 2001;21:2895-2900.

PUBLICATIONS

Sarkar S, Swiercz R, **Kantara C,** Hajjar K, Singh P. Annexin A2 mediates up-regulation of NF-κB, β-catenin, and stem cell in response to progastrin in mice and HEK-293 cells. Gastroenterology. 2011;140:583-595.

Singh P, **Kantara C,** Sarkar S, Maxwell C. Cancer Connections to Hormones and Growth Factors. *International Innovation*, Healthcare 2011, Issue 3, pp 70-72, ISSN: 2041-4552.http://www.research-europe.com/magazine/HEALTHCARE2/2011-3/pageflip.html.

Sarkar S, **Kantara C**, Singh P. Clathrin mediates endocytosis of Progastrin and activates MAPKs; Role of cell surface AnnexinA2. *Am J Physiol Gastrointest. Liver Physiol.* 2012 Jan 12. *In Press.*

Kantara C*, Sarkar S*, Ortiz I, Swiercz R, Davey R, Ullrich R, Singh P. Progastrin overexpression imparts tumorigenic/metastatic potential to embryonic epithelial cells: phenotypic differences between transformed and non-transformed stem cells.*Equally contributed to this work. March 2012. *International Journal of Cancer. In press.*

Fennewald S, **Kantara C**, Sastry S, Resto V. Laminin interaction with head and neck cancers cells under low fluid shear conditions leads to integrin activation and binding. March 2012. *Submitted to JBC.*

Szaniszlo P, Fennewald S, Qiu S, Vargas G, Shilagard T, **Kantara C**, Resto V. Temporal Characterization of Regional Lymphatic Metastasis in an Orthotopic Mouse Model for Head and Neck Squamous Cell Carcinoma. *In preparation.*

Kantara C, Ortiz I, Sarkar R, Ullrich R, Singh P. Combinatory effects of Curcumin ± siRNA DCAMKL-1 on colorectal cancer stem cells *in vitro* and *in vivo*: Novel treatment strategy. *In preparation.*

Kantara C, Ortiz I, Sarkar S, Ullrich R, Singh P. Tumorigenic potential of DCAMKL-1 and LGR5 positive colon cancer stem cells. *In preparation.*

Szaniszlo P, **Kantara C**, Fennewald S, Goldson T, Tao X, Elferink L, Resto V. Beta-1 Integrin is Essential for Growth, Anoikis Avoidance, and Adhesion to Laminin in Head and Neck Squamous Cell Carcinoma Cell Lines. *In preparation.*

Kantara C, Sarkar S, Singh P. Structure and function of DCAMKL-1 as a stem cell marker. Review.*In preparation.*

PATENTS

Singh, P (Inventor), **Kantara, C** (contributor), Sarkar, S (contributor), Maxwell, C (contributor) "Diagnosis of Epithelial Cancers (Primary and Metastatic) by Measuring ANXA2 Levels in the Serum". Final patent application number: D6986. Filed on June 28, 2010, by Dr. Benjamin Adler on behalf of UTMB.

Singh, P (Inventor), **Kantara, C** (contributor), Sarkar, S (contributor), Maxwell, C (contributor). Diagnosis of Benign and cancerous growths by measuring circulating tumor stem cells and serum annexinA2". Final patent application number D6987 UTMB-SING-P-10B, filed on June 29th 2011.

ABSTRACTS

Harrigal L, **Kantara C**, Chen M, Towers L, O'Connor K. sFRP-1 a potential ligand for α6β4 integrin that mediates ligand-independent phenotype in cancer cell migration. Summer Undergraduate Research Program at the University of Texas Medical Branch, Galveston Texas. September 2008. **Award: Excellent Research in Women's Health Honors.**

Li Z, He M, Yang L, Zhang X, **Kantara C**, Weiss H, Resto V, Xie J. The role of hedgehog signaling in radiation response in oral cancer. Poster presentation session for the Cancer Center Day 2009 at the University of Texas Medical Branch, Galveston, TX

Swiercz R, Sarkar S, **Kantara C**, Atanasov T, Singh P. Transcript sizes of stem cell marker, DCAMKL+1, differ significantly in cancer versus normal epithelial cells: potential for targeted therapy of cancer cells. 102th American Association of Cancer Research Conference, Orlando Florida, April 2010. Abstract #4359.

Kantara C, Sarkar S, May R, Houchen C, Shahid U, Singh P. DCAMKL+1 and CD44 positive stem/progenitor cells are significantly up-regulated in response to autocrine progastrin expression, associated with surprising transformation of HEK-293 cells, *in vitro* and *in vivo*. Digestive Disease Week, May 2010 Gastroenterology Vol. 138, Issue 5, Supplement 1, Page S-760. Poster presented at the National Student Research Forum. **Award: Best Poster in Oncology Research**.

Kantara C, Ortiz I, Sarkar S, Ullrich R, Singh P. Targeting the growth of cancer stem cells as spheroids, *in vitro*, using chemo dietary agents and RNAi. Stem Cells, Development and Cancer Conference, Vancouver, Canada, March 2011.Poster SessionB. Poster Presented at the Cancer Center Conference at the University of Texas Medical Branch. April 2010. **Award: Best Overall Student Poster.**

Szaniszlo P, **Kantara C**, Fennewald S, Goldson T, Tao X, Elferink L, Resto V. Beta-1 Integrin is Essential for Growth, Anoikis Avoidance, and Adhesion to Laminin in Head and Neck Squamous Cell Carcinoma Cell Lines. The American Head and Neck Society. Arlington, Virginia. May 2010. Abstract # P010.

Johnsrud A, **Kantara C**, Sarkar S, Swiercz R, Maxwell C, Kuo J, Singh P. Over-expression of progastrin renders HEK-293 cells tumorigenic: regulation of stem cells by progastrin/annexin 2. Poster presented at the Medical Student Summer Research Program at the University of Texas Medical Branch, June 2010. **Award: Best Overall Basic Science**.

Kuo J, **Kantara C**, Sarkar S, Swiercz R, Maxwell C, Johnsrud A, Singh P. Progastrin upregulates stem cell populations in the colonic crypts of mice: Functional implications.

Poster presented at the Medical Student Summer Research Program at the University of Texas Medical Branch, June 2010. **Award: NIDDK Research Enrichment and Preparation Training Program**.

Kantara C, Sarkar S, Swiercz R, Ullrich R, Singh P. Inhibitory Efficacy of Curcumin ± Stem Cell Specific RNAi on the growth of tumorospheres *in vitro*: Assay development and mechanisms of action. 102th American Association of Cancer Research Conference, Orlando Florida, April 2011. Abstract # 4363. Poster presented at the Neuroscience and Cell Biology Conference. **Award: Best Predoctoral Fellow Poster Presentation.**

Sarkar S, Maxwell C, **Kantara C**, Luthra G, Singal A, Qiu S, Bauer V, Okorodudu V, Singh P. Annexin A2 is increasingly expressed and released into the serum of patients positive for colonic growths/ tumors in relation to disease progression: Diagnostic Implications. 102th American Association of Cancer Research Conference, Orlando, Florida, April 2011. Abstract # Sa 1893. A-571.

Kantara C, Sarkar S, Swiercz R, Ortiz I, Singh P. Overexpression of Progastrin imparts Tumorigenic/metastatic Potential to Immortalized Embryonic Cells and Cancer cells: Role of Stem/progenitor Cell Markers and AnnexinA2. Digestive Disease Week, May 2011. Gastroenterology Vol. 140, Issue 5, Supplement 1, May 2011. Page S-341. **Platform Presentation.** Poster also presented at the Neuroscience and Cell Biology Conference. **Award: Best Predoctoral Fellow Poster Presentation.**

Kantara C, Ortiz I, Singh P. Targeting Caner Stem Cells (CSCs) with Curcumin ± RNAi against Stem-Cell markers, *In Vitro* and *In Vivo*: Effect on oncogenic-pathways. American Association of Cancer Research: New Horizons in Cancer Research, Gurgaon India, December 2011 Abstract. #C77.

Kantara C, Sarkar S, Maxwell C, Ullrich R, Singh P. Detection of circulating tumors cells (CTCs) in mice, using cancer stem cell (CSC) markers and a novel cell surface marker, AnnexinA2 .Submitted to the 103rd American Association of Cancer Research, Chicago, Illinois April 2012. Abstract #2378.

C, Kantara, S, Sarkar, C, Maxwell, R, Ullrich, Singh P. Circulating Tumors Cells (CTCs), positive for Cancer-Stem-Cell (CSC) Markers and cell-surface AnnexinA2, are significantly increased in mice bearing metastatic versus primary colon cancer tumors. Submitted to the Digestive Disease Week, San Diego, California, May 2012. Abstract# 1289642. **Platform Presentation.**

Kantara C, Ortiz, I, Sarkar S, Ullrich R, Singh P Targeting Caner Stem Cells (CSCs) with Curcumin±RNAi against Stem-Cell markers, In Vitro and In Vivo: Effect on oncogenic-pathways. Submitted to the Digestive Disease Week, San Diego, California, May 2012. Abstract#1290159.

Sarkar S, **Kantara C**, Singh P. Clathrin mediates endocytosis of progastrin (PG) and activates MAPKs; role of cell-surface associated AnnexinA2 (CS-ANXA2). Submitted to the Digestive Disease Week, San Diego, California, May 2012. Abstract#1289924.